SAPIENZA
UNIVERSITÀ DI ROMA

# Pharmacological modulation of lipid metabolism as a regulator of cellular plasticity, homeostasis, and stress responses in colon and liver cell models

*A dissertation in Fulfillment of the Requirements for the Degree of Doctor of Philosophy in Pharmacology and Toxicology*

**Francesco Vari**

*Department of Physiology and Pharmacology "V.Erspamer"*
*Sapienza University of Rome*

*Coordinator of the PhD program:*
Prof. Silvana Gaetani

*Thesis advisor:*
Prof. Anna Maria Giudetti

*ACADEMIC YEAR 2025-2026*

# Index


**1. Introduction** ..... 4

**1.1 Lipid metabolism: an overview** ..... **4**

**1.2 Intestinal lipid metabolism** ..... **5**

**1.3 Hepatic lipid metabolism** ..... **8**

**1.4 Distinct roles of DGAT1 and DGAT2 in lipid metabolism** ..... **10**

**1.5 Lipid droplets biogenesis and function in liver and intestine** ..... **14**

**1.6 Lipotoxicity associated with saturated fatty acids** ..... **16**

**1.7 Palmitic acid as a widely used inducer of lipotoxicity** ..... **17**

**1.8 Adaptive versus maladaptive responses to lipid overload** ..... **18**

**1.9 Role of PPAR$\alpha$ in lipid metabolism: structure, activation,** ..... **20**

**and metabolic functions** ..... **20**

**1.10 Oleoylethanolamide (OEA): a lipid signal orchestrating metabolic homeostasis** ..... **23**

**1.10.1 Biosynthesis and degradation of OEA** ..... 24

**1.10.2 PPAR$\alpha$-dependent OEA signaling in metabolic programming and satiety** ..... 26

**1.10.3 PPAR$\alpha$-independent actions of OEA** ..... 29

**1.10.4 OEA signaling in the intestine: lipid handling, chylomicron output, and high-fat stress adaptation** ..... 30

**1.10.5 OEA-PPAR$\alpha$ signaling as a regulator of hepatic lipid metabolism and homeostasis** ..... 31

**1.11 Omics approaches to investigate lipid metabolism** ..... **32**

**1.12 Aim of the study** ..... **37**

**1.13 References** ..... **41**

**2. Pharmacological potential of endocannabinoid and endocannabinoid-like compounds in protecting intestinal structure and metabolism under high-fat conditions** ..... 58

**Abstract** ..... **58**

**2.1 Introduction** ..... **59**

**2.2 Intestinal barrier: structure, properties, and role in gut health** ..... **61**

**2.3 Intestinal microbiota** ..... **64**

**2.4 Exploring the endocannabinoid system: functions and implications** ..... **65**

**2.5 OEA synthesis and metabolism** ..... **72**

**2.6 *In vitro* and *in vivo* approaches to investigate the effects of HFD** ..... **76**

**2.7 Effect of HFD on intestinal structure and function** ..... **78**

**2.8 Molecular mechanisms underlying HFD effects on intestine** ..... **81**

**2.9 HFD-induced gut microbiome alteration** ..... **82**

**2.10 HFDs disrupt intestinal nutrient transport** ..... **83**

**2.11 Systemic impacts of dysbiosis induced by HFDs** ..... **85**

**2.12 HFDs interfere with the endocannabinoid system** ..... **86**

**2.13 Dietary and therapeutic interventions to counteract HFD damage** ..... **88**

**2.14 Therapeutic potential of OEA in HFD induced intestinal dysfunction** **91**

**2.15 Conclusion** ..... **95**

**3. Lipotoxicity of palmitic acid is associated with DGAT1 downregulation and abolished by PPAR$\alpha$ activation in liver cells** 117

**Abstract** ..... **117**

**1. Introduction** ..... **118**

**2. Materials and Methods** ..... **121**

**3. Results** ..... **127**

**4. Discussion** ..... **140**

**5. References** ..... **144**

**4. Epithelial-mesenchymal transition shapes the lipotoxic response of colon cancer cells to palmitic acid** ..... 152

**Abstract** ..... **152**

**1. Introduction** ..... **153**

**2. Materials and Methods** ..... **156**

**3. Results** ..... **163**

**4. Discussion** ..... **180**

**5. Conclusions** ..... **187**

**6. References** ..... **188**

**5. A multi-omics map of OEA driven lipid remodeling in intestinal cell models** ..... 194

**Abstract** ..... **194**

**1. Introduction** ..... **196**

**2. Materials and Methods** ..... **197**

**3. Results** ..... **203**

**4. Discussion** ..... **227**

**6. General discussion and conclusions** ..... 229

**6.1 Limitations of the study and future perspectives** ..... **232**

**References** ..... **234**

# Abstract

Excess lipid accumulation is a well-established driver of metabolic dysfunction and tissue injury. However, the cellular impact of lipid overload is determined less by the absolute amount of fat than by its qualitative features and intracellular fate. Specifically, metabolic outcomes depend on the type of fatty acids involved and on how they are partitioned within the cell, whether directed toward β-oxidation, incorporated into membrane phospholipids for remodeling, or safely sequestered as neutral lipids within lipid droplets (LDs). When the cell's lipid-buffering capacity is overwhelmed, maladaptive programs are triggered, converging on endoplasmic reticulum (ER) stress, impaired autophagic flux, redox imbalance, and the activation of regulated cell death pathways. In parallel, bioactive lipid mediators derived from dietary fats, such as oleoylethanolamide (OEA), engage nutrient-sensing networks and can reprogram intracellular lipid trafficking and metabolism, thereby contributing to the restoration of cellular homeostasis. This dissertation aims to determine whether targeted modulation of lipid metabolism, through complementary molecular approaches, can shape cellular plasticity, enhance stress adaptation, and promote survival under lipid overload in hepatic and intestinal cell models. A central objective is to define the underlying metabolic rewiring using proteomics as a systems-level platform to capture global adaptive responses. First, using hepatocyte models, we dissected PA-induced lipotoxicity and identified a critical failure of neutral-lipid buffering linked to Diacylglycerol o-acyltransferase 1 (DGAT1) downregulation, accompanied by ER stress activation and

autophagy blockade. Pharmacological activation of Peroxisome Proliferator-Activated Receptor alpha (PPAR$\alpha$) restored adaptive lipid partitioning, rescued DGAT1 expression, improved mitochondrial efficiency, and abolished PA-induced cytotoxicity, supporting PPAR$\alpha$ as a mechanistically grounded lever to re-establish lipid homeostasis. Then, we demonstrate that epithelial-mesenchymal transition (EMT) profoundly conditions lipotoxic vulnerability in colorectal cancer cells: epithelial-like cells exhibit limited LDs biogenesis and high sensitivity to saturated fatty acids (i.e. palmitic acid, PA), whereas mesenchymal-like cells display a lipid-buffered phenotype enriched in LDs and enhanced resistance. Here, quantitative proteomics was pivotal in defining the baseline metabolic states and the PA-responsive networks that distinguish these phenotypes, revealing coordinated differences in LDs biogenesis, mitochondrial programs, stress-response modules, and cell-death signaling that would be difficult to capture with targeted assays alone. Finally, an integrated multi-omics workflow was used to delineate OEA metabolism across colon-derived models. This approach combined label-free quantitative proteomics (LC-MS/MS) with rapid SpiderMass lipidomic/metabolomic profiling and time-resolved OEA-d4 uptake kinetics. Proteome-wide analyses uncovered robust but highly context-dependent pathway reorganization, enabling separation of PPAR$\alpha$-aligned components from OEA-specific programs and linking lipid-signature changes to downstream network-level adaptations in trafficking, membrane dynamics, and stress resilience. Collectively, these findings position lipid partitioning as a determinant of cellular fate under lipid-induced stress and nominate DGAT1-dependent LDs buffering and OEA - PPAR$\alpha$ signaling as actionable nodes connecting metabolism to plasticity and stress adaptation.

Ultimately, proteomics provides the essential framework to resolve state-dependent cell mechanisms.

**Keywords:** Lipid metabolism; lipotoxicity; palmitic acid; oleoylethanolamide; PPAR$\alpha$; DGAT1; lipid droplets; ER stress; EMT; colorectal cancer cells; proteomics; multi-omics.

# 1. Introduction

## 1.1 Lipid metabolism: an overview

Lipids constitute a highly diverse and biologically essential class of molecules with structural, energetic, and signaling roles in mammalian cells. Beyond energy storage, lipids contribute to membrane organization, intracellular trafficking, and gene regulation, shaping fundamental cellular responses such as proliferation, differentiation, stress adaptation, and regulated cell death. Accordingly, lipid metabolism includes not only anabolic and catabolic pathways, but also tightly controlled signaling networks that link nutrient availability to cellular and whole-body physiology (1). At the biochemical level, lipid metabolism proceeds through a series of steps: fatty acid uptake, de novo lipogenesis, esterification into complex lipids, lipolysis, β-oxidation, and lipid remodeling. These processes are distributed across distinct organelles, plasma membrane, endoplasmic reticulum (ER), mitochondria, peroxisomes, and lipid droplets (LDs), enabling cells to direct lipid fluxes efficiently while preventing the toxic accumulation that arises when this balance fails (2). Fatty acids (FAs) are central intermediates in lipid metabolism and vary in chain length and degree of unsaturation, features that strongly influence their metabolic fate and biological activity. Long-chain saturated FAs (SFAs), such as palmitic acid (PA), are frequently linked to cellular stress responses, inflammatory signaling, and insulin resistance, whereas monounsaturated and polyunsaturated FAs (MUFAs/PUFAs) more often promote adaptive and protective responses - supporting membrane fluidity and facilitating safe neutral-lipid storage in LDs (3)(4). These differences suggest that lipid quality can matter as much as lipid quantity for metabolic outcomes.

At the systemic level, lipid homeostasis depends on coordinated inter-organ communication involving the intestine, liver, adipose tissue, skeletal muscle, and heart. Lipids are transported through the circulation within specialized lipoprotein particles, chylomicrons, very low density lipoproteins (VLDL), low density lipoproteins (LDL), and high density lipoproteins (HDL) transport lipids through the circulation., each defined by its apolipoprotein composition, lipid cargo, and tissue destination, thereby orchestrating organ-specific delivery and clearance (5). This program is regulated at the molecular level by nutrient-sensitive transcription factors and nuclear receptors. Peroxisome proliferator activated receptors (PPARs) govern fatty acid uptake and oxidation, sterol regulatory element binding proteins (SREBPs) control lipogenesis and cholesterol synthesis, and liver X receptors (LXRs) coordinate cholesterol efflux and sterol homeostasis. Together, these pathways integrate endocrine signals, mainly insulin and glucagon to dynamically reprogram metabolism across feeding-fasting cycles (6). When lipid handling capacity is overwhelmed, however, ectopic lipid deposition occurs in non adipose tissues, liver, skeletal muscle, pancreas, and intestine leading to the accumulation of bioactive lipid species that disrupt organelle function and intracellular signaling. This state, known as lipotoxicity, links obesity to insulin resistance, type 2 diabetes, and metabolic-associated fatty liver disease, and highlights new therapeutic targets in lipid metabolism (6).

## 1.2 Intestinal lipid metabolism

The intestine represents the primary interface between dietary lipids and systemic metabolism and plays a pivotal role in the systemic lipid homeostasis.

Traditionally viewed as a passive absorptive organ, it is now recognized as a dynamic metabolic and endocrine tissue that senses dietary lipids and generates lipid-derived signals influencing peripheral physiology (7). Dietary lipids are mainly ingested as triacylglycerols, cholesterol esters and phospholipids. In the intestinal lumen, these lipids are emulsified by bile acids to facilitate enzymatic digestion; pancreatic lipase/colipase hydrolyze triacylglycerols into free FAs (FFAs) and monoacylglycerols, while phospholipase A2 and cholesterol esterase process phospholipids and cholesterol esters, respectively (8). Absorption takes place mainly in the proximal small intestine. Here, fatty acids and monoacylglycerols enter enterocytes through passive diffusion and transporter mediated uptake. The latter involves membrane proteins such as CD36 and Fatty acid transport protein 4 (FATP4), which not only facilitate lipid entry but also influence intracellular lipid handling and signaling (9). Cholesterol absorption in the intestine depends primarily on Niemann-Pick C1-Like 1 (NPC1L1), a well-established drug target in the treatment of hypercholesterolemia. Blocking this transporter is indeed the mechanism exploited by ezetimibe, a drug that lowers plasma LDL cholesterol by inhibiting NPC1L1-mediated cholesterol uptake in the gut (Figure 1) (10); (11).

Within enterocytes, absorbed FAs are rapidly re-esterified into triacylglycerols in the ER and assembled into chylomicrons together with cholesterol esters, phospholipids, and apolipoprotein B48, a process requiring microsomal triacylglycerol transfer protein (MTP); chylomicrons are then secreted into the lymph and enter systemic circulation to deliver dietary lipids to peripheral tissues (12). Beyond transport, the intestine actively metabolizes lipids.

It carries out mitochondrial and peroxisomal β-oxidation and produces bioactive mediators such as oleoylethanolamide (OEA), which is induced by dietary fat and contributes to satiety while influencing intestinal lipid handling and systemic metabolism (13) (14). These effects are shaped by gut hormones (CCK, GLP-1, PYY), which regulate digestion and appetite, and by bile acids, which also act as signals through receptors such as FXR and TGR5 (15). With chronic high-fat feeding, intestinal lipid processing can shift alongside inflammation and barrier impairment, changes that may contribute to systemic metabolic dysfunction and motivate intestinal lipid pathways as therapeutic entry points for cardiometabolic risk (16).

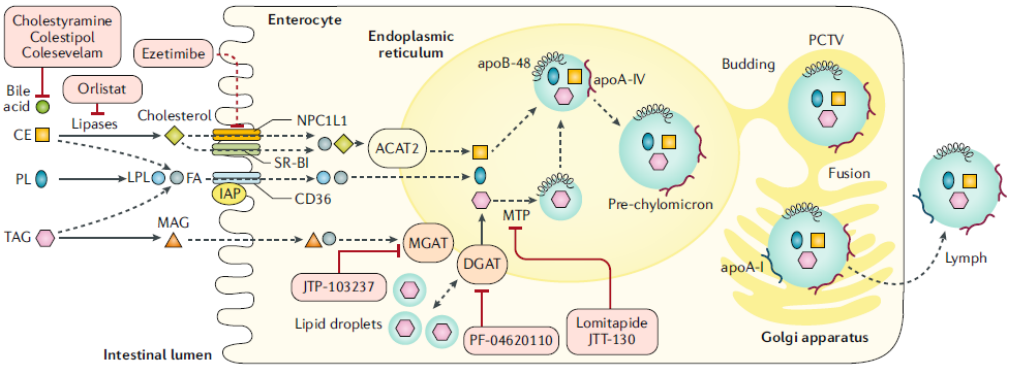


**Figure.1 Schematic representation of the main steps involved in intestinal lipid absorption and dietary lipid transport across enterocytes.** In the intestinal lumen, bile salts promote lipid emulsification, while lipases hydrolyze triglycerides (TAG), cholesteryl esters (CE), and phospholipids (PL), generating free fatty acids (FA), monoacylglycerols (MAG), and cholesterol. These products are taken up by enterocytes through membrane transporters and receptors, including NPC1L1, SR-BI, and CD36. Inside the enterocyte, cholesterol is esterified by ACAT2, whereas MAG and FA are re-esterified into TAG through MGAT and DGAT; a fraction of lipids may also be stored in cytoplasmic lipid droplets. In the endoplasmic reticulum, lipids are assembled with apoB-48 and apoA-IV through MTP to form the pre-chylomicron, which is then transported to the Golgi via PCTV (pre-chylomicron transport vesicles), further processed, and finally secreted into the lymph as mature chylomicrons.

## 1.3 Hepatic lipid metabolism

The liver is a key hub for lipid metabolism, integrating dietary lipids, fatty acids released from adipose tissue, and *de novo* synthesis to maintain systemic energy balance (17). Hepatic fatty acids mainly come from three sources: uptake of circulating non-esterified FAs, uptake of lipoprotein-derived FAs, and de novo lipogenesis (Figure 2). After feeding, insulin limits adipose lipolysis and promotes hepatic lipogenesis, whereas during fasting increased adipose lipolysis raises fatty-acid delivery to the liver (18). Fatty acid uptake by hepatocytes is mediated by both passive diffusion and transporter-dependent mechanisms. Proteins such as CD36 and fatty acid transport proteins (FATP) contribute to hepatic lipid influx, increased hepatic CD36 expression has been linked to steatosis, supporting its relevance as a potential pharmacological target (19). Once internalized, FAs are activated to acyl-CoA derivatives and directed toward distinct metabolic fates. One major route is mitochondrial and peroxisomal β-oxidation, a catabolic process that generates acetyl-CoA and reducing equivalents for ATP production; these oxidative programs are strongly controlled by fasting-responsive transcriptional networks centered on PPAR$\alpha$, making PPAR$\alpha$ activation a mechanistically grounded strategy to reduce hepatic lipid burden (20). Alternatively, FAs can be esterified into triacylglycerols and stored within LDs or incorporated into phospholipids and cholesterol esters. Importantly, triacylglycerol storage can function as an adaptive buffer that sequesters excess FAs into a relatively inert form, limiting the accumulation of more toxic lipid species and mitigating lipotoxic stress (21). De novo lipogenesis further contributes to hepatic triacylglycerol availability by converting excess carbohydrates into FAs; this pathway is classically driven by SREBP-1c in response to insulin and

by ChREBP in response to glucose-derived signals, thereby coupling carbohydrate oversupply to hepatic lipid synthesis (22); (23). Hepatic lipid export occurs through the assembly and secretion of very-low-density lipoprotein (VLDL) particles, a process requiring apolipoprotein B100 and microsomal triacylglycerol transfer protein (MTP), which facilitates lipid loading during lipoprotein assembly (24). Finally, hepatic zonation adds spatial complexity to lipid metabolism because hepatocytes differ along the porto - central axis: periportal cells are relatively enriched in oxidative pathways (including fatty acid β-oxidation), whereas pericentral cells show higher lipogenic activity. In fatty liver disease, this compartmentalization can be disrupted, influencing patterns of lipid accumulation and potentially modifying responses to metabolic therapies (25).

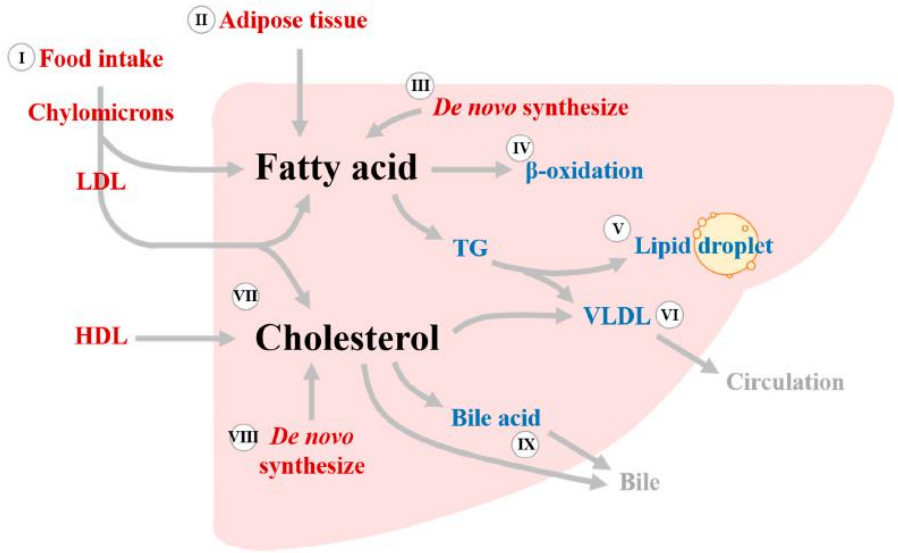


**Figure.2** Simplified schematic of hepatic lipid metabolism, showing the main sources and fates of fatty acids and cholesterol in the liver. Fatty acids derive from dietary lipids and circulating lipoproteins (I), adipose tissue (II), and de novo synthesis (III), and can be directed to beta-oxidation (IV), triglyceride (TG) synthesis and storage in lipid droplets (V), or very-low-density lipoprotein (VLDL) assembly and secretion (VI). Cholesterol is supplied by circulating lipoproteins, including low-density lipoproteins (LDL) and high-density lipoproteins (HDL), can also be synthesized de novo (VIII), and is utilized for bile

acid synthesis (IX) and biliary secretion. The diagram highlights the central role of the liver in coordinating lipid uptake, synthesis, storage, oxidation, and export.

## 1.4 Distinct roles of DGAT1 and DGAT2 in lipid metabolism

DGATs enzymes catalyze the terminal and committed step in triacylglycerol synthesis by converting diacylglycerol (DAG) and fatty acyl-CoA into triacylglycerols. This reaction constitutes a critical metabolic checkpoint, as it determines whether FAs are sequestered into a neutral and relatively inert storage form or redirected toward bioactive lipid species associated with lipotoxicity (26). In mammals, two distinct DGAT enzymes have been identified - DGAT1 and DGAT2 - which are encoded by separate genes, belong to different protein families, and perform non-redundant physiological functions (Figure 3). Although DGAT1 and DGAT2 catalyze the same biochemical reaction, they are structurally unrelated and exhibit distinct tissue distribution and substrate channeling properties. DGAT1, is a member of a gene family that includes acyl CoA:cholesterol acyltransferase (ACAT) 1 and ACAT2 and is broadly expressed across tissues, including the small intestine, liver, adipose tissue, skeletal muscle, and macrophages (27). In contrast, DGAT2 derives from a distinct gene family and is highly expressed in lipogenic tissues - particularly the liver and adipose tissue - where it plays a dominant role in endogenous triacylglycerol synthesis (28). DGAT1 is highly expressed in intestinal enterocytes and plays a major role in the re-esterification of dietary FAs into triacylglycerols during lipid absorption.

Following uptake of FAs and monoacylglycerols from the intestinal lumen, DGAT1 contributes to triacylglycerol synthesis within the ER, thereby supporting chylomicron assembly and secretion (29).

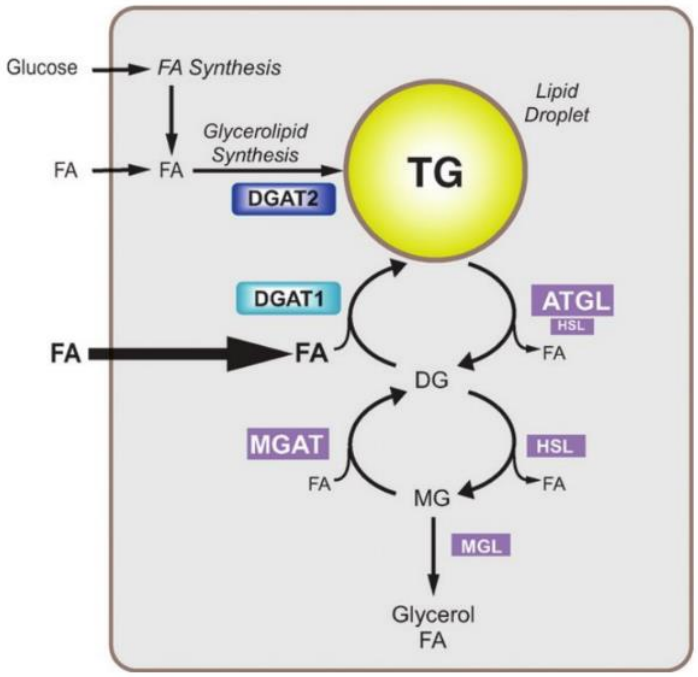


**Figure.3** Schematic representation of intracellular triglyceride metabolism and lipid droplets turnover. Fatty acids are supplied by extracellular uptake or de novo fatty acid synthesis (from glucose) and are incorporated into glycerolipids through Monoacylglycerol O-acyltransferase (MGAT) - and DGAT1/2-dependent reactions, leading to triglyceride (TG) synthesis and storage in lipid droplets. Triglycerides (TG) can be hydrolyzed by adipose triglyceride lipase (ATGL) to generate diacylglycerol (DG) and fatty acids (FA). DG is subsequently hydrolyzed by hormone-sensitive lipase (HSL) to monoacylglycerol (MG), which is finally converted into glycerol and FA by monoacylglycerol lipase (MGL).

Genetic deletion or pharmacological inhibition of DGAT1 alters the kinetics of intestinal triacylglycerol synthesis and postprandial chylomicronemia rather than completely abolishing lipid absorption, indicating the presence of compensatory triacylglycerol-synthetic pathways in enterocytes (30). Consistent with this role, DGAT1 preferentially utilizes exogenous, diet-derived FAs, distinguishing its function from DGAT2-mediated utilization of endogenously synthesized FAs (31).

Through these mechanisms, DGAT1 critically influences postprandial lipid handling and intestinal lipid-derived signaling (32).

From a pharmacological standpoint, DGAT1 has been investigated as a therapeutic target for obesity and metabolic disease; however, clinical development has been limited by gastrointestinal adverse effects, underscoring its essential physiological role in intestinal lipid handling (33). In contrast, DGAT2 is the predominant DGAT isoform involved in hepatic triacylglycerol synthesis, particularly in the context of de novo lipogenesis. DGAT2 preferentially channels newly synthesized FAs into triacylglycerols and LDs, thereby coupling excess carbohydrate availability to hepatic lipid storage (34). DGAT2 is closely associated with LDs and the ER, supporting its role in intracellular triacylglycerol accumulation rather than lipoprotein assembly. Genetic ablation of DGAT2 results in profound reductions in hepatic triacylglycerol content and is incompatible with normal development, highlighting its essential role in lipid homeostasis (35). In experimental models of hepatic steatosis, DGAT2 expression is upregulated and correlates with disease severity. Unlike DGAT1, DGAT2 plays a relatively minor role in intestinal lipid absorption. Its expression in enterocytes is substantially lower, and DGAT2 deficiency does not significantly impair chylomicron secretion, reinforcing the tissue-specific functional divergence between the two enzymes (36).

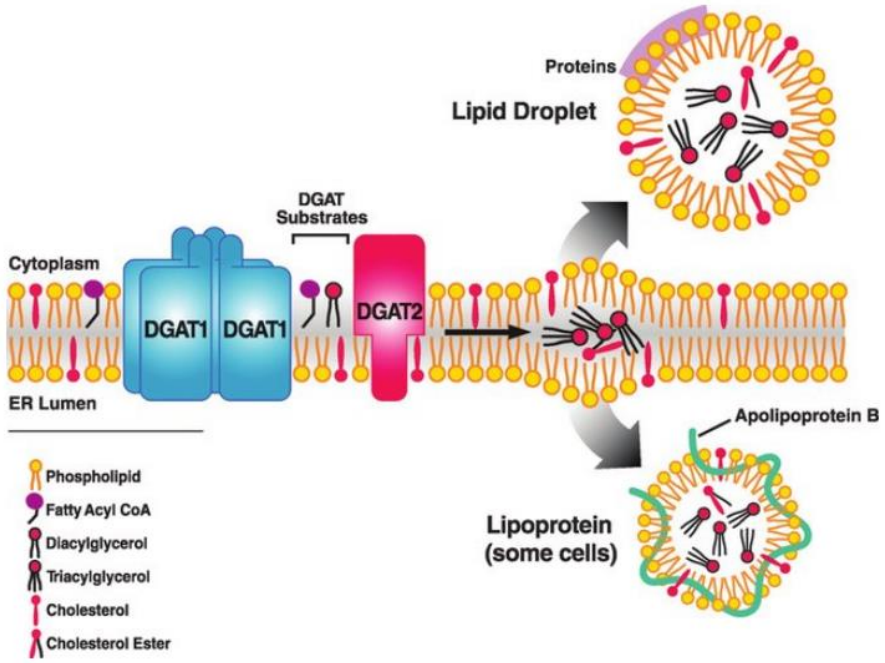


**Figure.4** Schematic model of DGAT1 and DGAT2 localization and function at the endoplasmic reticulum (ER) membrane. DGAT1 is shown as an integral ER membrane enzyme with both catalytic domains facing the ER lumen, whereas DGAT2 is positioned at the cytosolic side of the ER, where it uses diacylglycerol and fatty acyl-CoA to synthesize triacylglycerol. Newly synthesized triacylglycerols can be incorporated into lipid droplets, which bud from the ER and become coated with droplet-associated proteins, or in some cell types be used for apolipoprotein B-containing lipoprotein assembly. The diagram highlights the compartmentalized roles of DGAT enzymes in triglyceride synthesis, lipid droplet biogenesis, and lipoprotein production.

Beyond their role in triacylglycerol synthesis, DGAT enzymes exert broader regulatory functions in cellular lipid homeostasis and stress adaptation. By promoting triacylglycerol formation, DGAT activity can protect cells from SFA-induced lipotoxicity by limiting the availability of FAs for ceramide synthesis, ER stress, and mitochondrial dysfunction (37, 38). In this context, triacylglycerol accumulation may represent an adaptive, cytoprotective response to lipid overload rather than an inherently pathological process.

Consistently, DGAT1 has been shown to promote LD biogenesis during starvation by channeling autophagy-derived FAs into neutral lipid storage, thereby preserving mitochondrial function and limiting lipotoxic stress (39). In addition, DGAT1 activity is modulated by hypoxia-responsive pathways: hypoxia-inducible LD-associated protein (HILPDA) enhances DGAT1-mediated triacylglycerol synthesis and LDs formation in hepatocytes, linking oxygen availability to intracellular lipid partitioning (40). However, excessive or dysregulated DGAT activity - particularly DGAT2 - driven hepatic triacylglycerol synthesis - contributes to pathological lipid accumulation and the progression of metabolic liver disease (41). Together, these observations underscore the importance of tissue-specific and context-dependent regulation of DGAT activity in maintaining lipid homeostasis at the intersection of lipid storage, organelle protection, and cellular signaling.

## 1.5 Lipid droplets biogenesis and function in liver and intestine

In the liver and intestine, cytosolic LDs function as ER-derived organelles that integrate lipid storage with stress adaptation, and their impact on disease is strongly conditioned by LDs biogenesis, surface protein composition, and turnover. LDs formation initiates at the ER and requires coordinated neutral-lipid synthesis and recruitment of LD-coating proteins from the PLIN family, which regulate lipase access and thereby determine whether FAs are retained as neutral lipids or rapidly remobilized. In this context, PLIN3/TIP47 behaves as an early, exchangeable coat component: it associates with nascent LDs and is required for efficient LD maturation and triacylglycerol incorporation (42) (43). In hepatocytes, LDs expansion can be cytoprotective when it channels potentially lipotoxic FAs into triacylglycerol and sequesters them away from membranes; however,

persistent LDs accumulation and altered LDs coat composition can contribute to progressive liver injury and remodeling.

Consistent with a causal role for LDs coat proteins in hepatic pathogenesis, genetic loss of PLIN2 mitigates steatosis and metabolic injury *in vivo* (44) and liver-specific Plin2 deletion alleviates diet-induced hepatic steatosis, inflammation, and fibrosis (45). Morphological patterns of LD accumulation also map onto distinct mechanisms: microvesicular steatosis is tightly linked to mitochondrial dysfunction and oxidative stress (46), whereas variation in droplet size distributions within macrovesicular steatosis has been associated with differences in fibrogenic capacity in human liver (47). In enterocytes, LDs provide an essential buffering layer during dietary fat absorption and chylomicron assembly, and intestinal PLIN2 is functionally relevant to this process: Plin2 modulates enterocyte cytoplasmic LDs content and influences fecal lipid handling and diet-driven metabolic responses (48). Beyond lipid storage, LDs act as organizing centers for lipid mediator synthesis and therefore participate directly in intercellular signaling. LDs can compartmentalize eicosanoid-forming enzymes and have been demonstrated to operate as leukotriene-synthesizing organelles (49), with broader evidence supporting their role as specialized sites of eicosanoid production in inflammatory and neoplastic settings (50). In epithelial cancer contexts, LDs serve as reservoirs of cyclooxygenase-2 (COX-2) and sites of prostaglandin E2 ($PGE_2$) production, providing a direct mechanistic route by which LD abundance can modulate paracrine inflammatory tone and tumor-associated signaling. Importantly, PLIN proteins can couple LD biogenesis to inflammatory output: PLIN3 is required for robust LD formation and influences downstream inflammatory responses, including $PGE_2$ production in neutrophil-like cells (51) This signaling capacity is increasingly implicated in cancer progression

and microenvironmental communication, where LDs support metabolic flexibility and lipid-derived signaling required for growth, invasion, and stress resistance (52).

A concrete example is the PLIN2 axis in colorectal cancer, where PLIN2 has been reported to accelerate progression by combining tumor-intrinsic programs with microenvironmental remodeling, including macrophage reprogramming and CD36-linked EMT (53).

## 1.6 Lipotoxicity associated with saturated fatty acids

Lipotoxicity refers to a pathological state in which excess lipid exposure or accumulation in non-adipose tissues promotes cellular dysfunction and ultimately cell death. Crucially, lipotoxicity is not synonymous with triacylglycerol accumulation per se: the most damaging effects are typically attributed to specific lipid classes and intermediates ( saturated lipids, ceramides, DAGs, aberrant phospholipid species) that perturb organelle homeostasis and stress signaling (54). Among lipid species, long-chain SFAs - notably PA (C16:0) and stearate (C18:0) - are consistently associated with lipotoxic stress across multiple cell types (hepatocytes, myotubes, β-cells, cardiomyocytes, intestinal epithelial cells). In contrast, MUFAs such as oleate (C18:1) often buffer SFA toxicity by facilitating lipid neutralization through triacylglycerol synthesis and more permissive membrane remodeling (55). Mechanistically, SFA-driven lipotoxicity arises from interlocking stress modules. A prominent early axis is ER stress, driven in part by SFA-induced changes in membrane saturation and ER function, leading to unfolded protein response activation and pro-apoptotic outputs. This has been demonstrated clearly in pancreatic β-cells, where chronic PA exposure induces ER stress programs and apoptosis (56). A second major

axis is mitochondrial overload and dysfunction, where excess fatty-acid supply can exceed oxidative capacity, promoting incomplete oxidation, accumulation of lipid-derived intermediates, and stress amplification. In mouse models and mechanistic metabolic studies, mitochondrial overload and incomplete fatty-acid oxidation have been linked to insulin resistance (57). A third axis of relevance concerns alterations in sphingolipid levels, particularly the accumulation of ceramide, which can impair insulin signaling and enhance susceptibility to apoptosis. At the signaling level, ceramides have been shown to inhibit insulin-stimulated Akt/PKB activation (58). Importantly, causality is supported by *in vivo* intervention studies: blocking de novo ceramide synthesis improves insulin sensitivity and metabolic outcomes in diet-based models (59); (60). Finally, lipotoxicity is tightly connected to inflammatory signaling, where SFAs and SFA-driven stress pathways converge on kinases and innate immune circuits. A well-established example is the link between TLR4 signaling and fatty-acid associated insulin resistance in mouse models (61).

## 1.7 Palmitic acid as a widely used inducer of lipotoxicity

PA is among the most abundant SFAs in humans. It is commonly experimentally used because it robustly elicits lipotoxic phenotypes that mirror key features of metabolic diseases - impaired insulin signaling, inflammatory activation, ER stress, mitochondrial dysfunction, and programmed cell death. In in vitro systems, PA exposure (typically delivered complex to albumin to mimic physiological carriage) reproducibly induces ER stress and apoptosis in β-cell models, whereas oleate is comparatively less toxic and can counteract PA toxicity (62) (63). From a metabolic standpoint, palmitic acid (PA) is rapidly converted into

palmitoyl-CoA inside the cell. Under normal conditions, this molecule is safely disposed of either by being incorporated into triacylglycerols and stored in LDs, or by being fully broken down in the mitochondria. However, when these two disposal routes become overwhelmed or insufficient, palmitoyl-CoA is redirected toward alternative pathways that produce bioactive lipotoxic intermediates, most notably ceramides and saturated membrane lipids, which are inherently harmful to the cell. This metabolic rerouting helps explain why PA is particularly potent in disrupting insulin signaling and triggering pro-apoptotic cascades: a well-established molecular example is the ceramide-mediated inhibition of Akt, a key kinase in the insulin signaling pathway (64).

## 1.8 Adaptive versus maladaptive responses to lipid overload

When cells are exposed to excess lipids, they activate a coordinated set of adaptive responses to preserve metabolic homeostasis. A primary protective strategy consists in channeling excess FAs into neutral lipid storage within LDs. This process is often regarded as a "detoxification" mechanism, as triacylglycerol synthesis limits the accumulation of lipotoxic intermediates. Consistent with this view, experimental evidence shows that enhancing triacylglycerol formation and LD sequestration can protect cells from FA-induced cytotoxicity (65). In parallel, cells may increase fatty-acid oxidation to facilitate lipid disposal. However, when lipid supply chronically exceeds mitochondrial oxidative capacity, β-oxidation can become incomplete, thereby amplifying cellular stress rather than resolving it. Mechanistic studies in metabolic models have linked excessive lipid flux to mitochondrial overload and signatures of incomplete oxidation associated with insulin resistance (66).

In this adaptive framework, endogenous activation of lipid-sensing nuclear receptors, particularly PPAR$\alpha$, represents an additional mechanism through which cells coordinate lipid disposal and stress adaptation. Several lipid-derived molecules can act as physiological PPAR$\alpha$ activators, including long-chain unsaturated FAs, oxidized fatty-acid derivatives, eicosanoids, and N-acylethanolamines. These endogenous ligands do not simply serve as metabolic substrates, but also function as signals of lipid availability, promoting transcriptional programs involved in FA uptake, activation, mitochondrial and peroxisomal β-oxidation, and inflammatory control. Therefore, the balance between protective lipid mediators capable of engaging PPAR$\alpha$ and lipotoxic intermediates such as ceramides may influence whether lipid overload is resolved through adaptive remodeling or progresses toward cellular dysfunction (62-66).

Lipid stress also engages intracellular quality-control pathways. In enterocytes, for example, autophagy-related structures contribute to lipid trafficking and intracellular distribution, underscoring the involvement of organelle-level turnover mechanisms in lipid handling (67). When lipid exposure becomes sustained or excessive, these adaptive programs may be overwhelmed, leading to a maladaptive state characterized by persistent ER stress, mitochondrial dysfunction, chronic inflammatory signaling, and accumulation of toxic lipid species - most notably ceramides. The transition to this detrimental phase is strongly influenced by lipid composition, SFA-rich versus MUFA-rich environments, cellular oxidative capacity, and the efficiency of neutral lipid storage pathways. Accordingly, interventions that redirect lipid partitioning away from ceramide synthesis have been shown to markedly improve metabolic outcomes in murine models (68).

## 1.9 Role of PPARα in lipid metabolism: structure, activation, and metabolic functions

PPARα is a nuclear receptor that plays a central role in lipid metabolism, particularly in tissues with high oxidative capacity such as liver, intestine, heart, kidney, and skeletal muscle. Functioning as a transcriptional sensor of lipid availability, PPARα coordinates adaptive programs that favor fatty acid catabolism and energy homeostasis during fasting and nutrient deprivation (69). Like other nuclear receptors, PPARα has a modular architecture. The N-terminal A/B domain contains a ligand-independent activation function (AF-1) that contributes to basal transcriptional activity and can be tuned by post-translational modifications.

The highly conserved C domain forms the DNA-binding domain (DBD), featuring two zinc-finger motifs that enable sequence-specific recognition of peroxisome proliferator response elements (PPREs) in target gene promoters. A flexible hinge (D domain) supports protein-protein interactions, while the C-terminal E/F region contains the ligand-binding domain (LBD) and the ligand-dependent activation function (AF-2), where ligand-driven conformational changes govern coregulator recruitment and transcriptional output (70) (71). PPARα is activated by a range of endogenous lipid ligands, including unsaturated long-chain FAs and lipid-derived signaling mediators. Ligand engagement stabilizes an active receptor conformation that promotes coactivator binding and release of corepressors, switching PPARα from a repressed to a transcriptionally permissive state. Clinically, PPARα is the canonical target of fibrates (fenofibrate, gemfibrozil), which are used to lower plasma triacylglycerols and improve atherogenic dyslipidemia, although clinical benefit can be context-dependent and tolerability varies across individuals (72). At the

transcriptional level, ligand-bound PPARα heterodimerizes with retinoid X receptor (RXR) and binds PPAR responsive elements (PPREs) that typically consist of direct repeat motifs separated by one nucleotide (DR1 elements). This DNA-bound complex recruits coactivator assemblies (including histone-modifying and chromatin-remodeling activities) that enhance transcription, whereas in the absence of ligand, PPARα preferentially associates with corepressor complexes (NCoR/SMRT-containing assemblies) that maintain target loci in a transcriptionally restrained configuration. The regulated exchange of corepressors and coactivators is therefore a key mechanistic basis for ligand-dependent PPARα action and a central concept in pharmacological modulation of the receptor (73) (74).

Functionally, PPARα controls a broad gene network that promotes fatty acid uptake, activation, and oxidation. Canonical targets include genes involved in fatty acid transport and handling (CD36 and fatty acid–binding/activation systems), mitochondrial entry and oxidation (CPT1-dependent pathways), and peroxisomal β-oxidation (Acyl-CoA oxidase), thereby shifting cellular metabolism toward lipid disposal and reducing the intracellular accumulation of potentially harmful lipid intermediates (75). In the liver, this program is especially important during fasting, where PPARα supports the metabolic switch from carbohydrate reliance to fatty acid oxidation and ketogenesis. Consistent with this role, PPARα-deficient mice display impaired fasting adaptation characterized by defective fatty acid catabolism and ketone body production, predisposing to hypoketotic hypoglycemia and hepatic lipid accumulation (76).

Beyond the liver, PPARα plays a key role in regulating lipid metabolism in the intestine as well. In enterocytes, activation of PPARα drives specific transcriptional programs that enhance local fatty acid utilization and modulate the processing of dietary lipids, ultimately influencing their

systemic distribution. Concomitant with its regulation of lipid flux, PPAR$\alpha$ orchestrates a pleiotropic anti-inflammatory program. Mechanistically, this effect is largely mediated by transrepression, whereby ligand-activated PPAR$\alpha$ directly interacts with pro-inflammatory transcription factors, such as NF-κB and AP-1, thereby inhibiting their activity and reducing the expression of cytokines and acute-phase proteins, particularly under conditions of metabolic stress. This functional integration of lipid catabolism with the suppression of inflammatory signaling provides a compelling mechanistic rationale for targeting PPAR$\alpha$ in pathologies characterized by the intersection of dyslipidemia and chronic low-grade inflammation (76) (77). From a translational perspective, the clinical application of PPAR$\alpha$ pharmacology is nuanced by significant interspecies divergence in receptor expression and functional responsiveness. Rodents exhibit a marked peroxisome proliferative response and hepatomegaly upon PPAR$\alpha$ activation - phenomena largely absent in humans - which complicates the direct extrapolation of preclinical toxicological data to human safety profiles (78). These discrepancies have catalyzed the development of Selective PPAR$\alpha$ Modulators (SPPARMs), such as pemafibrate, designed to uncouple lipid-lowering efficacy from off-target adverse effects, thereby optimizing the therapeutic index in clinical settings (79)(80).

Overall, PPAR$\alpha$ integrates lipid sensing with transcriptional control of fatty acid catabolism and inflammation. Its tissue-specific actions in liver and intestine, its engagement by endogenous lipid mediators, and the opportunities (and limitations) of pharmacological activation together make PPAR$\alpha$ a central node in mechanistic and translational studies of lipid-driven metabolic disease (81) (82).

## 1.10 Oleoylethanolamide (OEA): a lipid signal orchestrating metabolic homeostasis

Oleoylethanolamide (OEA) is an endogenous lipid mediator belonging to the N-acylethanolamine (NAE) family. NAEs are structurally related to endocannabinoids, yet OEA is functionally distinct because it does not activate canonical cannabinoid receptors and instead acts primarily as a nutrient-responsive signal that couples lipid availability to coordinated metabolic and behavioral adaptations. Interest in OEA markedly increased after the demonstration that it induces satiety and reduces body-weight gain through activation of PPAR$\alpha$ (83). This evidence helped reposition OEA from a "peripheral lipid" to a signaling molecule capable of linking dietary fat ingestion to transcriptional programs of lipid handling and to measurable changes in feeding organization (84).

A central concept in OEA biology is that it behaves less like a classical endocrine hormone and more like an on-demand, locally produced lipid messenger. OEA production is particularly prominent in the proximal small intestine and is tightly regulated by nutritional state: OEA levels decrease during fasting and rise rapidly upon refeeding, consistent with a physiological role in translating dietary lipid ingestion into a postprandial signal that can shape subsequent ingestive behavior (85). This gut-centered localization is mechanistically meaningful because intestinal mucosal cells are directly exposed to the products of fat digestion- especially oleic acid- and can convert these substrates into OEA in a stimulus-dependent manner. In this framework, OEA integrates nutrient sensing with lipid partitioning and energy homeostasis, providing a functional bridge between local nutrient handling in the gut and metabolic adaptation in peripheral tissues.

### 1.10.1 Biosynthesis and degradation of OEA

OEA biosynthesis is classically described as a multi-step pathway that begins in membranes and culminates in the formation of free N-acylethanolamine. The first step involves N-acyltransferase (NAT) activity that transfers an acyl chain- typically from phosphatidylcholine - to phosphatidylethanolamine, generating a family of N-acylphosphatidylethanolamines (NAPEs). NAPEs are then converted into NAEs by NAPE-specific phospholipase D (NAPE-PLD), which cleaves NAPE to yield the corresponding NAE (including OEA) and phosphatidic acid. The molecular characterization of NAPE-PLD as an enzyme responsible for NAE formation is already reported (86) Importantly, NAE production is not necessarily restricted to a single route, and cellular studies indicate that modulating NAPE-PLD and related components reshapes NAPE/NAE pools, supporting both basal and stimulus-responsive regulation of NAE availability across contexts (87).

In the proximal small intestine, feeding acts as a strong physiological trigger for OEA mobilization. Mechanistic work shows that nutrient availability regulates both OEA formation and its degradation within intestinal mucosa, reinforcing the idea that local OEA levels reflect a dynamic balance between synthesis and catabolism rather than a static pool (88). This local control is also linked to fat handling at the epithelial interface: dietary fat-derived substrates contribute to OEA production, and epithelial sensing/transport steps can gate how much oleic acid becomes available for conversion into OEA, consistent with the intestine acting not only as an absorptive surface but also as a site of lipid-derived signal generation with systemic consequences.

OEA signaling is terminated predominantly by enzymatic hydrolysis to oleic acid and ethanolamine. Two intracellular hydrolases are particularly relevant: fatty acid amide hydrolase (FAAH) and N-acylethanolamine-hydrolyzing acid amidase (NAAA). FAAH is a widely expressed integral membrane enzyme of the amidase-signature family that hydrolyzes multiple fatty-acid amides; its foundational molecular characterization helped establish FAAH as a major "off-switch" for fatty acid amide signaling (89). Mechanistically, FAAH employs an unusual Ser-Ser-Lys catalytic triad, a feature supported by mutational and enzymology work (90), and its broader biochemical and pharmacological features (91) In contrast, NAAA is often discussed as a complementary, context-dependent hydrolase with distinct subcellular preferences and relevant roles in immune and intestinal compartments; its pharmacology has advanced substantially, enabling the use of selective inhibitors as tools to modulate endogenous NAE tone (92-94) From a translational standpoint, these catabolic enzymes are not only "terminators" of signaling but also leverage points for pharmacological modulation. By limiting hydrolysis, FAAH or NAAA inhibition can raise endogenous levels of OEA in a spatially and temporally constrained manner, potentially preserving the physiological on-demand logic of the pathway. Conversely, the rapid enzymatic breakdown of OEA has motivated the development of hydrolysis-resistant analogs that prolong signaling and enhance potency *in vivo* (95). Together, the synthesis - degradation cycle positions OEA as a fast-turnover lipid signal whose biology is strongly shaped by enzymatic control points that are, in principle, druggable.

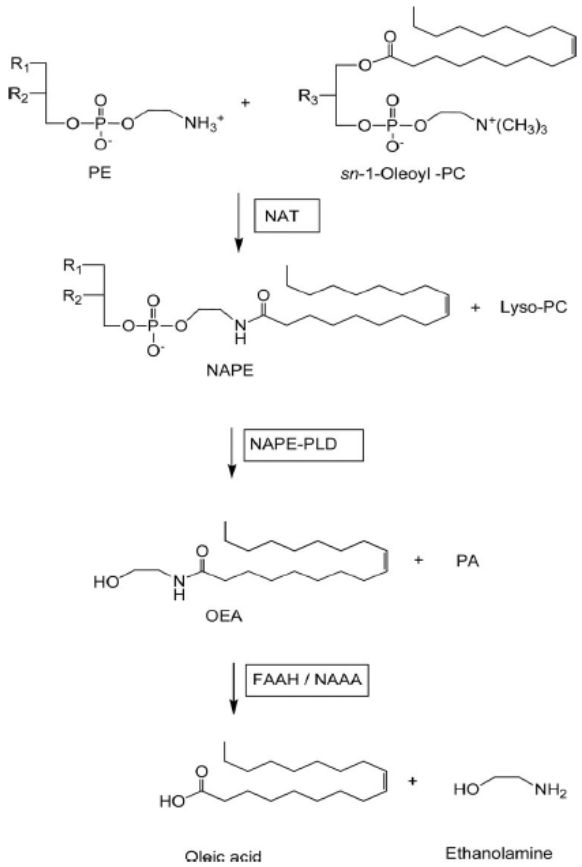


**Figure.5** Biosynthesis and degradation of OEA. Phosphatidylethanolamine (PE) is N-acylated with an oleoyl group donated by sn-1-oleoyl-phosphatidylcholine (PC) via N-acyltransferase (NAT) to form N-acylphosphatidylethanolamine (NAPE) and lyso-PC. NAPE is then hydrolyzed by NAPE-specific phospholipase D (NAPE-PLD) to generate OEA and phosphatidic acid (PA). Finally, OEA is degraded by FAAH and/or NAAA to yield oleic acid and ethanolamine.

### 1.10.2 PPAR$\alpha$-dependent OEA signaling in metabolic programming and satiety

OEA primarily targets PPAR$\alpha$, a lipid-sensing nuclear receptor that coordinates gene networks involved in fatty acid uptake, intracellular

transport, β-oxidation, and metabolic adaptation to lipid availability. The discovery that OEA induces satiety via PPAR$\alpha$ activation provided a mechanistic bridge between intestinal lipid sensing and nuclear receptor-dependent metabolic reprogramming (96). The satiating effect of OEA is primarily expressed through modifications in meal pattern organization rather than reductions in meal size. Specifically, OEA administration results in decreased meal frequency and prolonged inter-meal intervals, suggesting a regulatory role in feeding dynamics rather than a simple appetite-suppressing mechanism. This modulatory action on temporal feeding patterns is consistent with OEA's proposed role as a physiological satiety signal. Supporting the hypothesis of a gut-derived satiety mechanism, experimental evidence demonstrates that selective enhancement of OEA bioavailability in the proximal small intestine is sufficient to induce prolonged inter-meal satiety *in vivo* (97). A key refinement of this model is that intestinal OEA production is selectively engaged by fat ingestion and depends on epithelial lipid sensing/handling machinery. Duodenal lipid infusion stimulates OEA mobilization in the proximal small intestine, whereas infusion of non-lipid macronutrients does not reproduce this response; importantly, genetic disruption of either CD36 or PPAR$\alpha$ abrogates the satiety response induced by fat, indicating that OEA sits at the intersection of luminal lipid sensing and PPAR$\alpha$-dependent signaling outputs (98). Functionally, PPAR$\alpha$ activation by OEA promotes an oxidative metabolic bias by increasing expression of genes controlling fatty-acid activation and oxidation, including canonical mitochondrial and peroxisomal programs.

This facilitates lipid disposal and can limit the buildup of lipid intermediates that become deleterious under chronic oversupply (99 , 100). Beyond satiety, the OEA-PPAR$\alpha$ axis has broad metabolic consequences

that extend to peripheral tissues. *In vivo* studies show that OEA promotes fat utilization and reduces tissue triacylglycerol accumulation in wild-type animals, whereas these effects are lost in PPAR$\alpha$-deficient models, supporting a causal role for PPAR$\alpha$ in OEA-driven metabolic adaptation (101). In diet-based and genetic models of obesity, OEA administration lowers body-weight gain and improves hyperlipidemia, reinforcing that OEA impacts systemic lipid homeostasis and not only feeding behavior (102) Since PPAR$\alpha$ activation both promotes lipid breakdown and suppresses pro-inflammatory gene expression, OEA, by engaging PPAR$\alpha$, may simultaneously reduce lipid accumulation and dampen inflammation, two effects that are particularly relevant under conditions of metabolic stress (103). The importance of this pathway is supported by studies using modified OEA analogs that are resistant to hydrolysis - meaning they are not broken down as quickly in the body. These analogs activate PPAR$\alpha$ more potently and for longer, and produce stronger effects on appetite suppression and metabolism, suggesting that simply prolonging the duration of OEA signaling is enough to amplify its physiological benefits (104). Moreover, OEA plays a role in liver diseases beyond steatosis. In experimental models, OEA has been shown to attenuate liver fibrosis by inhibiting hepatic stellate cell activation, a process mediated at least in part by PPAR$\alpha$. These findings expand the conceptual framework of OEA, highlighting its involvement not only in metabolic regulation but also in tissue remodeling and chronic stress responses (105). Collectively, these findings position OEA as an endogenous ligand of PPAR$\alpha$ that promotes a transcriptional program favoring fatty acid oxidation, thereby coupling nutrient sensing to lipid utilization and potentially alleviating inflammation-associated metabolic stress.

### 1.10.3 PPAR$\alpha$-independent actions of OEA

Although PPAR$\alpha$ is the best-established target, OEA can influence physiology through additional receptors that enable faster, non-genomic signaling. One well-characterized PPAR$\alpha$-independent target of OEA is the transient receptor potential vanilloid 1 (TRPV1) channel. OEA has been shown to modulate TRPV1 activity, establishing a mechanistic link with sensory signaling and visceral afferent excitability (106). Moreover, *ex vivo* and *in vivo* experiments indicate that OEA can directly excite vagal sensory neurons and modulate short-term feeding responses through TRPV1-dependent mechanisms (107). These findings support the existence of a gut - brain signaling pathway that operates on a timescale faster than transcriptional remodeling (108). In parallel, OEA serves as an endogenous agonist of the Gs-coupled receptor GPR119, expressed in enteroendocrine L-cells. Activation of GPR119 increases intracellular cAMP and promotes GLP-1 secretion, linking lipid-derived signals to incretin release and glucose-metabolic coupling (109). This axis provides a mechanistic bridge between fat sensing and enteroendocrine outputs, suggesting that OEA can coordinate satiety not only through nuclear receptor signaling but also through hormone release that influences appetite and insulin secretion. More recently, OEA has been identified as an endogenous ligand for HIF-3$\alpha$, connecting OEA signaling to oxygen-sensitive transcriptional networks and suggesting an interface between lipid-derived mediators and hypoxia-inducible factor biology (110) Taken together, OEA can be conceptualized as a multi-receptor lipid messenger with layered kinetics: rapid sensory and endocrine effects can arise through TRPV1 and GPR119, while sustained metabolic adaptation is mainly mediated through PPAR$\alpha$-dependent

transcriptional programming, with emerging routes involving additional transcriptional regulators such as HIF-3$\alpha$.

### 1.10.4 OEA signaling in the intestine: lipid handling, chylomicron output, and high-fat stress adaptation

In the intestine, OEA acts as a key mediator linking dietary fat intake to both satiety signaling and lipid processing within enterocytes. After feeding, particularly following duodenal exposure to oleic acid, OEA levels rapidly increase in the mucosa of the proximal small intestine. This response is specific to lipid nutrients, as the infusion of non-lipid macronutrients does not elicit the same effect, supporting the concept that diet-derived oleic acid serves as the physiological precursor for OEA synthesis (111,112) Mechanistically, this pathway is tightly linked to epithelial fatty-acid sensing and transport. Genetic deletion of the membrane glycoprotein CD36 decreases jejunal OEA levels and disrupts the normal coupling between dietary fat and OEA signaling, supporting CD36 as a key upstream determinant of intestinal OEA tone and reinforcing the view that OEA is embedded in the machinery of intestinal lipid sensing rather than being a generic downstream lipid byproduct (113,114). Beyond its role in satiety signaling, intestinal OEA can also regulate how enterocytes handle absorbed FAs, determining whether they are oxidized locally, packaged into chylomicrons for systemic export, or channeled into lipid signaling pools. This regulatory function is conceptually analogous to the partitioning control exerted by the liver over lipid metabolism. *In vivo* and *ex vivo* experiments indicate that OEA increases FAT/CD36 expression in intestinal mucosa and isolated jejunal enterocytes and enhances fatty-acid uptake, suggesting that OEA can modulate the capacity of the epithelium

to import and process dietary FAs (115). At the level of lipoprotein secretion, OEA has been shown to modulate glycerolipid synthesis and chylomicron production in differentiated intestinal models. Specifically, it influences triacylglycerol synthesis and secretion, as well as apoB levels and microsomal triacylglycerol transfer protein (MTP) expression and activity. Notably, these intestinal effects may differ from those in the liver in terms of their dependence on PPAR$\alpha$, underscoring the tissue-specific regulatory pathways activated by a common lipid mediator (116).

This intestinal axis is also highly sensitive to chronic metabolic stress. In diet-induced obese rodents, the normal increase in jejunal OEA mobilization, triggered by feeding or lipid infusion, is markedly impaired. These findings suggest that prolonged nutrient overload may attenuate intestinal OEA production, thereby weakening a physiological brake on high-fat intake and potentially disrupting enterocyte lipid handling programs (117). In this sense, impaired intestinal OEA signaling may represent both a consequence of metabolic overload and a factor that contributes to the persistence of maladaptive feeding and lipid-handling patterns.

### 1.10.5 OEA-PPAR$\alpha$ signaling as a regulator of hepatic lipid metabolism and homeostasis

In the liver, the OEA-PPAR$\alpha$ axis acts as a key metabolic node linking lipid-derived signaling to fatty acid oxidation and protection against lipid overload. Although postprandial OEA mobilization primarily originates in the intestine, hepatic responsiveness to OEA is fully consistent with the canonical role of PPAR$\alpha$ in orchestrating fasting-like oxidative programs and sustaining lipid catabolism. OEA promotes fat utilization and reduces

tissue triacylglycerol accumulation *in vivo*, and these effects are lost in PPAR$\alpha$-deficient models, underscoring that a major fraction of OEA's systemic lipid-lowering phenotype is mediated by PPAR$\alpha$-dependent transcriptional control (118). Upon ligand binding, PPAR$\alpha$ induces an oxidative program that expands mitochondrial and peroxisomal β-oxidation capacity and broader lipid handling, thereby limiting the availability of FAs for net triacylglycerol storage; mapping of PPAR$\alpha$ target genes supports this role across oxidative and lipid metabolic pathways (119).

In diet-based obesity models, pharmacological elevation of OEA signaling reduces body-weight gain and improves hyperlipidemic features, consistent with sustained engagement of lipid catabolic programs (120). In liver disease contexts characterized by steatosis, inflammation, and progression toward fibrosis, PPAR$\alpha$ function is clinically relevant, and converging evidence supports the importance of maintaining or restoring PPAR$\alpha$-driven oxidative competence as a strategy to oppose lipid accumulation and inflammatory amplification (121). Beyond metabolic steatosis, OEA has also been reported to attenuate fibrogenic responses by targeting hepatic stellate cell, extending the potential relevance of this pathway from lipid accumulation to broader stress and remodeling programs in the liver (122).

## 1.11 Omics approaches to investigate lipid metabolism

The chemical diversity of lipids, their rapid remodeling, and tight coupling to signaling and organelle functions make lipid metabolism inherently multidimensional and difficult to capture with single-endpoint assays. For this reason, omics technologies particularly lipidomics, metabolomics, and

proteomics have become central to modern investigations of metabolic stress and lipotoxicity, enabling the parallel quantification of lipid species, pathway intermediates, and the protein networks that collectively shape phenotype (123)(124).

Lipidomics (typically MS-based) resolves lipid classes and molecular species with sufficient granularity to detect disease and stress-relevant shifts in saturation, acyl-chain length, and headgroup composition-features that often determine bioactivity more strongly than bulk lipid abundance (125) (126).

In lipotoxic contexts, lipidomics has been instrumental in linking metabolic dysfunction to the selective accumulation of bioactive lipid intermediates, particularly sphingolipids such as ceramides, which connect nutrient overload and inflammatory cues to impaired insulin signaling and cellular stress responses (127) At the same time, lipidomics helped refine the concept that neutral lipid storage can be adaptive: diverting FAs into triacylglycerols and LDs can reduce the pool available for toxic intermediates, thereby buffering lipotoxicity under specific conditions (128)

Methodologically, lipidomic and metabolomic profiling are most often performed by LC-MS(/MS) (targeted or untargeted), but complementary ambient and real-time MS approaches are increasingly relevant when the priority is rapid molecular readouts with minimal sample preparation. One notable example is SpiderMass/WALDI-MS, a platform designed for *in vivo*, real-time MS in which ion production occurs remotely from the mass spectrometer and the sampled material is transported to the analyzer in real time (Figure 6). SpiderMass uses resonant infrared laser ablation tuned to excite O-H bonds in endogenous water, which acts as an intrinsic ("endogenous") matrix in a MALDI-like process (water-assisted laser

desorption/ionization, WALDI), enabling direct desorption/ionization of lipids, metabolites, and proteins (129,130).

Importantly, beyond *in vivo* use, SpiderMass is also applicable *in vitro* and *ex vivo*, including cell cultures and fresh-frozen tissue sections (131,132) In such *in vitro*/*ex vivo* workflows, the key practical advantage is the potential to reduce preparative time and handling relative to extraction-heavy LC-MS pipelines, while maintaining conditions that are often closer to native chemistry. Consistent with this, an in-depth application study reports that fresh-frozen tissue sections can be analyzed by SpiderMass without any sample preparation, supporting rapid, more physiologically faithful molecular readouts (133). Because WALDI-MS can ionize multiple biomolecular classes, these SpiderMass measurements can be framed explicitly as rapid lipidomic profiling and metabolomic readouts (with detectable protein-level signals as well), providing fast molecular fingerprints that complement LC-MS depth and structural resolution when speed and near-native conditions are priorities (134)

Metabolomics complements lipidomics by measuring central carbon intermediates, redox cofactors, acylcarnitines, and energy-related metabolites that report on pathway activity and metabolic bottlenecks. This adds functional context to lipid signatures and supports inference about substrate utilization, mitochondrial capacity, and stress-associated rewiring (133) In lipotoxicity models, metabolomics is particularly useful for capturing shifts in energy/redox balance and patterns consistent with oxidative capacity limits (acylcarnitine and TCA-related signatures), helping determine whether fatty acid oversupply is matched by oxidation or instead coincides with incomplete oxidation and pathway congestion.

Because metabolic phenotypes are ultimately implemented by proteins, proteomics provides a uniquely powerful mechanistic bridge from altered

lipid/metabolite states to functional effectors. MS-based proteomics enables unbiased quantification of (1) enzymes and transporters controlling lipid synthesis, remodeling, trafficking, and β-oxidation; (2) organelle programs (mitochondrial OXPHOS and β-oxidation modules, peroxisomal oxidation, ER folding/lipid synthesis capacity, lipid-droplet structural and turnover proteins); and (3) stress-response and signaling networks that determine whether remodeling is adaptive or pathological. Crucially-especially for a thesis with substantial proteomic content, proteomics can move beyond abundance to capture regulatory layers such as post-translational modifications (phosphorylation, acetylation, ubiquitination) and proteostasis states that directly tune enzyme activity, organelle quality control, and stress signaling (134) In lipotoxic stress, proteomics can therefore reveal whether lipid and metabolite remodeling is accompanied by coordinated induction (or collapse) of oxidative machinery, rewiring of LDs biogenesis and turnover, activation of antioxidant defenses, and engagement of unfolded protein response and inflammatory programs - distinguishing transient compensation from sustained network remodeling and damage. Finally, while each omics layer is informative on its own, integration across lipidomics, metabolomics, and proteomics is often required to build causal, pathway-level models: lipid species changes can be mapped onto functional proxies of pathway activity (metabolites/flux surrogates) and anchored to the protein networks and regulatory nodes that implement adaptation (or drive failure) under metabolic stress (135).

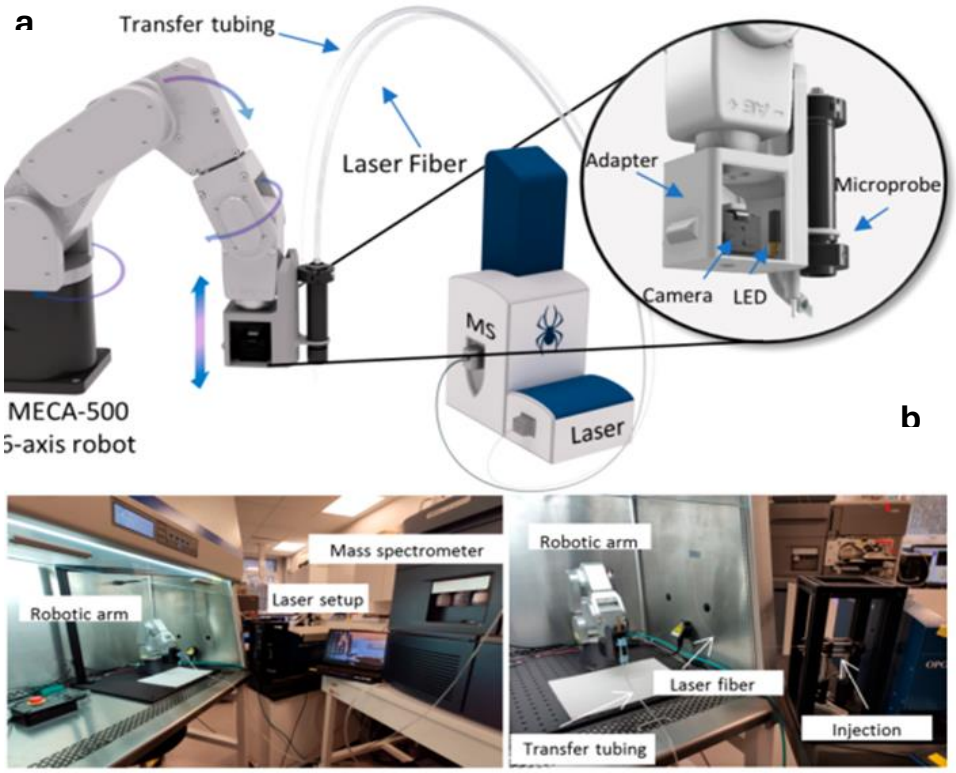


**Figure.6** Schematic representation of the robot-assisted SpiderMass technology and the general workflow of operation. (a) The SpiderMass probe is attached to the robotic arm via an adaptor. The zoomed-in view details the distance-sensing system, with a dedicated compartment for the camera and an LED laser pointer. Arrows indicate selected degrees of freedom of the 6-axis robotic arm. (b) Photographs of the robot-assisted SpiderMass MSI imaging setup: overall system layout including the robotic arm, laser system, and mass spectrometer (left), and a close-up of the robotic arm in the fume hood showing the laser fiber and transfer tubing, together with the laser injection interface (right).

## 1.12 Aim of the study

The overall aim of this study was to investigate whether pharmacological modulation of lipid metabolism can act as a regulator of cellular homeostasis, stress adaptation, and plasticity under conditions of lipid overload. The work was built on the concept that the biological outcome of fat exposure depends not only on the amount of lipid delivered to cells, but on how fatty acids are partitioned among oxidation, membrane remodeling, neutral-lipid storage, and the generation of bioactive intermediates that drive stress signaling (136) (136,137). In this framework, special attention was given to saturated fatty acid - induced lipotoxicity (using PA as a prototypical stressor), to the OEA- PPAR$\alpha$ axis as a druggable pathway promoting adaptive lipid handling (137,138) and to mechanisms that define susceptibility or resistance to lipid stress in intestinal, hepatic, and colon cell systems.

**Chapter 2** reports on the pharmacological potential of endocannabinoids and endocannabinoid-like mediators to preserve intestinal structure and metabolic function under high-fat conditions. The intestinal epithelium represents the first barrier exposed to dietary lipid flux and, far from acting as a passive surface, functions as a metabolically active tissue that responds to fat overload through coordinated changes in lipid processing, inflammatory tone, and barrier integrity (139 , 140). The review therefore investigated whether pharmacological manipulation of endogenous lipid mediators - with a focus on compounds within the endocannabinoid/NAE-related signaling space - could mitigate the epithelial architectural and metabolic alterations induced by high-fat exposure. The chapter aimed to define cytoprotective phenotypes at the level of epithelial organization and barrier-associated markers, and to link these outcomes to shifts in lipid-

handling pathways and stress-response readouts, thereby providing a mechanistic rationale for targeting gut lipid signaling as a strategy to improve systemic metabolic resilience.

**Chapter 3** dissects the cellular mechanisms by which PA induces lipotoxicity in hepatic cells, and tests whether reprogramming lipid metabolism through PPAR$\alpha$ activation can abolish the toxic phenotype. A central working hypothesis was that lipotoxicity does not simply result from triacylglycerol accumulation but rather reflects a failure of safe lipid buffering that increases the availability of harmful lipid species and amplifies organelle stress. Within this framework, the chapter investigated the relationship between PA-induced stress and the downregulation of DGAT1, a change expected to reduce triacylglycerol synthesis capacity and thereby impair the sequestration of neutral lipids into lipid droplets (LDs). The aim was to connect DGAT1-dependent triacylglycerol buffering to downstream stress modules, including ER stress, oxidative and mitochondrial dysfunction, and cell death signaling, and subsequently determine whether pharmacological activation of PPAR$\alpha$ by GW7647 could restore an adaptive metabolic state characterized by enhanced fatty acid catabolism and improved lipid partitioning, ultimately conferring protection against PA-induced toxicity in hepatocyte models (141,142). Selected findings were also confirmed in *Caenorhabditis elegans*, a widely used *in vivo* model for lipid metabolism studies, thereby extending the relevance of our observations from hepatocyte models to a whole-organism context.

**Chapter 4** reports how epithelial - mesenchymal transition (EMT) - as a major axis of cellular plasticity - shapes the response of colon cancer cells to PA-induced lipid stress. To address this, we leveraged an integrated omics strategy centered on basal proteomic profiling (supported by metabolic and

imaging readouts) in epithelial-like HCT15 and mesenchymal-like HCT116 models, asking whether EMT-linked cell states differ in their capacity to buffer saturated-fat overload through lipid storage. Strikingly, proteomics revealed a profound divergence in metabolic wiring and lipid-handling programs: HCT15 cells showed a predominantly glycolytic profile with reduced abundance of proteins involved in LDs biogenesis, whereas HCT116 cells exhibited an oxidative, "lipid-rich" proteomic signature, enriched in canonical LD/triacylglycerols - pathway components such as PLIN2, GPAT3, and DGAT1. Because EMT is associated with broad remodeling of metabolism, membrane dynamics, redox balance, and stress-response circuitry, this chapter therefore aimed to establish whether these proteome-defined states translate into differential vulnerability to PA and whether EMT rewires lipid routing - particularly triacylglycerols synthesis and LDs formation - in ways that either intensify maladaptive stress responses or enable protective adaptation. The work sought to connect EMT markers and functional state to quantitative endpoints of lipotoxicity (viability, stress signaling, mitochondrial integrity, and lipid accumulation patterns) and to interpret these differences as state-dependent metabolic wiring highlighted by proteomics.

**Chapter 5** aims to build an integrated molecular picture of the cellular state induced by OEA by combining omics approaches, so that coordinated pathway changes can be captured beyond what targeted assays alone would reveal. Because OEA can activate a PPAR$\alpha$-linked transcriptional program while also engaging additional lipid-sensing pathways, we expected a multi-layer remodeling of lipid handling, energy metabolism, and stress-response networks (143). Across all the three colon cell lines analyzed, OEA at 10 and 50 μM was well tolerated and consistently promoted to a lipid-handling phenotype, with increased neutral lipid

droplets at the higher dose and induction of CD36. SpiderMass kinetics with OEA-d4 indicated rapid uptake and redistribution, followed by marked, cell line-dependent persistence, suggesting differences in downstream turnover capacity. Proteomic profiling revealed clear but heterogeneous remodeling across models, while lipidomics and metabolomics showed a reproducible shift in membrane glycerophospholipids and signaling intermediates (including PE remodeling and increased PA/LPA/PS), together with alterations in lipid mediator pools. Comparison with the synthetic PPAR$\alpha$ agonist GW7647 helped estimate the PPAR$\alpha$-aligned component of the response and distinguish OEA-specific, context-dependent programs.

Overall, these data identify candidate effectors and pathway nodes through which OEA drives systems-level metabolic remodeling - reprogramming lipid uptake, storage, and membrane composition while reshaping stress-response, trafficking, and bioenergetic networks. Importantly, this work is ongoing: further mechanistic and functional studies are required to validate key nodes, define pathway hierarchy, and clarify PPAR$\alpha$-dependent versus independent components of the response.

## 1.13 References


1. *Yoon H, Shaw JL, Haigis MC, Greka A. Lipid metabolism in sickness and in health: Emerging regulators of lipotoxicity. Mol Cell. 2021 Sep;81(18):3708–30. doi:10.1016/j.molcel.2021.08.027*

2. *Kohlwein SD, Veenhuis M, van der Klei IJ. Lipid Droplets and Peroxisomes: Key Players in Cellular Lipid Homeostasis or A Matter of Fat—Store 'em Up or Burn 'em Down. Genetics. 2013 Jan 1;193(1):1–50. doi:10.1534/genetics.112.143362*

3. *Ertunc ME, Hotamisligil GS. Lipid signaling and lipotoxicity in metaflammation: indications for metabolic disease pathogenesis and treatment. J Lipid Res. 2016 Dec;57(12):2099–114. doi:10.1194/jlr.R066514*

4. *Obaseki E, Adebayo D, Bandyopadhyay S, Hariri H. Lipid droplets and fatty acid-induced lipotoxicity: in a nutshell. FEBS Lett. 2024 May 28;598(10):1207–14. doi:10.1002/1873-3468.14808*

5. *Feingold KR. Lipid and Lipoprotein Metabolism. Endocrinol Metab Clin North Am. 2022 Sep;51(3):437–58. doi:10.1016/j.ecl.2022.02.008*

6. *Dixon ED, Nardo AD, Claudel T, Trauner M. The Role of Lipid Sensing Nuclear Receptors (PPARs and LXR) and Metabolic Lipases in Obesity, Diabetes and NAFLD. Genes (Basel). 2021 Apr 26;12(5):645. doi:10.3390/genes12050645*

7. *Ko CW, Qu J, Black DD, Tso P. Regulation of intestinal lipid metabolism: current concepts and relevance to disease. Nat Rev Gastroenterol Hepatol. 2020 Mar 3;17(3):169–83. doi:10.1038/s41575-019-0250-7*

8. *Ko CW, Qu J, Black DD, Tso P. Regulation of intestinal lipid metabolism: current concepts and relevance to disease. Nat Rev Gastroenterol Hepatol. 2020 Mar 3;17(3):169–83. doi:10.1038/s41575-019-0250-7*

9. *Ko CW, Qu J, Black DD, Tso P. Regulation of intestinal lipid metabolism: current concepts and relevance to disease. Nat Rev Gastroenterol Hepatol. 2020 Mar 3;17(3):169–83. doi:10.1038/s41575-019-0250-7*

10. *Altmann SW, Davis HR, Zhu L ji, Yao X, Hoos LM, Tetzloff G, et al. Niemann-Pick C1 Like 1 Protein Is Critical for Intestinal Cholesterol Absorption. Science (1979). 2004 Feb 20;303(5661):1201–4. doi:10.1126/science.1093131*

11. *Garcia-Calvo M, Lisnock J, Bull HG, Hawes BE, Burnett DA, Braun MP, et al. The target of ezetimibe is Niemann-Pick C1-Like 1 (NPC1L1). Proceedings of the National Academy of Sciences. 2005 Jun 7;102(23):8132–7. doi:10.1073/pnas.0500269102*

12. *Ko CW, Qu J, Black DD, Tso P. Regulation of intestinal lipid metabolism: current concepts and relevance to disease. Nat Rev Gastroenterol Hepatol. 2020 Mar 3;17(3):169–83. doi:10.1038/s41575-019-0250-7*

13. *Fu J, Gaetani S, Oveisi F, Lo Verme J, Serrano A, Rodríguez de Fonseca F, et al. Oleylethanolamide regulates feeding and body weight through activation of the nuclear receptor PPAR-α. Nature. 2003 Sep;425(6953):90–3. doi:10.1038/nature01921*

14. *Schwartz GJ, Fu J, Astarita G, Li X, Gaetani S, Campolongo P, et al. The Lipid Messenger OEA Links Dietary Fat Intake to Satiety. Cell Metab. 2008 Oct;8(4):281–8. doi:10.1016/j.cmet.2008.08.005*

15. *Fiorucci S, Mencarelli A, Palladino G, Cipriani S. Bile-acid-activated receptors: targeting TGR5 and farnesoid-X-receptor in lipid and glucose disorders. Trends Pharmacol Sci. 2009 Nov;30(11):570–80. doi:10.1016/j.tips.2009.08.001*

16. *Rohr MW, Narasimhulu CA, Rudeski-Rohr TA, Parthasarathy S. Negative Effects of a High-Fat Diet on Intestinal Permeability: A Review. Advances in Nutrition. 2020 Jan;11(1):77–91. doi:10.1093/advances/nmz061*

17. *Donnelly KL, Smith CI, Schwarzenberg SJ, Jessurun J, Boldt MD, Parks EJ. Sources of fatty acids stored in liver and secreted via lipoproteins in patients with nonalcoholic fatty*

*liver disease. Journal of Clinical Investigation. 2005 May 2;115(5):1343–51. doi:10.1172/JCI23621*

18. *Donnelly KL, Smith CI, Schwarzenberg SJ, Jessurun J, Boldt MD, Parks EJ. Sources of fatty acids stored in liver and secreted via lipoproteins in patients with nonalcoholic fatty liver disease. Journal of Clinical Investigation. 2005 May 2;115(5):1343–51. doi:10.1172/JCI23621*

19. *Miquilena-Colina ME, Lima-Cabello E, Sánchez-Campos S, García-Mediavilla MV, Fernández-Bermejo M, Lozano-Rodríguez T, et al. Hepatic fatty acid translocase CD36 upregulation is associated with insulin resistance, hyperinsulinaemia and increased steatosis in non-alcoholic steatohepatitis and chronic hepatitis C. Gut. 2011 Oct;60(10):1394–402. doi:10.1136/gut.2010.222844*

20. *Kersten S, Seydoux J, Peters JM, Gonzalez FJ, Desvergne B, Wahli W. Peroxisome proliferator–activated receptor α mediates the adaptive response to fasting. Journal of Clinical Investigation. 1999 Jun 1;103(11):1489–98. doi:10.1172/JCI6223*

21. *Listenberger LL, Han X, Lewis SE, Cases S, Farese R V., Ory DS, et al. Triglyceride accumulation protects against fatty acid-induced lipotoxicity. Proceedings of the National Academy of Sciences. 2003 Mar 18;100(6):3077–82. doi:10.1073/pnas.0630588100*

22. *Moon YA. The SCAP/SREBP Pathway: A Mediator of Hepatic Steatosis. Endocrinology and Metabolism. 2017;32(1):6. doi:10.3803/EnM.2017.32.1.6*

23. *Iizuka K, Takao K, Yabe D. ChREBP-Mediated Regulation of Lipid Metabolism: Involvement of the Gut Microbiota, Liver, and Adipose Tissue. Front Endocrinol (Lausanne). 2020 Dec 3;11. doi:10.3389/fendo.2020.587189*

24. *Hussain MM, Shi J, Dreizen P. Microsomal triglyceride transfer protein and its role in apoB-lipoprotein assembly. J Lipid Res. 2003 Jan;44(1):22–32. doi:10.1194/jlr.R200014-JLR200*

25. *Cunningham RP, Porat-Shliom N. Liver Zonation – Revisiting Old Questions With New Technologies. Front Physiol. 2021 Sep 9;12. doi:10.3389/fphys.2021.732929*

26. *Yen CLE, Stone SJ, Koliwad S, Harris C, Farese R V. Thematic Review Series: Glycerolipids. DGAT enzymes and triacylglycerol biosynthesis. J Lipid Res. 2008 Nov;49(11):2283–301. doi:10.1194/jlr.R800018-JLR200*

27. *Cases S, Smith SJ, Zheng YW, Myers HM, Lear SR, Sande E, et al. Identification of a gene encoding an acyl CoA:diacylglycerol acyltransferase, a key enzyme in triacylglycerol synthesis. Proceedings of the National Academy of Sciences. 1998 Oct 27;95(22):13018–23. doi:10.1073/pnas.95.22.13018*

28. *Vecchiarelli AG, Neuman KC, Mizuuchi K. A propagating ATPase gradient drives transport of surface-confined cellular cargo. Proceedings of the National Academy of Sciences. 2014 Apr 24;111(13):4880–5. doi:10.1073/pnas.1401025111*

29. *Buhman KK, Smith SJ, Stone SJ, Repa JJ, Wong JS, Knapp FF, et al. DGAT1 Is Not Essential for Intestinal Triacylglycerol Absorption or Chylomicron Synthesis. Journal of Biological Chemistry. 2002 Jul;277(28):25474–9. doi:10.1074/jbc.M202013200*

30. *Buhman KK, Smith SJ, Stone SJ, Repa JJ, Wong JS, Knapp FF, et al. DGAT1 Is Not Essential for Intestinal Triacylglycerol Absorption or Chylomicron Synthesis. Journal of Biological Chemistry. 2002 Jul;277(28):25474–9. doi:10.1074/jbc.M202013200*

31. *Lee B, Fast AM, Zhu J, Cheng JX, Buhman KK. Intestine-specific expression of acyl CoA:diacylglycerol acyltransferase 1 reverses resistance to diet-induced hepatic steatosis and obesity in Dgat1 mice. J Lipid Res. 2010 Jul;51(7):1770–80. doi:10.1194/jlr.M002311*

32. *Yen CLE, Nelson DW, Yen MI. Intestinal triacylglycerol synthesis in fat absorption and systemic energy metabolism. J Lipid Res. 2015 Mar;56(3):489–501. doi:10.1194/jlr.R052902*

33. *Lee B, Fast AM, Zhu J, Cheng JX, Buhman KK. Intestine-specific expression of acyl CoA:diacylglycerol acyltransferase 1 reverses resistance to diet-induced hepatic steatosis and obesity in Dgat1 mice. J Lipid Res. 2010 Jul;51(7):1770–80. doi:10.1194/jlr.M002311*

34. *Nisticò C, Pagliari F, Chiarella E, Fernandes Guerreiro J, Marafioti MG, Aversa I, et al. Lipid Droplet Biosynthesis Impairment through DGAT2 Inhibition Sensitizes MCF7*

*Breast Cancer Cells to Radiation. Int J Mol Sci. 2021 Sep 18;22(18):10102. doi:10.3390/ijms221810102*

35. *Stone SJ, Myers HM, Watkins SM, Brown BE, Feingold KR, Elias PM, et al. Lipopenia and Skin Barrier Abnormalities in DGAT2-deficient Mice. Journal of Biological Chemistry. 2004 Mar;279(12):11767–76. doi:10.1074/jbc.M311000200*

36. *Yen CLE, Stone SJ, Koliwad S, Harris C, Farese R V. Thematic Review Series: Glycerolipids. DGAT enzymes and triacylglycerol biosynthesis. J Lipid Res. 2008 Nov;49(11):2283–301. doi:10.1194/jlr.R800018-JLR200*

37. *Listenberger LL, Han X, Lewis SE, Cases S, Farese R V., Ory DS, et al. Triglyceride accumulation protects against fatty acid-induced lipotoxicity. Proceedings of the National Academy of Sciences. 2003 Mar 18;100(6):3077–82. doi:10.1073/pnas.0630588100*

38. *Moliterni C, Vari F, Schifano E, Tacconi S, Stanca E, Friuli M, et al. Lipotoxicity of palmitic acid is associated with DGAT1 downregulation and abolished by PPARα activation in liver cells. J Lipid Res. 2024 Dec;65(12):100692. doi:10.1016/j.jlr.2024.100692*

39. *Nguyen TB, Louie SM, Daniele JR, Tran Q, Dillin A, Zoncu R, et al. DGAT1-Dependent Lipid Droplet Biogenesis Protects Mitochondrial Function during Starvation-Induced Autophagy. Dev Cell. 2017 Jul;42(1):9-21.e5. doi:10.1016/j.devcel.2017.06.003*

40. *de la Rosa Rodriguez MA, Deng L, Gemmink A, van Weeghel M, Aoun ML, Warnecke C, et al. Hypoxia-inducible lipid droplet-associated induces DGAT1 and promotes lipid storage in hepatocytes. Mol Metab. 2021 May;47:101168. doi:10.1016/j.molmet.2021.101168*

41. *Yamaguchi K, Yang L, McCall S, Huang J, Yu XX, Pandey SK, et al. Inhibiting triglyceride synthesis improves hepatic steatosis but exacerbates liver damage and fibrosis in obese mice with nonalcoholic steatohepatitis. Hepatology. 2007 Jun;45(6):1366–74. doi:10.1002/hep.21655*

42. *Wolins NE, Rubin B, Brasaemle DL. TIP47 Associates with Lipid Droplets. Journal of Biological Chemistry. 2001 Feb;276(7):5101–8. doi:10.1074/jbc.M006775200*

43. *Bulankina A V., Deggerich A, Wenzel D, Mutenda K, Wittmann JG, Rudolph MG, et al. TIP47 functions in the biogenesis of lipid droplets. Journal of Cell Biology. 2009 May 18;185(4):641–55. doi:10.1083/jcb.200812042*

44. *Carr RM, Peralta G, Yin X, Ahima RS. Absence of Perilipin 2 Prevents Hepatic Steatosis, Glucose Intolerance and Ceramide Accumulation in Alcohol-Fed Mice. PLoS One. 2014 May 15;9(5):e97118. doi:10.1371/journal.pone.0097118*

45. *Najt CP, Senthivinayagam S, Aljazi MB, Fader KA, Olenic SD, Brock JRL, et al. Liver-specific loss of Perilipin 2 alleviates diet-induced hepatic steatosis, inflammation, and fibrosis. American Journal of Physiology-Gastrointestinal and Liver Physiology. 2016 May 1;310(9):G726–38. doi:10.1152/ajpgi.00436.2015*

46. *Fromenty B, Berson A, Pessayre D. Microvesicular steatosis and steatohepatitis: role of mitochondrial dysfunction and lipid peroxidation. J Hepatol. 1997 Jan;26:13–22. doi:10.1016/S0168-8278(97)82328-8*

47. *Ferri F, Carotti S, Carpino G, Mischitelli M, Cantafora A, Molinaro A, et al. The Propensity of the Human Liver to Form Large Lipid Droplets Is Associated with PNPLA3 Polymorphism, Reduced INSIG1 and NPC1L1 Expression and Increased Fibrogenetic Capacity. Int J Mol Sci. 2021 Jun 5;22(11):6100. doi:10.3390/ijms22116100*

48. *Frank DN, Bales ES, Monks J, Jackman MJ, MacLean PS, Ir D, et al. Perilipin-2 Modulates Lipid Absorption and Microbiome Responses in the Mouse Intestine. PLoS One. 2015 Jul 6;10(7):e0131944. doi:10.1371/journal.pone.0131944*

49. *Silva AR, Pacheco P, Vieira-de-Abreu A, Maya-Monteiro CM, D'Alegria B, Magalhães KG, et al. Lipid bodies in oxidized LDL-induced foam cells are leukotriene-synthesizing organelles: a MCP-1/CCL2 regulated phenomenon. Biochimica et Biophysica Acta (BBA) - Molecular and Cell Biology of Lipids. 2009 Nov;1791(11):1066–75. doi:10.1016/j.bbalip.2009.06.004*

50. *Bozza PT, Bakker-Abreu I, Navarro-Xavier RA, Bandeira-Melo C. Lipid body function in eicosanoid synthesis: An update. Prostaglandins, Leukotrienes and Essential Fatty Acids (PLEFA). 2011 Nov;85(5):205–13. doi:10.1016/j.plefa.2011.04.020*

51. *Nose F, Yamaguchi T, Kato R, Aiuchi T, Obama T, Hara S, et al. Crucial Role of Perilipin-3 (TIP47) in Formation of Lipid Droplets and PGE2 Production in HL-60-Derived Neutrophils. PLoS One. 2013 Aug 1;8(8):e71542. doi:10.1371/journal.pone.0071542*

52. *Safi R, Menéndez P, Pol A. Lipid droplets provide metabolic flexibility for cancer progression. FEBS Lett. 2024 May 7;598(10):1301–27. doi:10.1002/1873-3468.14820*

53. *Yang F, Li Y, Shang X, Zhu Y, Hou W, Liu Y, et al. PLIN2 promotes colorectal cancer progression through CD36-mediated epithelial-mesenchymal transition. Cell Death Dis. 2025 Jul 10;16(1):510. doi:10.1038/s41419-025-07836-1*

54. *Unger RH. Lipotoxic Diseases. Annu Rev Med. 2002 Feb;53(1):319–36. doi:10.1146/annurev.med.53.082901.104057*

55. *Listenberger LL, Han X, Lewis SE, Cases S, Farese R V., Ory DS, et al. Triglyceride accumulation protects against fatty acid-induced lipotoxicity. Proceedings of the National Academy of Sciences. 2003 Mar 18;100(6):3077–82. doi:10.1073/pnas.0630588100*

56. *Ichinose K, Maeshima Y, Yamamoto Y, Kinomura M, Hirokoshi K, Kitayama H, et al. 2-(8-Hydroxy-6-Methoxy-1-Oxo-1H-2-Benzopyran-3-yl) Propionic Acid, an Inhibitor of Angiogenesis, Ameliorates Renal Alterations in Obese Type 2 Diabetic Mice. Diabetes. 2006 May 1;55(5):1232–42. doi:10.2337/db05-1367*

57. *Koves TR, Ussher JR, Noland RC, Slentz D, Mosedale M, Ilkayeva O, et al. Mitochondrial Overload and Incomplete Fatty Acid Oxidation Contribute to Skeletal Muscle Insulin Resistance. Cell Metab. 2008 Jan;7(1):45–56. doi:10.1016/j.cmet.2007.10.013*

58. *Schubert KM, Scheid MP, Duronio V. Ceramide Inhibits Protein Kinase B/Akt by Promoting Dephosphorylation of Serine 473. Journal of Biological Chemistry. 2000 May;275(18):13330–5. doi:10.1074/jbc.275.18.13330*

59. *Holland WL, Brozinick JT, Wang LP, Hawkins ED, Sargent KM, Liu Y, et al. Inhibition of Ceramide Synthesis Ameliorates Glucocorticoid-, Saturated-Fat-, and Obesity-Induced Insulin Resistance. Cell Metab. 2007 Mar;5(3):167–79. doi:10.1016/j.cmet.2007.01.002*

60. *Ussher JR, Koves TR, Cadete VJJ, Zhang L, Jaswal JS, Swyrd SJ, et al. Inhibition of De Novo Ceramide Synthesis Reverses Diet-Induced Insulin Resistance and Enhances Whole-Body Oxygen Consumption. Diabetes. 2010 Oct 1;59(10):2453–64. doi:10.2337/db09-1293*

61. *Shi H, Kokoeva M V., Inouye K, Tzameli I, Yin H, Flier JS. TLR4 links innate immunity and fatty acid–induced insulin resistance. Journal of Clinical Investigation. 2006 Nov 1;116(11):3015–25. doi:10.1172/JCI28898*

62. *Ichinose K, Maeshima Y, Yamamoto Y, Kinomura M, Hirokoshi K, Kitayama H, et al. 2-(8-Hydroxy-6-Methoxy-1-Oxo-1H-2-Benzopyran-3-yl) Propionic Acid, an Inhibitor of Angiogenesis, Ameliorates Renal Alterations in Obese Type 2 Diabetic Mice. Diabetes. 2006 May 1;55(5):1232–42. doi:10.2337/db05-1367*

63. *Listenberger LL, Han X, Lewis SE, Cases S, Farese R V., Ory DS, et al. Triglyceride accumulation protects against fatty acid-induced lipotoxicity. Proceedings of the National Academy of Sciences. 2003 Mar 18;100(6):3077–82. doi:10.1073/pnas.0630588100*

64. *Schubert KM, Scheid MP, Duronio V. Ceramide Inhibits Protein Kinase B/Akt by Promoting Dephosphorylation of Serine 473. Journal of Biological Chemistry. 2000 May;275(18):13330–5. doi:10.1074/jbc.275.18.13330*

65. *Listenberger LL, Han X, Lewis SE, Cases S, Farese R V., Ory DS, et al. Triglyceride accumulation protects against fatty acid-induced lipotoxicity. Proceedings of the National Academy of Sciences. 2003 Mar 18;100(6):3077–82. doi:10.1073/pnas.0630588100*

66. *Koves TR, Ussher JR, Noland RC, Slentz D, Mosedale M, Ilkayeva O, et al. Mitochondrial Overload and Incomplete Fatty Acid Oxidation Contribute to Skeletal Muscle Insulin Resistance. Cell Metab. 2008 Jan;7(1):45–56. doi:10.1016/j.cmet.2007.10.013*

67. *Khaldoun SA, Emond-Boisjoly MA, Chateau D, Carrière V, Lacasa M, Rousset M, et al. Autophagosomes contribute to intracellular lipid distribution in enterocytes. Mol Biol Cell. 2014 Jan;25(1):118–32. doi:10.1091/mbc.e13-06-0324*

68. *Holland WL, Brozinick JT, Wang LP, Hawkins ED, Sargent KM, Liu Y, et al. Inhibition of Ceramide Synthesis Ameliorates Glucocorticoid-, Saturated-Fat-, and Obesity-Induced Insulin Resistance. Cell Metab. 2007 Mar;5(3):167–79. doi:10.1016/j.cmet.2007.01.002*

69. *Kersten S, Seydoux J, Peters JM, Gonzalez FJ, Desvergne B, Wahli W. Peroxisome proliferator–activated receptor α mediates the adaptive response to fasting. Journal of Clinical Investigation. 1999 Jun 1;103(11):1489–98. doi:10.1172/JCI6223*

70. *Desvergne B, Wahli W. Peroxisome Proliferator-Activated Receptors: Nuclear Control of Metabolism*. Endocr Rev. 1999 Oct 1;20(5):649–88. doi:10.1210/edrv.20.5.0380*

71. *Bougarne N, Weyers B, Desmet SJ, Deckers J, Ray DW, Staels B, et al. Molecular Actions of PPARα in Lipid Metabolism and Inflammation. Endocr Rev. 2018 Oct 1;39(5):760–802. doi:10.1210/er.2018-00064*

72. *Bougarne N, Weyers B, Desmet SJ, Deckers J, Ray DW, Staels B, et al. Molecular Actions of PPARα in Lipid Metabolism and Inflammation. Endocr Rev. 2018 Oct 1;39(5):760–802. doi:10.1210/er.2018-00064*

73. *Desvergne B, Wahli W. Peroxisome Proliferator-Activated Receptors: Nuclear Control of Metabolism*. Endocr Rev. 1999 Oct 1;20(5):649–88. doi:10.1210/edrv.20.5.0380*

74. *Pawlak M, Lefebvre P, Staels B. Molecular mechanism of PPARα action and its impact on lipid metabolism, inflammation and fibrosis in non-alcoholic fatty liver disease. J Hepatol. 2015 Mar;62(3):720–33. doi:10.1016/j.jhep.2014.10.039*

75. *Bougarne N, Weyers B, Desmet SJ, Deckers J, Ray DW, Staels B, et al. Molecular Actions of PPARα in Lipid Metabolism and Inflammation. Endocr Rev. 2018 Oct 1;39(5):760–802. doi:10.1210/er.2018-00064*

76. *Kersten S, Seydoux J, Peters JM, Gonzalez FJ, Desvergne B, Wahli W. Peroxisome proliferator–activated receptor α mediates the adaptive response to fasting. Journal of Clinical Investigation. 1999 Jun 1;103(11):1489–98. doi:10.1172/JCI6223*

77. *Pawlak M, Lefebvre P, Staels B. Molecular mechanism of PPARα action and its impact on lipid metabolism, inflammation and fibrosis in non-alcoholic fatty liver disease. J Hepatol. 2015 Mar;62(3):720–33. doi:10.1016/j.jhep.2014.10.039*

78. *Corton JC, Peters JM, Klaunig JE. The PPARα-dependent rodent liver tumor response is not relevant to humans: addressing misconceptions. Arch Toxicol. 2018 Jan 2;92(1):83–119. doi:10.1007/s00204-017-2094-7*

79. *Arai H, Yamashita S, Yokote K, Araki E, Suganami H, Ishibashi S. Efficacy and Safety of Pemafibrate Versus Fenofibrate in Patients with High Triglyceride and Low HDL Cholesterol Levels: A Multicenter, Placebo-Controlled, Double-Blind, Randomized Trial. J Atheroscler Thromb. 2018 Jun 1;25(6):521–38. doi:10.5551/jat.44412*

80. *Bougarne N, Weyers B, Desmet SJ, Deckers J, Ray DW, Staels B, et al. Molecular Actions of PPARα in Lipid Metabolism and Inflammation. Endocr Rev. 2018 Oct 1;39(5):760–802. doi:10.1210/er.2018-00064*

81. *Bougarne N, Weyers B, Desmet SJ, Deckers J, Ray DW, Staels B, et al. Molecular Actions of PPARα in Lipid Metabolism and Inflammation. Endocr Rev. 2018 Oct 1;39(5):760–802. doi:10.1210/er.2018-00064*

82. *Kersten S, Seydoux J, Peters JM, Gonzalez FJ, Desvergne B, Wahli W. Peroxisome proliferator–activated receptor α mediates the adaptive response to fasting. Journal of Clinical Investigation. 1999 Jun 1;103(11):1489–98. doi:10.1172/JCI6223*

83. *Fu J, Gaetani S, Oveisi F, Lo Verme J, Serrano A, Rodríguez de Fonseca F, et al. Oleylethanolamide regulates feeding and body weight through activation of the nuclear receptor PPAR-α. Nature. 2003 Sep;425(6953):90–3. doi:10.1038/nature01921*

84. *Lu HC, Mackie K. Review of the Endocannabinoid System. Biol Psychiatry Cogn Neurosci Neuroimaging. 2021 Jun;6(6):607–15. doi:10.1016/j.bpsc.2020.07.016*

85. *Fu J, Astarita G, Gaetani S, Kim J, Cravatt BF, Mackie K, et al. Food Intake Regulates Oleoylethanolamide Formation and Degradation in the Proximal Small Intestine. Journal of Biological Chemistry. 2007 Jan;282(2):1518–28. doi:10.1074/jbc.M607809200*

86. *Okamoto Y, Morishita J, Tsuboi K, Tonai T, Ueda N. Molecular Characterization of a Phospholipase D Generating Anandamide and Its Congeners. Journal of Biological Chemistry. 2004 Feb;279(7):5298–305. doi:10.1074/jbc.M306642200*

87. *OKAMOTO Y, MORISHITA J, WANG J, SCHMID PC, KREBSBACH RJ, SCHMID HHO, et al. Mammalian cells stably overexpressing N -acylphosphatidylethanolamine-hydrolysing phospholipase D exhibit significantly decreased levels of N -acylphosphatidylethanolamines. Biochemical Journal. 2005 Jul 1;389(1):241–7. doi:10.1042/BJ20041790*

88. *Fu J, Astarita G, Gaetani S, Kim J, Cravatt BF, Mackie K, et al. Food Intake Regulates Oleoylethanolamide Formation and Degradation in the Proximal Small Intestine. Journal of Biological Chemistry. 2007 Jan;282(2):1518–28. doi:10.1074/jbc.M607809200*

89. *Cravatt BF, Giang DK, Mayfield SP, Boger DL, Lerner RA, Gilula NB. Molecular characterization of an enzyme that degrades neuromodulatory fatty-acid amides. Nature. 1996 Nov;384(6604):83–7. doi:10.1038/384083a0*

90. *McKinney MK, Cravatt BF. Evidence for Distinct Roles in Catalysis for Residues of the Serine-Serine-Lysine Catalytic Triad of Fatty Acid Amide Hydrolase. Journal of Biological Chemistry. 2003 Sep;278(39):37393–9. doi:10.1074/jbc.M303922200*

91. *Deutsch DG, Ueda N, Yamamoto S. The fatty acid amide hydrolase (FAAH). Prostaglandins, Leukotrienes and Essential Fatty Acids (PLEFA). 2002 Feb;66(2–3):201–10. doi:10.1054/plef.2001.0358*

92. *Bottemanne P, Muccioli GG, Alhouayek M. N-acylethanolamine hydrolyzing acid amidase inhibition: tools and potential therapeutic opportunities. Drug Discov Today. 2018 Aug;23(8):1520–9. doi:10.1016/j.drudis.2018.03.007*

93. *Piomelli D, Scalvini L, Fotio Y, Lodola A, Spadoni G, Tarzia G, et al. N -Acylethanolamine Acid Amidase (NAAA): Structure, Function, and Inhibition. J Med Chem. 2020 Jul 23;63(14):7475–90. doi:10.1021/acs.jmedchem.0c00191*

94. *Ponzano S, Bertozzi F, Mengatto L, Dionisi M, Armirotti A, Romeo E, et al. Synthesis and Structure–Activity Relationship (SAR) of 2-Methyl-4-oxo-3-oxetanylcarbamic Acid Esters, a Class of Potent N -Acylethanolamine Acid Amidase (NAAA) Inhibitors. J Med Chem. 2013 Sep 12;56(17):6917–34. doi:10.1021/jm400739u*

95. *Astarita G, Di Giacomo B, Gaetani S, Oveisi F, Compton TR, Rivara S, et al. Pharmacological Characterization of Hydrolysis-Resistant Analogs of Oleoylethanolamide with Potent Anorexiant Properties. J Pharmacol Exp Ther. 2006 Aug;318(2):563–70. doi:10.1124/jpet.106.105221*

96. *Fu J, Gaetani S, Oveisi F, Lo Verme J, Serrano A, Rodríguez de Fonseca F, et al. Oleylethanolamide regulates feeding and body weight through activation of the nuclear receptor PPAR-α. Nature. 2003 Sep;425(6953):90–3. doi:10.1038/nature01921*

97. *Fu J, Kim J, Oveisi F, Astarita G, Piomelli D. Targeted enhancement of oleoylethanolamide production in proximal small intestine induces across-meal satiety in rats. American Journal of Physiology-Regulatory, Integrative and Comparative Physiology. 2008 Jul;295(1):R45–50. doi:10.1152/ajpregu.00126.2008*

98. *Schwartz GJ, Fu J, Astarita G, Li X, Gaetani S, Campolongo P, et al. The Lipid Messenger OEA Links Dietary Fat Intake to Satiety. Cell Metab. 2008 Oct;8(4):281–8. doi:10.1016/j.cmet.2008.08.005*

99. *Pawlak M, Lefebvre P, Staels B. Molecular mechanism of PPARα action and its impact on lipid metabolism, inflammation and fibrosis in non-alcoholic fatty liver disease. J Hepatol. 2015 Mar;62(3):720–33. doi:10.1016/j.jhep.2014.10.039*

100. *Mandard S, Müller M, Kersten S. Peroxisome proliferator-activated receptor a target genes. Cell Mol Life Sci. 2004 Feb 1;61(4):393–416. doi:10.1007/s00018-003-3216-3*

101. *Guzmán M, Lo Verme J, Fu J, Oveisi F, Blázquez C, Piomelli D. Oleoylethanolamide Stimulates Lipolysis by Activating the Nuclear Receptor Peroxisome Proliferator-activated Receptor α (PPAR-α). Journal of Biological Chemistry. 2004 Jul;279(27):27849–54. doi:10.1074/jbc.M404087200*

102. *Fu J, Oveisi F, Gaetani S, Lin E, Piomelli D. Oleoylethanolamide, an endogenous PPAR-α agonist, lowers body weight and hyperlipidemia in obese rats. Neuropharmacology. 2005 Jun;48(8):1147–53. doi:10.1016/j.neuropharm.2005.02.013*

103. *Pawlak M, Lefebvre P, Staels B. Molecular mechanism of PPARα action and its impact on lipid metabolism, inflammation and fibrosis in non-alcoholic fatty liver disease. J Hepatol. 2015 Mar;62(3):720–33. doi:10.1016/j.jhep.2014.10.039*

104. *Astarita G, Di Giacomo B, Gaetani S, Oveisi F, Compton TR, Rivara S, et al. Pharmacological Characterization of Hydrolysis-Resistant Analogs of Oleoylethanolamide with Potent Anorexiant Properties. J Pharmacol Exp Ther. 2006 Aug;318(2):563–70. doi:10.1124/jpet.106.105221*

105. *Chen L, Li L, Chen J, Li L, Zheng Z, Ren J, et al. Oleoylethanolamide, an endogenous PPAR-α ligand, attenuates liver fibrosis targeting hepatic stellate cells. Oncotarget. 2015 Dec 15;6(40):42530–40. doi:10.18632/oncotarget.6466*

106. *Wang X, Miyares RL, Ahern GP. Oleoylethanolamide excites vagal sensory neurones, induces visceral pain and reduces short-term food intake in mice via capsaicin receptor TRPV1. J Physiol. 2005 Apr 6;564(2):541–7. doi:10.1113/jphysiol.2004.081844*

107. *Wang X, Miyares RL, Ahern GP. Oleoylethanolamide excites vagal sensory neurones, induces visceral pain and reduces short-term food intake in mice via capsaicin receptor TRPV1. J Physiol. 2005 Apr 6;564(2):541–7. doi:10.1113/jphysiol.2004.081844*

108. *Wang X, Miyares RL, Ahern GP. Oleoylethanolamide excites vagal sensory neurones, induces visceral pain and reduces short-term food intake in mice via capsaicin receptor TRPV1. J Physiol. 2005 Apr 6;564(2):541–7. doi:10.1113/jphysiol.2004.081844*

109. *Lauffer LM, Iakoubov R, Brubaker PL. GPR119 Is Essential for Oleoylethanolamide-Induced Glucagon-Like Peptide-1 Secretion From the Intestinal Enteroendocrine L-Cell. Diabetes. 2009 May 1;58(5):1058–66. doi:10.2337/db08-1237*

110. *Diao X, Ye F, Zhang M, Ren X, Tian X, Lu J, et al. Identification of oleoylethanolamide as an endogenous ligand for HIF-3α. Nat Commun. 2022 May 9;13(1):2529. doi:10.1038/s41467-022-30338-z*

111. *Fu J, Astarita G, Gaetani S, Kim J, Cravatt BF, Mackie K, et al. Food Intake Regulates Oleoylethanolamide Formation and Degradation in the Proximal Small Intestine. Journal of Biological Chemistry. 2007 Jan;282(2):1518–28. doi:10.1074/jbc.M607809200*

112. *Schwartz GJ, Fu J, Astarita G, Li X, Gaetani S, Campolongo P, et al. The Lipid Messenger OEA Links Dietary Fat Intake to Satiety. Cell Metab. 2008 Oct;8(4):281–8. doi:10.1016/j.cmet.2008.08.005*

113. *Guijarro A, Fu J, Astarita G, Piomelli D. CD36 gene deletion decreases oleoylethanolamide levels in small intestine of free-feeding mice. Pharmacol Res. 2010 Jan;61(1):27–33. doi:10.1016/j.phrs.2009.09.003*

114. *Schwartz GJ, Fu J, Astarita G, Li X, Gaetani S, Campolongo P, et al. The Lipid Messenger OEA Links Dietary Fat Intake to Satiety. Cell Metab. 2008 Oct;8(4):281–8. doi:10.1016/j.cmet.2008.08.005*

115. *Yang Y, Chen M, Georgeson KE, Harmon CM. Mechanism of oleoylethanolamide on fatty acid uptake in small intestine after food intake and body weight reduction. American Journal of Physiology-Regulatory, Integrative and Comparative Physiology. 2007 Jan;292(1):R235–41. doi:10.1152/ajpregu.00270.2006*

116. *Pan X, Schwartz GJ, Hussain MM. Oleoylethanolamide differentially regulates glycerolipid synthesis and lipoprotein secretion in intestine and liver. J Lipid Res. 2018 Dec;59(12):2349–59. doi:10.1194/jlr.M089250*

117. *Igarashi M, DiPatrizio N V., Narayanaswami V, Piomelli D. Feeding-induced oleoylethanolamide mobilization is disrupted in the gut of diet-induced obese rodents.*

*Biochimica et Biophysica Acta (BBA) - Molecular and Cell Biology of Lipids. 2015 Sep;1851(9):1218–26. doi:10.1016/j.bbalip.2015.05.006*

118. *Guzmán M, Lo Verme J, Fu J, Oveisi F, Blázquez C, Piomelli D. Oleoylethanolamide Stimulates Lipolysis by Activating the Nuclear Receptor Peroxisome Proliferator-activated Receptor α (PPAR-α). Journal of Biological Chemistry. 2004 Jul;279(27):27849–54. doi:10.1074/jbc.M404087200*

119. *Mandard S, Müller M, Kersten S. Peroxisome proliferator-activated receptor a target genes. Cell Mol Life Sci. 2004 Feb 1;61(4):393–416. doi:10.1007/s00018-003-3216-3*

120. *Fu J, Oveisi F, Gaetani S, Lin E, Piomelli D. Oleoylethanolamide, an endogenous PPAR-α agonist, lowers body weight and hyperlipidemia in obese rats. Neuropharmacology. 2005 Jun;48(8):1147–53. doi:10.1016/j.neuropharm.2005.02.013*

121. *Pawlak M, Lefebvre P, Staels B. Molecular mechanism of PPARα action and its impact on lipid metabolism, inflammation and fibrosis in non-alcoholic fatty liver disease. J Hepatol. 2015 Mar;62(3):720–33. doi:10.1016/j.jhep.2014.10.039*

122. *Chen L, Li L, Chen J, Li L, Zheng Z, Ren J, et al. Oleoylethanolamide, an endogenous PPAR-α ligand, attenuates liver fibrosis targeting hepatic stellate cells. Oncotarget. 2015 Dec 15;6(40):42530–40. doi:10.18632/oncotarget.6466*

123. *Watson AD. Thematic review series: Systems Biology Approaches to Metabolic and Cardiovascular Disorders. Lipidomics: a global approach to lipid analysis in biological systems. J Lipid Res. 2006 Oct;47(10):2101–11. doi:10.1194/jlr.R600022-JLR200*

124. *Patti GJ, Yanes O, Siuzdak G. Metabolomics: the apogee of the omics trilogy. Nat Rev Mol Cell Biol. 2012 Apr 22;13(4):263–9. doi:10.1038/nrm3314*

125. *Watson AD. Thematic review series: Systems Biology Approaches to Metabolic and Cardiovascular Disorders. Lipidomics: a global approach to lipid analysis in biological systems. J Lipid Res. 2006 Oct;47(10):2101–11. doi:10.1194/jlr.R600022-JLR200*

126. *Hu T, Zhang J. Mass-spectrometry-based lipidomics. J Sep Sci. 2018 Jan 27;41(1):351–72. doi:10.1002/jssc.201700709*

127. *SUMMERS S. Ceramides in insulin resistance and lipotoxicity. Prog Lipid Res. 2006 Jan;45(1):42–72. doi:10.1016/j.plipres.2005.11.002*

128. *Listenberger LL, Han X, Lewis SE, Cases S, Farese R V., Ory DS, et al. Triglyceride accumulation protects against fatty acid-induced lipotoxicity. Proceedings of the National Academy of Sciences. 2003 Mar 18;100(6):3077–82. doi:10.1073/pnas.0630588100*

129. *Ogrinc N, Saudemont P, Balog J, Robin YM, Gimeno JP, Pascal Q, et al. Water-assisted laser desorption/ionization mass spectrometry for minimally invasive in vivo and real-time surface analysis using SpiderMass. Nat Protoc. 2019 Nov 9;14(11):3162–82. doi:10.1038/s41596-019-0217-8*

130. *Fatou B, Saudemont P, Leblanc E, Vinatier D, Mesdag V, Wisztorski M, et al. In vivo Real-Time Mass Spectrometry for Guided Surgery Application. Sci Rep. 2016 May 18;6(1):25919. doi:10.1038/srep25919*

131. *Ogrinc N, Saudemont P, Balog J, Robin YM, Gimeno JP, Pascal Q, et al. Water-assisted laser desorption/ionization mass spectrometry for minimally invasive in vivo and real-time surface analysis using SpiderMass. Nat Protoc. 2019 Nov 9;14(11):3162–82. doi:10.1038/s41596-019-0217-8*

132. *Zirem Y, Ledoux L, Roussel L, Maurage CA, Tirilly P, Le Rhun É, et al. Real-time glioblastoma tumor microenvironment assessment by SpiderMass for improved patient management. Cell Rep Med. 2024 Apr;5(4):101482. doi:10.1016/j.xcrm.2024.101482*

133. *Patti GJ, Yanes O, Siuzdak G. Metabolomics: the apogee of the omics trilogy. Nat Rev Mol Cell Biol. 2012 Apr 22;13(4):263–9. doi:10.1038/nrm3314*

134. *Aebersold R, Mann M. Mass spectrometry-based proteomics. Nature. 2003 Mar;422(6928):198–207. doi:10.1038/nature01511*

135. *Hasin Y, Seldin M, Lusis A. Multi-omics approaches to disease. Genome Biol. 2017 Dec 5;18(1):83. doi:10.1186/s13059-017-1215-1*

136. *Yoon H, Shaw JL, Haigis MC, Greka A. Lipid metabolism in sickness and in health: Emerging regulators of lipotoxicity. Mol Cell. 2021 Sep;81(18):3708–30. doi: 10.1016/j.molcel.2021.08.027*

137. *Fu J, Gaetani S, Oveisi F, Lo Verme J, Serrano A, Rodríguez de Fonseca F, et al. Oleylethanolamide regulates feeding and body weight through activation of the nuclear receptor PPAR-α. Nature. 2003 Sep;425(6953):90–3. doi:10.1038/nature01921*

138. *Kersten S, Seydoux J, Peters JM, Gonzalez FJ, Desvergne B, Wahli W. Peroxisome proliferator–activated receptor α mediates the adaptive response to fasting. Journal of Clinical Investigation. 1999 Jun 1;103(11):1489–98. doi:10.1172/JCI6223*

139. *Ko CW, Qu J, Black DD, Tso P. Regulation of intestinal lipid metabolism: current concepts and relevance to disease. Nat Rev Gastroenterol Hepatol. 2020 Mar 3;17(3):169–83. doi:10.1038/s41575-019-0250-7*

140. *Rohr MW, Narasimhulu CA, Rudeski-Rohr TA, Parthasarathy S. Negative Effects of a High-Fat Diet on Intestinal Permeability: A Review. Advances in Nutrition. 2020 Jan;11(1):77–91. doi:10.1093/advances/nmz061*

141. *Bougarne N, Weyers B, Desmet SJ, Deckers J, Ray DW, Staels B, et al. Molecular Actions of PPARα in Lipid Metabolism and Inflammation. Endocr Rev. 2018 Oct 1;39(5):760–802. doi:10.1210/er.2018-00064*

142. *Listenberger LL, Han X, Lewis SE, Cases S, Farese R V., Ory DS, et al. Triglyceride accumulation protects against fatty acid-induced lipotoxicity. Proceedings of the National Academy of Sciences. 2003 Mar 18;100(6):3077–82. doi:10.1073/pnas.0630588100*

143. *Fu J, Gaetani S, Oveisi F, Lo Verme J, Serrano A, Rodríguez de Fonseca F, et al. Oleylethanolamide regulates feeding and body weight through activation of the nuclear receptor PPAR-α. Nature. 2003 Sep;425(6953):90–3. doi:10.1038/nature01921*

# 2. Pharmacological potential of endocannabinoid and endocannabinoid-like compounds in protecting intestinal structure and metabolism under high-fat conditions


## Abstract

The intestine plays a crucial role in nutrient absorption, digestion, and regulation of metabolic processes. Intestinal structure and functions are influenced by several factors, with dietary composition being one of the most significant. Diets rich in various types of fats, including saturated, monounsaturated, and polyunsaturated fats, have distinct effects on intestinal cell metabolism and overall intestinal health. High consumption of saturated fats, frequently found in animal products, has been associated with inflammation, altered gut microbiota composition, and impaired intestinal barrier function, with potential consequences such as metabolic disorders, obesity, and insulin resistance. In contrast, monounsaturated fats, found in foods such as olive oil and avocado, promote intestinal cell integrity, reducing inflammation and supporting a healthier microbiome.

Polyunsaturated fatty acids, especially omega-3 fatty acids, have shown anti-inflammatory effects and may improve the function and adaptability of intestinal cells, promoting better nutrient absorption and immune regulation. Recent evidence suggests that endocannabinoids and endocannabinoid-like compounds, such as oleoylethanolamide have a protective effect on the function and structure of the intestine. These

endocannabinoid pathways modulating compounds can act on receptors in the intestinal epithelium, improving the intestinal barrier and counteracting inflammation, facilitating a more favorable environment for intestinal health. Understanding how different fats influence intestinal metabolism and the protective role of endocannabinoids and endocannabinoid-like compounds is essential to developing dietary strategies to improve intestinal health and prevent diet-related diseases. This review explores the impact of high fats on intestinal metabolism and the main role of endocannabinoids and endocannabinoid-like compounds on these effects.

## 2.1 Introduction

The human intestinal system is a highly intricate organ in terms of physiological functions and structural organization. It is essential for digestion, nutrient absorption, immune defense, and maintaining symbiotic relationships with the gut microbiota [1]. Comprising the small and large intestines, the gut is uniquely structured to perform these multifaceted roles through specialized anatomical formations, a diverse cellular composition, and a dynamic biochemical environment. Recent advancements in research techniques have unveiled the intricate organization and functioning of the gut, illustrating how its structural complexities support physiological functions critical to human health [1].

The small intestine, consisting of the distinct regions of the duodenum, jejunum, and ileum, has a highly folded mucosal surface with villi and microvilli on epithelial cells. This extensive surface area facilitates the efficient absorption of nutrients, electrolytes, and water, including sugars, monovalent ions, and amino acids [2]. The lamina propria, a connective

tissue layer within each villus, contains blood and lymphatic vessels that transport absorbed nutrients and lipids to the body [1-2].

The large intestine is divided into the ascending, transverse, descending, and sigmoid sections, which include the cecum, colon, and rectum, facilitating feces formation and excretion. Lacking villi, it has deep crypts with cells that produce mucus, aiding in lubrication. Its main function is absorbing water, electrolytes, vitamins, and the anaerobic fermentation of dietary fibers. Paracellular or transcellular pathways regulate the movement of solutes across the epithelium, with active transport for nutrient and electrolyte absorption [1-2]. Most digestion and absorption processes occur in the duodenum, jejunum, and ileum, where nutrients are absorbed into capillaries and lymphatic vessels. Unabsorbed material moves into the colon, where water is absorbed, and feces are formed and stored [1]. High-fat diets (HFDs) are known to have a significant impact on gut health, contributing to various metabolic disorders such as dysbiosis, increased intestinal permeability, and inflammation, all of which impair the gut's ability to regulate nutrient absorption and protect against harmful pathogens. These alterations in intestinal function are linked to systemic metabolic dysfunction, including obesity and insulin resistance [3]. Recent research has highlighted the potential therapeutic role of endocannabinoids and endocannabinoid-like compounds in mitigating the negative effects of HFDs. Among endocannabinoid-like compounds, oleoylethanolamide (OEA) has garnered significant interest due to its beneficial effects on various physiological functions, including the regulation of dietary fat intake, energy balance, and intestinal motility, as well as its influence on eating behavior [4]. In the small intestine, particularly in the duodenum and jejunum, OEA levels fluctuate in response to nutritional status, decreasing during periods of starvation and rising upon refeeding [5]. Recent research

has demonstrated that administering OEA to rodents can provide protection against inflammation and alter the composition of the intestinal microbiota [6]. This review aims to examine the effects of HFDs on intestinal barrier function and structure, discussing how endocannabinoids and endocannabinoid-like compounds, particularly OEA, may safeguard the gut from damage induced by HFDs.

## 2.2 Intestinal barrier: structure, properties, and role in gut health

The intestinal barrier is a multifunctional interface critical for nutrient absorption and immune defense. It comprises epithelial cells, mucosa, immune components, and microbiota, all of which maintain a selectively permeable structure that allows the passage of essential nutrients and water while restricting pathogenic organisms and toxins [7-8]. Recent advancements in single-cell RNA sequencing have revealed the cellular diversity of the gut [1]. The intestinal epithelium consists of five main cell types: enterocytes, goblet cells, enteroendocrine cells, Paneth cells, and M cells, derived from stem cells in the crypts. Enterocytes absorb nutrients via specific transporters, goblet cells secrete mucus, Paneth cells produce antimicrobial peptides (AMPs), and enteroendocrine cells release hormones regulating digestion and appetite [8]. The mucus layer, produced by goblet cells, primarily consisting of mucin proteins, represents the first layer of defense. Consistent with their functions, mucins are classified as transmembrane and secretory. Transmembrane mucins include MUC1, MUC3A/B, MUC4, MUC12, MUC13, MUC15, MUC17, MUC20, and MUC21 that, thanks to their transmembrane structure, also participate in signal transduction. The secretory mucins are classified as gel-forming and non-gel-forming mucins. The gel-forming mucins include MUC2,

MUC5AC, MUC5B, MUC6, and MUC19, and among them, MUC2 is the most typical gel-forming mucin expressed in the jejunum, ileum, and colon [9]. The mucus layer physically separates microbiota from the epithelial cells, reducing direct interactions with pathogens. Beneath this, the epithelial layer supports barrier integrity by producing AMPs and aiding nutrient transport [8, 10]. AMPs are small, naturally occurring proteins that play a crucial role in the innate immune response by attracting immune cells to the site of infection, promoting inflammation, and enhancing the activity of other immune components [11]. Thus, AMPs play an essential role in the first line of defense against pathogens, including bacteria, viruses, fungi, and parasites. The primary structure of AMPs exhibits considerable variability. Larger AMPs, composed of 100 amino acids or more, often share similarities with lytic enzymes, nutrient-binding proteins, or proteins with specific binding sites for microbial macromolecules. Conversely, most AMPs are smaller and primarily involved in disrupting the structural integrity or functionality of microbial cell membranes. They can also directly inhibit specific adenosine triphosphate (ATP)-dependent enzymes through their interaction with ATP. In humans, the principal classes of AMPs are cathelicidins and defensins, with defensins further classified into alpha ($\alpha$) and beta ($\beta$) types [12]. Additionally, certain AMPs contribute to tissue repair and regeneration by facilitating cell migration and proliferation, which are crucial for effective wound healing [13]. Tight junctions (TJs), composed of proteins such as claudins, occludins, and Zonula Occludens (ZO), seal the space between adjacent enterocytes, preventing the passage of harmful pathogens and toxins into the bloodstream. Adherens junctions (AJs), formed by cadherins and linked to the actin cytoskeleton, provide mechanical strength and regulate cell-cell adhesion. Desmosomes offer additional structural support by connecting

intermediate filaments between cells, ensuring tissue resilience under mechanical stress [7-8]. Gap junctions (GJ), made of connexins, allow for the direct transfer of ions and small molecules between cells, enabling coordinated cellular activity. Together, these junctions ensure the proper functioning of the intestinal barrier, maintaining a selective permeability essential for digestion and immune defense [8]. Due to the impermeability of the intestinal epithelium to hydrophilic solutes, specific transporters mediate nutrient passage via transcellular and paracellular pathways. The transcellular pathway involves active transport, endocytosis, and nutrientspecific transporters, while the paracellular pathway allows ions and hydrophilic molecules through junctional complexes. Under pathological conditions, increased epithelial permeability allows the translocation of harmful agents, such as luminal antigens and microbial toxins, which can activate afferent nerves and lead to visceral hypersensitivity. This enhanced permeability is associated with diseases like inflammatory bowel disease (IBD), celiac disease, and irritable bowel syndrome (IBS) [7]. The function of the intestine is also closely related to neural and immune components [14]. The GI tract is regulated by the enteric nervous system (ENS), a complex, autonomous network that controls digestive functions independently of the central nervous system. The ENS comprises sensory neurons, motor neurons, and interneurons that coordinate muscular movements and the intestine's secretory and absorptive activities, involving the autonomic nervous system (ANS). The ANS contributes to GI regulation by transmitting sensory signals to the brain via parasympathetic and sympathetic pathways. This bidirectional gut-brain connection influences not only motility and secretions but also visceral sensitivity and pain perception [14].

## 2.3 Intestinal microbiota

The intestinal microbiota, also known as gut microbiota, refers to the vast community of microorganisms, including bacteria, viruses, fungi, and archaea, which reside in the GI tract, particularly the intestines. The intestinal microbiota influences ENS development and interacts with immune and epithelial cells by producing metabolites that support colon cell health, the immune system, barrier function, metabolic processes, and gut-brain communication [7, 14-15]. Beneficial bacteria in the gut, including Bifidobacteria and Firmicutes, ferment dietary fibers, especially non-digestible carbohydrates such as cellulose, pectin, and resistant starch, to produce short-chain fatty acids (SCFAs) [7]. SCFAs, which include butyrate, propionate, and acetate, produced in a roughly 3:1:1 ratio, play a significant role in maintaining gut health and supporting various physiological processes [16]. The amounts of SCFAs vary significantly among fecal samples, being influenced by individual lifestyle and health conditions [17-18]. Acetate is produced primarily by bacteria such as Bacteroides. Propionate, primarily produced by Firmicutes, is important for regulating lipid metabolism. Butyrate, produced by specific bacteria such as Faecalibacterium prausnitzii and Butyrivibrio fibrisolvens, is a primary energy source for colonocytes (cells lining the colon) and has anti-inflammatory properties.

Bacterial metabolites also encompass valeric acid, which is produced through the gut microbiota fermentation of dietary fibers, as well as isovalerate and isobutyrate, both of which are branched SCFA derived from the fermentation of branched-chain amino acids that result from undigested proteins reaching the colon. Valeric acid is noted for its anti-inflammatory properties and influence on energy metabolism; it has also been studied for

its effects on mood and anxiety [19-20]. Isovaleric acid, primarily generated from the fermentation of leucine, has been linked to various effects on muscle metabolism and energy production, and it may contribute to gut health by promoting relaxation of colonic smooth muscle through the PKA pathway [21]. Isobutyrate has been associated with several physiological effects, particularly concerning the insulin signaling pathway. Indeed, isobutyrate enhances lipid and glucose metabolism in adipocytes, which may improve insulin sensitivity [22]. SCFAs enhance TJ integrity, increase mucus production, and support antiinflammatory responses by modulating immune cell activity [23]. Additionally, specific microbial strains and metabolites influence immune reactions through the gut-brain and gut-liver axes, impacting local and systemic immunity [8, 14].

## 2.4 Exploring the endocannabinoid system: functions and implications

The endocannabinoid system (ECS) is a complex signaling network that regulates various physiological processes, including energy balance, lipid metabolism, appetite, inflammation, and neuroprotection [24-25]. ECS comprises endocannabinoids, natural compounds that resemble the cannabinoids found in cannabis, cannabinoid receptors, and enzymes involved in both the synthesis and degradation of endocannabinoids. Particularly, the degradative enzymes include fatty acid amide hydrolase (FAAH) and monoacylglycerol lipase (MAGL) that tightly regulate endocannabinoid levels to ensure proper signaling and prevent receptor overstimulation [25]. Dysregulation of FAAH and MAGL activity can lead to altered endocannabinoid signaling, contributing to conditions like chronic pain, obesity, and metabolic disorders [6, 26]. There are two main

types of cannabinoid receptors: CB1, which is found primarily in the brain and central nervous system, and CB2, which is found primarily in peripheral organs and the immune system. Beyond the classical CB1 and CB2 pathways, endocannabinoids also interact with transient receptor potential (TRP) channels and PPARs, further broadening their functional repertoire [27]. Anandamide (AEA), a lipid-signaling molecule belonging to the N-acylethanolamine (NAE) family, and 2-arachidonoylglycerol (2-AG) are the most extensively studied endocannabinoids. Endocannabinoid-like compounds are endogenous lipid mediators structurally related to AEA; they share several steps of synthesis and degradation with AEA but have distinct receptorbinding profiles. These molecules, including OEA, palmitoylethanolamide (PEA), stearoylethanolamide (SEA), N-linoleoylethanolamine (LEA), and N-docosahexaenoylethanolamine (DHEA), do not directly activate CB1 or CB2 receptors but modulate physiological processes through other pathways. OEA is a prominent member of the NAE family, particularly recognized for its significant role in the GI system. It is distinguished as the most potent NAE agonist for the peroxisome proliferator-activated receptor $\alpha$ (PPAR$\alpha$) through which it exerts anorectic effects [28]. In addition to its appetite-suppressing properties, OEA demonstrates antiinflammatory, neuroprotective, and analgesic effects, likely mediated by PPAR$\alpha$ activation, although PPAR$\alpha$-independent mechanisms may also play a role [29]. Notably, OEA exhibits *in vitro* affinity for the GPR119 receptor, although its anorectic effect does not seem to rely on this receptor interaction [30]. Furthermore, OEA promotes protein kinase C (PKC)- dependent phosphorylation and activation of the TRPV1 channel, thereby contributing to the excitation of sensory nerves [31]. In the rat brain, OEA levels are approximately one-third that of PEA and SEA, with a significant increase observed during

cerebral ischemia, suggesting a potential neuroprotective role for the NAE family through various molecular mechanisms [32]. A randomized clinical trial demonstrated that dietary supplement with PEA added with polydatin induced a markedly improved abdominal pain severity in patients with IBS [33]. Moreover, PEA can also display its bioactive effect throughout GPR119 and GPR55, although the interaction with the latter has been questioned [30]. Although it shares several bioactivities with PEA, SEA does not interact with PPAR$\alpha$ receptors but shows affinity for the GPR119 receptor [32]. SEA has anti-inflammatory, anorectic, and neuroprotective effects [34]. While SEA has received less attention, emerging evidence suggests it may contribute to cellular homeostasis and metabolic regulation [35]. LEA has not been as extensively studied as other members of the NAE family despite sharing similar bioactivities with OEA and PEA. LEA reduced food intake in a manner dependent on PPAR$\alpha$ activation, like the effects of OEA and PEA [32]. Given its high intestinal concentration, it is suggested that LEA's anorectic effects may also involve GPR119, where it exhibits comparable activity to OEA, although this remains to be validated [32]. Over the past decade, DHEA has emerged as a new member of the NAE family with distinct neuronal properties [36], leading to its designation as synaptamide [37]. DHEA exhibits nanomolar affinity for GPR110, a G protein-coupled receptor highly expressed in the hippocampus [38] and promotes neurite outgrowth and synapse formation in wild-type neurons throughout GPR110 activation [39-40]. Additionally, DHEA has GPR110-dependent antiinflammatory effects, reducing pro-inflammatory cytokines in LPS-treated microglia and decreasing neuroinflammation in mice [41-43]. DHEA levels in the brain are significantly higher than AEA, and its concentration correlates with brain docosahexaenoic acid levels. Limited research has explored DHEA's physiological role in peripheral tissues [32].

The endocannabinoid-like compounds often interact synergistically with endocannabinoids, amplifying or modulating ECS activity. For instance, PEA has been observed to enhance the activity of AEA by reducing FAAHmediated degradation, a phenomenon known as the "entourage effect" [44]. The role of endocannabinoids in gut structure and function The ECS is extensively expressed throughout the GI tract, encompassing enterocytes, immune cells, and ENS [45-46]. This system plays a pivotal role in gut physiology, intricately modulating motility, permeability, and inflammatory responses. Importantly, various studies, primarily summarized in Table 1, highlight the dual role of cannabinoids in modulating intestinal permeability, which has significant implications for both healthy and inflammatory conditions. Under physiological conditions, the action of endocannabinoids in the GI tract is predominantly mediated by the CB1 receptor [47]. However, CB1 activation can increase epithelial permeability by reducing TJ expression, creating conditions that may promote obesity [48]. On the contrary, in pathological states, both CB1 and CB2 reduce abnormal GI motility and permeability [49]. In Caco-2 cells, AEA and 2-AG exacerbated apically EDTAinduced TEER decrease but facilitated a concentration-dependent recovery of basolateral TEER. These effects were inhibited by the CB1 receptor antagonist AM251 and the TRPV1 antagonist capsazepine in the case of AEA [50]. Apical application of AEA and 2-AG worsened hyperpermeability in Caco2 cells exposed to inflammatory cytokines throughout CB1, and co-application of AEA with a FAAH inhibitor, or 2-AG with a MAGL inhibitor, further decreased TEER [51]. FAAH and MAGL inhibitors, such as URB597 and JZL184, caused concentration-dependent drops in TEER in Caco-2 cells. Furthermore, URB597 and JZL184 worsened TEER reductions in cells exposed to inflammatory cytokines and hypoxia. The effects were absent in CB1

knockdown Caco-2 cells [52]. Alcohol-induced increased intestinal permeability is reversed by inhibiting the CB1 receptor with selective CB1 receptor antagonists [53]. *In vivo* research reinforced ECS involvement, particularly the CB1 receptor, in the control of intestinal permeability. Chronic stimulation of the CB1 receptor with the agonist HU210 in wildtype mice led to an increased permeability [54]. Conversely, CB1 knockout mice, compared to wild-type mice, experienced more severe intestinal barrier disruption after exposure to immobilization and acoustic stress [55]. The ECS has an intriguing connection with the gut microbiota. Germ-free mice showed increased CB1 receptor and endocannabinoid levels, effects that were reversed by the reconstitution of gut microflora [56]. Antibiotics also affect the ECS, increasing CB2 receptor expression, especially under stress conditions [57]. Probiotics Lactobacillus acidophilus can enhance CB2 receptors and reduce mice's visceral hypersensitivity [58-59]. Baseline levels of NAEs were positively associated with gut bacterial diversity and beneficial SCFA-producing species like Bifidobacterium and Faecalibacterium. Increased AEA correlated with elevated butyrate levels, increased AEA and PEA, and reduced inflammatory cytokines. On the other hand, 2-AG and OEA were associated with higher levels of the anti-inflammatory cytokine IL-10, highlighting the ECS's role in mediating anti-inflammatory actions via the gut microbiota [59]. In this context, the use of prebiotics or probiotics for improving the tone of the ECS, and endocannabinoids such as PEA, to restore the normal intestinal microbiota has been reported to ameliorate GI dysfunctions [60-61]. The ECS and the CB2 receptor play an essential role in intestinal inflammation [61]. AEA has been shown to suppress neutrophil migration through the CB2 receptor, although 2-AG, another CB2 receptor agonist, does not show the same effect [61]. Studies in mice have shown that CB2 receptor absence leads to more

severe disease and higher intestinal neutrophil accumulation, suggesting that CB2 activation helps prevent excessive immune responses [61]. Pharmacological activation of CB2 or the elevation of endocannabinoid levels through FAAH inhibition has been shown to protect against an experimental mouse model of colitis [62]. AEA can also reverse the inflammation-induced increase in intestinal pathogenic bacteria, such as Pseudomonas, by inducing several AMPs, and can increase the abundance of beneficial bacteria that produce the SCFA butyrate. Thus, increasing endogenous AEA through FAAH inhibitors has been reported as an effective treatment for inflammation-based diseases [63]. PEA has demonstrated significant benefits in reducing inflammation in colitis models [64]. Beyond CB2 receptors, PEA also influences enteric glial cells, which are critical for regulating inflammation and maintaining the integrity of the intestinal lining [65]. Furthermore, the regulation of the level of PEA and AEA through enzymes such as FAAH and NAAA offers a possible strategy to control inflammation in the gut and improve mucosal integrity [161]. Moreover, OEA treatment in rodents protects against inflammatory events and changes the intestinal microbiota composition [6]. Results demonstrated that CB1 signaling may be a useful strategy to reduce intestinal permeability in aging-related gut inflammatory conditions [66]. Based on emerging data, endocannabinoids may serve as valuable biomarkers for intestinal diseases such as IBS, IBD, and colorectal cancer (CRC) [67]. The observed elevations in plasma levels of AEA and OEA in patients with ulcerative colitis (UC) and Crohn's disease (CD), along with the increased levels of 2-AG in CD and CRC patients, highlight their potential role in disease pathology. Furthermore, the upregulation of the 2-AG synthesizing enzyme diacylglycerol lipase (DAGL) alpha in intestinal biopsies from CD patients, coupled with the altered expression of GPR119,

underscores the involvement of ECS in these conditions [68]. The ability of NAEs to promote the expansion of Enterobacteriaceae, a hallmark of inflammatory bowel disease, suggests that these compounds not only reflect disease status but may also contribute to disease progression. Given these findings, endocannabinoids could be utilized as biomarkers to diagnose and monitor intestinal diseases, provide insights into disease mechanisms, and potentially guide therapeutic strategies [69].

| Endocannabinoid | | Endocannabinoid-like | | Cannabinoid |
|---|---|---|---|---|
| MAIN TYPES | | | | |
| 2-AG<br>AEA  | | PEA<br>DHEA<br>LEA<br>OEA<br>SEA  | | THC<br>CBD  |
| MAIN RECEPTORS | | | | |
| CB1-CB2 | | PPARα-TRPV1-GPR119-GRPR110 | | CB1-CB2 |
| **Compound(s)** | **Model / Species** | **Experimental Design** | **Effect / Outcome** | **Ref.** |
| AEA, 2-AG | Caco-2 cells | EDTA-induced TEER decrease | Exacerbated TEER decrease when applied apically | Alhamoruni et al., 2010 |
| AEA, 2-AG | Caco-2 cells | Inflammatory condition induced by cytokines | Exacerbated TEER decrease when applied apically | Alhamoruni et al., 2012 |
| HU210 (CB1 Agonist) | Mice | CB1 Induction | Increased permeability | Maccioni et al., 2025 |
| | CB1 knockout mice | Immobilization and acoustic stress induced | More severe intestinal barrier disruption in CB1 knockout mice compared to wild type | Zoppi et al., 2012 |
| AEA | Mice-T84 cells | CB2 induction | Suppress neutrophil transmigration | Szabady et al., 2018 |
| AEA | Mice | Inflammatory condition induced | Induced AMPs and the abundance of beneficial bacteria | Sultan et al., 2021 |
| PEA | Mice | Colitis model | Reduced inflammation | Borrelli et al., 2015 |
| | Rats-IEC6 cells | Aging model | Aging and the reduction of CB1 expression are correlated with decreased intestinal integrity | Lee et al., 2023 |
| SR141716A (CB1 antagonist) | Mice | CB1 antagonism | Increased gut integrity, increased beneficial gut bacteria and boosts of SCFA production | Mehrpouya-Bahrami et al., 2017 |
| CP55940 (CB1-CB2 agonist) | Mice | CB1 induction | Restored intestinal permeability induced by high fat diet | Cuddihey et al., 2022 |
| CBD, THC | Mice | HFD rich in cholesterol | Reduced gut microbiota disturbances, reduced intestinal inflammation | Gorelick et al., 2022 |
| PEA | Mice | HFD | Improved gut barrier integrity and growth of beneficial microbes | Schwartz et al., 2008 |

**Table 1.** Endocannabinoids (AEA and 2-AG), endocannabinoid-like compounds (OEA and PEA), and cannabinoids THC (delta-9-tetrahydrocannabinol) and CBD (cannabidiol) modulate intestinal health through multiple mechanisms.

These include enhancing intestinal barrier integrity, regulating gut microbiota composition, modulating inflammatory responses, and influencing metabolic pathways.

Experimental models reveal receptor-specific effects involving cannabinoid receptors, PPAR$\alpha$, TRPV1, and others, highlighting their therapeutic potential in gastrointestinal and metabolic disorders.

## 2.5 OEA synthesis and metabolism

OEA, an endocannabinoid-like compound, has garnered attention as a potential therapeutic agent for different diseases due to its unique mechanisms of action, distinct from those of traditional endocannabinoids. OEA synthesis occurs in the proximal small intestine in response to dietary fat intake through a two-step process (Figure 1) [70].

First, the enzyme N-acyl transferase (NAT) catalyzes the bonding between the free amino group of phosphatidylethanolamine (PE) and the oleoyl group in sn1-oleoyl-phosphatidylcholine. This reaction forms N-acylphosphatidylethanolamine (NAPE). In the second step, NAPE is hydrolyzed by N-acylphosphatidyl-ethanolamine-specific phospholipase D (NAPE-PLD), producing phosphatidic acid and OEA. The biosynthesis of OEA and other bioactive lipid amides is modulated by bile acids [70-71]. During feeding, OEA levels in the duodenal and jejunal mucosa increase due to enhanced activity of NAPE-PLD, while fasting promotes degradation through increased FAAH activity [71-72]. Localization studies confirm that OEA biosynthesis and hydrolysis occur in intestinal epithelial and lamina propria cells. Unlike classical satiety peptides, OEA acts as a paracrine signal within the gut to extend postprandial intervals, underscoring its therapeutic potential for obesity and metabolic disorders [73]. OEA does not activate CB1 or CB2 receptors. Instead, it primarily activates PPAR$\alpha$, regulating genes critical to fat absorption and fatty acid metabolism [74]. Interestingly, activation of PPAR$\alpha$ itself also contributes to this process by modulating the expression of satiety-associated proteins,

including apolipoprotein A-IV, enhancing its role in appetite control [75]. In addition to PPAR$\alpha$-mediated effects, OEA interacts with GPR119 and TRPV1, which contribute to other physiological processes, including energy homeostasis, inflammation, and sensory regulation [73]. Furthermore, recent research has revealed that OEA functions as an endogenous ligand for hypoxia-inducible factor 3-alpha (HIF-3$\alpha$). This novel role links OEA to the regulation of lipid metabolism and obesity while integrating oxygen-dependent pathways into its metabolic functions [73]. The anorexigenic effects of exogenously administered OEA are accompanied by activation of specific brain regions, including the hypothalamic paraventricular nucleus and the brainstem, which are associated with satiety control [76]. Notably, OEA does not suppress food intake when administered intracerebrally, and its effects are blocked by capsaicin-induced desensitization of peripheral sensory fibers. However, it has been demonstrated that vagal afferent fibers are not strictly necessary for both behavioral and neurochemical effects of OEA [76-77]. Within a few minutes after its intraperitoneal administration, an increased concentration of intact OEA is observed in different brain areas, with associated inhibition of food intake. These data support the hypothesis that OEA, probably through circulation, rapidly reaches the brain and inhibits eating by acting directly on selected brain nuclei [76]. These findings establish OEA as a peripheral lipid mediator regulating feeding behavior [78].

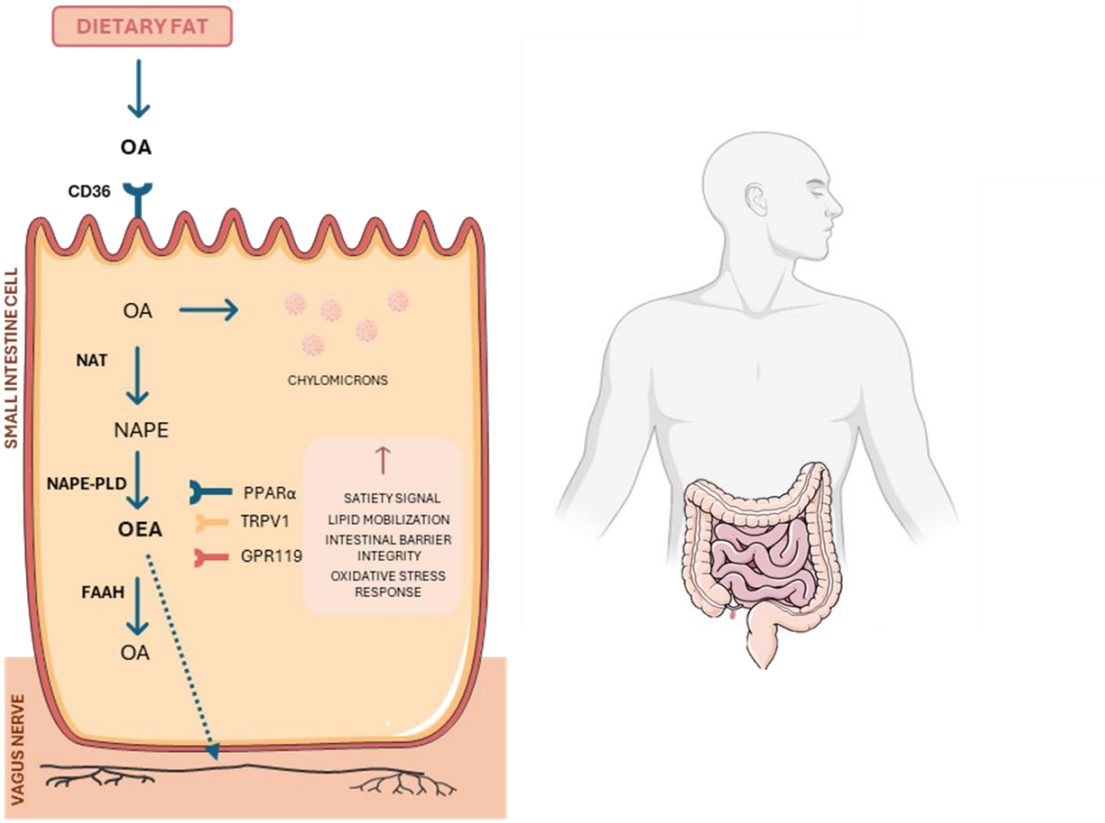


**Figure 1. Mechanism of OEA production in small intestinal cells and its role in metabolic regulation.** Dietary fat containing oleic acid (OA) is metabolized in enterocytes, producing NAPE and subsequent synthesis of OEA via NAPE-PLD enzymatic activity. OEA interacts with receptors such as PPAR$\alpha$, TRPV1, and GPR119, modulating satiety signals, lipid mobilization, intestinal barrier integrity, and oxidative stress response. FAAH breaks down OEA into OA and ethanolamine. The diagram also compares OEA production under diets with high and low oleic acid content, highlighting its physiological impact through vagus nerve activation.

Intraperitoneal injection of OEA ensures its efficacy by bypassing GI degradation [75]. However, a study by Nielsen et al. demonstrated that an oral dose of 10 mg/kg OEA in 24-hour-starved rats is nearly as effective as intraperitoneal administration. The study observed a significant reduction in radiolabeled [3 H]OEA during its transit from the stomach to the intestine, primarily due to extensive enzymatic hydrolysis by FAAH. Despite this, 0.48% of the administered dose remained intact in the intestinal tissue after 90 min, effectively inhibiting food intake by 15.5%.

This retained amount, 11 times higher than the endogenous level of 0.354 nmol/g, accounts for its anorectic efficacy.

Importantly, the study confirmed that OEA's anorectic effects are mediated by the intact molecule rather than its radiolabeled metabolites, oleate, and ethanolamine. Tests with oral ethanolamine (1.88 mg/kg) and oleate (8.68 mg/kg) independently showed no significant impact on food intake, emphasizing that the anorectic effects are specific to intact OEA administration. The finding that this simple and naturally occurring compound holds potential for oral use is highly advantageous for anti-obesity medicine development [78-79]. Drug delivery involves methods and technologies designed to transport therapeutic compounds to their target sites in the body, ensuring maximum efficacy and minimal side effects [80]. A study presents PEGylated liposomes encapsulating OEA to enhance its solubility and bioavailability for stroke therapy. Intravenously administered liposomes demonstrated controlled release, reduced neuronal apoptosis, and attenuated inflammation in ischemic stroke models [81]. OEA, contrary to other satiety agents like cholecystokinin, not only suppresses meal size but also prolongs the intervals between meals, providing a unique mechanism for appetite regulation [72]. Unlike CB1 receptor antagonists, which have been associated with severe psychiatric side effects, OEA offers a safer alternative with minimal adverse effects for anti-obesity therapies [82].

## 2.6 *In vitro* and *in vivo* approaches to investigate the effects of HFD

HFD formulations are frequently employed in experimental research to investigate how elevated lipids influence metabolic processes, cellular function, and the overall health of biological systems [14].

The duration of feeding and the types of fats used, whether saturated, unsaturated, or a combination, are critical factors influencing experimental outcomes [8]. The HFDs used in vivo studies vary significantly in macronutrient composition, particularly in the ratio of saturated fatty acids (SFA) to unsaturated fatty acids [83]. These formulations typically provide 40%–60% of total calories from fats [84]. HFD formulations rich in SFA, reproducing a Western diet model, combine fats from sources like lard or palm oil [19]. Short-term exposure to these diets (1-7 days) primarily focuses on rapid metabolic changes, including intestinal proliferation, insulin resistance, and lipid absorption [7, 85], while medium-term studies (8-12 weeks) evaluate systemic effects, such as gut barrier disruption, inflammation, and the onset of non-alcoholic fatty liver disease (NAFLD) [86]. Long-term protocols (6-12 months) assess chronic adaptations, such as obesity, tumorigenesis, and immune dysregulation [7]. For example, mice fed 60% fat diets for 9–14 months showed significant increases in intestinal stem cell proliferation and tumor development [10]. *In vitro*, HFD conditions are often achieved by exposing cultured cells to lipid-rich media. This is typically accomplished by supplementing the media with free fatty acids (FFAs), such as palmitate, oleate, or a combination of these fatty acids, to mimic the cellular environment associated with HFDs [87]. The concentration and preparation of these fatty acids, including their conjugation with carriers like bovine serum albumin (BSA), are carefully

controlled to prevent lipotoxicity while maintaining physiological relevance [88]. Even *in vitro*, the composition of macromolecules is adapted to simulate the metabolic conditions occurring *in vivo*. Short-term studies (24–72 h) focus on acute responses, such as changes in lipid absorption, barrier integrity, and inflammatory signaling, while long-term experiments (lasting several weeks) investigate chronic adaptations, including stem cell proliferation, epithelial integrity, and metabolic dysregulation [88-89]. Organoid-based 3D cultures are widely used for their ability to mimic intestinal microarchitecture and cellular dynamics. These systems incorporate Matrigel scaffolds and collagen support to create structural and biochemical environments, allowing assessment of epithelial proliferation, gene expression, and permeability changes [90]. For example, canine colonoid-derived monolayers have been shown to model gut barrier dysfunction induced by palmitic acid through reductions in TJ proteins like ZO-1 and E-cadherin [91]. Hydrogel scaffolds and synthetic matrices further enhance the versatility of these models, enabling the incorporation of extracellular matrix (ECM) components and growth factors that support differentiation and metabolic responses [92]. These systems frequently use Caco-2 and HT29-MTX cells to replicate enterocytes and mucus-producing goblet cells, allowing for studies of permeability and nutrient transport [91]. Additionally, microfluidic platforms, such as gut-on-chip devices, integrate fluid dynamics to emulate physiological conditions, including nutrient flow and mechanical stress [92].

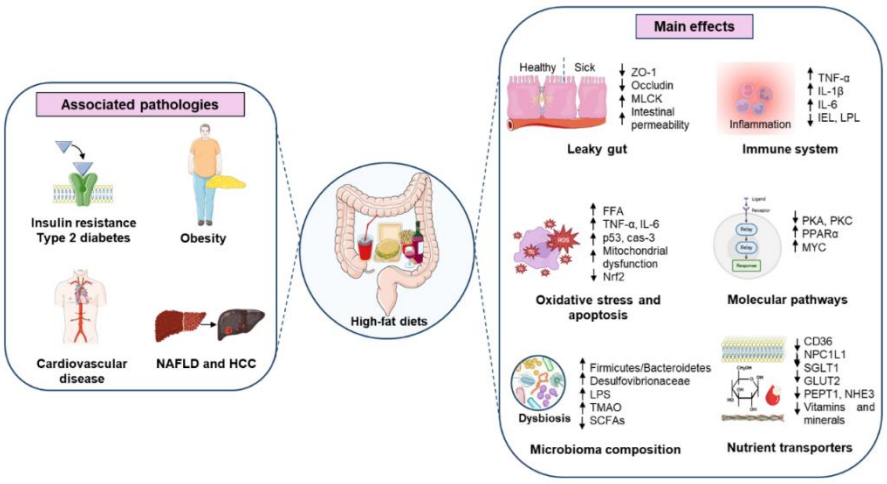


**Figure 2. Main effects of HFDs on intestinal structure and metabolism.** HFD is associated with several metabolic diseases, including insulin resistance, type 2 diabetes mellitus (T2DM), obesity, cardiovascular disease, NAFLD, and hepatocellular carcinoma (HCC). These effects are mediated through alterations in gut structure and function, leading to increased permeability (leaky gut).

## 2.7 Effect of HFD on intestinal structure and function

The type of dietary fat can significantly influence intestinal structure, with SFAs potentially having detrimental effects, while monounsaturated fatty acids (MUFA) and polyunsaturated fatty acids (PUFA) offer protective benefits (Figure 2). SFAs, commonly found in animal products and processed foods, can disrupt the intestinal barrier, leading to increased permeability and a higher risk of metabolic disorders [93]. In contrast, MUFAs, which are present in olive oil and avocados, are generally regarded

as beneficial for gut health. They enhance the integrity of the intestinal barrier and support the metabolism of intestinal cells, potentially reducing inflammation and fostering a more balanced gut microbiome [94]. PUFAs, particularly omega-3s found in fatty fish and flaxseeds, are recognized for their anti-inflammatory effects. Additionally, these fatty acids improve cell membrane fluidity, which aids in nutrient absorption and helps regulate immune responses [94]. HFD stimulates pro-inflammatory signaling pathways, increasing tumor necrosis factor alpha (TNF-$\alpha$), IL-1$\beta$, and IL-6 levels [1, 8]. Mice fed an HFD composed of 60% calories from fat, primarily SFA, exhibited reduced levels of ZO-1 and occludin and increased expression of TNF-$\alpha$ and IL-6, which activated myosin light chain kinase (MLCK), leading to TJ disruption and increased permeability [95-96]. In mouse models of HFD-induced obesity, inflammatory cytokines are associated with a marked increase in intestinal permeability. Instead, anti-inflammatory cytokines like IL22 enhance gut barrier function by promoting PI3K-mediated intestinal epithelial cell proliferation, supporting wound healing, and reducing fatty acid-induced endoplasmic reticulum stress [95-96]. Similarly, IL-17 aids gut barrier TJ organization through actin1-mediated occludin-F-actin association. These cytokines, critical for maintaining barrier integrity, are often diminished in HFD-fed subjects, weakening gut defenses against barrier breakdown [8]. Moreover, HFDinduced dysbiosis exacerbates intestinal permeability by accelerating damage to TJ proteins in the small intestinal mucosa [96]. Intestinal barrier damage due to inflammation is not limited to local effects but has systemic consequences. Once permeability is increased, luminal toxins and bacterial antigens like lipopolysaccharide (LPS) can enter the bloodstream, leading to endotoxemia [1, 97]. Endotoxemia exacerbates systemic inflammation and is strongly linked to metabolic diseases such as insulin resistance, type

2 diabetes, and obesity. This highlights the broader implications of gut permeability alterations and how an HFD can contribute to metabolic dysregulation [8, 93]. Oxidative stress plays a key role in amplifying inflammation and microbial disruptions, impairing intestinal permeability under HFD conditions [1, 8]. Excess dietary fats, especially SFAs, increase reactive oxygen species (ROS) in epithelial cells, damaging TJ cell structures. In HFD-fed animals, markers like lipid peroxides rise, and antioxidant enzymes are depleted, making epithelial cells more vulnerable to ROS damage [8]. The resulting oxidative environment activates pathways like the nuclear factor-κB (NF-κB), which promotes inflammation and further disrupts TJs, worsening intestinal permeability. High oxidative stress can also induce apoptosis, forming gaps in the intestinal lining that allow the passage of harmful substances [8]. The transition from a normal fat diet (13% fat) to an HFD (60% fat) in mice caused a shift from carbohydrate to fat metabolism and significantly increased cellular proliferation in intestinal crypts [98]. Single-cell RNA sequencing revealed the activation of stress response pathways, upregulation of lipid metabolism genes, and enhanced lipid absorption capacity within 3 days, highlighting rapid intestinal adaptation to dietary changes [98]. A study analyzed the effects of HFDs in 12- month-old mice, revealing reduced villus length, colon length, and crypt depth, indicative of atrophic and structural dysfunction. Increased intestinal stem cells (ISCs) enhanced regenerative capacity but predisposed to colorectal cancer [99]. Exposure to HFD compromises intestinal immunity by reducing intraepithelial lymphocytes (IEL) and lamina propria lymphocytes (LPL) within 1 day, with effects intensifying over 3 weeks [92, 100]. A recent study revealed a sex-dependent response to 14 weeks of HFD administration in C57BL/6J mice. Both sexes demonstrated HFDinduced gut dysbiosis, but females

experienced a more pronounced colonic inflammation, marked by increased expression of TLR4, IL6, and IL-1β, associated with greater intestinal permeability with altered expression of occludin and claudins [99]. FFAs were toxic to intestinal T-cells *in vitro* and *in vivo*; lipase inhibitors partially preserved epithelial integrity, reducing luminal FFA, whereas statins failed to protect against FFA toxicity, confirming damage was mediated primarily through the intestinal lumen [101]. A model of intestinal barrier obtained with human intestinal cells (Caco-2) treated for 4 days with palmitic acid showed reduced expression of junctional proteins (E-cadherin, ZO1, occludin, tricellulin) and increasing paracellular permeability [90]. Palmitic acid also induced an inflammatory response with elevated IL-8 levels, effects not observed with oleic acid [22]. Palmitic acid was reported to disrupt gut epithelium homeostasis in colonoid-derived monolayers, reducing ZO-1 expression and Transepithelial-Transendothelial Electrical Resistance (TEER) within 24 h [91].

## 2.8 Molecular mechanisms underlying HFD effects on intestine

At the molecular level, HFD effects are mediated by different signaling pathways. PPAR$\alpha$, a nuclear receptor activated by dietary lipids, drives crypt expansion and villus elongation but also promotes lipid droplet accumulation, linking structural changes to functional impairments [102-103]. Protein kinases such as PKA and PKC, which regulate nutrient transporter activity, are inhibited under HFD conditions, further exacerbating the malabsorption of lipids, carbohydrates, and proteins [104]. MYC plays a dual role in nutrient absorption and metabolic regulation.

While its normal activity supports efficient glucose and lipid absorption, excessive MYC activity, particularly in obesity, exacerbates metabolic dysfunction [105]. HFDs significantly disrupt the intricate balance of intestinal hormone signaling and impair the gut-liver axis, both of which are crucial for maintaining energy homeostasis. A recent study registered how MYC disruption promotes glucagon-like peptide-1 (GLP-1) production, a hormone that improves glucose homeostasis by stimulating insulin secretion and enhancing glucose absorption [106]. Under normal conditions, dietary fats in the small intestine stimulate the release of appetite-regulating hormones, including cholecystokinin, GLP-1, and peptide YY (PYY). These hormones work synergistically to slow gastric emptying, reduce hunger, and enhance feelings of satiety. However, chronic exposure to an HFD diminishes these regulatory mechanisms, resulting in faster gastric emptying, blunted hormonal responses, and weakened gut-liver communication. These deleterious effects drive excessive energy intake, weight gain, and dysregulated lipid and glucose metabolism [107].

## 2.9 HFD-induced gut microbiome alteration

The composition and function of gut microbiome are profoundly shaped by dietary patterns, with HFDs emerging as a significant factor in altering microbial dynamics and contributing to systemic health outcomes [108-109]. The relationship between HFDs and microbiomes has been increasingly recognized as a key player in metabolic, inflammatory, and neoplastic diseases [110]. HFDs induce notable shifts in the gut microbiota, disrupting homeostasis and leading to dysbiosis [111]. Some diets, such as those rich in SFA from lard and palm oil, are associated with reduced

microbial diversity and a pronounced increase in the Firmicutes/Bacteroidetes ratio, a hallmark linked to enhanced energy extraction and weight gain [112-113]. Additionally, HFDs induce the growth of proinflammatory taxa, such as Desulfovibrionaceae, which produce LPS capable of compromising the gut barrier, inducing systemic inflammation via toll-like receptors (TLRs) and establishing a pathway to metabolic dysfunction [111]. These changes are associated with decreased levels of beneficial metabolites, such as SCFAs [110, 114]. In addition, the microbial metabolism of dietary fats leads to an increase in secondary bile acids, which contribute to systemic inflammation and insulin resistance [111]. In contrast, diets rich in MUFAs and PUFAs have a milder effect on microbial diversity and support a more balanced microbiota. Their anti inflammatory properties reduce pro-inflammatory cytokines while promoting the production of SCFAs by gut bacteria. Butyrate not only provides energy for colonic epithelial cells but also strengthens TJs, improving gut barrier stability and reducing susceptibility to damage caused by dietary fats [115].

## 2.10 HFDs disrupt intestinal nutrient transport

Beyond systemic impacts, HFDs exert profound effects on intestinal physiology including crypt elongation, villus shortening, and microvilli disruption. These changes significantly reduce the absorptive surface area, limiting nutrient uptake [104]. Furthermore, high-fat, high-sucrose, low-fiber diets caused intestinal shortening in mice compared to mice fed normal chow [103]. Increased crypt depth is one of the hallmarks of HFD-induced intestinal remodeling. ISC proliferation under HFD conditions results in crypt expansion but at the expense of differentiation into

functional absorptive enterocytes. This imbalance results in a reduced number of mature enterocytes, the main cells responsible for efficient nutrient absorption. Paneth cells, essential for maintaining the ISC niche, are also affected by compromising epithelial homeostasis [115-116]. Lipid transporters, including FAT/CD36, FATPs, and NPC1L1, are essential for the transport of long-chain fatty acids and cholesterol, from the lumen into enterocytes. Chronic HFD exposure significantly reduces the expression of these transporters, leading to inefficient lipid uptake [104]. Intracellular lipid droplet accumulation within enterocytes, a hallmark of HFD-fed animals, further disrupts lipid processing and absorption [103, 117]. Compensatory upregulation of proteins such as liver fatty acidbinding protein (L-FABP) and microsomal triglyceride transfer protein (MTTP) reflects the intestine's attempt to manage excess lipid intake but exacerbates systemic dyslipidemia in mice long-term fed on an HFD [118]. Moreover, in a murine model, chronic HFD consumption enhances intestinal lipid absorption by upregulating FATP-4 and MTTP, increasing cell proliferation, and expanding the absorptive area [119]. Carbohydrate absorption is mediated by SGLT1 and GLUT2. HFDs reduce the expression of these transporters, impairing glucose absorption [104, 118]. The effect, coupled with systemic metabolic dysfunctions like insulin resistance, highlights the widespread consequences of intestinal transporter dysregulation [115]. The absorption of di- and tripeptides is facilitated by PEPT1, while NHE3, an antiporter that contributes to blood buffering capacity, maintains the ionic balance that ensures protein digestion. HFDs impair the functionality of these transporters, leading to reduced protein absorption/digestion and amino acid deficiencies [116]. The altered bile acid metabolism consequent to HFD consumption significantly impairs fat-soluble vitamin (A, D, E, and K) absorption. Bile acids are critical for micelle

formation, which facilitates the solubilization and uptake of these vitamins. Disruptions in bile acid recycling reduce micelle formation, limiting the bioavailability of these essential micronutrients [98]. Moreover, HFD-associated inflammation induces the downregulation of mineral transporters and compromises the uptake of calcium, magnesium, zinc, and iron, exacerbating deficiencies linked to metabolic syndrome [120-121].

## 2.11 Systemic impacts of dysbiosis induced by HFDs

The consequences of HFD-induced dysbiosis extend across multiple physiological systems, manifesting most prominently as metabolic disorders. Obesity, a condition strongly associated with HFD consumption, is exacerbated by the enhanced capacity of microbiota to harvest energy from food and the promotion of adipogenesis through altered SCFA profiles [112]. Dysbiosis also supports the development of insulin resistance by promoting low-grade systemic inflammation and impairing insulin signaling pathways [108]. Furthermore, increased intestinal barrier permeability, driven by reduced butyrate production and impaired TJ, amplifies the translocation of microbial products such as LPS into the bloodstream, causing metabolic endotoxemia [110]. In the liver, altered bile acid metabolism and lipid accumulation, facilitated by intestinal microbial shifts, contribute to NAFLD [113]. HFD is linked to cardiovascular disease partly through the alteration of gut microbiota. In this condition, an increased population of facultative anaerobes, including Escherichia coli, enhances the breakdown of dietary choline into TMA. Once absorbed, TMA is oxidized in the liver to form trimethylamine N-oxide (TMAO). Elevated TMAO levels contribute to atherosclerosis, exacerbating vascular plaque formation [122]. HFDs also enhance the carcinogenic potential of the gut microbiota through the overproduction of secondary bile acids and the

sustained activation of pro-inflammatory pathways, creating a microenvironment conducive to tumorigenesis, particularly in colorectal tissues [109-110].

## 2.12 HFDs interfere with the endocannabinoid system

The effects of cannabinoids on intestinal metabolism can have both therapeutic and adverse consequences, influencing conditions like IBS, IBD, and obesity [26]. HFDs have been shown to upregulate ECS activity through increased endocannabinoid levels, particularly AEA and 2-AG. Through CB1 and CB2, these endocannabinoids amplify lipogenesis and decrease energy expenditure, contributing to obesity [74, 123-124]. Elevated AEA levels are driven by increased activity of NAPE-PLD, the enzyme responsible for endocannabinoid biosynthesis, particularly in adipose tissues. Likewise, HFDs enhance DAGL expression, furthering 2-AG synthesis in white and brown adipose tissues [125]. The dysregulation of ECS components by HFDs is not limited to adipose tissues; alterations are also observed in the liver and brain, contributing to systemic metabolic and inflammatory dysfunctions. The overactivation of CB1 receptors in the hypothalamus under HFD conditions promotes hyperphagia, decreases thermogenesis, and fat deposition in peripheral tissues, exacerbating obesity and its associated comorbidities [74]. A recent study highlights that SR141716A, a CB1 receptor antagonist, mitigates diet-induced obesity by reducing inflammation, improving gut barrier integrity, and modulating the gut microbiome. SR141716A increases beneficial gut bacteria, particularly Akkermansia muciniphila, and boosts SCFA production, including propionate and butyrate, which support metabolic and anti-inflammatory processes [125]. These effects are independent of caloric

restriction, emphasizing the therapeutic potential of CB1 antagonists in managing obesity and metabolic disorders. Conversely, some studies indicate that CB1 activation exerts protective effects in response to HFDs. Mice consuming HFD, rich in sucrose, showed increased intestinal permeability and reduced levels of 2-AG and related monoacylglycerols in the colonic epithelium. These effects were more pronounced in CB1-deficient mice [126-127]. In a mouse model of Western diet-induced obesity, with chronic access to an HFD and a high-sucrose diet, a reduced endocannabinoid level with increased permeability in the large-intestinal epithelium has been reported. Moreover, CB1−/− mice fed on the obesogenic diet experienced decreased expression of TJ proteins and increased expression of inflammatory markers in the large-intestinal epithelium [126-127]. In another study, mice fed on an HFD showed increased intestinal permeability restored by activation of the CB1 receptor [126]. The phytocannabinoids CBD and THC have also demonstrated regulatory effects on intestinal permeability and microbiota composition. Indeed, mice fed on an HFD rich in cholesterol experienced gut microbiota disturbances, marked by an elevated Bacteroidetes/Firmicutes ratio and an increased abundance of Mucispirillum schaedleri, contributing to intestinal inflammation and NAFLD progression. Administration of THC (2.5 mg/kg) and CBD (2.39 mg/kg) reversed these detrimental alterations, with CBD particularly effective at restoring Firmicutes, reducing inflammatory microbes, and increasing beneficial bacteria such as Clostridia and Ruminococcaceae [128]. These results suggest that CBD can modulate the gut-liver axis and potentially alleviate NAFLD. In a model of HFD-induced intestinal dysfunction, PEA showed significant protective effects by improving gut barrier integrity and promoting the growth of beneficial microbes like Bifidobacterium and Turicibacter sanguinis, which supported

intestinal homeostasis [129]. Moreover, PEA reduced intestinal inflammation, enhanced serotonin synthesis, and decreased kynurenine levels by modulating tryptophan metabolism [130]. Research suggests that HFDs can influence the activity and expression of FAAH and MAGL, potentially altering endocannabinoid tone and its related physiological effects. A study demonstrated that an HFD increased the activity of MAGL in the hypothalamus, a key brain region involved in the regulation of appetite and energy homeostasis. This enhancement of MAGL activity may contribute to the dysregulation of appetite and feeding behaviors observed in obesity [131]. Furthermore, HFD-induced obesity has been shown to modulate FAAH expression in various tissues. A study reports that chronic exposure to HFD in mice led to a decrease in FAAH expression in the liver, which could result in higher levels of AEA [132]. This could potentially exacerbate the inflammatory response and increase the risk of metabolic diseases, as AEA is involved in both immune modulation and fat metabolism [133]. Inflammatory mediators, such as cytokines and FFAs, have been shown to regulate the activity of both FAAH and MAGL [134-135]. Additionally, HFD-induced changes in the gut microbiota could further influence endocannabinoid signaling by modulating enzyme activity [136-137].

## 2.13 Dietary and therapeutic interventions to counteract HFD damage

Therapeutic interventions against HFDs have become a critical area of research due to the increasing prevalence of obesity and metabolic diseases such as type 2 diabetes, NAFLD, and cardiovascular diseases. Studies have explored both nonpharmacological and pharmacological interventions to

mitigate these effects. Dietary modifications are one of the primary approaches, with several studies showing that reducing dietary fat intake, particularly SFA, can significantly improve metabolic outcomes. A randomized trial demonstrated that a Mediterranean diet, which is lower in SFA and higher in MUFA, led to improved insulin sensitivity and a reduction in markers of inflammation in individuals with metabolic syndrome [138]. Furthermore, supplementation with omega-3 fatty acids, known for their anti-inflammatory properties, has shown promising results in both animal and human studies. A study found that omega-3 supplementation attenuated HFD-induced hepatic steatosis and improved lipid profiles in mice, suggesting potential therapeutic benefits [139-140]. Given the significant health burden of HFD-induced dysbiosis, strategies to restore microbial balance have garnered considerable attention. Emerging therapeutic strategies include the use of probiotics and prebiotics, which can modulate the gut microbiota and potentially mitigate the inflammatory effects induced by HFDs. A study found that probiotics administration to mice fed on an HFD reduced systemic inflammation and improved insulin sensitivity, suggesting a potential role for gut microbiota modulation in preventing metabolic dysfunction [141]. The inclusion of prebiotics, such as inulin and resistant starch, selectively supports the growth of beneficial bacteria, while replacing SFA with unsaturated fats, such as those found in extra virgin olive oil, has shown promise in promoting a healthier microbial profile [142-143]. Dietary interventions focusing on increasing fiber intake have been demonstrated to enhance microbial diversity and SCFA production, counteracting the deleterious effects of HFDs [109, 144]. The supplementation of dietary fiber, omega-3 fatty acids, or prebiotics has shown the potential to mitigate the negative effects of HFDs on gut permeability [89]. Fiber supports TJ integrity, while omega-3 fatty acids

exhibit anti-inflammatory properties that counteract the effects of SFAs [89]. Moreover, certain probiotics, such as Lactobacillus and Bifidobacterium strains, are also beneficial as they reduce gut inflammation and support TJ maintenance [8].

The development of postbiotics, which include bioactive compounds like SCFAs and bacteriocins, provides another promising avenue for harnessing the microbiome's therapeutic potential without requiring live microbes [144]. Pharmacological treatments also play a key role in counteracting the negative effects of HFDs. For instance, metformin, a commonly prescribed drug for type 2 diabetes, improves insulin sensitivity and reduces fat accumulation in the liver. Additionally, newer agents targeting specific metabolic pathways, such as the GLP-1 agonist liraglutide, have been shown to reduce fat mass and improve glycemic control in patients with obesity and type 2 diabetes [145]. Fibrates, including fenofibrate, are hypolipidemic drugs that activate PPAR$\alpha$ to combat metabolic disorders linked to HFD. A recent study reveals that the activation of PPAR$\alpha$, through synthetic agonists, alleviates palmitic acid-induced lipotoxicity, restoring key cellular processes, such as autophagy and endoplasmic reticulum homeostasis [146]. Considering that chronic inflammation is a hallmark of HFDinduced gut damage, the use of nonsteroidal anti-inflammatory drugs and other anti-inflammatory agents has been studied for their potential to alleviate inflammation and improve intestinal barrier function. For example, mesalazine (a common treatment for IBD) has shown some promise in reducing intestinal inflammation and improving gut permeability in preclinical studies involving HFD-fed animals [147]. However, long-term use of non-steroidal anti-inflammatory drugs can lead to GI side effects, limiting their therapeutic applicability. As mentioned above, oxidative stress plays a significant role in gut injury associated with

HFDs. Studies have suggested that antioxidants like N-acetylcysteine (NAC) and curcumin can reduce oxidative damage, modulate inflammatory pathways, and improve intestinal permeability [145]. NAC, for instance, has shown promise in reducing intestinal inflammation and maintaining the integrity of the epithelial barrier in animal models. However, the clinical translation of these findings remains to be fully explored [145, 148]. Exercise is another cornerstone of therapeutic interventions. Regular physical activity helps to counteract the negative effects of an HFD by improving muscle insulin sensitivity and promoting weight loss. A study showed that moderate-intensity exercise significantly reduced the risk of developing type 2 diabetes in individuals with prediabetes, even when they maintained an HFD [148]. In animal models, exercise combined with dietary changes has been shown to reduce liver fat content and improve metabolic function [147]. Emerging therapeutic approaches, such as fecal microbiota transplantation (FMT), offer innovative solutions for reestablishing microbial equilibrium in dysbiotic individuals. By introducing a diverse and healthy microbial community, FMT has demonstrated efficacy in reversing dysbiosis in conditions such as Clostridium difficile infection and potentially HFDinduced metabolic disorders [108, 112].

## 2.14 Therapeutic potential of OEA in HFD induced intestinal dysfunction

OEA positively regulates lipid metabolism by stimulating fatty acid uptake, decreasing lipid accumulation in hepatocytes, and enhancing fatty acid oxidation and lipolysis [3, 5]. Moreover, OEA exerts prominent roles in intestinal physiology, contributing to overall gut health [6] (Figure 3). The

intestine, particularly the small intestine, is equipped with PPAR$\alpha$ receptors, like other metabolically active tissues such as the liver and skeletal muscle, making this organ highly responsive to OEA [72]. OEA has been shown as a potential therapy for obesity-related liver disorders like NAFLD [3]. In HFD-fed rats, daily intraperitoneal injection of OEA (10 mg/kg) for 2 weeks reduced liver fat accumulation and improved lipid metabolism by decreasing lipogenic markers and enhancing lipid oxidation through PPAR$\alpha$ activation [3]. OEA also reduced oxidative and endoplasmic reticulum stress and improved liver function by lowering markers of oxidative damage and increasing antioxidant enzymes [3]. In an experimental model of mouse liver fibrosis, OEA mitigates liver fibrosis by targeting hepatic stellate cells via a PPAR$\alpha$dependent pathway. OEA reduces fibrosis markers such as $\alpha$-SMA and collagen, alleviates inflammation, and modulates extracellular matrix remodeling while suppressing TGF-$\beta$1 signaling. Notably, these protective effects were absent in PPAR$\alpha$ knockout models, highlighting the critical role of PPAR$\alpha$ in mediating OEA's antifibrotic actions [149]. A study reported how the intraperitoneal injection of OEA exerted significant cardioprotective effects in HFD-induced diabetic rats with myocardial ischemia-reperfusion injury. OEA pretreatment reduced creatine kinase, lactate dehydrogenase, and malondialdehyde levels. Additionally, OEA reduced myocardial infarct size, improved myocardial tissue structure, and mitigated cell apoptosis. Through TRPV1 receptors, OEA activated the PI3K/Akt signaling pathway, reducing apoptosis-related caspase-3, and enhancing the antiapoptotic Bcl-2/Bax ratio [150]. Intraperitoneal OEA administration in HFD-fed mice reversed dopamine deficiency induced by the diet in a PPAR$\alpha$-dependent manner [151]. A recent study, in mice long-term (12 weeks) treated with HFD, has introduced an "intestinal OEA factory" designed for the

controlled in situ release of OEA. This was achieved by engineering Lactobacillus paracasei F19 (LP) to express the human NAPE gene, enabling the production of OEA in response to a dietary supply of ultra-low oleate. This innovative system resulted in a significant weight reduction and improved metabolic dysfunction. Additionally, there was a notable improvement in depressive and anxiety-like behaviors, which correlated with the restoration of duodenal barrier function, the reestablishment of the Firmicutes/Bacteroidetes ratio, and an increase in beneficial bacteria, including Lactobacillus, Prevotella, and Parabacteroides [152]. OEA exhibits potent anti-inflammatory effects by reducing levels of pro-inflammatory cytokines such as TNF-$\alpha$ and IL-6 in HFD feeding. It simultaneously enhances anti-inflammatory markers like IL-10, promoting a shift toward a balanced immune response [6]. OEA has demonstrated the ability to increase lipid oxidation, specifically in the jejunum of HFD-fed C57BL/6J mice, by increasing PPAR$\alpha$, FAT/CD36, and FATP1 expression. Similar effects were observed in the liver and duodenum but not in the ileum. This action prevents excessive lipid accumulation in different tissues, thereby improving metabolic parameters like insulin sensitivity and lipid profiles [71]. OEA promotes a shift in mice microbiota composition toward a "lean-like" profile, characterized by increased Bacteroidetes and reduced Firmicutes populations. These changes are accompanied by decreased expression of pro-inflammatory cytokines in Peyer's patches, underscoring the dual role of OEA in microbiota modulation and immune homeostasis [153]. OEA has been shown to restore epithelial integrity *in vitro* by modulating PPAR$\alpha$ and TRPV1 receptor pathways [154]. A study using intestinal Caco-2 cells demonstrated that OEA prevents the hypoxia-induced reduction in TEER, a measure of barrier integrity, and maintains TJ function. By stabilizing TEER, OEA prevents the paracellular passage of

macromolecules and harmful substances, including LPS [103]. A pilot study in healthy young adult men demonstrated that an oral supplement containing spermidine, nicotinamide, PEA, and OEA decreased TNF-$\alpha$ and ROS in stimulated macrophages [155]. Moreover, a double-blind placebocontrolled study demonstrated that 2 months' supplementation with a complex of epigallocatechin-3-gallate with NAPE ameliorated oxidative stress-related markers of overweight and class I obese subjects [156].

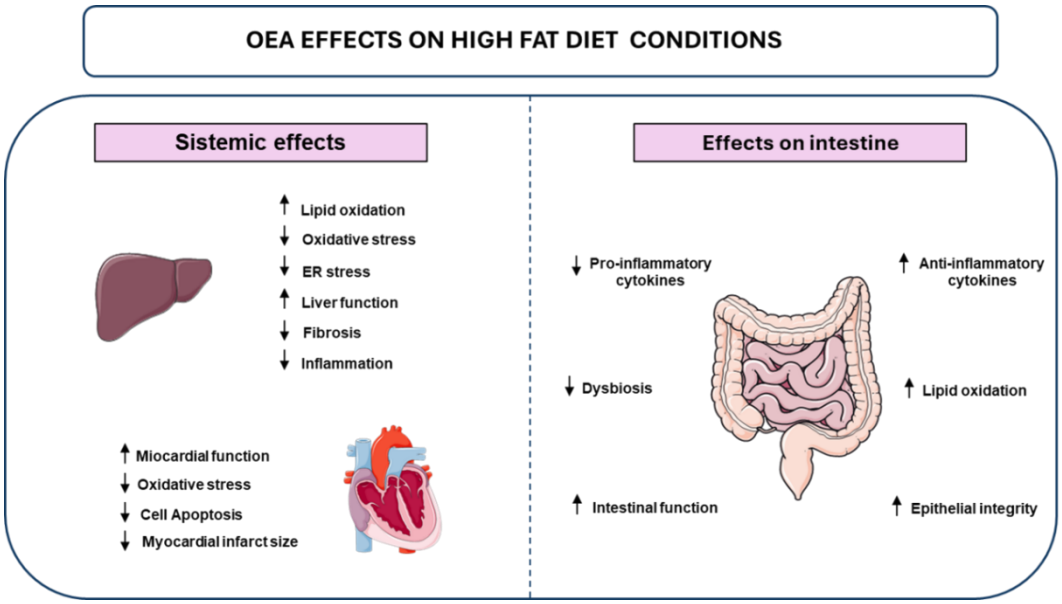


**Figure 3. Systemic and intestinal effects of OEA.** At a systemic level, OEA has beneficial effects on lipid metabolism, enhances cardiovascular function, and mitigates inflammation. Within the intestinal environment, OEA plays a crucial role in strengthening the integrity of the intestinal barrier, modulating microbiota composition, and regulating local inflammatory responses, all of which contribute to maintaining overall gut health.

## 2.15 Conclusion

In conclusion, the interplay between HFDs and the ECS plays a critical role in the development of metabolic disorders, including obesity and intestinal dysfunction. HFDs enhance the activity of the ECS by increasing the levels of endocannabinoids such as AEA and 2-AG, which affect various metabolic pathways, including lipid metabolism and energy balance. This dysregulation contributes to systemic metabolic and inflammatory dysfunctions, exacerbating obesity and related comorbidities [24].

While cannabinoids like THC and CBD show potential for therapeutic applications in modulating gut permeability and microbiota composition, their effects can vary depending on the context and the specific receptors they target. Compounds such as OEA, which work through alternative pathways such as PPAR$\alpha$ activation, offer promising therapeutic prospects due to their ability to improve intestinal barrier integrity, reduce inflammation, and support metabolic health without the adverse effects of traditional ECS-targeted agents [73]. OEA is a promising therapeutic agent for addressing the harmful consequences of HFDs by simultaneously targeting appetite regulation, gut health, inflammation, and metabolic processes. OEA has the potential to treat metabolic syndrome and related disorders. Together, these findings underscore the complex role of the ECS in mediating the effects of HFDs and highlight the potential of targeting specific ECS components, including OEA, to develop novel therapies for obesity, intestinal dysfunction, and related metabolic disorders. Future investigations should focus on determining optimal dosing strategies and exploring synergistic effects with other treatments. Despite advancements in research, there are still several gaps that have not been fully addressed.

While cannabinoid receptors (CB1 and CB2) and their endogenous ligands have been identified, the precise mechanisms through which they interact with other cellular signaling pathways are not fully understood. Moreover, the processes involved in the synthesis and degradation of endocannabinoids are not fully characterized. Also, it must be considered that significant differences may occur in responses to the endocannabinoid system among individuals, influenced by sex, genetic, environmental, and lifestyle factors [157-158]. Many studies have focused on specific endocannabinoid compounds without exploring their interactions with other dietary components or the gut microbiome, which may influence their pharmacological effects [159]. In addition, it should be noted that some endocannabinoids, such as 2-AG, represent a source of arachidonic acid for prostaglandin synthesis [131]. Thus, the administration of endocannabinoids, or strategies to increase their synthesis, may have far-reaching effects that go beyond the CB1 and CB2 receptors. Another point that is to be considered is the lack of standardized methodologies across studies, leading to variability in results and conclusions [160]. Several studies have utilized small sample sizes or animal models that may not fully represent human physiology, limiting the applicability of their findings to clinical settings. Also, a few studies have attempted to translate preclinical findings into human trials, highlighting a significant gap in our understanding of the therapeutic potential of endocannabinoid compounds. To address these gaps, future research needs to adopt more comprehensive approaches, including larger, well-controlled clinical trials that consider the multifactorial nature of diet and metabolism. Research on drugs that modulate the ECS is ongoing, but there are still significant challenges in creating effective medications that are free from side effects. More clinical trials are needed to establish the efficacy and safety of

endocannabinoid-based treatments for various conditions. This includes understanding optimal dosing, delivery methods, and potential side effects. This could provide a clearer understanding of the role of endocannabinoids in intestinal health. In the future, more mechanistic studies are warranted to elucidate the detailed mechanisms of action of endocannabinoids in the gut. In addition, better-designed clinical trials are needed to explore the full therapeutic potential of endocannabinoids on and through the gut.

## 4. References


1. *Hickey JW, Becker WR, Nevins SA, Horning A, Perez AE, Zhu C, et al. Organization of the human intestine at single-cell resolution. Nature. 2023;619(7970):572-584. doi:10.1038/s41586-023-05915-x.*

2. *Nigam Y, Knight J, Williams N. Gastrointestinal tract 5: the anatomy and functions of the large intestine. Nursing Times 10th ed. Vol. 2019;115:50-53.*

3. *Giudetti AM, Vergara D, Longo S, Friuli M, Eramo B, Tacconi S, et al. Oleoylethanolamide reduces hepatic oxidative stress and endoplasmic reticulum stress in high-fat diet-fed rats. Antioxidants. 2021;10(8):1289. doi:10.3390/antiox10081289.*

4. *Tutunchi H, Saghafi-Asl M, Ostadrahimi A. A systematic review of the effects of oleoylethanolamide, a high-affinity endogenous ligand of PPAR-α, on the management and prevention of obesity. Clin. Exp. Pharmacol. Physiol. 2020;47(4):543-552. doi:10.1111/1440-1681.13238.*

5. *Bowen KJ, Kris-Etherton PM, Shearer GC, West SG, Reddivari L, Jones PJH. Oleic acid-derived oleoylethanolamide: a nutritional science perspective. Prog. Lipid Res. 2017;67:1-15. doi:10.1016/j.plipres.2017.04.001.*

6. *De Filippo C, Costa A, Becagli MV, Monroy MM, Provensi G, Passani MB. Gut microbiota and oleoylethanolamide in the regulation of intestinal homeostasis. Front. Endocrinol. (Lausanne). 2023;14:1135157. doi:10.3389/fendo.2023.1135157.*

7. *Shalon D, Culver RN, Grembi JA, Folz J, Treit PV, Shi H, et al. Profiling the human intestinal environment under physiological conditions. Nature. 2023;617(7961):581-591. doi:10.1038/s41586-023-05989-7.*

8. *Di Tommaso N, Gasbarrini A, Ponziani FR. Intestinal barrier in human health and disease. Int. J. Environ. Res. Public Health. 2021;18(23):12836. doi:10.3390/ijerph182312836.*

9. *Qiao Y, He C, Xia Y, Ocansey DKW, Mao F. Intestinal mucus barrier: a potential therapeutic target for IBD. Autoimmun. Rev. 2025;24(2):103717. doi:10.1016/j.autrev.2024.103717.*

10. *Birchenough GMH, Schroeder BO, Sharba S, Arike L, Recktenwald CV, Puértolas-Balint F, et al. Muc2-dependent microbial colonization of the jejunal mucus layer is diet sensitive and confers local resistance to enteric pathogen infection. Cell Rep. 2023;42(2):112084. doi:10.1016/j.celrep.2023.112084*

11. *Gagandeep KR, Narasingappa RB, Vyas GV. Unveiling mechanisms of antimicrobial peptide: actions beyond the membranes disruption. Heliyon. 2024;10(19):e38079. doi:10.1016/j.heliyon.2024.e38079.*

12. *Yang R, Ma X, Peng F, Wen J, Allahou LW, Williams GR, et al. Advances in antimicrobial peptides: from mechanistic insights to chemical modifications. Biotechnol. Adv. 2025;81:108570. doi:10.1016/j.biotechadv.2025.108570.*

13. *Duarte-Mata DI, Salinas-Carmona MC. Antimicrobial peptides' immune modulation role in intracellular bacterial infection. Front. Immunol. 2023;14:1119574. doi:10.3389/fimmu.2023.1119574.*

14. *Greenwood-Van Meerveld B, Johnson AC, Grundy D. Gastrointestinal physiology and function. Handb. Exp. Pharmacol., 1-16. 2017. doi:10.1007/164_2016_118.*

15. *Fukasawa N, Tsunoda J, Sunaga S, Kiyohara H, Nakamoto N, Teratani T, et al. The gut-organ axis: clinical aspects and immune mechanisms. Allergol. Int. 2025;74(2):197-209. doi:10.1016/j.alit.2025.01.004.*

16. *O'Riordan KJ, Collins MK, Moloney GM, Knox EG, Aburto MR, Fülling C, et al. Short chain fatty acids: microbial metabolites for gut-brain axis signalling. Mol. Cell Endocrinol. 2022;546:111572. doi:10.1016/j.mce.2022.111572.*

17. *Huda-Faujan N, Abdulamir AS, Fatimah AB, Anas OM, Shuhaimi M, Yazid AM, et al. The impact of the level of the intestinal short chain fatty acids in inflammatory bowel disease patients versus healthy subjects. Open Biochem J. 2010;4:53-58. doi:10.2174/1874091X01004010053.*

18. *Zhang D, Peng R, Yang D. A preliminary study on the changes of fecal short-chain fatty acids in patients with traumatic spinal cord injury in the chronic phase. Spinal Cord. Ser. Cases. 2025;11(1):3. doi:10.1038/s41394-025-00698-x.*

19. *Xiong RG, Zhou DD, Wu SX, Huang SY, Saimaiti A, Yang ZJ, et al. Health benefits and side effects of short-chain fatty acids. Foods. 2022;11(18):2863. doi:10.3390/foods11182863.*

20. *Gharib M, Samani LN, Panah ZE, Naseri M, Bahrani N, Kiani K. The effect of valeric on anxiety severity in women undergoing hysterosalpingography. Glob. J. Health Sci. 2015;7(3):358-363. doi:10.5539/gjhs.v7n3p358.*

21. *Blakeney BA, Crowe MS, Mahavadi S, Murthy KS, Grider JR. Branched short-chain fatty acid isovaleric acid causes colonic smooth muscle relaxation via cAMP/PKA pathway. Dig. Dis. Sci. 2019;64(5):1171-1181. doi:10.1007/s10620-018-5417-5.*

22. *Heimann E, Nyman M, Pålbrink AK, Lindkvist-Petersson K, Degerman E. Branched short-chain fatty acids modulate glucose and lipid metabolism in primary adipocytes. Adipocyte. 2016;5(4):359-368. doi:10.1080/21623945.2016.1252011.*

23. *Ney LM, Wipplinger M, Grossmann M, Engert N, Wegner VD, Mosig AS. Short chain fatty acids: key regulators of the local and systemic immune response in inflammatory diseases and infections. Open Biol. 2023;13(3):230014. doi:10.1098/rsob.230014.*

24. *Piomelli D. The molecular logic of endocannabinoid signalling. Nat. Rev. Neurosci. 2003;4(11):873-884. doi:10.1038/nrn1247.*

25. *Di Marzo V, Matias I. Endocannabinoid control of food intake and energy balance. Nat. Neurosci. 2005;8(5):585-589. doi:10.1038/nn1457.*

26. *Cravatt BF, Demarest K, Patricelli MP, Bracey MH, Giang DK, Martin BR, et al. Supersensitivity to anandamide and enhanced endogenous cannabinoid signaling in mice lacking fatty acid amide hydrolase. Proc. Natl. Acad. Sci. U. S. A. 2001;98(16):9371-9376. doi:10.1073/pnas.161191698.*

27. *Lo VJ, Fu J, Astarita G, La Rana G, Russo R, Calignano A, et al. The nuclear receptor peroxisome proliferator-activated receptor-α mediates the anti- inflammatory actions of palmitoylethanolamide. Mol. Pharmacol. 2005;67(1):15-19. doi:10.1124/mol.104.006353*

28. *Fu J, Gaetani S, Oveisi F, Lo Verme J, Serrano A, Rodríguez de Fonseca F, et al. Oleylethanolamide regulates feeding and body weight through activation of the nuclear receptor PPAR-alpha. Nature. 2003;425(6953):90-93. doi:10.1038/nature01921.*

29. *Suardíaz M, Estivill-Torrús G, Goicoechea C, Bilbao A, de Fonseca FR. Analgesic properties of oleoylethanolamide (OEA) in visceral and inflammatory pain. Pain. 2007;133(1):99-110. doi:10.1016/j.pain.2007.03.008.*

30. *Im DS. GPR119 and GPR55 as receptors for fatty acid ethanolamides, oleoylethanolamide and palmitoylethanolamide. Int. J. Mol. Sci. 2021;22(3):1034. doi:10.3390/ijms22031034.*

31. *Ahern GP. Activation of TRPV1 by the satiety factor oleoylethanolamide. J Biol Chem. 2003;278(33):30429-30434. doi:10.1074/jbc.M305051200.*

32. *Mock ED, Gagestein B, van der Stelt M. Anandamide and other N-acylethanolamines: a class of signaling lipids with therapeutic opportunities. Prog. Lipid Res. 2023;89:101194. doi:10.1016/j.plipres.2022.101194.*

33. *Cremon C, Stanghellini V, Barbaro MR, Cogliandro RF, Bellacosa L, Santos J, et al. Randomised clinical trial: the analgesic properties of dietary supplementation with palmitoylethanolamide and polydatin in irritable bowel syndrome. Aliment. Pharmacol. Ther. 2017;45(7):909-922. doi:10.1111/apt.13958*

34. *Winiarska-Mieczan A, Kwiecień M, Jachimowicz-Rogowska K, Donaldson J, Tomaszewska E, Baranowska-Wójcik E. Anti-inflammatory, antioxidant, and neuroprotective effects of polyphenols-polyphenols as an element of diet therapy in depressive disorders. Int. J. Mol. Sci. 2023;24(3):2258. doi:10.3390/ijms24032258*

35. *Di Marzo V, Melck D, Bisogno T, De Petrocellis L. Endocannabinoids: endogenous cannabinoid receptor ligands with neuromodulatory action. Trends Neurosci. 1998;21(12):521-528. doi:10.1016/s0166-2236(98)01283-1.*

36. *Kim HY, Spector AA. N-Docosahexaenoylethanolamine: a neurotrophic and neuroprotective metabolite of docosahexaenoic acid. Mol. Asp. Med. 2018;64:34-44. doi:10.1016/j.mam.2018.03.004.*

37. *Kim HY, Spector AA, Xiong ZM. A synaptogenic amide N-docosahexaenoylethanolamine promotes hippocampal development. Prostagl. Other Lipid Mediat. 2011;96(1-4):114-120. doi:10.1016/j.prostaglandins.2011.07.002.*

38. *Lee JW, Huang BX, Kwon H, Rashid MA, Kharebava G, Desai A, et al. Orphan GPR110 (ADGRF1) targeted by N-docosahexaenoylethanolamine in development of neurons and cognitive function. Nat. Commun. 2016;7(1):13123. doi:10.1038/ncomms13123.*

39. *Huang BX, Hu X, Kwon HS, Fu C, Lee JW, Southall N, et al. Synaptamide activates the adhesion GPCR GPR110 (ADGRF1) through GAIN domain binding. Commun Biol. 2020;3(1):109. doi:10.1038/s42003-020-0831-6.*

40. *Qu X, Qiu N, Wang M, Zhang B, Du J, Zhong Z, et al. Structural basis of tethered agonism of the adhesion GPCRs ADGRD1 and ADGRF1. Nature. 2022;604(7907):779-785. doi:10.1038/s41586-022-04580-w.*

41. *Park T, Chen H, Kevala K, Lee JW, Kim HY. N-Docosahexaenoylethanolamine ameliorates LPS-induced neuroinflammation via cAMP/PKA-dependent signaling. J. Neuroinflammation. 2016;13(1):284. doi:10.1186/s12974-016-0751-z.*

42. *Meijerink J, Poland M, Balvers MG, Plastina P, Lute C, Dwarkasing J, et al. Inhibition of COX-2-mediated eicosanoid production plays a major role in the anti-inflammatory effects of the endocannabinoid N-docosahexaenoylethanolamine (DHEA) in macrophages. Br. J. Pharmacol. 2015;172(1):24-37. doi:10.1111/bph.12747.*

43. *Park T, Chen H, Kim HY. GPR110 (ADGRF1) mediates anti- inflammatory effects of N-docosahexaenoylethanolamine. J. Neuroinflammation. 2019;16(1):225. doi:10.1186/s12974-019-1621-2.*

44. *Srivastava RK, Lutz B, Ruiz de Azua I. The microbiome and gut endocannabinoid system in the regulation of stress responses and metabolism. Front. Cell Neurosci. 2022;16:867267. doi:10.3389/fncel.2022.867267*

45. *Cani PD, Geurts L, Matamoros S, Plovier H, Duparc T. Glucose metabolism: focus on gut microbiota, the endocannabinoid system and beyond. Diabetes Metab. 2014;40(4):246-257. doi:10.1016/j.diabet.2014.02.004.*

46. *Galiazzo G, Giancola F, Stanzani A, Fracassi F, Bernardini C, Forni M, et al. Localization of cannabinoid receptors CB1, CB2, GPR55, and PPARα in the canine gastrointestinal tract. Histochem Cell Biol. 2018;150(2):187-205. doi:10.1007/s00418-018-1684-7.*

47. *Izzo AA, Sharkey KA. Cannabinoids and the gut: new developments and emerging concepts. Pharmacol. Ther. 2010;126(1):21-38. doi:10.1016/j.pharmthera.2009.12.005.*

48. *Maccarrone M, Bab I, Bíró T, Cabral GA, Dey SK, Di Marzo V, et al. Endocannabinoid signaling at the periphery: 50 years after THC. Trends Pharmacol. Sci. 2015;36(5):277-296. doi:10.1016/j.tips.2015.02.008.*

49. *Duncan M, Mouihate A, Mackie K, Keenan CM, Buckley NE, Davison JS, et al. Cannabinoid CB 2 receptors in the enteric nervous system modulate gastrointestinal contractility in lipopolysaccharide-treated rats. Am. J. Physiology- Gastrointestinal Liver Physiol. 2008;295(1):G78-G87. doi:10.1152/ajpgi.90285.2008*

50. *Alhamoruni A, Lee AC, Wright KL, Larvin M, O'Sullivan SE. Pharmacological effects of cannabinoids on the Caco-2 cell culture model of intestinal permeability. J. Pharmacol. Exp. Ther. 2010;335(1):92-102. doi:10.1124/jpet.110.168237.*

51. *Alhamoruni A, Wright K, Larvin M, O'Sullivan S. Cannabinoids mediate opposing effects on inflammation-induced intestinal permeability. Br. J. Pharmacol. 2012;165(8):2598-2610. doi:10.1111/j.1476-5381.2011.01589.x.*

52. *Karwad MA, Couch DG, Theophilidou E, Sarmad S, Barrett DA, Larvin M, et al. The role of CB1 in intestinal permeability and inflammation. FASEB J. 2017;31(8):3267-3277. doi:10.1096/fj.201601346R.*

53. *Maccioni L, Dvorácskó S, Godlewski G, Cinar R, Iyer MR, Gao B, et al. Gut cannabinoid receptor 1 regulates alcohol binge-induced intestinal permeability. eGastroenterology. 2025;3(1):e100173. doi:10.1136/egastro-2024-100173.*

54. *Muccioli GG, Naslain D, Bäckhed F, Reigstad CS, Lambert DM, Delzenne NM, et al. The endocannabinoid system links gut microbiota to adipogenesis. Mol. Syst. Biol. 2010;6(1):392. doi:10.1038/msb.2010.46.*

55. *Zoppi S, Madrigal JLM, Pérez-Nievas BG, Marín-Jiménez I, Caso JR, Alou L, et al. Endogenous cannabinoid system regulates intestinal barrier function in vivo through cannabinoid type 1 receptor activation. Am. J. Physiology-Gastrointestinal Liver Physiology. 2012;302(5):G565-G571. doi:10.1152/ajpgi.00158.2011.*

56. *Manca C, Boubertakh B, Leblanc N, Deschênes T, Lacroix S, Martin C, et al. Germ-free mice exhibit profound gut microbiota-dependent alterations of intestinal endocannabinoidome signaling. J. Lipid Res. 2020;61(1):70-85. doi:10.1194/jlr.R*

57. *Guida F, Turco F, Iannotta M, De Gregorio D, Palumbo I, Sarnelli G, et al. Antibiotic-induced microbiota perturbation causes gut endocannabinoidome changes, hippocampal neuroglial reorganization and depression in mice. Brain Behav. Immun. 2018;67:230-245. doi:10.1016/j.bbi.2017.09.001.*

58. *Aguilera M, Vergara P, Martínez V. Stress and antibiotics alter luminal and wall-adhered microbiota and enhance the local expression of visceral sensory-related systems in mice. Neurogastroenterol. Motil. 2013;25(8):e515-e529. doi:10.1111/nmo.12154.*

59. *Vijay A, Kouraki A, Gohir S, Turnbull J, Kelly A, Chapman V, et al. The anti-inflammatory effect of bacterial short chain fatty acids is partially mediated by endocannabinoids. Gut Microbes. 2021;13(1):1997559. doi:10.1080/19490976.2021.1997559*

60. *Turco F, Brugnatelli V, Abalo R. Neuro-gastro-cannabinology: a novel paradigm for regulating mood and digestive health. Med. Cannabis Cannabinoids. 2023;6(1):130-137. doi:10.1159/000534007.*

61. *Szabady RL, Louissaint C, Lubben A, Xie B, Reeksting S, Tuohy C, et al. Intestinal P-glycoprotein exports endocannabinoids to prevent inflammation and maintain homeostasis. J. Clin. Investigation. 2018;128(9):4044-4056. doi:10.1172/JC*

62. *Andrzejak V, Muccioli GG, Body-Malapel M, El Bakali J, Djouina M, Renault N, et al. New FAAH inhibitors based on 3-carboxamido-5-aryl-isoxazole scaffold that protect against experimental colitis. Bioorg Med. Chem. 2011;19(12):3777-3786. doi:10.1016/j.bmc.2011.04.057.*

63. *Sultan M, Wilson K, Abdulla OA, Busbee PB, Hall A, Carter T, et al. Endocannabinoid anandamide attenuates acute respiratory distress syndrome through modulation of microbiome in the gut-lung Axis. Cells. 2021;10(12):3305. doi:10.3390/cells10123305.*

64. *Borrelli F, Romano B, Petrosino S, Pagano E, Capasso R, Coppola D, et al. Palmitoylethanolamide, a naturally occurring lipid, is an orally effective intestinal anti-inflammatory agent. Br. J. Pharmacol. 2015;172(1):142-158. doi:10.1111/bph.12907.*

65. *Zeisel A, Hochgerner H, Lönnerberg P, Johnsson A, Memic F, van der Zwan J, et al. Molecular architecture of the mouse nervous system. Cell. 2018;174(4):999-1014.e22. doi:10.1016/j.cell.2018.06.021.*

66. *Lee Y, Kim Y, Park S, Heo G, Chung HY, Im E. Cannabinoid receptor type 1 in the aging gut regulates the mucosal permeability via miR-191-5p. Front. Endocrinol. (Lausanne). 2023;14:14. doi:10.3389/fendo.2023.1241097.*

67. *Cuddihey H, MacNaughton WK, Sharkey KA. Role of the endocannabinoid system in the regulation of intestinal homeostasis. Cell Mol Gastroenterol Hepatol. 2022;14(4):947-963. doi:10.1016/j.jcmgh.2022.05.015.*

68. *Grill M, Högenauer C, Blesl A, Haybaeck J, Golob-Schwarzl N, Ferreirós N, et al. Members of the endocannabinoid system are distinctly regulated in inflammatory bowel disease and colorectal cancer. Sci. Rep. 2019;9(1):2358. doi:10.1038/s41598-019-38865-4.*

69. *Fornelos N, Franzosa EA, Bishai J, Annand JW, Oka A, Lloyd-Price J, et al. Growth effects of N-acylethanolamines on gut bacteria reflect altered bacterial abundances in inflammatory bowel disease. Nat. Microbiol. 2020;5(3):486-497. doi:10.1038/s41564-019-0655-7.*

70. *Igarashi M, Iwasa K, Yoshikawa K. Feeding regulation by oleoylethanolamide synthesized from dietary oleic acid. Prostagl. Leukot. Essent. Fat. Acids. 2021;165:102228. doi:10.1016/j.plefa.2020.102228Ignatowska-*

71. *Fu J, Astarita G, Gaetani S, Kim J, Cravatt BF, Mackie K, et al. Food intake regulates oleoylethanolamide formation and degradation in the proximal small intestine. J. Biol. Chem. 2007;282(2):1518-1528. doi:10.1074/jbc.*

72. *Terrazzino S, Berto F, Carbonare MD, Fabris M, Guiotto A, Bernardini D, et al. Stearoylethanolamide exerts anorexic effects in mice via downregulation of liver stearoyl-coenzyme A desaturase-1 mRNA expression. FASEB J. 2004;18(13):1580-1582. doi:10.1096/fj.03-1080fje.*

73. *Diao X, Ye F, Zhang M, Ren X, Tian X, Lu J, et al. Identification of oleoylethanolamide as an endogenous ligand for HIF-3α. Nat. Commun. 2022;13(1):2529. doi:10.1038/s41467-022-30338-z.*

74. *Iannotti FA, Vitale RM. The endocannabinoid system and PPARs: focus on their signalling crosstalk, action and transcriptional regulation. Cells. 2021;10(3):586. doi:10.3390/cells10030586.*

75. *Tso P, Liu M. Apolipoprotein A-IV, food intake, and obesity. Physiol. Behav. 2004;83(4):631-643. doi:10.1016/j.physbeh.2004.07.032.*

76. *Romano A, Friuli M, Eramo B, Gallelli CA, Koczwara JB, Azari EK, et al. "To brain or not to brain": evaluating the possible direct effects of the satiety factor oleoylethanolamide in the central nervous system. Front. Endocrinol. (Lausanne). 2023;14:1158287. doi:10.3389/fendo.2023.1158287.*

77. *Karimian Azari E, Ramachandran D, Weibel S, Arnold M, Romano A, Gaetani S, et al. Vagal afferents are not necessary for the satiety effect of the gut lipid messenger oleoylethanolamide.*

*Am. J. Physiology-Regulatory, Integr. Comp. Physiology. 2014;307(2):R167-R178. doi:10.1152/ajpregu.00067.2014*

*78. Rodríguez de Fonseca F, Navarro M, Gómez R, Escuredo L, Nava F, Fu J, et al. An anorexic lipid mediator regulated by feeding. Nature. 2001;414(6860):209-212. doi:10.1038/35102582.*

*79. Nielsen MJ, Petersen G, Astrup A, Hansen HS. Food intake is inhibited by oral oleoylethanolamide. J. Lipid Res. 2004;45(6):1027-1029. doi:10.1194/jlr.C300008-JL*

*80. De Jong WH, Borm PJ. Drug delivery and nanoparticles:applications and hazards. Int. J. Nanomedicine. 2008;3(2):133-149. doi:10.2147/ijn.s596.*

*81. Wu S, Yang X. OEA loaded liposomes with the neuroprotective effect for stroke therapy. Front. Chem. 2022;10:1014208. doi:10.3389/fchem.2022.1014208.*

*82. Romano A, Coccurello R, Giacovazzo G, Bedse G, Moles A, Gaetani S. Oleoylethanolamide: a novel potential pharmacological alternative to cannabinoid antagonists for the control of appetite. Biomed. Res. Int. 2014;2014:203425-203510. doi:10.1155/2014/203425.*

*83. Recena AL, Aparecida do Amaral L, Serafim de Souza R, Jacobowski AC, Freitas dos Santos E, Rodrigues Macedo ML. Nonalcoholic fatty liver disease induced by high-fat diet in C57bl/6 models. Nutrients. 2019;11(12):3067. doi:10.3390/nu11123067.*

*84. Nguyen S, Shao D, Tomasi LC, Braun A, de Mattos ABM, Choi YS, et al. The effects of fatty acid composition on cardiac hypertrophy and function in mouse models of diet-induced obesity. J. Nutr. Biochem. 2017;46:137-142. doi:10.1016/j.jnutbio.2017.05.009.*

*85. Keles U, Kalem-Yapar N, Hultén H, Zhao L, Kaldis P. Impact of short-term lipid overload on whole-body physiology. Mol. Cell Biol. 2025;45(2):47-58. doi:10.1080/10985549.2024.2438814.*

*86. Jiang S, Miao Z. High-fat diet induces intestinal mucosal barrier dysfunction in ulcerative colitis: emerging mechanisms and dietary intervention perspective. Am. J. Transl. Res. 2023;15(2):653-677.*

87. *Moliterni C, Vari F, Schifano E, Tacconi S, Stanca E, Friuli M, et al. Lipotoxicity of palmitic acid is associated with DGAT1 downregulation and abolished by PPARα activation in liver cells. J. Lipid Res. 2024;65(12):100692. doi:10.1016/j.jlr.2024.100692.*

88. *Ko CW, Qu J, Black DD, Tso P. Regulation of intestinal lipid metabolism: current concepts and relevance to disease. Nat. Rev. Gastroenterol. Hepatol. 2020;17(3):169-183. doi:10.1038/s41575-019-0250-7.*

89. *An J, Wang Q, Yi S, Liu X, Jin H, Xu J, et al. The source of the fat significantly affects the results of high-fat diet intervention. Sci. Rep. 2022;12(1):4315. doi:10.1038/s41598-022-08249-2.*

90. *Gori M, Altomare A, Cocca S, Solida E, Ribolsi M, Carotti S, et al. Palmitic acid affects intestinal epithelial barrier integrity and permeability in vitro. Antioxidants. 2020;9(5):417. doi:10.3390/antiox9050417*

91. *Nagao I, Ambrosini YM. High-fat diet enhances cell proliferation and compromises intestinal permeability in a translational canine intestinal organoid model. BMC Mol. Cell Biol. 2024;25(1):14. doi:10.1186/s12860-024-00512-w*

92. *Zeiringer S, Wiltschko L, Glader C, Reiser M, Absenger-Novak M, Fröhlich E, et al. Development and characterization of an in vitro intestinal model including extracellular matrix and macrovascular endothelium. Mol. Pharm. 2023;20(10):5173-5184. doi: 10.1021/acs.molpharmaceut.3c00532.*

93. *Hariri N, Thibault L. High-fat diet-induced obesity in animal models. Nutr. Res. Rev. 2010;23(2):270-299. doi: 10.1017/S0954422410000168.*

94. *Memmola R, Petrillo A, Di Lorenzo S, Altuna SC, Habeeb BS, Soggiu A, et al. Correlation between olive oil intake and gut microbiota in colorectal cancer prevention. Nutrients. 2022;14(18):3749. doi:10.3390/nu14183749.*

95. *Dang Y, Ma C, Chen K, Chen Y, Jiang M, Hu K, et al. The effects of a high-fat diet on inflammatory bowel disease. Biomolecules. 2023;13(6):905. doi:10.3390/biom13060905.*

96. *Rohr MW, Narasimhulu CA, Rudeski-Rohr TA, Parthasarathy S. Negative effects of a high-fat diet on intestinal permeability: a review. Adv. Nutr. 2020;11(1):77-91. doi:10.1093/advances/nmz061.*

97. *Xie Y, Ding F, Di W, Lv Y, Xia F, Sheng Y, et al. Impact of a high-fat diet on intestinal stem cells and epithelial barrier function in middle-aged female mice. Mol. Med. Rep. 2020; 21:1133-1144. doi:10.3892/mmr.2020.10932.*

98. *Enriquez JR, McCauley HA, Zhang KX, Sanchez JG, Kalin GT, Lang RA, et al. A dietary change to a high-fat diet initiates a rapid adaptation of the intestine. Cell Rep. 2022;41(7):111641. doi:10.1016/j.celrep.2022.111641.*

99. *Lefebvre C, Tiffay A, Breemeersch CE, Dreux V, Bôle-Feysot C, Guérin C, et al. Sex-dependent effects of a high fat diet on metabolic disorders, intestinal barrier function and gut microbiota in mouse. Sci. Rep. 2024;14(1):19835. doi:10.1038/s41598-024-70931-4.*

100. *Tanaka S, Nemoto Y, Takei Y, Morikawa R, Oshima S, Nagaishi T, et al. High-fat diet-derived free fatty acids impair the intestinal immune system and increase sensitivity to intestinal epithelial damage. Biochem. Biophys. Res. Commun. 2020;522(4):971-977. doi:10.1016/j.bbrc.2019.11.158.*

101. *Shi C, Li H, Qu X, Huang L, Kong C, Qin H, et al. High fat diet exacerbates intestinal barrier dysfunction and changes gut microbiota in intestinal- specific ACF7 knockout mice. Biomed. and Pharmacother. 2019;110:537-545. doi:10.1016/j.biopha.2018.11.100.*

102. *Stojanovic O, Altirriba J, Rigo D, Spiljar M, Evrard E, Roska B, et al. Dietary excess regulates absorption and surface of gut epithelium through intestinal PPARalpha. Nat Commun. 2021;12(1):7031. doi:10.1038/s41467-021-27133-7.*

103. *Karwad MA, Couch DG, Wright KL, Tufarelli C, Larvin M, Lund J, et al. Endocannabinoids and endocannabinoid-like compounds modulate hypoxia- induced permeability in CaCo-2 cells via CB1, TRPV1, and PPARα. Biochem. Pharmacol. 2019;168:465-472. doi:10.1016/j.bcp.2019.07.017*

104. *Torelli Hijo AH, Coutinho CP, Alba-Loureiro TC, Moreira Leite JS, Bargi- Souza P, Goulart-Silva F. High fat diet modulates the protein content of nutrient transporters in the small intestine of mice: possible involvement of PKA and PKC activity. Heliyon. 2019;5(10):e02611. doi:10.1016/j.heliyon.2019.e02611.*

105. *Luo Y, Yang S, Wu X, Takahashi S, Sun L, Cai J, et al. Intestinal MYC modulates obesity-related metabolic dysfunction. Nat. Metab. 2021;3(7):923-939. doi:10.1038/s42255-021-00421-8.*

106. *Little TJ, Horowitz M, Feinle-Bisset C. Modulation by high-fat diets of gastrointestinal function and hormones associated with the regulation of energy intake: implications for the pathophysiology of obesity. Am. J. Clin. Nutr. 2007;86(3):531-541. doi:10.1093/ajcn/86.3.531.*

107. *Hou K, Wu ZX, Chen XY, Wang JQ, Zhang D, Xiao C, et al. Microbiota in health and diseases. Signal Transduct. Target Ther. 2022;7(1):135. doi:10.1038/s41392-022-00974-4.*

108. *Pflughoeft KJ, Versalovic J. Human microbiome in health and disease. Annu. Rev. Pathology Mech. Dis. 2012;7(1):99-122. doi:10.1146/annurev-pathol-011811-132421.*

109. *de Vos WM, Tilg H, Van Hul M, Cani PD. Gut microbiome and health: mechanistic insights. Gut. 2022;71(5):1020-1032. doi:10.1136/gutjnl-2021-326789.*

110. *Malesza IJ, Malesza M, Walkowiak J, Mussin N, Walkowiak D, Aringazina R, et al. High-fat, western-style diet, systemic inflammation, and gut microbiota: a narrative review. Cells. 2021;10(11):3164. doi:10.3390/cells10113164.*

111. *Zsálig D, Berta A, Tóth V, Szabó Z, Simon K, Figler M, et al. A review of the relationship between gut microbiome and obesity. Appl. Sci. 2023;13(1):610. doi:10.3390/app13010610.*

112. *Andújar-Tenorio N, Prieto I, Cobo A, Martínez-Rodríguez AM, Hidalgo M, Segarra AB, et al. High fat diets induce early changes in gut microbiota that may serve as markers of ulterior altered physiological and biochemical parameters related to metabolic syndrome. Effect of virgin olive oil in comparison to butter. PLoS One. 2022;17(8):e0271634. doi:10.1371/journal.pone.0271634.*

113. *Nogal A, Valdes AM, Menni C. The role of short-chain fatty acids in the interplay between gut microbiota and diet in cardio-metabolic health. Gut Microbes. 2021;13(1):1-24. doi:10.1080/19490976.2021.1897212*

114. *Losacco MC, de Almeida CFT, Hijo AHT, Bargi-Souza P, Gama P, Nunes MT, et al. High-fat diet affects gut nutrients transporters in hypo and hyperthyroid mice by PPAR-a independent mechanism. Life Sci. 2018;202:35-43. doi:10.1016/j.lfs.2018.03.053.*

115. *Beyaz S, Mana MD, Roper J, Kedrin D, Saadatpour A, Hong SJ, et al. High-fat diet enhances stemness and tumorigenicity of intestinal progenitors. Nature. 2016;531(7592):53-58. doi:10.1038/nature17173.*

116. *D'Aquila T, Zembroski AS, Buhman KK. Diet induced obesity alters intestinal cytoplasmic lipid droplet morphology and proteome in the postprandial response to dietary fat. Front. Physiol. 2019;10:180. doi:10.3389/fphys.2019.00180.*

117. *Wisniewski JR, Friedrich A, Keller T, Mann M, Koepsell H. The impact of high-fat diet on metabolism and immune defense in small intestine mucosa. J Proteome Res. 2015;14(1):353-365. doi:10.1021/pr500833v.*

118. *Petit V, Arnould L, Martin P, Monnot MC, Pineau T, Besnard P, et al. Chronic high-fat diet affects intestinal fat absorption and postprandial triglyceride levels in the mouse. J. Lipid Res. 2007;48(2):278-287. doi:10.1194/jlr.M600283-JL*

119. *Jais A, Bruning JC. Hypothalamic inflammation in obesity and metabolic disease. J Clin Invest. 2017;127(1):24-32. doi:10.1172/JCI88878.*

120. *Kawai T, Autieri MV, Scalia R. Adipose tissue inflammation and metabolic dysfunction in obesity. Am. J. Physiology-Cell Physiol. 2021;320(3):C375-C391. doi:10.1152/ajpcell.00379.2020.*

121. *Yoo S, Jung SC, Kwak K, Kim JS. The role of prebiotics in modulating gut microbiota: implications for human health. Int. J. Mol. Sci. 2024;25(9):4834. doi:10.3390/ijms25094834.*

122. *Kasper P, Martin A, Lang S, Kütting F, Goeser T, Demir M, et al. NAFLD and cardiovascular diseases: a clinical review. Clin. Res. Cardiol. 2021;110(7):921-937. doi:10.1007/s00392-020-01709-7.*

123. *Pertwee RG, Howlett AC, Abood ME, Alexander SPH, Di Marzo V, Elphick MR, et al. International union of basic and clinical pharmacology. LXXIX. Cannabinoid receptors and their ligands: beyond $CB_1$ and $CB_2$. Pharmacol. Rev. 2010;62(4):588-631. doi:10.1124/pr.110.003004.*

124. *Lu HC, Mackie K. Review of the endocannabinoid system. Biol. Psychiatry Cogn. Neurosci. Neuroimaging. 2021;6(6):607-615. doi:10.1016/j.bpsc.2020.07.016.*

125. *Mehrpouya-Bahrami P, Chitrala KN, Ganewatta MS, Tang C, Murphy EA, Enos RT, et al. Blockade of CB1 cannabinoid receptor alters gut microbiota and attenuates inflammation and diet-induced obesity. Sci. Rep. 2017;7(1):15645. doi:10.1038/s41598-017-15154-6.*

126. *Cuddihey H, Cavin JB, Keenan CM, Wallace LE, Vemuri K, Makriyannis A, et al. Role of CB1 receptors in the acute regulation of small intestinal permeability: effects of high-fat diet. Am J Physiol Gastrointest Liver Physiol. 2022;323(3):G219-G238. doi:10.1152/ajpgi.00341.2021.*

127. *Wiley MB, DiPatrizio NV. Diet-induced gut barrier dysfunction is exacerbated in mice lacking cannabinoid 1 receptors in the intestinal epithelium. Int J Mol Sci. 2022;23(18):10549. doi:10.3390/ijms231810549.*

128. *Gorelick J, Assa-Glazer T, Zandani G, Altberg A, Sela N, Nyska A, et al. THC and CBD affect metabolic syndrome parameters including microbiome in mice fed high fat-cholesterol diet. J. Cannabis Res. 2022;4(1):27. doi:10.1186/s42238-022-00137-w.*

129. *Pirozzi C, Coretti L, Opallo N, Bove M, Annunziata C, Comella F, et al. Palmitoylethanolamide counteracts high-fat diet-induced gut dysfunction by reprogramming microbiota composition and affecting tryptophan metabolism. Front. Nutr. 2023;10:1143004. doi:10.3389/fnut.2023.1143004.*

130. *Schwartz GJ, Fu J, Astarita G, Li X, Gaetani S, Campolongo P, et al. The lipid messenger OEA links dietary fat intake to satiety. Cell Metab. 2008;8(4):281-288. doi:10.1016/j.cmet.2008.08.005.*

131. *Nomura DK, Morrison BE, Blankman JL, Long JZ, Kinsey SG, Marcondes MCG, et al. Endocannabinoid hydrolysis generates brain prostaglandins that promote neuroinflammation. Science. 2011;334(6057):809-813. doi:10.1126/science.1209200.*

132. *DiPatrizio NV, Astarita G, Schwartz G, Li X, Piomelli D. Endocannabinoid signal in the gut controls dietary fat intake. Proc Natl Acad Sci U S A. 2011;108(31):12904-12908. doi:10.1073/pnas.1104675108.*

133. *Ignatowska-Jankowska BM, Baillie GL, Kinsey S, Crowe M, Ghosh S, Owens RA, et al. A cannabinoid CB1 receptor-positive allosteric modulator reduces neuropathic pain in the mouse with no psychoactive effects. Neuropsychopharmacology. 2015;40(13):2948-2959. doi:10.1038/npp.2015.148.*

134. *Tandon P, Abrams ND, Carrick DM, Chander P, Dwyer J, Fuldner R, et al. Metabolic regulation of inflammation and its resolution: current status, clinical needs, challenges, and opportunities. J. Immunol. 2021;207(11):2625-2630. doi:10.4049/jimmunol.2100829*

135. *Sipe JC, Chiang K, Gerber AL, Beutler E, Cravatt BF. A missense mutation in human fatty acid amide hydrolase associated with problem drug use. Proc. Natl. Acad. Sci. 2002;99(12):8394-8399. doi:10.1073/pnas.082235799.*

136. *Ramesh D, Gamage TF, Vanuytsel T, Owens RA, Abdullah RA, Niphakis MJ, et al. Dual inhibition of endocannabinoid catabolic enzymes produces enhanced antiwithdrawal effects in morphine-dependent mice. Neuropsychopharmacology. 2013;38(6):1039-1049. doi:10.1038/npp.2012.269.*

137. *Kumar Singh A, Cabral C, Kumar R, Ganguly R, Kumar Rana H, Gupta A, et al. Beneficial effects of dietary polyphenols on gut microbiota and strategies to improve delivery efficiency. Nutrients. 2019;11(9):2216. doi:10.3390/nu11092216.*

138. *Papadaki A, Nolen-Doerr E, Mantzoros CS. The effect of the mediterranean diet on metabolic health: a systematic review and meta-analysis of controlled trials in adults. Nutrients. 2020;12(11):3342. doi:10.3390/nu12113342.*

139. *Kuda O, Rossmeisl M, Kopecky J. Omega-3 fatty acids and adipose tissue biology. Mol. Asp. Med. 2018;64:147-160. doi:10.1016/j.mam.2018.01.004.*

140. *Cani PD, Amar J, Iglesias MA, Poggi M, Knauf C, Bastelica D, et al. Metabolic endotoxemia initiates obesity and insulin resistance. Diabetes. 2007;56(7):1761-1772. doi:10.2337/db06-1491.*

141. *Davani-Davari D, Negahdaripour M, Karimzadeh I, Seifan M, Mohkam M, Masoumi S, et al. Prebiotics: definition, types, sources, mechanisms, and clinical applications. Foods. 2019;8(3):92. doi:10.3390/foods8030092.*

142. *Wang Z, Klipfell E, Bennett BJ, Koeth R, Levison BS, Dugar B, et al. Gut flora metabolism of phosphatidylcholine promotes cardiovascular disease. Nature. 2011;472(7341):57-63. doi:10.1038/nature09922.*

143. *Liu L, Li Q, Yang Y, Guo A. Biological function of short-chain fatty acids and its regulation on intestinal health of poultry. Front. Vet. Sci. 2021;8:736739. doi:10.3389/fvets.2021.736739.*

144. *Herman R, Kravos NA, Jensterle M, Janež A, Dolžan V. Metformin and insulin resistance: a review of the underlying mechanisms behind changes in GLUT4-mediated glucose transport. Int. J. Mol. Sci. 2022;23(3):1264. doi:10.3390/ijms23031264.*

145. *Blagov AV, Orekhova VA, Sukhorukov VN, Melnichenko AA, Orekhov AN. Potential use of antioxidant compounds for the treatment of inflammatory bowel disease. Pharmaceuticals (Basel). 2023;16(8):1150. doi:10.3390/ph16081150.*

146. *Mishra J, Stubbs M, Kuang L, Vara N, Kumar P, Kumar N. Inflammatory bowel disease therapeutics: a focus on probiotic engineering. Mediat. Inflamm. 2022;2022:9621668-9621715. doi:10.1155/2022/9621668.*

147. *Van der Windt DJ, Sud V, Zhang H, Tsung A, Huang H. The effects of physical exercise on fatty liver disease. Gene Expr. 2018;18(2):89-101. doi:10.3727/105221617*

148. *Knowler WC, Barrett-Connor E, Fowler SE, Hamman RF, Lachin JM, Walker EA, et al. Reduction in the incidence of type 2 diabetes with lifestyle intervention or metformin. N. Engl. J. Med. 2002;346(6):393-403. doi:10.1056/NEJ*

149. *Chen L, Li L, Chen J, Li L, Zheng Z, Ren J, et al. Oleoylethanolamide, an endogenous PPAR-α ligand, attenuates liver fibrosis targeting hepatic stellate cells. Oncotarget. 2015;6(40):42530-42540. doi:10.18632/oncotarget.6466.*

150. *Yao E, Luo L, Lin C, Wen J, Li Y, Ren T, et al. OEA alleviates apoptosis in diabetic rats with myocardial ischemia/reperfusion injury by regulating the PI3K/Akt signaling pathway through activation of TRPV1. Front. Pharmacol. 2022;13:964475. doi:10.3389/fphar.2022.964475.*

151. *Tellez LA, Medina S, Han W, Ferreira JG, Licona-Limon P, Ren X, et al. A gut lipid messenger links excess dietary fat to dopamine deficiency. Science. 2013;341(6147):800-802. doi:10.1126/science.1239275.*

152. *Seguella L, Corpetti C, Lu J, Pesce M, Basili Franzin S, Palenca I, et al. Oleoylethanolamide-producing Lactobacillus paracasei F19 improves metabolic and behavioral disorders by restoring intestinal permeability and microbiota-gut-brain axis in high-fat diet-induced obese male mice. Brain Behav. Immun. 2025;127:25-44. doi:10.1016/j.bbi.2025.02.014.*

153. *Di Paola M, Bonechi E, Provensi G, Costa A, Clarke G, Ballerini C, et al. Oleoylethanolamide treatment affects gut microbiota composition and the expression of intestinal cytokines in Peyer's patches of mice. Sci. Rep. 2018;8(1):14881. doi:10.1038/s41598-018-32925-x*

154. *Karwad MA, Macpherson T, Wang B, Theophilidou E, Sarmad S, Barrett DA, et al. Oleoylethanolamine and palmitoylethanolamine modulate intestinal permeability in vitro via TRPV1 and PPARalpha. FASEB J. 2017;31(2):469-481. doi:10.1096/fj.201500132.*

155. *Rhodes CH, Hong BV, Tang X, Weng CY, Kang JW, Agus JK, et al. Absorption, anti-inflammatory, antioxidant, and cardioprotective impacts of a novel fasting mimetic*

*containing spermidine, nicotinamide, palmitoylethanolamide, and oleoylethanolamide: a pilot dose-escalation study in healthy young adult men. Nutr. Res. 2024;132:125-135. doi:10.1016/j.nutres.2024.10.006.*

*156. Cazzola R, Rondanelli M. N-Oleoyl-Phosphatidyl-Ethanolamine and epigallo catechin-3-gallate mitigate oxidative stress in overweight and class I obese people on a low-calorie diet. J. Med. Food. 2020;23(3):319-325. doi:10.1089/jmf.2019.0145.*

*157. Meccariello R, Santoro A, D'Angelo S, Morrone R, Fasano S, Viggiano A, et al. The epigenetics of the endocannabinoid system. Int. J. Mol. Sci. 2020;21(3):1113. doi:10.3390/ijms21031113.*

*158. Mohammad AA, Urban Spillane L, Pittman B, Flynn LT, De Aquino JP, Bassir NA, et al. Sex differences in the acute effects of oral THC: a randomized, placebo-controlled, crossover human laboratory study. Psychopharmacol. Berl. 2024;241(10):2145-2155. doi:10.1007/s00213-024-06625-6.*

*159. Cani PD, Plovier H, Van Hul M, Geurts L, Delzenne NM, Druart C, et al. Endocannabinoids - at the crossroads between the gut microbiota and host metabolism. Nat. Rev. Endocrinol. 2016;12(3):133-143. doi:10.1038/nrendo.2015.211.*

*160. Gouvea-Silva JG, Costa-Oliveira Cda, Ramos YJ, Mantovanelli DF, Cardoso MS, Viana-Oliveira LD, et al. Is there enough knowledge to standardize a Cannabis sativa L medicinal oil preparation with a high content of cannabinoids? Cannabis Cannabinoid Res. 2023;8(3):476-486. doi:10.1089/can.2022.0076.*

*161. Alhouayek M, Bottemanne P, Subramanian KV, Lambert DM, Makriyannis A, Cani PD, et al. N -Acylethanolamine-hydrolyzing acid amidase inhibition increases colon N -palmitoylethanolamine levels and counteracts murine colitis. FASEB J. 2015;29(2):650-661. doi:10.1096/fj.14-255208.*

# 3. Lipotoxicity of palmitic acid is associated with DGAT1 downregulation and abolished by PPAR$\alpha$ activation in liver cells


## Abstract

Lipotoxicity refers to the harmful effects of excess fatty acids on metabolic health, and it can vary depending on the type of fatty acids involved. Saturated and unsaturated fatty acids exhibit distinct effects, though the precise mechanisms behind these differences remain unclear. Here, we investigated the lipotoxicity of palmitic acid (PA), a saturated fatty acid, compared with oleic acid (OA), a monounsaturated fatty acid, in the hepatic cell line HuH7. Our results demonstrated that PA, unlike OA, induces lipotoxicity, endoplasmic reticulum (ER) stress, and autophagy inhibition. Compared with OA, PA treatment leads to less lipid droplet (LD) accumulation and a significant reduction in the mRNA and protein level of diacylglycerol acyltransferase 1 (DGAT1), a key enzyme of triacylglycerol synthesis. Using modulators of ER stress and autophagy, we established that DGAT1 downregulation by PA is closely linked to these cellular pathways. Notably, the ER stress inhibitor 4-phenylbutyrate can suppress PA-induced DGAT1 downregulation. Furthermore, knockdown of DGAT1 by siRNA or with A922500, a specific DGAT1 inhibitor, resulted in cell death, even with OA. Both PA and OA increased the oxygen consumption rate; however, the increase associated with PA was only partially coupled to ATP synthesis. Importantly, treatment with GW7647 a specific PPAR$\alpha$ agonist mitigated the lipotoxic effects of PA, restoring PA-induced ER stress, autophagy block, and DGAT1 suppression.

In conclusion, our study highlights the crucial role of DGAT1 in PA-induced lipotoxicity, broadening the knowledge of the mechanisms underlying hepatic lipotoxicity and providing the basis for potential therapeutic interventions.

**Keywords**: Diacylglycerol acyltransferase; endoplasmic reticulum stress; hepatic cells; lipid droplets; lipotoxicity.

## 1.Introduction

Excess dietary fatty acids are often linked to pathological conditions such as obesity, insulin resistance, type 2 diabetes mellitus, and cardiovascular diseases (1). Among factors contributing to these conditions, a key role is played by the overload of triacylglycerols (TAGs) in sites other than adipose tissue, where lipids generally should not accumulate (2). The main form of TAG storage in cells is lipid droplets (LD), dynamic organelles found in all cell types, from yeast to humans. Regardless of their morphology, LDs share a similar structural organization, consisting of a phospholipid monolayer surrounding a core filled with neutral lipids, primarily TAGs and sterol esters (3). Various proteins, including perilipins (PLIN), associate with the monolayer to regulate different aspects of LD dynamics, such as growth and degradation, and are thought to influence LD positioning within the cell (3). LDs are closely associated with the endoplasmic reticulum (ER) (3,4) where a significant proportion of cellular TAG is synthesized via the glycerol 3-phosphate pathway, which involves the esterification of fatty acids to a glycerol 3-phosphate backbone (5-8). The final and committed step of TAG synthesis is the esterification of fatty acyl-CoA, catalyzed by diacylglycerol acyltransferase (DGAT) 1 and DGAT2.

These enzymes differ in their biochemical, cellular, and physiological functions: DGAT1 is exclusively localized in the ER (9,10) while DGAT2 is found in the ER and around LDs (9,10). They have non-redundant roles; DGAT1 preferentially deals with exogenous fatty acids, whereas DGAT2 is important for TAG synthesis with de novo lipogenesis-derived fatty acids. Both enzymes are considered potential therapeutic targets for various diseases (11).

The accumulation of lipids in the liver, known as steatosis, can lead to more severe pathological conditions, such as steatohepatitis and cirrhosis (12). Considering the liver's essential role in regulating lipid homeostasis, alteration of hepatic metabolism can impact the health of the entire organism. Evidence shows that the type of dietary fatty acids can differently influence liver function. While a diet high in saturated fatty acids induces toxicity and cell death, an excess of monounsaturated or polyunsaturated fatty acids, although causing steatosis, is typically not toxic (13). This has shifted the prevailing paradigm that lipid accumulation is always toxic; instead, TAG accumulation may act as a protective mechanism against the harmful effects of free fatty acids (FFA). The greater the FFAs incorporated into TAGs, the lower their associated toxicity. Exposing hepatocytes to excess long-chain saturated fatty acids (SFA) induces inflammation, inhibits insulin signaling, and promotes ER stress, ultimately leading to cell death (15,16). In contrast, unsaturated fatty acids are not toxic at comparable concentrations and can protect cells from SFA-induced lipotoxicity (17-19). Both *in vitro* and *in vivo* studies have demonstrated that inactivating or downregulating stearoyl-CoA desaturase 1 (SCD1), the key enzyme responsible for introducing double bonds into long-chain SFA (20), increases lipotoxicity, underscoring the role of acyl chain unsaturation in modulating toxicity.

Despite this knowledge, the exact molecular mechanisms underlying these effects remain partially understood and often controversial. Therefore, elucidating the impact of different lipid species on lipotoxicity is essential to develop targeted therapies for liver diseases.

Saturated palmitic acid (PA) and monounsaturated fatty acid oleic acid (OA) are among the most prevalent fatty acids in diet and serum (21). Studies indicate that PA exerts a toxic effect on the liver, while OA is non-cytotoxic and can protect against PA-induced toxicity (22,23). Additionally, the endogenous conversion of PA to OA can reduce hepatotoxicity by promoting incorporation into TAG (24). With this study, we explored the molecular mechanisms underlying SFA lipotoxicity in hepatic cells. We found that PA-induced lipotoxicity was associated with ER stress and autophagy block. Notably, PA treatment led to fewer and smaller LD accumulation than OA, indicating a reduced capacity for incorporating into TAG. PA significantly downregulated DGAT1 expression at both mRNA and protein levels, with a mechanism dependent on ER stress and autophagy. PPAR$\alpha$ activation alleviated PA-associated lipotoxicity and restored DGAT1 expression. In the simple animal model Caenorhabditis elegans, PA reduced lifespan, induced ER stress, and led to the accumulation of LDs with distinct morphologies compared to OA. In conclusion, by highlighting the role of DGAT1 as a key regulator of saturated fat-associated lipotoxicity, this study could be useful in setting up new therapeutic approaches for high-fat diet-associated liver disease treatments.

## 2.Materials and Methods

### 2.1 Cell treatments and reagents

Human hepatocellular carcinoma cell lines Huh-7 and HepG2 were maintained in Dulbecco's Modified Eagle Me- dium (DMEM) low glucose with 10% fetal bovine serum (FBS), 100 U/ml penicillin, 100 μg/ml streptomycin, and 2 mM glutamine. Cells were cultured at 37◦C with 5% partial pressure of $CO_2$ in a humidified atmosphere. Oleic acid (OA, COD. 75090), palmitic acid (PA, COD. 506345), palmitoleic acid (C16:1, COD. 76169), stearic acid (C 18:0, COD. 85679), and bovine serum albumin (BSA), and fraction V fatty acid-free (COD. 03117057001) were purchased from Merck. Fatty acids were dissolved in fatty-acid-free BSA at a final molar ratio of ~2:1 fatty acids/BSA, close to the value observed in human serum (25), and diluted to a proper final concentration in DMEM just before cell treatments. Thapsigargin (COD. sc- 24017), Myriocin (COD. sc-201397), and Tunicamycin (COD. Sc3506a) were purchased from Santa Cruz. Bafilomycin (COD. 54645S) and LY294002 (COD. 9901) were from Cell Signaling. GW7647 (COD. HY-13861), A922500 (COD. HY- 10038), 4-phorbol butyrate (PBA, COD. HY-A0281), and Torin 1 (COD. HY13003) were from MedChemExpress. 2-tetradecyl glycidic acid (TDGA) was kindly provided by Dr M. Guzma´ n (School of Biology, Complutense University, 28,040). Cell viability was assayed on adherent cells by the crystal violet assay method exactly as reported in (26). Intracellular peroxide was detected using 2′,7′-dichlorofluorescein diac- etate (DCFH-DA, Sigma-Aldrich) staining as reported in (27).

DGAT1 silencing by siRNA transfection. For the siRNA transfection experiments, Huh-7 cells were seeded in plates at 60% confluence and were transfected with a pool of three different DGAT1 siRNAs or with negative control (CRH5722).

The oligonucleotides were purchased from Cohesion Biosciences (London, United Kingdom). Ac- cording to the manufacturer's instructions, the cells were transfected with 20 nM of siRNA using ScreenFect®siRNA (S- 4001) (ScreenFect). After 48 h, cells were harvested for mRNA and protein extraction.

## 2.2 *Caenorhabditis elegans* growth conditions and lifespan assay

Nematodes were cultured as reported in (28). Lifespan analysis was conducted at 16◦C and death was recorded when the nematodes ceased responding to gentle touch with a platinum wire. For the fertility assay, synchronized N2 worms were incubated at 16◦C on NGM plates seeded with various treatments to allow for embryo laying. Subsequently, indi- vidual animals were transferred onto a fresh plate daily, and the total number of progenies was counted using a Zeiss Axiovert 25 microscope. This process was continued until the mother worms ceased laying eggs.

## 2.3 LDs staining and fluorescence analyses

Oil Red O (ORO) and BODIPY stain protocols were used for LD analysis. Following fatty acid treatments, HuH-7 cells were washed with PBS, fixed with 4% paraformaldehyde in PBS pH 7.4 for 20 min, at room temperature, and stained with 0.5% ORO solution in isopropanol for 1 h. After PBS washing, the LD number and area were quantified using FIJI software version 2.9.0/1.53. To enhance LD detection, Z-stack projection was used to combine images from different focal planes, ensuring that LDs across z-axes were captured. The resulting

12 bit images were converted to 8 bit, Gaussian blurred (sigma = 1), and a threshold of 25. The images were then converted to a binary mask, and adjacent objects were sepa- rated using the watershed function. The "analyze particle" function identified LDs in a single cell. For BODIPY staining, cells were seeded onto coverslips in 12-well plates at 60%–80% confluence. After treatment, cells were washed twice with PBS and incubated for 15 min at 37◦C with BODIPY 493/503 at a dilution of 1:1000 in PBS from a 1 mg/ml stock solution. After that, coverslips were washed three times with PBS and used for rapid image acquisition. Images were captured with a Zeiss

LSM900 confocal laser scanning microscope (Zeiss) equipped with a 63×/1.40 NA oil immersion objective. In *C. elegans*, ORO staining was performed on 1-day adult worms treated with fatty acids from embryo hatching. Worms were collected and fixed in a 60% isopropanol for 10 min, and stained with a working ORO solution (0.5% ORO in iso- propanol/water 3:2). Following incubation for 1 h at room temperature, worms were centrifuged, washed with M9 buffer, and visualized under an Axio Observer fluorescence microscope (Zeiss) equipped with Apotome 3. Worms were

imaged at two magnifications: 10X (with a 100 μm scale bar) and 63X objectives (with a 10 μm scale bar). LD assessment was

conducted using FIJI software version 2.9.0/1.53. In the case of BODIPY 493/503 staining animals were processed as described in (29).

## 2.4 RNA extraction and RT-qPCR analyses

Total RNA was extracted from cell pellets with the Easy- Pure RNA kit (TransGen Biotech Co., Ltd). RNA quantifica- tion was performed using a NanoDrop One

Spectrophotometer (Thermo Scientific). For cDNA synthesis HIScript III RT SuperMix for qPCR (+gDNA wiper) kit was used (Vazyme Biotech), following the manufacturer's in- structions. Gene expression analyses were performed through real-time PCR using iTaq Universal Sybr Green Supermix (Bio-Rad) run on the CFX Connect Real-time System (BioRad). A comparative analysis was performed. Glyceral- dehyde-3-phosphate dehydrogenase (*GAPDH*) and *RPLP0* were evaluated as housekeeping genes, resulting in stable overall samples. *RPLP0* was chosen as the reference gene. Primer se- quences are reported in supplemental Table S1. For analyses in worms, RNA was extracted from 200 1-day- old wild-type adults using the miRNeasy Micro Kit (Qiagen). The Real-time analysis was conducted using the ICycler IQ Multicolor Real-Time Detection System (Bio-Rad), according to (29). Selective primers (200 nM) were utilized, and their sequences are provided in supplemental Table S1.

## 2.5 Oxygen consumption rate (OCR) measurements

Oxygen consumption rate (OCR) was measured with a polarographic approach using a Clark-type oxygen electrode in a water-jacketed chamber (Hansatech Instruments, Nor- folk, UK) (30). Briefly, after trypsinization, cells were resuspended in a "respiration" buffer (buffer A = 75 mM sucrose, 5 mM $KH_2PO_4$, 40 mM KCl, 0.5 mM EDTA, 3 mM $MgCl_2$, 30 mM Tris-HCl, pH 7.4) and inserted inside the water- jacketed chamber (final volume 1 ml). For the determination of the "respiratory fingerprint," cells were treated with oligomycin (2 μg/μl), CCCP (1 μM), antimycin A (15 nM), and rotenone (1 μM).

## 2.6 Western blot

Proteins were extracted from cells using RIPA lysis buffer (Cell Signaling #9806). Total protein levels were determined using the Bradford method (Bio-Rad Labora- tories). After boiling for 5 min, proteins were loaded and separated by SDS-polyacrylamide gel electrophoresis. The samples were then transferred onto a nitrocellulose mem- brane (Bio-Rad Laboratories) and blocked at room temperature for 1 h using 5% (w/v) non-fat milk in TBS-Tris buffer (Tris-buffered saline (TBS) plus 0.5% (v/v) Tween- 20, TTBS). The membranes were incubated with the following primary antibodies: Glucose regulatory protein 78 (GRP78) (76-E6) (Santa Cruz # sc-13539, rat 1:1000), microtubule-associated protein 1$\alpha$/1$\beta$-light chain 3 (MAP LC3$\alpha$/$\beta$ (G-4) Santa Cruz #sc-398822, mouse 1:1000), P62 (SQSTM1/p62 (D-3) Santa Cruz #sc-28359, Mouse 1:1000),

DGAT1 (Santa Cruz #sc-32861, rabbit 1:1000), DGAT2 (Novus Biologicals, #NBP1-71701, mouse 1:1000), SCD1 (Santa Cruz #sc-58420, Mouse 1:1000), Adipose Triglyceride Lipase (ATGL, Santa Cruz, sc-365278, mouse 1:1000), PERK (Santa Cruz sc377400, mouse 1:1000), spliced XBP1 (XBP1s, Cell Signaling, 40435s, rabbit 1:1000), Beclin1 (Cell Signaling, 3495s, rabbit 1:1000). After washing with TTBS, the blots were incubated with peroxidase-conjugated monoclonal secondary antibodies (Sigma-Aldrich) at 1:10.000 dilutions at room temperature for 1–2 h. The blots were then washed thoroughly in TTBS. Western blotting analyses were per- formed using the Amersham ECL Advance Western Blot- ting Detection Kit (GE Healthcare) and the ChemiDoc system (Bio-Rad) was used for chemiluminescence measurement.

## 2.7 Fatty acid β-oxidation measurements

The rate of fatty acid oxidation (FAO) was determined as the formation of labeled $CO_2$ (31). Briefly, Huh-7 cells were incubated at 37◦C in the presence of 0.5 mM albumin-bound [1–$^{14}$C]PA (0.1 Ci/mol). After 20 min, reactions were stopped by 0.3 ml of 2 M perchloric acid (reactions proceed at a linear rate up to 45 min). At the same time, 0.15 ml of benzethonium hydroxide (1 M in methanol) was injected into a center well containing a filter paper. Samples were allowed to equilibrate for an additional hour at 4◦C, and the center well (with the $CO_2$ fixed as bicarbonate) was transferred into vials for radioactivity counting. To evaluate the contribution of peroxisome to β-oxidation, experiments were conducted in the presence of 5 μM TDGA, an irreversible specific inhibitor of carnitine-palmitoyltransferase-1 (CPT1), a mitochondrial rate-limiting enzyme for long-chain FAO, as reported in (32). TDGA was added to cells 1h before measurements.

## 2.8 Thin-layer chromatography (TLC) analysis of lipids

Total lipids were extracted using methyl-tert-butyl ether, as reported in (33). Lipids were loaded on silica gel plates for thin-layer chromatography (TLC) separation. Plates were developed with hexane/ethyl ether/acetic acid (70/30/1; v/v/v) for neutral lipid separation, with toluene/methanol (70/30; v/v) for sphingolipid separation. After development, plates were uniformly sprayed with 10% cupric sulfate in 8% aqueous phosphoric acid, allowed to dry for 10 min at room temperature, and then placed into a 145◦C oven for 10 min, as reported in (34). The ChemiDoc system (Bio-Rad) was used to measure spot intensity. Different lipid species were identified by developing specific standards in the same experimental conditions.

## 2.9 Statistical analysis

Results are expressed as means ± standard deviation (SD). Statistical differences were evaluated using GraphPad Prism version 8.3.0 for Windows. The comparison was made using one-way analysis of variance (ANOVA) and 2-way ANOVA for oxygraphy experiments. After Tukey post hoc analysis, differences between groups were considered statistically significant when $P < 0.05$.

# 3. Results

## 3.1 Lipotoxicity and lipid droplets accumulation

We first established a lipid accumulation model with OA or PA in liver cells to investigate the underlying lipotoxicity mechanism. Therefore, we conducted vitality assays in two different hepatic cell lines Huh-7 and HepG2. A dose- and time-dependent decrease in cell viability was measured after treatments with PA, compared to BSA and OA, in both cell lines, with a greater effect in Huh-7 cells (Supplementary Figures 1A, 1B and 3D, 3E). A slight but significant reduction in cell viability was observed by prolonging (>48 hours) the incubation with maximal concentrations of OA (Supplementary Figures 1A, B and 3D, E).

ORO staining and chromatographic analyses were used to follow the development of lipid accumulation. Compared to PA, OA induced a greater number of larger and brighter LDs in the central region of the cells. In contrast, PA was incorporated into smaller, less numerous, and evenly distributed LDs (Figures 1A-C). TLC analysis confirmed significantly higher TAG accumulation upon equimolar administration of OA than PA (Figure 1D).

We analyzed the expression of key enzymes involved in LD metabolism. PA significantly reduced DGAT1 protein levels compared to OA and BSA (Figures

1E, F), while OA markedly increased DGAT2 expression relative to the other groups (Figures 1E, F). These changes were correlated with lower DGAT1 mRNA levels in PA-treated cells compared to those treated with BSA and OA, and higher DGAT2 mRNA levels in OA-treated cells compared to BSA and PA (Figure 1G). No significant changes were observed in the levels of ATGL, an enzyme involved in the lipolysis of TAG into diacylglycerols and free fatty acids (Supplementary Figure 2). Additionally, mRNA levels of PLIN2 and PLIN3, proteins closely associated with LDs and involved in their remodeling, were significantly elevated in PA-treated cells compared to BSA and OA (Figure 1G).

Given the marked reduction of DGAT1 expression induced by PA, we investigated its potential role in lipotoxicity. We conducted experiments where OA was added to cells silenced for DGAT1 (siDGAT1) or treated with the specific DGAT1 inhibitor A922500. In the siDGAT1 cells, DGAT1 expression was drastically reduced at both mRNA and protein levels (Figures 1H, L), without inducing compensatory effects on the DGAT2 isoform (Figure 1I). Under these conditions, OA/siRNA cells accumulated fewer LDs than control cells (OAsh). At a concentration that diminished TAG synthesis by about 50% (data not shown), A922500 induced a reduction in LD accumulation in cells treated with OA (OA/DGAT1i) (Figure 1A-C), In both scenarios, reduced cell viability was noted (Figure 1M), compared with OA, mirroring the conditions observed in PA-treated cells.

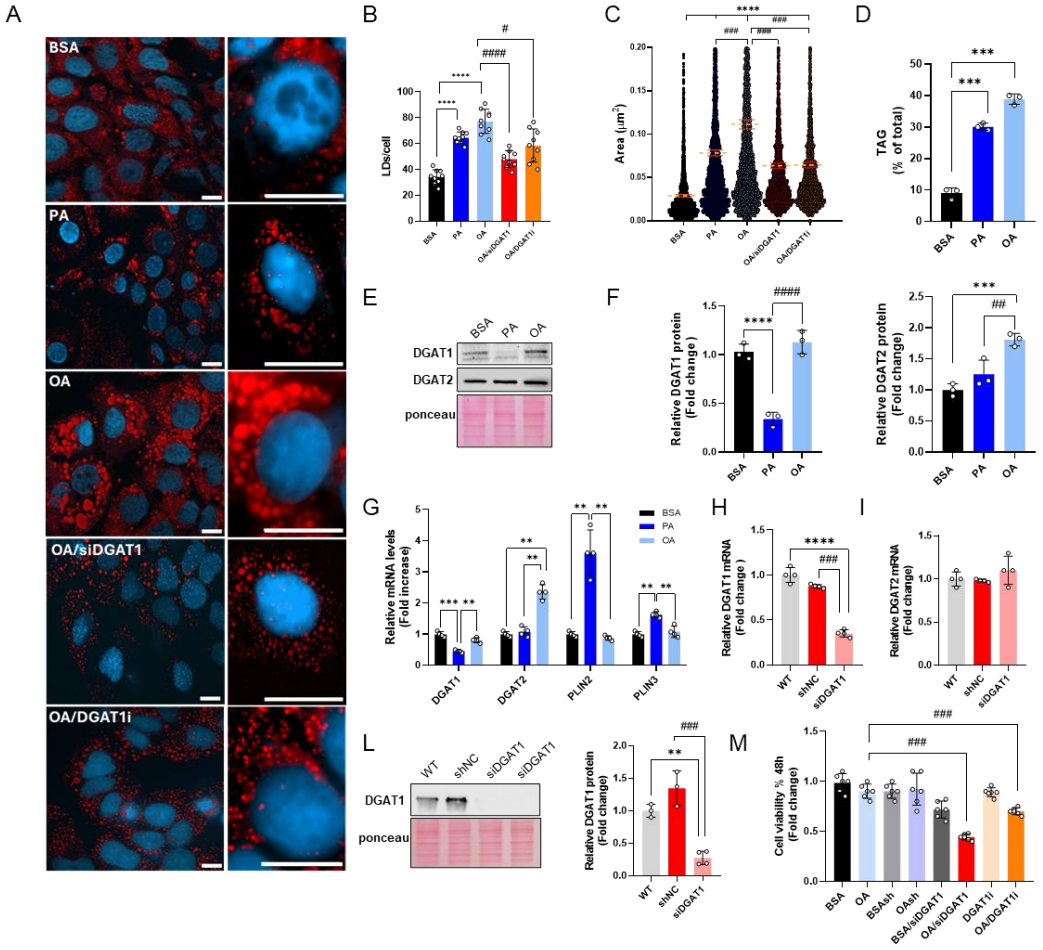


**Fig. 1. Analysis of LD and lipid metabolic enzymes in Huh-7 cells.** A: Representative images obtained by confocal microscopy of Huh-7 cells stained with Oil Red O and DAPI after treatments for 24 h with BSA, 200 µM PA, or 200 µM OA, 200 µM OA + siRNADGAT1 (OA/siDGAT1), and 200 µM OA + 40 µM DGAT1 inhibitor (OA/DGAT1i). Image acquisition through Axio Observer fluorescence microscope (Zeiss) equipped with Apotome 3, magnification 40x air, and 63x oil (scale bar 10 µm). B, C: The number of LD/cells and area were obtained with FIJI software. Red bars represent the mean values of the area. (D) Triacylglycerol (TAG) quantification after TLC analysis. Values are expressed as % of total neutral lipids. (E, F) Representative Western blot, and relative quantifications, of DGAT1, and DGAT2 from Huh-7 cells treated with BSA, 200 µM PA, or 200 µM OA. (G) Real-time RTPCR analysis of DGAT1, DGAT2, perilipin (PLIN) 2, and PLIN3 in Huh-7 cells treated 24 h with BSA, 200 µM PA, or 200 µM OA. (H, I) Real-time RT-PCR and (J) Western blot analysis of DGAT1 in Huh-7 cells silenced for DGAT1 with siRNA. (K) Cell viability assay. Values are means ± SD. Asterisks indicate differences compared to the control, while hashtags denote group differences. (*) $P < 0.05$; (**) $P < 0.01$; (***) $P < 0.005$; (****) $P < 0.001$.

## 3.2 Palmitic acid-induced DGAT1 downregulation is related to ER stress and autophagy block

ER stress and autophagy are closely associated with lipotoxicity, especially in the context of excess FFAs and disrupted lipid metabolism (16). We found that PA, compared to OA, induced ER stress, as indicated by increased expression of XBP1s and GRP78, along with decreased expression of PERK, which are specific ER stress markers (Figure 2A). Additionally, PA significantly increased the LC3-II/LC3-I ratio and p62 expression (Figure 2B). Treatment with bafilomycin 1, which targets the vacuole-type H+ -ATPase preventing lysosomal acidification, does not increase the amount of autophagic dots promoted by PA treatment, confirming that PA inhibits the autophagic flux (Figure 2B). Similar results were observed in the hepatoblastoma cell line HepG2, where PA, compared to OA, induced ER stress, an autophagic block, and a significant reduction in DGAT1 protein expression (see Supplementary Figure 3).

To explore the association between DGAT1 and ER stress we measured DGAT1 expression in the presence of Thapsigargin and tunicamycin, two specific ER stress activators. In treatments with Thapsigargin and tunicamycin, DGAT1 expression was significantly reduced (Figure 2C). In the same context, DGAT2 expression did not change (Figure 2C). Notably, the specific ER stress inhibitor PBA, at a concentration reducing PA-induced XBP1s, restored DGAT1 expression (Figure 2D).

To further investigate whether the PA-induced reduction of DGAT1 was related to the block of autophagy flux, we used LY294002 and Torin 1, two autophagy activators. Both compounds increased DGAT1 but not DGAT2 expression (Figure 2E). These findings suggest that DGAT1 suppression depends on ER stress and autophagy block.

Interestingly, LY294002 and Torin 1 promoted LD accumulation in HuH-7 cells, and the effect was completely prevented by bafilomycin and DGAT1i (Figure 2F). These findings support the notion that DGAT1 plays a crucial role in LD formation associated with the autophagic process.

To assess the impact of fatty acid unsaturation on lipotoxicity, we treated cells with various fatty acids, including PA, OA, palmitoleic acid, and stearic acid. Analysis of BODIPY-stained LDs revealed morphological differences among the treatment groups (Figure 2G). Quantitative analysis of LDs showed that PA and stearic acid resulted in fewer and smaller LDs than OA and palmitoleic acid (Figures 2H, I). Notably, palmitoleic acid exhibited no significant cytotoxicity at the same concentration as PA, while stearic acid was cytotoxic, unlike OA (Figure 2L). Since SCD1 is the key enzyme in fatty acid desaturation, we investigated the modulation of SCD1 by these fatty acids. Compared to BSA, the monounsaturated fatty acids palmitoleic acid and OA significantly reduced SCD1 protein expression (Figure 2M). In contrast, saturated fatty acids did not alter SCD1 expression. Additionally, OA treatment led to a marked decrease in SCD1 mRNA levels compared to PA (Figure 2N).

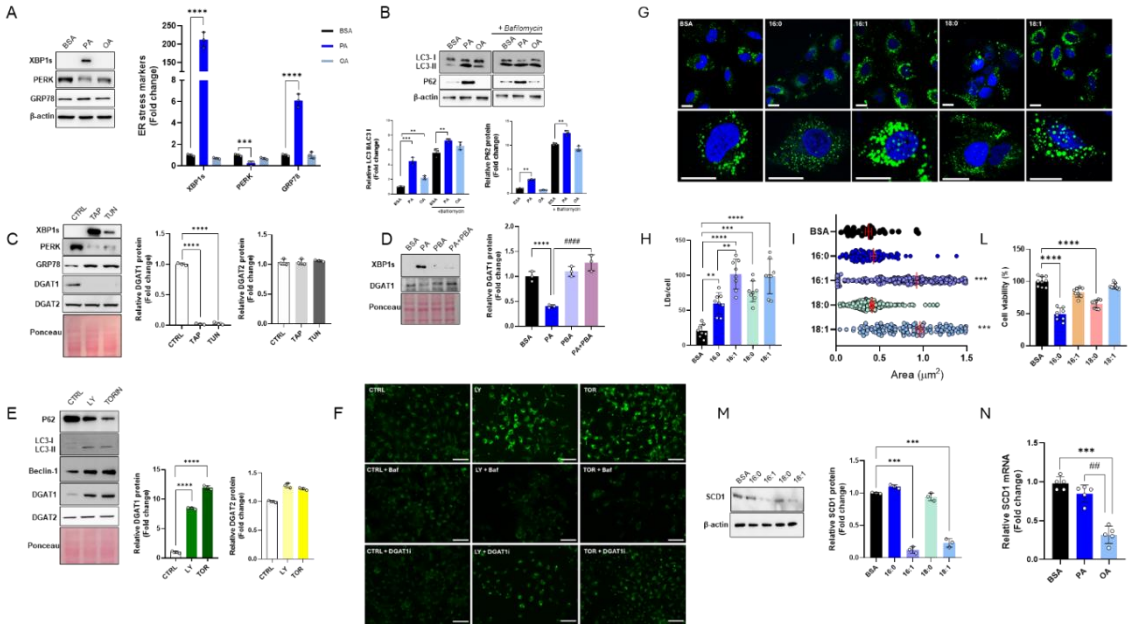

**Fig. 2. DGAT1 inhibition is related to endoplasmic reticulum stress and autophagy block and depends on fatty acyl-chain saturation.** A: Western blot analysis, and relative quantification, of spliced XBP1 (XBP1s), PERK, and GRP78 in cells treated with BSA, 200 μM PA, or 200 μM OA. B: Western blot analysis and relative quantification of LC3I, LC3II, and P62 in cells treated with BSA, 200 μM PA, or 200 μM OA, in the presence or absence of 200 nM Bafilomycin added 2h before incubation ending. C: Western blot analysis, of XBP1s, PERK, GRP78, DGAT1, and DGAT2, and relative quantification of DGAT1 and DGAT2, in control (CTRL) and cells treated with 1 μM Thapsigargin and 1 μM Tunicamycin for 24 h. D: Western blot analysis of XBP1s and DGAT1, and relative quantification of DGAT1, in BSA cells and treated with 500 nM 4-phorbol butyrate (PBA) for 24 h. E: Western blot analysis of LC3I, LC3II, Beclin-1, DGAT1, and DGAT2, and relative quantification of DGAT1 and DGAT2 in CTRL and cells treated with 10 μM LY20094002 and 200 nM Torin 1. F: Images of BODIPY-stained Huh-7 neutral lipids, obtained by fluorescent microscopy after treatments with 10 μM LY20094002 and 200 nM Torin 1, in the presence or absence of 200 nM Bafilomycin and 40 μM DGAT1 inhibitor. (Scale bar 100 μm). G: Confocal microscopy after BODIPY and DAPI stains nuclei in Huh-7 cells treated for 24 h with BSA, 200 μM PA, 200 μM palmitoleic acid (C16:1), 200 μM stearic acid (C18:0), 200 μM OA. H, I: The measurements of numbers and area of LDs/cells were obtained with FIJI software. Red bars represent the mean values of the LD area. J: Vitality test for Huh-7 cells treated for 24 h with BSA, 200 μM PA, 200 μM C16:1, 200 μM C18:0, and 200 μM OA. K: Western blot analysis of stearoyl-

CoA desaturase-1 (SCD1) and relative quantification in Huh-7 cells treated with BSA, 200 μM PA, 200 μM C16:1, 200 μM C18:0, and 200 μM OA. L: Realtime RT-PCR analysis of SCD1 in Huh-7 cells treated for 24 h with BSA, 200 μM PA, or 200 μM OA. Asterisks indicate differences compared to the control, while hashtags among groups. Values are means ± SD. (*) $P < 0.05$; (**) $P < 0.01$; (***) $P < 0.005$; (****) $P < 0.001$.

## 3.3 Palmitic and oleic acid are differently metabolized in hepatic cells

Once internalized, fatty acids can be stored as TAG, converted into phospholipids and sphingolipids (such as ceramide and sphingomyelin), or undergo β-oxidation for ATP production (Figure 3A). To investigate the fate of PA and OA in liver cells, we incubated the cells with (1-$^{14}$C)PA (53 mCi/mmol) or (1-$^{14}$C) OA (53 mCi/mmol) for 4 hours, followed by TLC analysis of total lipids. Our results indicate that PA and OA are differently distributed in cell lipids. Specifically, PA is incorporated into cholesteryl esters and phospholipids to a greater extent than OA, while OA is more significantly incorporated into TAG compared to PA (Figure 3B). PA is a substrate for the *de novo* synthesis of ceramide, a toxic lipid species (35). Although we found no significant differences in ceramide levels between PA- and OA-treated cells (data not shown), PA compared to OA-treated cells induced significantly higher mRNA expression of ceramide synthase 6 (*cers6*), which synthesizes C16 acyl chain ceramides (Figure 3C). Importantly, treatment with myriocin, an inhibitor of the key enzyme in *de novo* ceramide synthesis, did not alleviate PA-associated lipotoxicity (Figure 3D), suggesting that this pathway is not involved in PA-induced lipotoxicity.

We evaluated the potential link between PA-induced lipotoxicity and changes in mitochondrial function by measuring the oxygen consumption rate (OCR). Compared to BSA, PA, and OA increased basal respiration, with OA exhibiting

a more pronounced effect (Figure 3E). The higher basal respiration observed in OA-treated cells was associated with enhanced ATP-dependent respiration. In contrast, the increase in OCR induced by PA was uncoupled from ATP synthesis, indicating reduced oxidative phosphorylation (OXPHOS) efficiency, whereas OA improved this efficiency. OA also resulted in lower non-mitochondrial respiration compared to the elevated level of PA-treated cells. Furthermore, OA increased the respiratory reserve (RR), which was diminished in PA-treated cells (Figure 3E). When basal respiration was measured in the presence of TDGA, a specific irreversible inhibitor of CPT1, OA-induced basal respiration was greatly reduced than PA (Figure 3F). These results suggest that β-oxidation from OA contributes more than PA to OCR. To differentiate the contributions of mitochondria and peroxisomes to β-oxidation, we measured the rate of labeled $CO_2$ production in the presence of TDGA. The peroxisomal β-oxidation, determined as the difference between total and TDGA-sensitive β-oxidation, was significantly higher in PA-treated cells than in OA-treated cells (Figure 3G) and correlated with increased levels of $H_2O_2$ (Figure 3H). The observed differences in β-oxidation were not linked to changes in CPT1 mRNA levels, which remained stable across treatments (Figure 3I). However, we noted a small but significant increase in PPAR$\alpha$ mRNA levels, a key regulator of fatty acid metabolism in the liver, particularly in OA-treated cells (Figure 3L).

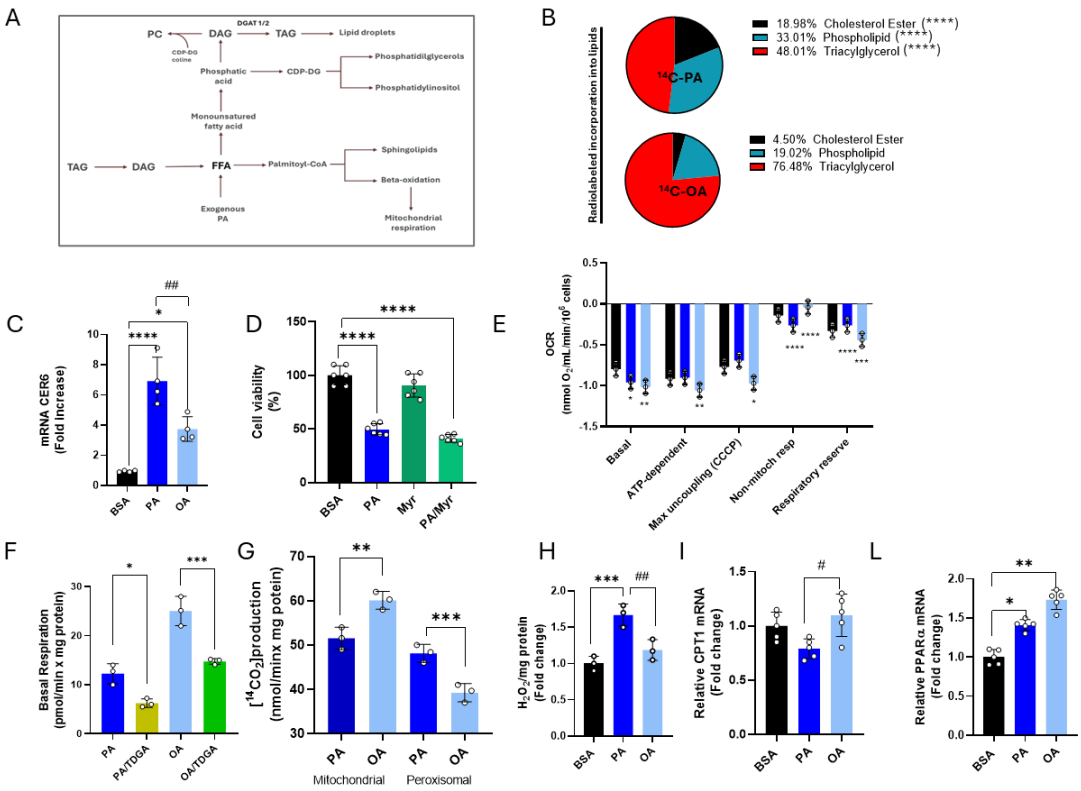


**Fig. 3. Lipid composition and bioenergetics parameters of Huh-7 cells.** A: Schematic representation of the fate of exogenous added fatty acids (FFA) in cells. Once entered in the cells, FFA can be converted into esters of SH-CoA and incorporated into complex lipids or β-oxidized. B: Distribution of [1-14C]-PA or [1-14C]-OA in Huh-7 after 4 h of incubation with the labeled substrates. C: Real-time RT-PCR analysis of CER6 in Huh-7 cells treated for 48 h with BSA, 200 μM PA, or 200 μM OA. D: Vitality test for Huh-7 cells treated for 24 h with BSA, 200 μM PA, 3.7 μM Myriocin (Myr), and PA + Myr. E: Basal respiration measurements in Huh-7 cells treated for 24 h with BSA, 200 μM PA, or 200 μM OA. Cells were inserted in the oxygraphic chamber and treated with 2 μg/μl oligomycin, 1 μM CCCP, 15 nM antimycin A, and 1 μM rotenone. Basal = basal cell respiration value; ATP-dependent = basal-oligomycin value (ATP-dep.); Max uncoupling (CCCP) = CCCP value (MaxUN); non-mitochondrial respiration = basal-CCCP value (Non-mit.); Respiratory Reserve = CCCP-antimycin A value (RR). Oligomycin: inhibitor of complex V of mitochondrial oxidative phosphorylation (ATP synthase). CCCP: carbonyl cyanide m-chlorophenylhydrazone, an uncoupler of mitochondrial oxidative phosphorylation; antimycin A: inhibitor of complex III of mitochondrial oxidative phosphorylation. Data are reported as nmol O2/ml/min/106 cells. F: Basal respiration of Huh-7 cells treated for 24 h with BSA, 200 μM PA, or 200 μM OA, in the presence or absence of 5 μM 2-tetradecyl glycidic acid (TDGA). G: β-oxidation

in Huh-7 cells treated with BSA, 200 μM PA, or 200 μM OA, in the presence of or absence of 5 μM TDGA. The picture reports the mitochondrial and peroxisomal contribution to the total β-oxidation. H: Hydrogen peroxide (H2O2) production from Huh-7 cells after 24 h with BSA, 200 μM PA, or 200 μM OA. (I, J) Realtime RT-PCR analysis of CPT1 and PPARα in Huh-7 cells 24-hour-treated with BSA, 200 μM PA, or 200 μM OA. Asterisks indicate differences compared to the control, while hashtags among groups. Values are means ± SD. (*) $P < 0.05$; (**) $P < 0.01$; (***) $P < 0.005$; (****) $P < 0.001$.

## 3.4 PPARα activation reverses palmitic acid-induced lipotoxicity

PPARα agonists can mitigate hepatic fatty acid accumulation by stimulating β-oxidation (36). Additionally, PPARα can modulate DGAT expression (37). To investigate the role of PPARα in PA-inducing DGAT1 downregulation, we utilized the synthetic PPARα agonist GW7647. As expected, GW7647 significantly increased PPARα mRNA levels (Figure 4A). Co-incubation with PA further enhanced PPARα expression beyond that observed in PA-treated cells (Figure 4A). This was also reflected in CPT1 mRNA levels, which were significantly elevated in the GW7647/PA combination compared to PA alone (Figure 4B). Additionally, the PA/GW7647 combination significantly reduced PA-associated lipotoxicity (Figure 4C) and improved cell morphology altered by PA treatment (Figure 4D). Co-incubation with the PPARα activator notably decreased the PA-induced expression of ER stress and autophagy markers (Figure 4E). GW7647 also upregulated DGAT1 at both the protein and mRNA levels compared to PA alone (Figures 4E, F), while DGAT2 mRNA expression remained largely unchanged (Figure 4G). Interestingly, BODIPY-stained cells treated with the PA/GW7647 combination showed greater accumulation of green-stained droplets than those treated with PA alone (Figure 4H).

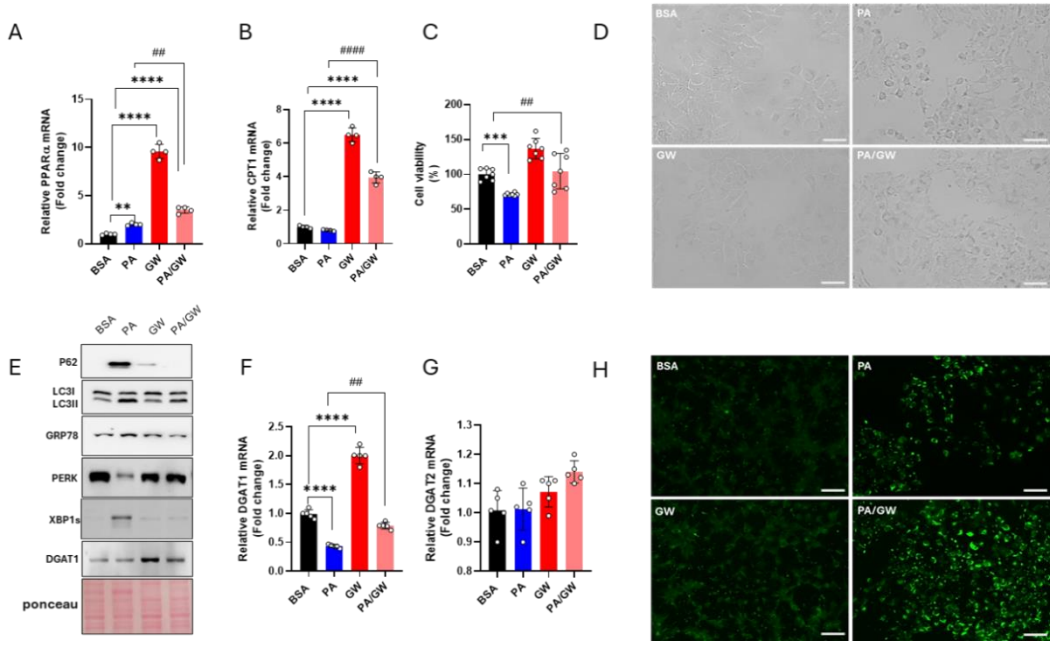


**Fig. 4. PPAR$\alpha$ agonists rescue PA-induced lipotoxicity in hepatic cells.** A, B: Real-time RT-PCR analysis of PPAR$\alpha$ and CPT1 in Huh7 cells 24-hour-treated with BSA, 200 μM PA, 10 μM GW7647, 200 μM PA + 10 μM GW7647. C: Crystal violet vitality test in Huh-7 cells incubated for 24 h with BSA, 200 μM PA, 10 μM GW7647, 200 μM PA + 10 μM GW7647. D: Bright field microscopy images of HuH7 cells treated with BSA, 200 μM PA, 10 μM GW7647, 200 μM PA + 10 μM GW7647. E: Western blot analysis of P62, LC3I, LC3II, GRP78, PERK, XBP1s, and DGAT1 in Huh-7 cells treated with BSA, 200 μM PA, 10 μM GW7647, 200 μM PA + 10 μM GW7647. F, G: Real-time RT-PCR analysis of DGAT1 and DGAT2 in Huh-7 cells treated for 24 h with BSA, 200 μM PA, 10 μM GW7647, 200 μM PA + 10 μM GW7647. H: Images of BODIPY-stained Huh-7 neutral lipids, obtained by fluorescent microscopy after cell treatments with BSA, 200 μM PA, 10 μM GW7647, 200 μM PA + 10 μM GW7647. (Scale bar 100 μm). Asterisks indicate differences compared to the control, while hashtags among groups. Values are means ± SD. (**) $P < 0.01$; (***) $P < 0.005$; (****) $P < 0.001$.

## 3.5 Metabolic alterations induced by palmitic acid in *Caenorhabditis elegans* mirror those seen in cultured liver cells

*Caenorhabditis elegans* is a valuable model organism for studying a wide range of human diseases at both metabolic and genomic levels *in vivo*. This nematode has been widely utilized across various research fields (27,28,38). Notably, its intestine retains many specialized liver functions (39), and key aspects of lipid metabolism are conserved between nematodes and mammals, with lipid synthesis and modification occurring primarily in the *Caenorhabditis elegans* intestine (40). We assessed whether PA could replicate its effects in *Caenorhabditis elegans*. ORO-stained LDs in the worms exhibited characteristics like those observed in liver cells, with OA inducing more abundant and larger LDs than PA (Figure 5A-C). Viability analysis of the wild-type population revealed that PA significantly reduced nematode lifespan compared to BSA, with 50% of viability reached at day 9 (Figure 5D). In the same experimental conditions, OA treatment induced an extended lifespan with 50% viability reached at day 14, while the BSA (control) was at day 10 (Figure 5D). Fertility analysis (Figure 5E) indicated a notable increase, compared with BSA, in offspring numbers after OA supplementation. Examination of apoptotic bodies, quantified under fluorescence microscopy after acridine orange staining, revealed an elevated number of apoptotic bodies following both PA and OA treatments at 3 days (Figure 5F). This effect intensified at 7 days of adulthood, with PA treatment resulting in a higher accumulation of apoptotic bodies, than OA (Figure 5F).

We analyzed the expression of genes related to ER stress, such as *atf6* and the spliced and unspliced forms of *xbp1* (Figure 5G). While *atf6* increased in OA-treated nematodes, compared to controls and PA-treated nematodes, a significant increase in both spliced and unspliced forms of the *xbp1* gene was measured in PA-treated nematodes compared to BSA- and OA-treated

nematodes (Figure 5G). Additionally, the mRNA levels of *dgat1* and *dgat2* were higher in OA compared to both PA and BSA (Figure 5G), while the *dgat1* gene did not significantly change in PA, compared with controls.

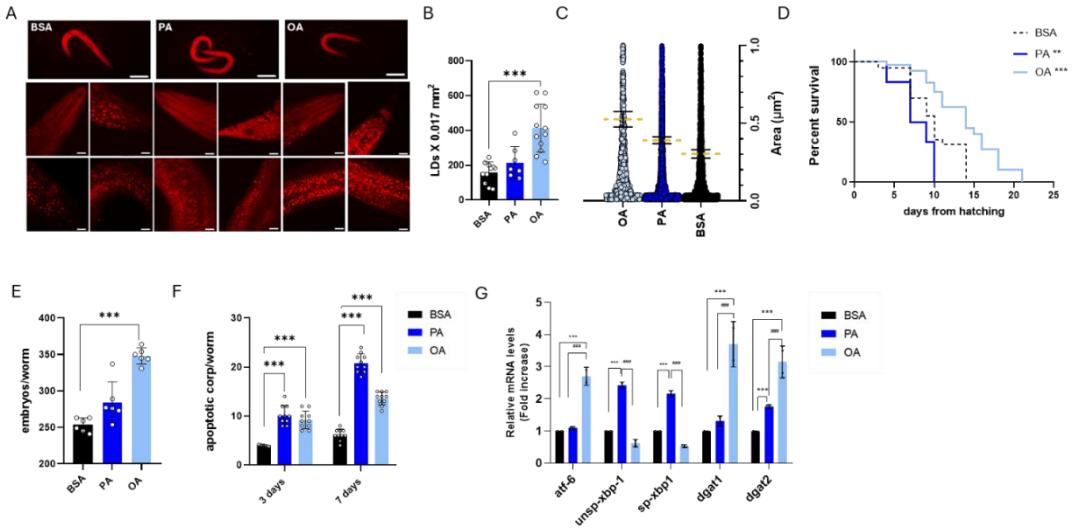


**Fig. 5. Impact of OA and PA on nematode life span, lipid metabolism enzymes, and ER stress**. A: Oil Red O staining of 1-day adult worms treated with BSA, 200 µM OA, or 200 µM PA and (B-C) related LD number and area quantification. D: Kaplan-Meier survival plot of N2 worms fed with heat-killed OP50 and supplemented with BSA, 200 µM OA, or 200 µM PA. E: Average embryo production per worm. F: Apoptotic corpses in 3-day adults and 7-day adults supplemented with 200 µM OA or 200 µM PA compared to the BSA treated control population. G: Real-time qPCR analysis of Atf-6, unsp-Xbp-1, sp-Xbp-1, Dgat-1, and Dgat-2 genes in treated 1-day adults. Asterisks indicate the P-values (log-rank test) normalized to the control. Hashtags refer to differences among groups. (***) $P < 0.005$; (****) $P < 0.001$.

## 4. Discussion

Lipotoxicity resulting from chronic high exposure to FFAs poses a significant threat to cellular health and is implicated in various metabolic diseases. Understanding the mechanisms is crucial for developing strategies to mitigate the effects of lipotoxicity and improve metabolic health. The lipotoxicity of saturated fatty acids is closely associated with ER stress and the inhibition of autophagic flux, contributing to cellular dysfunction and metabolic diseases (41-46). We report that PA increases cell death, activates ER stress responses, and impairs autophagic function in two different hepatic cell models and in the in vivo model Caenorhabditis elegans. The use of *C. elegans*, a well-established model for lipid metabolism studies, provided a whole-organism context to validate selected PA-induced metabolic alterations beyond the cellular level. In contrast to OA, PA leads to lower LD accumulation and DGAT1 downregulation, which may contribute to lipotoxicity and metabolic dysfunction. Studies have highlighted the crucial role of DGAT1 in TAG recycling and its protective effects against FFA-induced lipotoxicity (47). DGAT1 regulates TAG levels during adipocyte differentiation, promoting proper lipid storage, and preventing lipotoxicity (48). Its role in adipogenesis and metabolic regulation highlights its significance in maintaining overall metabolic health. In this study, we demonstrated for the first time the role of ER stress and impaired autophagy induced by PA in regulating DGAT1, highlighting the complex interplay between lipid metabolism and cellular stress responses. Consistent with previous findings (49,50), we observed that knocking down DGAT1 using specific inhibitors like A922500 or through siRNA increased lipotoxicity in the presence of OA, emphasizing DGAT1's protective role in lipid metabolism. Additionally, the fact that palmitoleic acid does not induce lipotoxic effects, unlike PA,

highlights the importance of fatty acid saturation in determining cellular outcomes.

DGAT1 and DGAT2 both reside in the ER and play essential roles in lipid metabolism (51,52). Following treatment with OA, we observed the upregulation of DGAT2 in hepatic cells, as reported in (53), and *Caenorhabditis elegans*. These findings highlight the importance of DGAT2 in lipid metabolism across various biological systems. By increasing DGAT2 levels, OA may provide a protective mechanism against lipotoxicity. Enhanced TAG synthesis can help sequester excess FFAs thereby reducing the risk of metabolic dysfunction. The differential regulation of DGAT2, PLIN2, and PLIN3 in response to PA and OA directly correlates with the structural differences in LDs that we observed and previously reported (54). The PLIN family of proteins, including PLIN2 and PLIN3, is crucial in regulating LD biology (55). PLIN2 has a crucial role in maintaining LD morphology (56,57), with the knockdown of PLIN2 leading to enlarged LDs and increased hydrolytic activity of TAGs (58). The PLIN3 functions as an LD stabilizer and is essential for intracellular lipid trafficking (59). Recent studies indicated that PLIN3 is associated with micro-droplets (60). Furthermore, the upregulation of PLIN2 in conditions of pathological lipid accumulation in the liver has been reported (61). The increase in PLIN2 may represent a compensatory mechanism to counteract elevated lipid levels and reduce lipotoxicity, particularly since an autophagy block can hinder effective lipid turnover and exacerbate cellular stress (62). PLIN2 knockdown in mice enhances autophagy and protects against severe ER stress-induced hepatosteatosis and hepatocyte apoptosis (62).

When TAG synthesis is impaired, excess FFAs accumulate in the cytoplasm. To mitigate the effects of this excess, cells can redirect FFAs toward membrane phospholipids (63). Additionally, inhibiting DGAT1 can reduce TAG flux and

increase phospholipid synthesis (64). While this adaptive mechanism can temporarily alleviate stress from excess FFAs, it may have long-term consequences for cellular function, such as altered membrane composition, which could lead to membrane instability or dysfunction over time. Fully saturated membrane glycerolipids can induce ER stress (54). The preferential incorporation of PA into phospholipids, we measured, may indeed contribute to ER stress. According to the findings of (65), both PA and OA elevate basal respiration rates, indicating that both fatty acids enhance mitochondrial activity and overall metabolic demand in cells. However, OA is associated with more efficient ATP synthesis, suggesting better coupling of respiration to ATP production. In contrast, PA partially uncouples respiration from ATP synthesis, potentially leading to increased energy expenditure, mitochondrial stress, and dysfunction. This difference may be attributed to the structural properties of the fatty acids; unsaturated fats like OA typically have a more favorable impact on mitochondrial functions (66). The uncoupling of respiration from ATP synthesis and the resulting increase in $H_2O_2$ production may contribute to the lipotoxic effects of PA we observed. Lipotoxicity has been linked to oxidative stress in various cellular models (67-70), primarily through the increase of reactive oxygen species (ROS) and a decrease in antioxidant defenses (71). Our results highlight distinct metabolic responses elicited by PA compared to OA, particularly concerning non-mitochondrial oxygen consumption and peroxisomal β-oxidation. The relative contributions of peroxisomal versus mitochondrial ROS can vary based on the cell type, metabolic state, and the specific fatty acids present. In some cell models, oxidative stress induced by peroxisomal $H_2O_2$ may lead to more pronounced lipotoxic effects than those caused by mitochondrial ROS (72). Given that peroxisomal β-oxidation influences oxygen consumption and $H_2O_2$ production (73), we cannot rule out the contribution of this metabolic pathway to PA-induced oxidative stress. CPT1 is crucial for fatty acid transport

into the mitochondrial matrix. Since CPT1 expression remains unchanged across groups, it suggests that fatty acid transport into the mitochondria for β-oxidation is not the rate-limiting step in this context. The measured activation of PPAR$\alpha$ may indicate signaling through other pathways that enhance fatty acid oxidation independently of CPT1 expression. While FFAs can be toxic when excessively accumulated, they are not inherently harmful if their levels are properly regulated and adequately oxidized (74). Efficient mitochondrial β-oxidation enables cells to utilize FFAs for energy, preventing the detrimental effects associated with lipid overload. Enhancing mitochondrial β-oxidation has been shown to mitigate the lipotoxic effects of PA in various cell models (64-67). Therefore, strategies aimed at increasing β-oxidation (e.g., specific dietary interventions, or pharmacological agents) may be beneficial in treating conditions related to lipotoxicity. PPAR$\alpha$ plays a crucial role in regulating peroxisomal fatty acid oxidation, which is important for lipid metabolism and energy homeostasis. PPAR$\alpha$ is activated by various ligands, including fatty acids and their derivatives, with PA and OA-reported ligands of PPAR$\alpha$ (75). We observed a modest but significant increase in PPAR$\alpha$ expression following treatment with PA, with a more pronounced effect from OA. The downregulation of DGAT1 in response to PA suggests that this regulation likely occurs independently of direct control by PPAR$\alpha$. Research suggests that under inflammatory conditions, PPAR$\alpha$ activation may downregulate specific target genes as part of a broader adaptive response to manage lipid overload and cellular stress (75). This raises the question of whether a similar mechanism is at play with PA, warranting further investigation. PPAR$\alpha$ has been shown to play a crucial role in determining cell fate during ER stress and autophagy inhibition (76). Our results indicate that the PPAR$\alpha$ agonist GW7647 completely alleviates PA-induced ER stress and autophagy block while simultaneously upregulating

DGAT1 expression. Further investigations are needed to clarify how this affects DGAT1 expression.

Our data highlight the intricate relationship between fatty acid metabolism, ER stress, autophagy, and cellular health. By prioritizing strategies to enhance fatty acid oxidation while regulating DGAT1 activity, it may be possible to mitigate the lipotoxic effects of PA and promote improved metabolic outcomes.

## 5. References


1. *Wu JHY, Micha R, Mozaffarian D. (2019) Dietary fats and cardiometabolic disease: mechanisms and effects on risk factors and outcomes. Nat. Rev. Cardiol. 16, 581-601.*
2. *Van Herpen NA, Schrauwen-Hinderling VB. (2008) Lipid accumulation in non-adipose tissue and lipotoxicity. Physiol. Behav. 94, 231-241.*
3. *Olzmann JA, Carvalho P. (2019) Dynamics and functions of lipid droplets. Nat. Rev. Mol. Cell Biol. 20, 137-155.*
4. *Blanchette-Mackie EJ, Dwyer NK, Barber T, Coxey RA, Takeda T, Rondinone CM, et al. (1995) Perilipin is located on the surface layer of intracellular lipid droplets in adipocytes. J. Lipid Res. 36, 1211-1226.*
5. *Kennedy E, Smith S, Weiss S. (1956) New synthesis of lecithin in an isolated enzyme system. Nature. 178, 594-595.*
6. *Coleman RA, Mashek DG. (2011) Mammalian triacylglycerol metabolism: synthesis, lipolysis, and signaling. Chem. Rev. 111, 6359-6386.*
7. *Takeuchi K, Reue K. (2009) Biochemistry, physiology, and genetics of GPAT, AGPAT, and lipin enzymes in triglyceride synthesis. Am. J. Physiol. Endocrinol. Metab. 296, E1195-E1209.*
8. *Kennedy E. (1957) Biosynthesis of phospholipids. Fed. Proc. 16, 847-853.*

9. *Bhatt-Wessel B, Jordan TW, Miller JH, Peng L. (2018) Role of DGAT enzymes in triacylglycerol metabolism. Arch. Biochem. Biophys. 655, 1-11.*
10. *Wilfling F, Wang H, Haas JT, Krahmer N, Gould TJ, Uchida A, et al. (2013) Triacylglycerol synthesis enzymes mediate lipid droplet growth by relocalizing from the ER to lipid droplets. Dev. Cell. 24, 384-399.*
11. *Yen CE, Stone SJ, Koliwad S, Harris C, Farese RV Jr. (2008) DGAT enzymes and triacylglycerol biosynthesis. J. Lipid Res. 49, 2283-2301.*
12. *Geng Y, Faber KN, de Meijer VE, Blokzijl H, Moshage H. (2021) How does hepatic lipid accumulation lead to lipotoxicity in non-alcoholic fatty liver disease? Hepatol. Int. 15, 21-35.*
13. *Henique C, Mansouri A, Fumey G, Lenoir V, Girard J, Bouillaud F, et al. (2010) Increased mitochondrial fatty acid oxidation is sufficient to protect skeletal muscle cells from palmitate-induced apoptosis. J. Biol. Chem. 285, 36818-36827.*
14. *Listenberger LL, Han X, Lewis SE, Cases S, Farese RV Jr, Ory DS, et al. (2003) Triglyceride accumulation protects against fatty acid-induced lipotoxicity. Proc. Natl. Acad. Sci. U. S. A. 100, 3077-3082.*
15. *Wei Y, Topczewski F, Pagliassotti MJ. (2006) Saturated fatty acids induce endoplasmic reticulum stress and apoptosis independently of ceramide in liver cells. Am. J. Physiol. Endocrinol. Metab. 291, E275-E281.*
16. *Liu X, Green RM. (2019) Endoplasmic reticulum stress and liver diseases. Liver Res. 3, 55-64.*
17. *Coll T, Eyre E, Rodriguez-Calvo R, Palomer X, Sanchez RM, Merlos M, et al. (2008) Oleate reverses palmitate-induced insulin resistance and inflammation in skeletal muscle cells. J. Biol. Chem. 283, 11107-11116.*
18. *Li Y, Hruby A, Bernstein AM, Ley SH, Wang DD, Chiuve SE, et al. (2015) Saturated fats compared with unsaturated fats and sources of carbohydrates in relation to risk of coronary heart disease: a prospective cohort study. J. Am. Coll. Cardiol. 66, 1538-1548.*

19. *Geng T, Hu W, Broadwater MH, Snider JM, Bielawski J, Russo SB, et al. (2013) Fatty acids differentially regulate insulin resistance through endoplasmic reticulum stress-mediated induction of tribbles homolog: a potential link between dietary fat composition and the pathophysiological outcomes of obesity. Diabetologia. 56, 2078-2087.*
20. *Li ZZ, Berk M, McIntyre TM, Feldstein AE. (2009) Hepatic lipid partitioning and liver damage in nonalcoholic fatty liver disease: role of stearoyl-CoA desaturase. J. Biol. Chem. 9, 5637-5644.*
21. *Carta G, Murru E, Banni S, Manca C. (2017) Palmitic acid: physiological role, metabolism, and nutritional implications. Front. Physiol. 8, 902.*
22. *Urso CJ, Zhou H. (2021) Palmitic acid lipotoxicity in microglia cells is ameliorated by unsaturated fatty acids. Int. J. Mol. Sci. 22, 9093.*
23. *Nemecz M, Constantin A, Dumitrescu M, Alexandru N, Filippi A, Tanko G, et al. (2019) The distinct effects of palmitic and oleic acid on pancreatic beta cell function: the elucidation of associated mechanisms and effector molecules. Front. Pharmacol. 9, 1554.*
24. *Wei Y, Wang D, Pagliassotti MJ. (2007) Saturated fatty acid-mediated endoplasmic reticulum stress and apoptosis are augmented by trans-10, cis-12-conjugated linoleic acid in liver cells. Mol. Cell Biochem. 1-2, 105-113.*
25. *Alsabeeh N, Chausse B, Kakimoto PA, Kowaltowski AJ, Shirihai O. (2018) Cell culture models of fatty acid overload: problems and solutions. Biochim. Biophys. Acta Mol. Cell Biol. Lipids. 1863, 143-151.*
26. *Feoktistova M, Geserick P, Leverkus M. (2016) Crystal violet assay for determining viability of cultured cells. Cold Spring Harb. Protoc. 2016, pdb.prot087379.*
27. *Salbini M, Quarta A, Russo F, Giudetti AM, Citti C, Cannazza G, et al. (2021) Oxidative stress and multi-organel damage induced by two novel phytocannabinoids, CBDB and CBDP, in breast cancer cells. Molecules. 26, 5576.*

28. *Schifano E, Conta G, Preziosi A, Ferrante C, Batignani G, Mancini P, et al. (2022) 2-hydroxyisobutyric acid (2-HIBA) modulates ageing and fat deposition in Caenorhabditis elegans. Front. Mol. Biosci. 23, 986022.*

29. *Schifano E, Zinno P, Guantario B, Roselli M, Marcoccia S, Devirgiliis C, et al. (2019) The foodborne strain Lactobacillus fermentum MBC2 triggers pept-1-dependent pro-longevity effects in Caenorhabditis elegans. Microorganisms. 7, 45.*

30. *Gnocchi D, Afonso MB, Cavalluzzi MM, Lentini G, Ingravallo G, Sabba C, et al. (2023) Inhibition of lysophosphatidic acid receptor 6 upregulated by the choline-deficient L-amino acid-defined diet prevents hepatocarcinogenesis in mice. Mol. Carcinog. 62, 577-582.*

31. *Giudetti AM, De Domenico S, Ragusa A, Maffia M, Vergara D. (2019) A specific lipid metabolic profile is associated with the epithelial-mesenchymal transition program. Biochim. Biophys. Acta Mol. Cell Biol. Lipids. 1864, 344-357.*

32. *Priore P, Giudetti AM, Natali F, Gnoni GV, Geelen MJH. (2007) Metabolism and short-term metabolic effects of conjugated linoleic acids in rat hepatocytes. Biochim. Biophys. Acta. 1771, 1299-1307.*

33. *Matyash V, Liebisch G, Kurzchalia TV, Shevchenko A, Schwudke D. (2008) Lipid extraction by methyl-tert-butyl ether for high-throughput lipidomics. J. Lipid Res. 49, 1137-1146.*

34. *Giudetti AM, Guerra F, Longo S, Santoro L, Bucci C. (2020) An altered lipid metabolism characterizes Charcot-Marie-Tooth type 2B peripheral neuropathy. Biochim. Biophys. Acta Mol. Cell Biol. Lipids. 1865, 158805.*

35. *Summers SA, Chaurasia B, Holland WL. (2019) Metabolic messengers: ceramides. Nat. Metab. 1, 1051-1058.*

36. *Rakhshandehroo M, Knoch B, Muller M, Kersten S. (2010) Peroxisome proliferator-activated receptor alpha target genes. PPAR Res. 2010, 612089.*

37. *Rakhshandehroo M, Hooiveld G, Muller M, Kersten S. (2009) Comparative analysis of gene regulation by the transcription factor PPARalpha between mouse and human. PLoS One. 4, e6796.*

38. *Kimura KD, Tissenbaum HA, Liu Y, Ruvkun G. (1997) Daf-2, an insulin receptor-like gene that regulates longevity and diapause in Caenorhabditis elegans. Science. 277, 942-946.*

39. *O'Reilly LP, Perlmutter DH, Silverman GA, Pak SC. (2014) alpha1-antitrypsin deficiency and the hepatocytes - an elegans solution to drug discovery. Int. J. Biochem. Cell Biol. 47, 109-112.*

40. *Watts JL, Ristow M. (2017) Lipid and carbohydrate metabolism in Caenorhabditis elegans. Genetics. 207, 413-446.*

41. *Yang L, Guan G, Lei L, Lv Q, Liu S, Zhan X, et al. (2018) Palmitic acid induces human osteoblast-like Saos-2 cell apoptosis via endoplasmic reticulum stress and autophagy. Cell Stress Chaperones. 23, 1283-1294.*

42. *Zeng X, Zhu M, Liu X, Chen X, Yuan Y, Li L, et al. (2020) Oleic acid ameliorates palmitic acid induced hepatocellular lipotoxicity by inhibition of ER stress and pyroptosis. Nutr. Metab. (Lond). 17, 11.*

43. *Varshney R, Varshney R, Mishra R, Gupta S, Sircar D, Roy P. (2018) Kaempferol alleviates palmitic acid-induced lipid stores, endoplasmic reticulum stress and pancreatic beta-cell dysfunction through AMPK/mTOR-mediated lipophagy. J. Nutr. Biochem. 57, 212-227.*

44. *Rada P, Gonzalez-Rodriguez A, Garcia-Monzon C, Valverde AM. (2020) Understanding lipotoxicity in NAFLD pathogenesis: is CD36 a key driver? Cell Death Dis. 11, 802.*

45. *Amir M, Czaja MJ. (2011) Autophagy in nonalcoholic steatohepatitis. Expert Rev. Gastroenterol. Hepatol. 5, 159-166.*

46. *Trauner M, Arrese M, Wagner M. (2010) Fatty liver and lipotoxicity. Biochim. Biophys. Acta. 1801, 299-310.*

47. *Chitraju C, Mejhert N, Haas JT, Diaz-Ramirez LG, Grueter CA, Imbriglio JE, et al. (2017) Triglyceride synthesis by DGAT1 protects adipocytes from lipid-induced ER stress during lipolysis. Cell Metab. 26, 407-418.e3.*

48. *Yu Y, Zhang Y, Oelkers P, Sturley SL, Rader DJ, Ginsberg HN. (2002) Posttranscriptional control of the expression and function of diacylglycerol acyltransferase-1 in mouse adipocytes. J. Biol. Chem. 277, 50876-50884.*

49. *Geng Y, Arroyave-Ospina JC, Buist-Homan M, Plantinga J, Olinga P, Reijngoud D, et al. (2023) Differential effects of oleate on vascular endothelial and liver sinusoidal endothelial cells reveal its toxic features in vitro. J. Nutr. Biochem. 114, 109255.*

50. *Van Rijn JM, Ardy RC, Kuloglu Z, Harter B, van Haaften-Visser DY, van der Doef HPJ, et al. (2018) Intestinal failure and aberrant lipid metabolism in patients with DGAT1 deficiency. Gastroenterology. 155, 130-143.e15.*

51. *Stone SJ, Levin MC, Zhou P, Han J, Walther TC, Farese RV Jr. (2009) The endoplasmic reticulum enzyme DGAT2 is found in mitochondria-associated membranes and has a mitochondrial targeting signal that promotes its association with mitochondria. J. Biol. Chem. 284, 5352-5361.*

52. *McFie PJ, Banman SL, Stone SJ. (2018) Diacylglycerol acyltransferase-2 contains a C-terminal sequence that interacts with lipid droplets. Biochim. Biophys. Acta Mol. Cell Biol. Lipids. 1863, 1068-1081.*

53. *McFie PJ, Chumala P, Katselis GS, Stone SJ. (2021) DGAT2 stability is increased in response to DGAT1 inhibition in gene edited HepG2 cells. Biochim. Biophys. Acta Mol. Cell Biol. Lipids. 1866, 158991.*

54. *Eynaudi AB, Diaz-Castro F, Borquez JC, Bravo-Sagua R, Parra V, Troncoso R. (2021) Differential effects of oleic and palmitic acids on lipid droplet-mitochondria interaction in the hepatic cell line HepG2. Front. Nutr. 8, 775382.*

55. *Itabe H, Yamaguchi T, Nimura S, Sasabe N. (2017) Perilipins: a diversity of intracellular lipid droplet proteins. Lipids Health Dis. 16, 1-11.*

56. *Xu S, Zou F, Diao Z, Zhang S, Deng Y, Zhu X, et al. (2019) Perilipin 2 and lipid droplets provide reciprocal stabilization. Biophys. Rep. 5, 145-160.*

57. *Sztalryd C, Brasaemle DL. (2017) The perilipin family of lipid droplet proteins: gatekeepers of intracellular lipolysis. Biochim. Biophys. Acta Mol. Cell Biol. Lipids. 1862, 1221-1232.*

58. *Wu Y, Chen K, Li L, Hao Z, Wang T, Liu Y, et al. (2022) Plin2-mediated lipid droplet mobilization accelerates exit from pluripotency by lipidomic remodeling and histone acetylation. Cell Death Differ. 29, 2316-2331.*

59. *Nose F, Yamaguchi T, Kato R, Aiuchi T, Obama T, Hara S, et al. (2013) Crucial role of perilipin-3 (TIP47) in formation of lipid droplets and PGE2 production in HL-60-derived neutrophils. PLoS One. 8, e71542.*

60. *Bartholomew SR, Bell EH, Summerfield T, Newman LC, Miller EL, Patterson B, et al. (2012) Distinct cellular pools of perilipin 5 point to roles in lipid trafficking. Biochim. Biophys. Acta. 1821, 268-278.*

61. *Wang Y, Zhou J, Yang Q, Li X, Qiu Y, Zhang Y, et al. (2024) Therapeutic siRNA targeting PLIN2 ameliorates steatosis, inflammation, and fibrosis in steatotic liver disease models. J. Lipid Res. 65, 100635.*

62. *Tsai T, Chen E, Li L, Saha P, Lee H, Huang L, et al. (2017) The constitutive lipid droplet protein PLIN2 regulates autophagy in liver. Autophagy. 13, 1130-1144.*

63. *Shyu P, Ng BSH, Ho N, Chaw R, Seah YL, Marvalim C, et al. (2019) Membrane phospholipid alteration causes chronic ER stress through early degradation of homeostatic ER-resident proteins. Sci. Rep. 9, 8637.*

64. *Lovsletten NG, Vu H, Skagen C, Lund J, Kase ET, Thoresen GH, et al. (2020) Treatment of human skeletal muscle cells with inhibitors of diacylglycerol acyltransferases 1 and 2 to explore isozyme-specific roles on lipid metabolism. Sci. Rep. 10, 238.*

65. *Yuzefovych L, Wilson G, Rachek L. (2010) Different effects of oleate vs. palmitate on mitochondrial function, apoptosis, and insulin signaling in L6 skeletal muscle cells: role of oxidative stress. Am. J. Physiol. Endocrinol. Metab. 299, E1096-E1105.*

66. *Sivasubramanian MK, Monteiro R, Balasubramanian P, Subramanian M. (2023) Palmitic acid induces oxidative stress, senescence and downregulates glutamate transporter expression in human brainstem astrocytes. Physiology. 38, S1.*

67. *Huang L, Zeng X, Li B, Wang C, Zhou M, Lang H, et al. (2021) Dihydromyricetin attenuates palmitic acid-induced oxidative stress by promoting autophagy via SIRT3-ATG4B signaling in hepatocytes. Nutr. Metab. (Lond). 18, 83.*

68. *Alnahdi A, John A, Raza H. (2019) Augmentation of glucotoxicity, oxidative stress, apoptosis and mitochondrial dysfunction in HepG2 cells by palmitic acid. Nutrients. 11, 1979.*

69. *Chen P, Liu H, Xiang H, Zhou J, Zeng Z, Chen R, et al. (2019) Palmitic acid-induced autophagy increases reactive oxygen species via the Ca2+/PKCalpha/NOX4 pathway and impairs endothelial function in human umbilical vein endothelial cells. Exp. Ther. Med. 17, 2425-2432.*

70. *Szczepanska P, Rychlicka M, Groborz S, Kruszynska A, Ledesma-Amaro R, et al. (2023) Studies on the anticancer and antioxidant activities of resveratrol and long-chain fatty acid esters. Int. J. Mol. Sci. 24, 7167.*

71. *Elsner M, Gehrmann W, Lenzen S. (2011) Peroxisome-generated hydrogen peroxide as important mediator of lipotoxicity in insulin-producing cells. Diabetes. 60, 200-208.*

72. *Jo DS, Park NY, Cho DH. (2020) Peroxisome quality control and dysregulated lipid metabolism in neurodegenerative diseases. Exp. Mol. Med. 52, 1486-1495.*

73. *Castillo HB, Shuster SO, Tarekegn LH, Davis CM. (2024) Oleic acid differentially affects de novo lipogenesis in adipocytes and hepatocytes. Chem. Commun. (Camb). 60, 3138-3141.*

74. *Houten SM, Violante S, Ventura FV, Wanders RJ. (2016) The biochemistry and physiology of mitochondrial fatty acid beta-oxidation and its genetic disorders. Annu. Rev. Physiol. 78, 23.*

75. *Choi SE, Jung IR, Lee YJ, Lee SJ, Lee JH, Kim Y, et al. (2011) Stimulation of lipogenesis as well as fatty acid oxidation protects against palmitate-induced INS-1 beta-cell death. Endocrinology. 152, 816-827.*

76. *Bougarne N, Weyers B, Desmet SJ, Deckers J, Ray DW, Staels B, et al. (2018) Molecular actions of PPARalpha in lipid metabolism and inflammation. Endocr. Rev. 39, 760-802.*

77. *Xu, L., Zhang, X., Tian, Y., Fan, Z., Li, W., Liu, M., et al. (2020). The critical role of PPARα in the binary switch between life and death induced by endoplasmic reticulum stress. Cell Death Dis. 11, 691.*

# 4. Epithelial-mesenchymal transition shapes the lipotoxic response of colon cancer cells to palmitic acid

## Abstract

Saturated fatty acids such as palmitic acid (PA) can induce lipotoxic stress, whereas monounsaturated fatty acids like oleic acid (OA) often promote adaptive responses through lipid droplets (LDs) formation. Here, we reveal that epithelial-mesenchymal transition (EMT) profoundly influences the lipotoxic response of colorectal cancer cells. Using the epithelial-like HCT15 and mesenchymal-like HCT116 cell lines, we combined proteomic, metabolic, and imaging analyses to elucidate how EMT status determines lipid storage capacity and resistance to PA-induced toxicity. A Basal proteomic profiling highlighted a striking divergence in metabolic changes: HCT15 cells displayed enhanced glycolysis and reduced expression of LDs biogenesis proteins, while HCT116 cells exhibited oxidative metabolism and a "lipid-rich" proteomic signature enriched in PLIN2, GPAT3, and DGAT1. Functionally, PA triggered massive cytotoxicity and failed to induce LDs in HCT15 cells, correlating with DGAT1/2 downregulation and suppressed triacylglycerol synthesis. In contrast, HCT116 cells showed modest LDs accumulation, preserved mitochondrial function, and strong resistance to lipotoxic stress. OA treatment restored LDs formation and cell viability in both

models, underscoring the protective role of unsaturated fatty acids. Notably, forced EMT induction in HCT15 cells by PMA markedly enhanced LDs accumulation and reduced PA-induced death, confirming that EMT confers metabolic plasticity and lipid-buffering capacity.

These findings demonstrate that EMT status modulates differential lipid handling and stress adaptation in colon cancer cells, linking mesenchymal transition to enhanced LDs biogenesis and survival under lipotoxic conditions.

## 1. Introduction

The colon, or large intestine, is a pivotal component of the digestive tract, primarily responsible for absorbing nutrients, water, electrolytes, and vitamins from the intestinal lumen (1). The epithelial cells lining the colon form a continuous layer connected by tight junctions (TJs) between neighboring epithelial cells, which are crucial for maintaining the integrity of the intestinal barrier (2). E-cadherin (E-cad), a calcium-dependent adhesion molecule, is prominently located at these junctions. Functional cell adhesion relies on the interaction between E-cad and cytoplasmic proteins known as catenins (3). Specifically, β-catenin (β-cat) binds to the cytoplasmic domain of E-cad, linking it to the actin cytoskeleton, thereby contributing to tissue integrity and robust cell-cell adhesion (4), (5).

Disruption of this epithelial integrity is a hallmark of the epithelial-mesenchymal transition (EMT), a dynamic process through which epithelial cells lose polarity and adhesion, acquiring mesenchymal features such as increased motility and invasiveness. EMT plays a critical role not only in development and wound healing but also in cancer progression, where it enhances metastatic potential and confers resistance to various stressors, including nutrient overload and

lipotoxicity (6). The intestinal barrier is extremely sensitive to dietary influences, with certain components capable of inducing dysfunction. A shift from traditional to a Western diet, particularly rich in saturated fats, can compromise membrane integrity, leading to gastrointestinal disorders and triggering local and systemic inflammation (7). Under high-fat dietary conditions, enzymes known as diacylglycerol O-acyltransferases (DGAT1 and DGAT2) play a crucial role in lipid metabolism. These enzymes catalyze the final step of triacylglycerol (TAG) synthesis, converting diacylglycerol and acyl-CoA into TAG. Intestinal DGAT1 is essential for dietary fat absorption and storage. In response to a high-fat diet (HFD), DGAT1 activity is upregulated, facilitating the conversion of excess diacylglycerols into TAG, which helps regulate lipid levels within intestinal cells and prevents the toxic accumulation of free fatty acids (FFAs) (8). DGAT2 also contributes to lipid accumulation in intestinal cells by supporting TAG synthesis, especially when dietary fat intake is elevated.

Nutrient overload can induce endoplasmic reticulum (ER) stress, triggering the unfolded protein response (UPR), which governs the autophagy pathway, crucial for lipid metabolism (9). The effects of ER stress and autophagy can vary by tissue. Recently, we demonstrated a differential regulation of DGAT1 and DGAT2 under lipotoxicity induced by palmitic acid (PA) in hepatic cancer cell lines (10).

PA, a saturated fatty acid, and oleic acid (OA), a monounsaturated fatty acid, are the most abundant fatty acids in the diet and plasma, representing 31% and 27% of total plasma non-esterified fatty acid, respectively (11). These fatty acids exert distinct effects on cellular metabolism. PA is often associated with pro-inflammatory responses and has been implicated in promoting cancer cell proliferation and survival (12). In contrast, OA has been linked to anti-inflammatory effects and may inhibit cancer cell growth through various

mechanisms, including the modulation of signaling pathways related to apoptosis and cell cycle regulation (13), (14). Research has shown that PA can impair intestinal barrier integrity and induce inflammation by disrupting paracellular permeability and altering TJ expression and localization (15).

Beyond classical apoptotic and necrotic mechanisms, ferroptosis has recently emerged as a distinct form of regulated cell death characterized by the accumulation of lipid peroxides derived from polyunsaturated fatty acids and critically dependent on enzymes such as acyl-CoA synthetase long chain family member 4 (ACSL4) and iron metabolism pathways (16). Several studies have shown that saturated fatty acids, including PA, can create conditions that favor ferroptosis, especially in cells with impaired lipid droplets (LDs) formation and reduced capacity to neutralize toxic lipid intermediates. In this context, comparing epithelial- and mesenchymal-like intestinal cells may provide novel insights into the relationship between lipotoxicity, EMT, and vulnerability to ferroptosis (17).

This study aims to compare the effects of PA and OA on two human colon cancer cell lines, HCT15 and HCT116, which exhibit distinct cellular characteristics. HCT116 cells display a mesenchymal-like phenotype, characterized by increased migratory and invasive capabilities, reduced E-cad expression, and alterations in cell adhesion properties (18). Conversely, HCT15 cells retain epithelial traits, including stronger cell-cell adhesion and lower motility, potentially rendering them more susceptible to lipid-induced stress and membrane dysfunction (19). From a genomic perspective, HCT116 cells are *TP53* wild-type, whereas HCT15 cells harbor a *TP53* loss-of-function mutation, a distinction that may also affect their metabolic responses (20). We found that HCT15 and HCT116 respond differently to PA treatment, regarding both lipotoxicity and LDs accumulation. Proteomic analysis showed distinct differences between the two cell lines that

align with their EMT phenotypes. Moreover, the EMT transition was able to partially reverse these differences, further supporting the idea that EMT underlies the divergent cellular behaviors observed in HCT15 and HCT116. Together, these results underscore the importance of EMT in shaping lipotoxic responses and highlight the potential of EMT-targeting strategies for modulating metabolic stress associated with fatty acid overload.

## 2. Materials and Methods

### 2.1 Cell treatments and reagents

HCT15 and HCT116 human colon cancer cell lines were maintained in Dulbecco's Modified Eagle Medium (DMEM, Sigma-Aldrich D5546) low glucose with 10% fetal bovine serum (FBS, Capricorn HI-12A), 100 U/mL penicillin, 100 μg/mL streptomycin (Sigma-Aldrich #P4333), and 2 mM glutamine (Sigma-Aldrich G7513). Cells were cultured at 37 °C with 5% partial pressure of CO2 in a humidified atmosphere. Both cell lines were regularly tested for mycoplasma contamination using a Mycoplasma Detection Kit (Aurogene, REP-MYSNC-100). OA (COD. 75090), PA (COD. 506345), and bovine serum albumin (BSA), fraction V fatty acid-free (COD. 03117057001) were purchased from Merck (Darmstadt, Germany). Fatty acids were dissolved in fatty-acid-free BSA at 8 mM concentration and were subsequently diluted to the desired final concentration in DMEM immediately before cell treatments. For cell treatments with PA and OA, we chose the concentration of 0.2 mM, which represents the physiological postprandial intestinal concentration (21), (22) and is within the concentration range of FFAs in human *plasma* (i.e., 0.2-2 mM) (22), (23). For EMT induction, colon cancer cells were plated onto a 6-well plate for 24 hours. Cells were then treated in triplicate with 100 nM Phorbol 12-myristate 13-acetate (PMA, Santa

Cruz sc-3576) for 24 h before being subjected to PA treatment for an additional 24 h. For autophagy inhibition of colon cancer cells 100 μM of chloroquine (Cell signaling #14774) were added 4h before incubation ending.

## 2.2 Cell viability assay

Cell viability was evaluated using the crystal violet assay on adherent cells. Cells were seeded in a 96-well plate at a density of 10,000 cells per well. After treatment, cells were washed with phosphate-buffered saline (PBS) and fixed with 4% paraformaldehyde (PFA) for 30 minutes at room temperature. The cells were then stained with 0.1% crystal violet (Sigma Aldrich, Cat. no. C0775) solution for 1 hour at room temperature. The stain was removed through multiple washes with distilled water until the solution was clear. The plate was left to air dry. To solubilize the crystal violet, 100% ethanol was added, and the absorbance of the dye was measured at 550 nm.

## 2.3 Analysis of proteomic data

Whole-cell lysates from colorectal cancer cell lines HCT15 and HCT116, treated with palmitic acid (PA) or with bovine serum albumin (BSA) as vehicle control, were subjected to label-free quantitative proteomic analysis. Proteins were extracted using a lysis buffer supplemented with protease and phosphatase inhibitors. Protein concentrations were determined using the bicinchoninic acid (BCA) assay. A total of 50 μg of protein per sample was used for downstream processing. Protein samples were reduced, alkylated, and subjected to trypsin digestion overnight at 37 °C using a filter-aided sample preparation (FASP) approach. For this, Amicon Ultra-0.5 mL centrifugal filters with a 30 kDa molecular weight cut-off (Millipore) were used. After digestion, samples were

additionally treated with NaCl and 5% trifluoroacetic acid (TFA) to ensure effective acidification and removal of interfering substances. Samples were then dried and reconstituted in 60 µL of 0.1% formic acid (FA). A volume of 20 µL from each sample was desalted using an Evotip Pure (Evosep, Denmark) according to the manufacturer's protocol. Peptides were analysed using an Evosep One liquid chromatography (LC) system coupled to a timsTOF HT mass spectrometer (Bruker Daltonics, Germany). The LC system operated under the 60 Samples Per Day (60 SPD) method, using a C18 performance column (EV1109; 8 cm × 150 µm, 1.5 µm particle size) maintained at 40 °C. The analytical column was connected to a fused silica emitter (10 µm inner diameter, Bruker Daltonics), integrated into a CaptiveSpray ion source (Bruker). Data were acquired in DIA-PASEF (data-independent acquisition with parallel accumulation and serial fragmentation) mode, recording spectra over an m/z range of 100-1700 and an ion mobility range of $1/K_0$ = 1.51 $V \cdot cm^{-2}$ to 0.6 $V \cdot cm^{-2}$. Data analysis was performed using DIA-NN (Data-Independent Acquisition by Neural Networks). The DIA-NN output was further processed using Perseus version 1.6.10.43 for statistical analysis and data visualization. Differential expression analysis was performed using a t-test with a significance threshold of $p < 0.01$. Venn diagrams illustrating protein overlap and uniqueness between the two cell lines were generated using InteractiVenn (24). Additional analyses were performed using Profiler (25) for functional enrichment and STRING for interactome analysis (26).

## 2.4 Analysis of cellular bioenergetic profiles using Seahorse XFp

For bioenergetic studies, 10.000 cells/well were seeded in the XFp cell culture miniplates. The results were normalized to total cell number following DAPI staining. The assay was executed in XF DMEM Medium pH 7.4 media (Agilent, Santa Clara, California, United States; Cat. #103575-100) containing 5.5 mM

glucose (Agilent, Cat. #103577-100), 2 mM L-glutamine (Agilent, Cat. #103579-100) and 1 mM sodium pyruvate (Agilent, Cat. #103578-100). Next, cells were incubated at 37 °C in a non-$CO_2$ incubator for 1 h. Oxygen consumption rate (OCR) and extracellular acidification rate (ECAR) were measured under basal conditions and in response to sequentially injected compounds at a final concentration of 1.5 μM oligomycin (Sigma-Aldrich Cat. #O4876), 2 μM FCCP (Sigma-Aldrich Cat. #C2920), and 0.5 μM rotenone (Sigma-Aldrich Cat. #R8875) + 0.5 μM antimycin A (Sigma-Aldrich Cat. #A8674) and 50 mM of 2-deoxy-D-glucose (2-DG, Sigma-Aldrich Cat. #D6134). Stocks of compounds were prepared in the same DMEM media and loaded into the delivery ports of Seahorse cartridges. The parameters related to respiration were assessed, including non-mitochondrial respiration (OCR after rotenone-antimycin A injection), basal mitochondrial respiration (ΔOCR between the steady state and after rotenone-antimycin A injection), ATP-linked respiration (ΔOCR between basal mitochondrial respiration and after oligomycin injection), and maximal mitochondrial respiration (ΔOCR between non-mitochondrial respiration and after FCCP injection). The parameters related to glycolysis were assessed, including non-glycolytic acidification (ECAR after 2-DG injection), glycolysis (ΔECAR between the steady state and after 2-DG injection), maximal glycolytic capacity (ΔECAR between non-glycolytic acidification and after oligomycin injection), and glycolytic reserve (ΔECAR between the steady state and after oligomycin injection).

## 2.5 BODIPY staining

BODIPY 493/503 staining was performed on cells cultured on coverslips (60-80% confluency) in 12-well plates. After treatment, cells were washed with PBS and

incubated for 15 minutes at 37 °C with the dye (1:1000 dilution from a 1 mg/mL stock in PBS). Following three washes with PBS, the slides were mounted using Dako Fluorescent Mounting Medium (Agilent, Santa Clara, CA, USA) and imaged with an inverted confocal microscope (Zeiss Axio Observer Z1 equipped with an LSM 780 scanning head; Zeiss, Germany). Images were acquired with ZEN Black software using the 63×/1.4 oil-immersion objective with a 20 μm scale bar. LDs number and area were quantified using FIJI software (version 2.9.0/1.53). For each condition, three representative images were acquired using identical microscope settings. Quantification was performed using the "Analyze Particles" function, with size and circularity filters set to exclude background noise. This function provided measurements of both LDs number and total area per field of view. All data were normalized to the number of cells per image.

## 2.6 Thin-layer chromatography (TLC)

Total lipids were extracted from HCT15 and HCT116 cells using methyl-tert-butyl ether as an extraction solvent, as reported in (27). Extracted lipids were loaded on silica gel plates for thin-layer chromatography (TLC) analysis. Plates were developed with hexane/ethyl ether/acetic acid (70/30/1; *v*/*v*/*v*). After development, plates were uniformly sprayed with 10% cupric sulfate in 8% aqueous phosphoric acid, allowed to dry for 10 minutes at room temperature, and then placed into a 145 °C oven for 10 minutes, as reported in (28). Different lipid species were identified by developing specific standards under the same experimental conditions. Spot intensity was measured by densitometric analysis.

## 2.7 RNA extraction and Real Time-qPCR analyses

Total RNA was extracted from HCT15 and HCT116 cells with TRI reagent® (Zymo Research, R2050-1). RNA quantification was performed using a NanoDrop One Spectrophotometer (Thermo Scientific). For cDNA synthesis, HIScript III RT SuperMix for qPCR (+gDNA wiper) kit was used (Vazyme Biotech), following the manufacturer's instructions. Gene expression analyses were performed through real-time RT-PCR using iTaq Universal Sybr Green Supermix (Bio-Rad), run on the Rotor-Gene Q 6000 System (Qiagen). A comparative analysis was performed. Glyceraldehyde-3-phosphate dehydrogenase (GAPDH) and β-actin were evaluated as housekeeping genes, resulting in stable overall samples. GAPDH was chosen as the reference gene. All predesigned primers were obtained from Bio-Rad (more information is available at www.bio-rad.com/PrimePCR). The list of primers is reported in Supplementary Table 1.

## 2.8 Western blot

Proteins were extracted from cells using RIPA lysis buffer (Cell Signaling #9806). Total protein levels were determined using the Bradford method (Bio-Rad Laboratories). After boiling for 5 min, proteins were loaded and separated by SDS-polyacrylamide gel electrophoresis. The samples were then transferred onto a nitrocellulose membrane (Bio-Rad Laboratories) and blocked at room temperature for 1 hour using 5 % (*w*/*v*) non-fat milk in TBS-Tris buffer (Tris-buffered saline (TBS) plus 0.5 % (*v*/*v*) Tween-20, TTBS). The membranes were incubated with the primary antibodies reported in Supplementary Table 2. After washing with TTBS, the blots were incubated with peroxidase-conjugated monoclonal secondary antibodies (Sigma-Aldrich) at 1:10.000 dilutions at room temperature for 1-2 hours. The blots were then washed thoroughly in TTBS. Western blotting analyses were performed using the Amersham ECL Advance

Western Blotting Detection Kit (GE Healthcare, Little ChaOEAnt, UK), and the ChemiDoc system (Bio-Rad) was used for chemiluminescence measurement. Densitometric analysis of the immunoblots was performed using Image LabTM Version 6.0.1 2017 (Bio-Rad Laboratories, Inc.) software.

## 2.9 Statistical analysis

Results are expressed as means ± standard deviation (SD). Statistical differences were evaluated using GraphPad Prism version 8.3.0 for Windows. The comparison was made using a one-way analysis of variance (ANOVA). After Tukey's post hoc analysis, differences between groups were considered statistically significant when $p<0.05$. For proteomic data, statistical analyses were carried out using Perseus version 1.6.10.43. Label-free quantification (LFQ) intensities were $\log_2$-transformed and normalized prior to analysis. Proteins identified in at least two biological replicates were retained. Missing values were imputed as constants (missing = 0). Differentially expressed proteins were determined by two-sample *t*-test using six biological replicates per condition. Differentially expressed proteins were identified using a significance threshold of $p < 0.01$ for the main analysis, and $p < 0.05$ for exploratory comparisons.

# 3.Results

## 3.1 Proteomic profiling of HCT15 and HCT116 cell lines

We performed an unbiased, exploratory global proteomic analysis ($p < 0.01$) to delineate baseline molecular differences between the colorectal cancer cell lines HCT15 and HCT116. Approximately 6.000 proteins were identified across the two models. Hierarchical clustering (Figure 1a) resolved two distinct expression clusters: Cluster 1 comprised proteins markedly upregulated in HCT15 and downregulated in HCT116, whereas Cluster 2 included proteins enriched in HCT116 and suppressed in HCT15, indicating clearly segregated proteomic phenotypes.

Functional enrichment analysis (Figure 1b) demonstrated that HCT15 cells preferentially engage glycolytic pathways, while HCT116 cells predominantly rely on oxidative metabolism. In Supplementary Table 3 proteins that are upregulated in HCT15 or HCT116 cells are categorized based on their functions. Consistently, LDHA and LDHB, key enzymes orchestrating the metabolic equilibrium between glycolysis and oxidative phosphorylation, were significantly upregulated in HCT15 than HCT116 cells (Supplementary Table 4). This metabolic divergence was corroborated by Seahorse flux analysis, showing elevated basal respiration in HCT116 and enhanced glycolytic activity in HCT15 (Figure 1c).

Volcano plot analysis further revealed robust differential protein expression between the two cell lines (Figure 1d). While most proteins clustered around the origin ($\log_2$ fold change $\approx 0$), reflecting overall comparable expression levels,

distinct subsets exhibited significant positive or negative fold changes with strong statistical confidence, indicating cell line-specific regulatory signatures.

Consistent with their predominantly epithelial phenotype, HCT15 cells displayed higher levels of E-cadherin, whereas HCT116 cells showed increased Zeb-1 expression. Non-phosphorylated β-catenin, a key regulator of EMT, was also elevated in HCT15 relative to HCT116. Conversely, HCT116 cells expressed higher levels of PKC$\alpha$, a known EMT inducer, together with NDRG1, a context-dependent EMT modulator. In addition, HCT15 cells exhibited increased abundance of multiple epithelial markers, supporting a more differentiated and cohesive epithelial phenotype (Supplementary Table 3 and Table 4). Western blot analysis of core EMT regulators corroborated our proteomic findings (Figure 1e).

The Venn diagram (Figure 1f) confirmed both shared and exclusive proteomic features, with 6.060 proteins common to both lines, 88 detected only in HCT15, and 159 unique to HCT116 (Supplementary Table 5 and Table 6). Proteins exclusive to HCT116 were enriched in pathways related to EMT, hypoxia, and p53 signaling, whereas those unique to HCT15 were predominantly associated with apoptosis and inflammatory processes (Figure 1g, Supplementary Table 5 and Table 6). Notably, a substantial proportion of the exclusive proteins in both cell lines mapped to lipid metabolism. HCT15 lacked several proteins required for LDs biogenesis, which were instead uniquely expressed in HCT116, PLIN2, DHRS3, and reduced levels of CAV-1, GPAT3, DGAT, LDAF1, MFN2 compared to HCT116 (Supplementary Table 3-6). Moreover, enzymes involved in cholesterol esterification, such as ACAT1 and ACAT2, and the autophagy-associated protein ATG2A were more expressed in HCT15 than HCT116 cells. The consistency of our results with data from the Human Protein Atlas database further strengthens our observations (29). The differences between HCT15 and HCT116 cells in LDs-associated proteins suggest two distinct cell strategies.

HCT116 cells display a "lipid-rich" phenotype, characterized by enhanced lipid storage that supports rapid growth, membrane biosynthesis, and stress resistance. In contrast, HCT15 cells preferentially rely on lipid recycling and autophagy to maintain energy balance and ensure survival under metabolic stress conditions. This trait is functionally relevant, as LDs formation is essential for buffering lipid-induced toxicity and maintaining metabolic homeostasis under elevated fatty acid exposure.

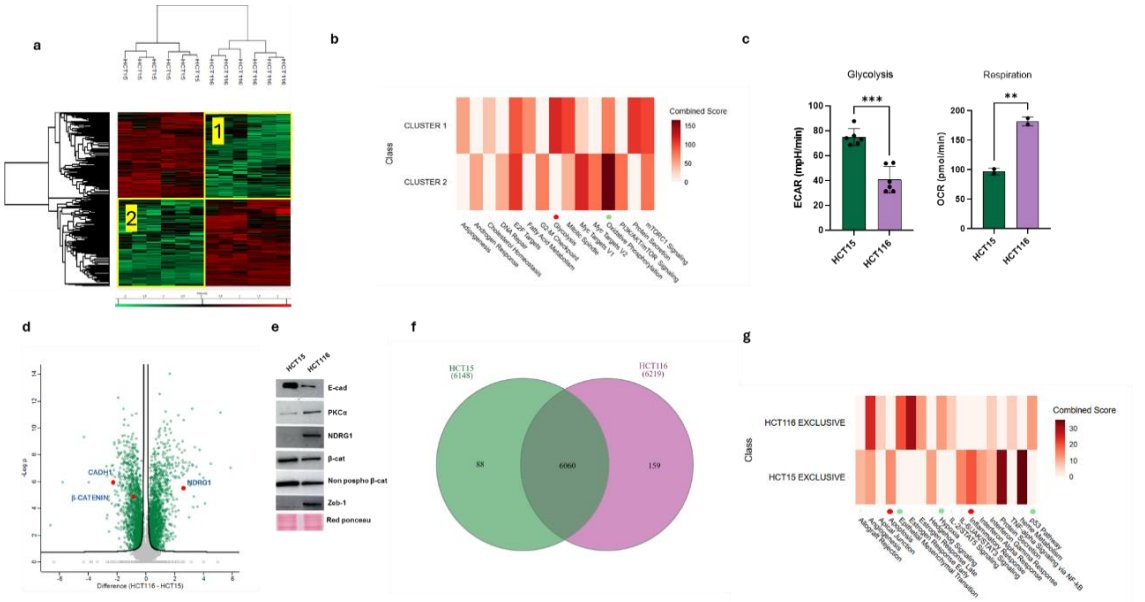


**Figure 1. Comparative proteomic profile of HCT15 and HCT116 cells**. **(a)** Heatmap and hierarchical clustering of differentially expressed proteins between HCT15 and HCT116 colorectal cancer cell lines, derived from quantitative proteomic profiling. The color scale ranges from green (downregulated) to red (upregulated), with black indicating no variation in expression. The analysis identifies two major clusters (Cluster 1 and Cluster 2), which reflect distinct proteomic signatures between the cell lines. **(b)** Functional enrichment analysis of basal proteomic profiles, highlighting the most significantly enriched biological processes and signaling pathways in both cell lines. Red and green dots correspond to pathways with predominant protein contributions in HCT15 and HCT116 cells, respectively. **(c)** Basal metabolic phenotyping of the two cell lines, illustrated through oxygen consumption rate (OCR) and extracellular acidification rate (ECAR) measurements, which indicate mitochondrial respiration

and glycolytic activity, respectively. **(d)** Volcano plot depicting differentially expressed proteins between HCT116 and HCT15 cells. The x-axis represents $\log_2$ fold-change (HCT116 vs. HCT15), while the y-axis indicates $-\log_{10}$ p-value. (**e**) Western blot validation of selected proteins involved in cell adhesion and intracellular signaling, including E-cadherin, PKC$\alpha$, NDRG1, β-catenin, non-phospho β-catenin, and ZEB1, in both cell lines. Ponceau S staining served as a total-protein loading control. **(f)** Venn diagram showing shared and unique proteins identified in HCT15 and HCT116 cell lines. **(g)** Functional enrichment analysis of cell-line-exclusive proteins, illustrating biological processes and pathways predominantly associated with proteins uniquely detected in HCT15 (red) or HCT116 (green) cells.

## 3.2 Palmitic acid differentially induces lipid droplets formation in HCT15 and HCT116 cells

PA significantly decreased HCT15 cell viability, causing approximately 40% and 80% cell death at 24 and 48 hours, respectively, as determined by crystal violet staining (Supplementary Figure 1a). Conversely, HCT116 cells were remarkably resistant to PA, exhibiting only ~20% loss of viability at 48 hours (Supplementary Figure 1b). Based on the proteomic results, we sought to further investigate the metabolism of LDs in the two cell lines. We selected PA, a saturated fatty acid classically associated with lipotoxic stress, and OA, a monounsaturated fatty acid known to counteract PA-induced toxicity and promote neutral lipid storage. This approach enabled us to examine how fatty acid composition modulates cell viability and lipid accumulation.

Bright-field microscopy showed that PA exposure markedly altered HCT15 cell morphology, inducing pronounced cell shrinkage, rounding, detachment, and a clear reduction in cell density (Supplementary Figure 1c). Co-treatment with OA partially restored cell morphology and confluence, indicating a protective effect of OA against PA-induced cytotoxicity. In stark contrast, HCT116 cells displayed

minimal morphological changes upon PA treatment, maintaining normal morphology and adherence without substantial loss of confluence or evident cell death under any condition (Supplementary Figure 1d).

Consistent with these observations, Together, these results demonstrate a marked cell line-specific sensitivity to saturated fatty acid exposure, with HCT116 cells being substantially more resistant to PA-induced cytotoxicity than HCT15 cells.

Fluorescence microscopy further revealed robust LDs accumulation in both cell lines following OA treatment compared with BSA (Figure 2a, d). OA-derived LDs were significantly larger in HCT15 than in HCT116 cells (Figure 2c, f). HCT15 cells failed to accumulate appreciable LDs in response to PA alone (Figure 2a, d), whereas HCT116 cells formed modest LDs under PA treatment (Figure 2b, e), albeit fewer and smaller than those induced by OA (Figure 2e, f). Co-treatment with PA and OA promoted LDs formation to levels comparable to OA alone in both cell lines, indicating a dominant effect of OA on lipid storage (Figure 2a-f).

Expression analysis of the TAG-synthesizing enzymes DGAT1 and DGAT2 revealed further differences between the cell lines. In HCT15 cells, PA significantly downregulated DGAT1 and DGAT2 mRNA levels, with partial rescue by OA co-treatment (Figure 2g). In contrast, PA treatment did not significantly alter DGAT1 or DGAT2 expression in HCT116 cells relative to BSA. Notably, basal DGAT1 expression was substantially higher in HCT116 than in HCT15 cells (Figure 1h), in agreement with our proteomic data and with The Human Protein Atlas (29), potentially contributing to the enhanced lipid storage capacity of HCT116 cells. To corroborate these findings, total lipids were extracted after 24 hours of FA treatment and analyzed by TLC (Figure 2i, j and supplementary Figure 2). OA induced a significant increase in TAG content in both cell lines relative to controls. Notably, PA treatment led to ~38% TAG

accumulation in HCT116 cells but less than 15% in HCT15 cells (Figure 3a, b). As expected, PA/OA co-treatment increased TAG levels, consistent with the microscope analysis of LDs accumulation (Figure 1a).

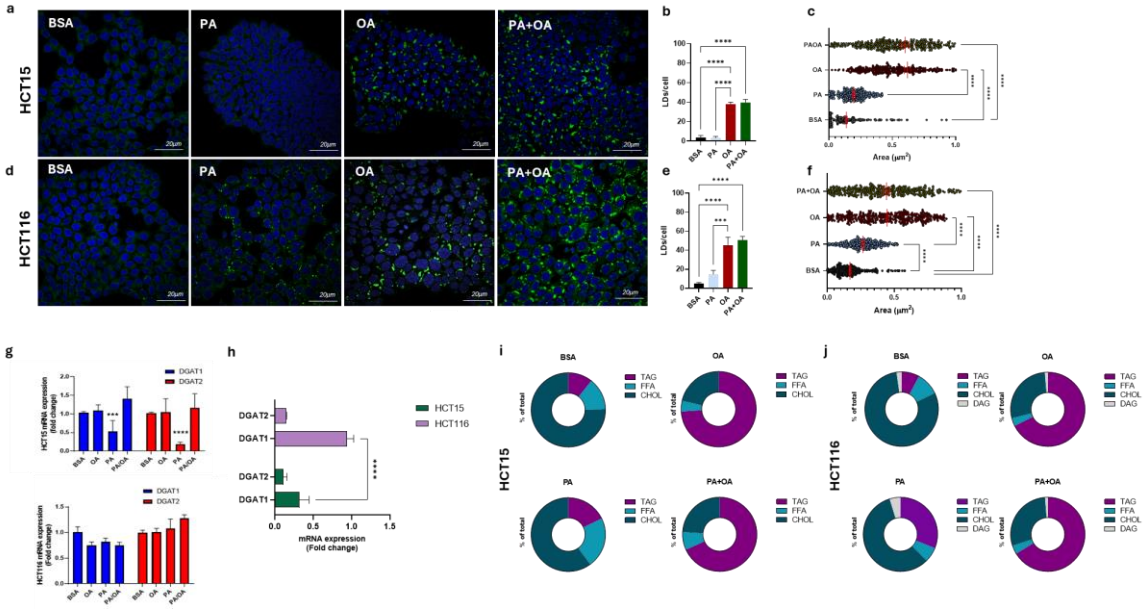


**Figure 2. Lipid droplet metabolism in HCT15 and HCT116 cells.** Representative confocal microscopy images showing lipid droplets (LDs, green; stained with BODIPY) and nuclei (blue; stained with DAPI) in HCT15 (a) and HCT116 (d) cells treated for 24 h with BSA (control), palmitic acid (PA, 200 µM), oleic acid (OA, 200 µM), or their combination (PA+OA, 1:1 ratio, 200 µM each). Scale bar: 20 µm. Quantification of LD number per cell in HCT15 (b) and HCT116 (e), and LD area (µm²) in HCT15 (c) and HCT116 (f) under the indicated conditions. (g) Relative mRNA expression levels of DGAT1 and DGAT2 in HCT15 and HCT116 cells, as determined by qRT-PCR. Data are expressed as fold change versus BSA. (h) Basal DGAT1 and DGAT2 expression comparison between HCT15 and HCT116. (i, j) Thin-layer chromatography (TLC) analysis of intracellular neutral lipids, including triacylglycerols (TAG), free fatty acids (FFA), cholesterol (Chol), and diacylglycerols (DAG), and their relative quantification by densitometric analysis in (i) HCT15 and (j) HCT116 cells after 24 h of treatment. Each lipid species is expressed as a percentage of the total neutral lipid content and normalized to the control group (BSA). Data represent the mean ± SD of three independent experiments. (**p < 0.01; ***p < 0.001; ****p < 0.0001 versus BSA).

## 3.3 Palmitic acid shapes the proteomic landscape of HCT15 and HCT116 colon cancer cells

We performed a proteomic analysis on HCT15 and HCT116 cells after PA treatment for 24 hours. Hierarchical clustering of proteomic data revealed two major clusters for both cell lines. In HCT15 cells Cluster 2 comprised proteins upregulated by PA, while Cluster 1 included proteins downregulated by PA (Figure 3a). In HCT116 cells Cluster 2 contained proteins downregulated by PA, whereas Cluster 1 comprised proteins upregulated by PA (Figure 3b). Functional enrichment analysis, performed with Profiler (based on combined score and gene count) using MSigDB_HALLMARK_2020 database, shows that PA treatment in HCT15 cells primarily upregulated proteins involved in apoptosis, fatty acid metabolism, UV response, xenobiotic metabolism, and mTORC1 signaling (Figure 3c) (25). By contrast, in HCT116 cells, the upregulated proteins were mainly associated with adipogenesis, oxidative phosphorylation, and MYC target gene sets V1 (Figure 3d). The proteins driving these pathways are listed and grouped by cell line and functional category (Figure 3e). These findings suggest that HCT15 cells respond to PA by activating multiple stress-related programs, including apoptotic signaling, metabolic adaptation, and xenobiotic defense, indicating a higher sensitivity to lipid-induced stress. In contrast, HCT116 cells appear to reprogram their metabolism toward energy production and lipid accumulation.

The Venn diagrams comparing upregulated proteins in the two cell lines (p-value $< 0.05$) following PA exposure reveal 8 shared proteins (GLB1L2, HMOX1,

LMAN2, FAR1, SQSTM1, PNPLA2, REEP4, and TRAPPC3), probably involved in common adaptive responses to the treatment (Figure 3f, Supplementary Table 7). Moreover, proteins upregulated by PA exclusively in HCT15 or HCT116 cells were 114 and 87 respectively (Figure 3f). Among up-regulated proteins in HCT116 cells after PA treatment, we found PLIN2 (Supplementary Table 7) a central regulator of LDs biogenesis and stabilization (30).

PCA of normalized proteomic data ($p < 0.01$) was performed to assess both treatment-induced differences and replicate homogeneity (Figure 3g). In HCT15 cells, PC1 (66%) and PC2 (8%) clearly separate BSA and PA-treated cells. A similar pattern of separation was observed in HCT116 cells (PC1=65% and PC2=8.25%). Since PC1 captures the largest source of variability, its separation of the groups indicates that the dominant difference in the dataset is driven by the effect of PA treatment, whereas PC2 accounts for a smaller portion of variability, likely reflecting secondary or subtle differences.

Transcription factors involved in the upregulation of proteins by PA were obtained by enrichment analysis using ChEA3, followed by interaction validation with STRING (Supplementary Figure 3). In HCT15 cells, the top-ranked transcriptional factors up-regulated by PA are protein involved in cellular responses to ER stress: CEBPG, NCOA1, GLMP, ZBED3, ATF5, NR1H4, ZNF335, DDIT3, and ZNF852. STRING analysis highlighted that ATF5, CEBPG, and DDIT3 show significant interactions with the upregulated proteins, suggesting a central role in mediating the cellular response of HCT15 to PA. In HCT116 cells, the top-ranked transcription factors XBP1, ATMIN, ZNF761, MSANTD1, THAP7, ZNF653, ESR1, ZNF883, TIGD5, and GTF2B. Notably, ESR1 and GTF2B, were found to interact with key proteins of lipid metabolism, including PLIN2 and CPT1A, both upregulated by PA treatment of HCT116 cells.

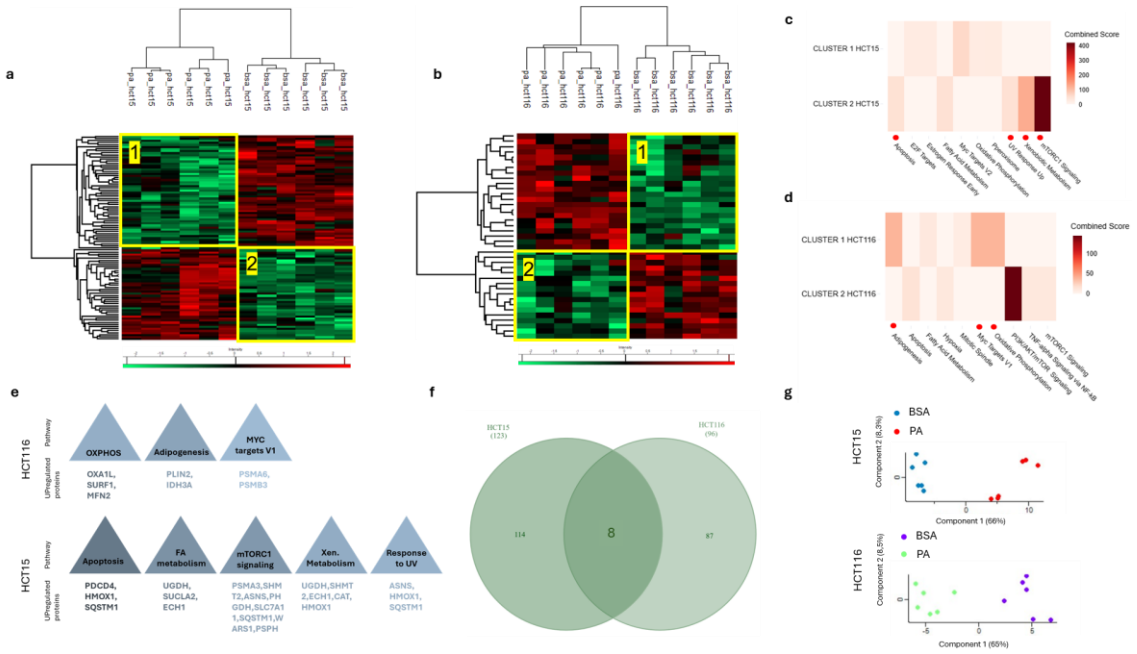


**Figure 3. Proteomic analysis of HCT15 and HCT116 cells following palmitic acid treatment.** Heatmap representation of proteomic profiles in (a) HCT15 and (b) HCT116 cells after treatment with PA (200 μM, 24 h). Cluster 2 includes proteins upregulated in HCT15, whereas cluster 1 comprises proteins upregulated in HCT116 in response to PA. Functional enrichment analyses of upregulated proteins in (c) HCT15 and (d) HCT116 cells highlight enriched biological processes and pathways, with the most significantly affected ones shown in red. (e) Enrichment analysis of representative upregulated proteins belonging to major functional categories. (f) Venn diagram showing shared and unique subsets of significantly upregulated proteins ($p < 0.005$) in HCT15 and HCT116 cells following PA treatment. (g) Principal component analysis (PCA) illustrating the distribution of biological replicates and overall proteomic variance between treatments and cell lines.

## 3.4 The proteomic profile of HCT15 cells indicates that palmitic acid activates a specific cell death pathway

Building on the proteomic evidence revealing a distinct pro-apoptotic signature in PA-treated HCT15 cells, we investigated, by western blot (Figure 4a) the molecular mechanisms underlying PA-induced cell death. PA treatment dramatically elevated the p-ERK/ERK ratio in HCT15 cells compared to BSA or OA in both cell lines (Figures 4a-c). This hyperactivation coincided with striking p53 stabilization and marked suppression of YAP protein expression, orchestrating a molecular switch toward cell death commitment.

Interestingly, proteomic analysis indicated a modulation of proteins associated with apoptosis, as a higher expression of Bax and reduced level of antiapoptotic Bcl-2, in HCT15 compared with HCT116 cells (Supplementary Table 4). Our comprehensive analysis of cell death markers by western blot (Figure 4d) revealed a complex picture that extends beyond classical apoptosis. Bax expression, which confirmed its major expression in HCT15 than HCT116 cells, remained unchanged in HCT15 cells but was significantly reduced in HCT116 cells following PA exposure (Figure 4d, e). While PA treatment selectively suppressed the anti-apoptotic protein Bcl-2 in HCT15 cells and upregulated this antiapoptotic marker in HCT116 cells (Figure 4d, f), suggesting fundamentally different cellular responses to saturated fatty acid stress. The activation of PARP-1 and proteolytic cleavage of caspase-7, hallmarks of apoptotic execution, were evident in PA-treated HCT15 but not HCT116 cells (Figure 4d, g, h). Several additional observations point toward ferroptosis as a concurrent or even predominant mechanism of PA-induced cell death in HCT15 cells. Most

compellingly, PA treatment upregulated ACSL4 in HCT15 cells, while downregulating this enzyme in HCT116 cells (Figure 4d, i).

In line with this, PA treatment induced a marked increase in P16 expression in HCT15 cells while decreasing this marker in HCT116 cells (Figure 4d, j), further supporting a cell line specific stress response consistent with ferroptosis vulnerability. Concomitantly, PA downregulated GPx4 expression in HCT15 but not in HCT116 cells (Figure 4d, k). Given that, GPx4 represents the central defense against ferroptosis by neutralizing lipid peroxides (31), its suppression coupled with ACSL4 elevation creates a molecular environment primed for ferroptosis cell death. Proteomic analysis in PA-treated HCT15 cells confirms significant upregulation of multiple ferroptosis-related proteins, including SLC7A11, HMOX1, SESN2, SQSTM1/p62, and CAT (Supplementary Table 7).

Beyond its cytotoxic effects, PA exposure triggered a profound disintegration of epithelial architecture in HCT15 cells, marked by a striking downregulation of essential junctional proteins, including E-cadherin, β-catenin, and ZO-1, at both protein and transcript levels (Figures 4m-o). Such a collapse of intercellular adhesion is a hallmark of epithelial destabilization and has been strongly associated with cancer aggressiveness and metastatic potential (32), (33). Remarkably, co-treatment with OA largely rescued this phenotype, reinstating the expression of junctional proteins and safeguarding epithelial cohesion (Figure 4l-n). In contrast, HCT116 cells exhibited a striking resistance to PA challenge, with only negligible perturbations in junctional marker expression under identical conditions (Figure 4l-n).

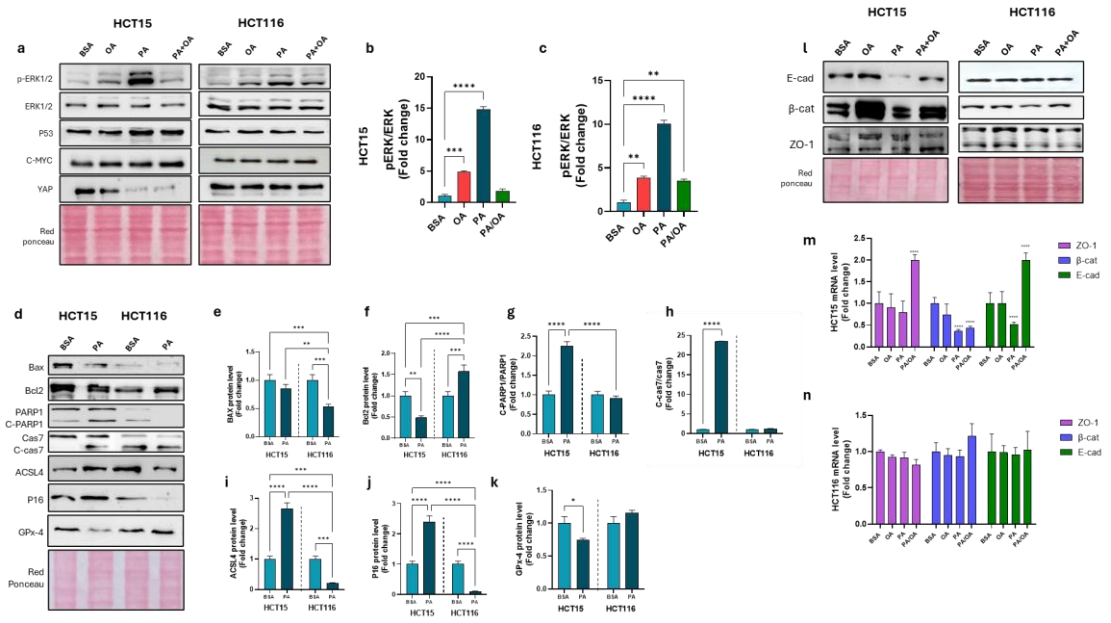


**Figure 4. Cell signaling, tight junctions, and cell death programs in HCT15 and HCT116 cells.** (a) Representative Western blot analysis of pERK1/2, total ERK1/2, P53, C-MYC, and YAP in HCT15 and HCT116 cells after 24 h of treatment with BSA (control), OA (200 μM), PA (200 μM), or PA+OA (1:1 ratio, 200 μM each). Quantification of pERK/ERK ratios in (b) HCT15 and (c) HCT116. (d) Western blot analysis of apoptosis-related markers (Bax, Bcl2, PARP1, cleaved PARP1 (C-PARP1), caspase 7 (Cas7), cleaved caspase 7 (C-Cas7)), ACSL4, P16, and GPx4, and (e–k) relative quantifications, including C-PARP1/total PARP1 and C-Cas7/total Cas7 ratios in both cell lines treated with BSA or PA. (l) Representative Western blot analysis of tight junction proteins E-cadherin (E-cad), β-catenin (β-cat), and ZO-1 in HCT15 and HCT116 cells. (m, n) Relative mRNA expression levels of ZO-1, β-cat, and E-cad in HCT15 and HCT116 cells after 24 h of treatment with BSA, OA, PA, or PA+OA. Values represent the mean ± SD of at least three independent experiments. (*$p < 0.05$; **$p < 0.01$; ***$p < 0.005$; ****$p < 0.001$).

## 3.5 Palmitic acid reprogram energy metabolism in colon cancer cells

Among differential expressed proteins in the two colorectal cancers following PA treatment, we identify many mitochondrial proteins (Supplementary Table 7). To elucidate the impact of fatty acid exposure on mitochondrial functionality, we performed comprehensive bioenergetic profiling using Seahorse XF technology and OXPHOS complex analysis in HCT15 and HCT116 intestinal cells (Figure 5).

HCT15 cells demonstrated marked metabolic vulnerability to PA treatment, exhibiting a dramatic suppression of basal respiration and ATP-linked mitochondrial respiration (Figure 5a, b) that persisted throughout the measurement period. This respiratory impairment was accompanied by reduction in extracellular acidification (Figure 5a), indicating no compensatory shift toward glycolytic metabolism. These last data are also confirmed by significant reduction in glycolysis and glycolytic reserve in PA-treated HCT15 cells (Figure 5b). Proteomics analysis of PA-treated HCT15 cells further supporting OCR data indicating downregulation of proteins involved in mitochondrial oxidative phosphorylation and dynamics (NDUFAF1, NDUFA3, NDUFA10, SURF1, OXA1L, COX20, MFN2, NDUFS3, ATPAF1, ACAD9, LONP1, YMEL1), (Supplementary Table 7). In striking contrast, OA treatment maintained near-normal respiratory capacity, suggesting preservation of mitochondrial function.

HCT116 cells displayed remarkable metabolic resilience across PA treatments (Figure 5f-j). PA treatments resulted in only modest alterations in basal respiration and ATP-linked mitochondrial respiration, with minimal impact on extracellular acidification rates, glycolysis and glycolytic reserve (Figure 5g) indicating maintained oxidative capacity and metabolic flexibility. OA treatment

in HCT116 cells increased mitochondrial basal respiration and ATP-linked respiration, with a minimal increase also in glycolysis (Figure 5g).

Western blot analysis of OXPHOS subunit complexes provided mechanistic insights into the observed respiratory defects. In HCT15 cells, PA treatment induced significant downregulation of CI (NDUFB8 subunit) and CII (SDHB subunit) (Figure 5c, d). HCT116 cells showed minimal changes in OXPHOS complex expression, with a trend toward an increase in CII expression (Figure 5h, i). Coherent with the higher basal respiration of HCT116 cells under OA treatment, both CI, and CII were upregulated by OA in HCT116 cells (Figure 5h, i).

AMPK, a crucial nutrient and energy sensor, plays a central role in maintaining cellular energy homeostasis (34). Our data revealed that PA treatment led to a marked increase in the phosphorylation of AMPK (pAMPK) relative to total AMPK levels in both cell lines (Figure 5c, e, h, j). Differently, OA treatment did not significantly affect AMPK activation in HCT116 cells, while enhanced AMPK phosphorylation in HCT15 cells. Importantly, co-treatment with OA did not counteract the PA-induced phosphorylation of AMPK, suggesting that PA triggers a persistent activation of the AMPK pathway independent of OA (data not shown).

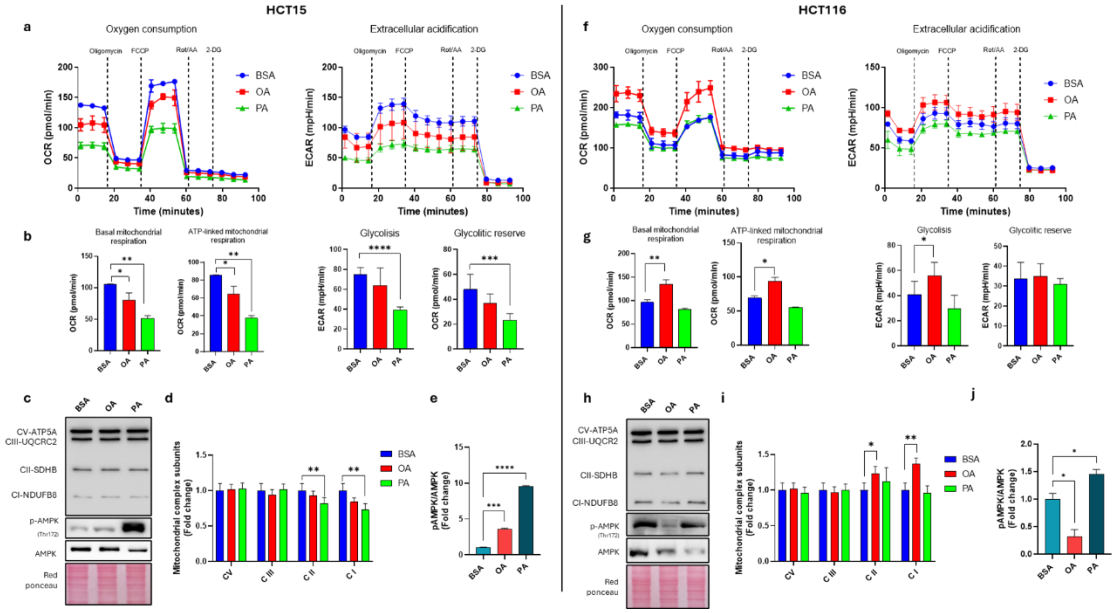


**Figure 5. Energy metabolism in HCT15 and HCT116 cells.** (a, f) Oxygen consumption rate (OCR) and extracellular acidification rate (ECAR) profiles were assessed using a Seahorse XFp Analyzer in HCT15 and HCT116 cells after 24 h of treatment with BSA (control), OA (200 μM), or PA (200 μM). (b, g) Bioenergetic parameters, including basal respiration, ATP-linked respiration, glycolysis, and glycolytic reserve, were derived from OCR/ECAR curves. Representative Western blot analysis of total OXPHOS, phosphorylated AMPK (p-AMPK, Thr172), and total AMPK in (c) HCT15 and (h) HCT116 cells, with relative quantification of mitochondrial complex subunits and p-AMPK/AMPK ratios in (d) HCT15 and (i) HCT116. Ponceau S staining was used as a total protein loading control. Values represent the mean ± SD of at least three independent experiments. (*$p < 0.05$; **$p < 0.01$; ***$p < 0.005$; ****$p < 0.001$).

## 3.6 EMT enhances resistance to palmitic acid-induced lipotoxicity in HCT15 cells

To further dissect whether the differential sensitivity of HCT15 and HCT116 colorectal cancer cells to the lipotoxic effects of PA could be mechanistically linked to EMT, we assessed the impact of PA in the presence of PMA, a well-characterized EMT inducer (Figure 6a) (35). At the molecular level, PMA treatment induced clear EMT-related changes in HCT15 cells, as reflected by downregulation of the epithelial marker E-cadherin and modulation of key signaling molecules (Figure 6b). Specifically, PMA reduced PKC$\alpha$ and p53 expression, while markedly increasing NDRG1 levels in both cell lines, a signature consistent with a shift toward a mesenchymal-like phenotype (32) (33). Phase-contrast microscopy revealed that PA alone elicited profound stress responses in HCT15 cells, manifested by cell rounding and detachment (Supplementary Figure 4). Remarkably, co-treatment with PMA attenuated these cytotoxic features, preserving cell morphology and suggesting that EMT activation exerts a protective role against PA-induced lipotoxic stress. In sharp contrast, HCT116 cells exhibited only minimal morphological alterations across all treatment conditions, highlighting their intrinsic resistance to PA cytotoxicity (Supplementary Figure 4).

Cell viability assays further substantiated these observations: in HCT15 cells, PA markedly reduced survival at 24 h, an effect that was almost completely reversed by PMA co-treatment (Figure 6c). Conversely, in HCT116 cells, neither PA nor PMA significantly impacted viability (Figure 6d). Such remodeling underscores the capacity of EMT to enhance cell survival under metabolic stress conditions. Notably, LDs accumulation was markedly enhanced in HCT15 cells exposed to the PA-PMA combination compared to PA alone, while no such effect was evident in HCT116 cells (Figure 6e, f). Given that LDs biogenesis represents a

well-established adaptive mechanism to buffer FFA-induced lipotoxicity in hepatocytes (36) (37), our data strongly suggest that PMA-induced EMT promotes LDs accumulation as a cytoprotective strategy in HCT15 cells. Collectively, these findings support the hypothesis that EMT activation by PMA confers a protective advantage against PA-induced lipotoxicity, particularly in HCT15 cells, by driving a mesenchymal-like phenotype associated with enhanced LDs synthesis and activation of pro-survival pathways.

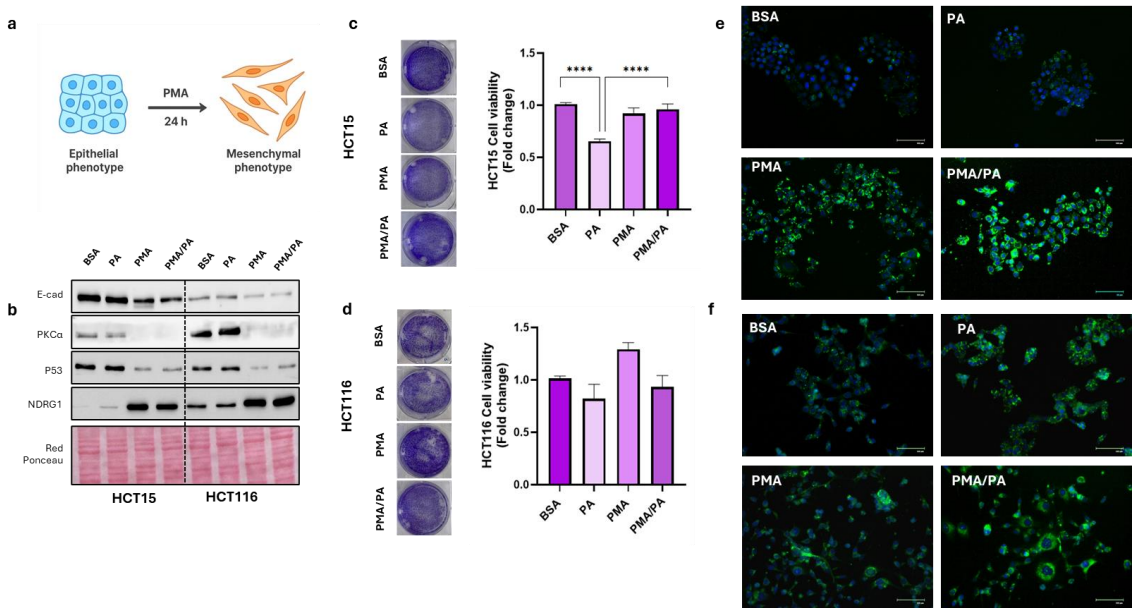


**Figure 6. EMT confers resistance to palmitic acid-induced lipotoxicity in HCT15 cells.** (a) Schematic illustration of the effect of phorbol 12-myristate 13-acetate (PMA) in inducing epithelial–mesenchymal transition (EMT). (b) Representative Western blot analysis of EMT markers (Zeb1, E-cadherin, PKC$\alpha$, P53, and NDRG1) in HCT15 and HCT116 cells treated for 24 h with BSA (control), PA (200 μM), PMA (100 nM), or PMA+PA. Ponceau S staining was used as a loading control. (c, d) Cell viability assessed by the Crystal Violet assay in HCT15 (c) and HCT116 (d) cells under the same conditions. (e, f) Representative BODIPY staining images showing lipid droplet accumulation (green) in PMA/PA-treated HCT15 (e) and HCT116 (f) cells. Scale bars: 100 μm. Values are expressed as mean ± SD of at least three independent experiments. (*$p < 0.05$; **$p < 0.01$; ***$p < 0.005$; ****$p < 0.001$).

## 4. Discussion

Our findings reveal a fundamental relationship between EMT status and cellular vulnerability to saturated fatty acid-induced stress in colorectal cancer. The striking differential sensitivity of HCT15 and HCT116 cells to PA extends beyond simple cytotoxicity, encompassing divergent metabolic reprogramming, lipid handling capacity, and activation of distinct cell death pathways. These observations align with emerging evidence that EMT confers broad metabolic plasticity and stress resistance in cancer cells (32), (38), but our study uniquely demonstrates how this phenotypic state specifically modulates responses to dietary lipid exposure.

The mesenchymal-like phenotype of HCT116 cells, characterized by elevated Zeb-1, PKC$\alpha$, and NDRG1 expression alongside reduced E-cadherin, appears to establish a pre-adapted metabolic state capable of buffering lipotoxic stress. This interpretation is consistent with recent work demonstrating that mesenchymal cancer cells exhibit enhanced metabolic flexibility and can efficiently redirect excess nutrients toward biosynthetic pathways rather than toxic accumulation (39). Conversely, the epithelial characteristics of HCT15 cells, robust cell-cell junctions, high E-cadherin expression, and organized polarity, may paradoxically render these cells more vulnerable to membrane lipid perturbations that disrupt cellular architecture.

The inability of HCT15 cells to accumulate LDs in response to PA represents a critical metabolic failure that likely drives their enhanced sensitivity to lipotoxicity. Our observation that PA downregulates DGAT1 and DGAT2 expression specifically in HCT15 cells provides a molecular mechanism for this deficiency. These findings resonate strongly with recent studies in hepatocytes demonstrating that DGAT1 downregulation under PA exposure compromises the cell capacity to sequester toxic FFA into neutral lipid stores (10). The concept

of LDs as "metabolic buffers" that protect cells from lipotoxicity is well established in liver biology (40), (41), and our data extend this paradigm to colorectal cancer cells, suggesting that LDs biogenesis capacity fundamentally determines cellular fate under lipid stress.

The proteomic identification of elevated PLIN2 expression in HCT116 cells following PA treatment supports this interpretation, as PLIN2 is a key structural protein that stabilizes nascent LDs and prevents their premature lipolysis (42). The coordinated upregulation of both PLIN2 and maintained DGAT expression in HCT116 cells likely creates a permissive environment for lipid storage that is absent in HCT15 cells.

Our observation that PA induces simultaneous activation of apoptotic markers and ferroptosis signatures in HCT15 cells challenges traditional views of cell death as discrete, mutually exclusive pathways. The constellation of findings, ACSL4 upregulation, GPx4 downregulation, iron metabolism dysregulation, alongside PARP-1 cleavage, caspase-7 activation, and Bcl-2 suppression, strongly suggests a hybrid ferroptosis-apoptosis mechanism. This interpretation aligns with emerging evidence that cells under metabolic stress can activate multiple death pathways simultaneously, with the outcome representing the integrated effect of these signals (43).

ACSL4 has a central role in incorporating polyunsaturated fatty acids into membrane phospholipids, making it a critical determinant of ferroptosis susceptibility. Its selective upregulation in PA-treated HCT15 cells, coupled with GPx4 downregulation creates a highly permissive context for lipid peroxidation-driven damage. Unlike apoptosis, ferroptosis is not caspase-dependent but rather relies on oxidative and lipid imbalance, and our model supports this hypothesis. In contrast, HCT116 cells, thanks to their enhanced metabolic plasticity and efficient lipid storage, appear less susceptible to ferroptosis. This is particularly

relevant given that saturated fatty acids like PA can promote conditions favoring ferroptosis in cells with impaired antioxidant defenses and compromised lipid storage (44). The proteomic identification of coordinated upregulation of ferroptosis-related proteins, SLC7A11, HMOX1, SESN2, SQSTM1/p62, and CAT, further supports the activation of this pathway.

The possible engagement of ferroptosis and apoptotic machinery might reflect the severity of metabolic disruption in PA-treated HCT15 cells. Classical apoptosis typically requires ATP and functional mitochondria, yet our bioenergetic profiling revealed catastrophic metabolic failure in these cells. Under such conditions, alternative ATP-independent death pathways like ferroptosis may become increasingly important. The hybrid nature of cell death in this context may thus represent not redundancy but rather complementary mechanisms ensuring elimination of severely compromised cells.

The comprehensive bioenergetic failure observed in PA-treated HCT15 cells, characterized by suppressed mitochondrial respiration, and impaired glycolytic capacity, reveals that lipotoxicity extends far beyond simple membrane perturbation. The proteomic evidence of downregulated OXPHOS complex proteins (NDUFA9, SURF1, OXA1L) and mitochondrial dynamics regulators (MFN2, LONP2, YMEL1) suggests that PA actively dismantles mitochondrial infrastructure in susceptible cells. This interpretation differs from models proposing simple substrate overload and instead suggests active suppression of mitochondrial biogenesis or accelerated mitochondrial degradation.

The inability of HCT15 cells to compensate for respiratory failure by upregulating glycolysis represents a particularly striking metabolic inflexibility. In contrast, cancer cells typically exhibit remarkable metabolic plasticity, readily switching between oxidative phosphorylation and glycolysis depending on substrate availability and oxygen tension (the Warburg effect). The loss of this

flexibility in PA-treated HCT15 cells may reflect either direct glycolytic enzyme inhibition or broader disruption of metabolic regulatory networks. The reduction in both glycolysis and glycolytic reserve suggests fundamental impairment of glucose metabolism.

The metabolic resilience of HCT116 cells, maintaining near-normal respiratory and glycolytic capacity despite PA exposure, likely contributes significantly to their survival advantage. Their ability to even increase mitochondrial respiration under OA treatment demonstrates intact metabolic machinery capable of adapting to lipid substrate availability. This metabolic competence may stem from their mesenchymal phenotype, which has been associated with enhanced mitochondrial function and oxidative metabolism in multiple cancer contexts (45).

These metabolic distinctions may, at least in part, derive from differences in p53 functionality between the two cell lines. Beyond its established roles in cell-cycle arrest and apoptosis, p53 is a central regulator of cellular metabolism. Wild type p53 supports mitochondrial oxidative phosphorylation, maintains mitochondrial integrity, and suppresses excessive glycolytic activity, thereby ensuring an efficient and balanced bioenergetic state (46). Conversely, loss or dysfunction of p53 disrupts this homeostasis, leading to impaired mitochondrial respiration and a compensatory shift toward glycolysis, a hallmark of metabolic rewiring consistently demonstrated in both cultured cells and *in vivo* models. In this context, the proteomic differences observed between HCT116 (p53 wild type) and HCT15 (p53 mutant) are consistent with their distinct metabolic phenotypes and reinforce the concept that p53 status shapes both metabolic and phenotypic traits in colorectal cancer cells.

The higher baseline expression of PKC$\alpha$ and NDRG1 in HCT116 cells, and their further modulation by PMA-induced EMT in HCT15 cells, points to these

proteins as potential mediators of lipotoxic resistance. The well-established roles of PKC$\alpha$ in regulating TJ dynamics and cell survival signaling (47), (48) position it as a key effector in maintaining barrier function under stress. Its activation may promote cytoskeletal remodeling that stabilizes membrane integrity during lipid challenges, while simultaneously activating pro-survival pathways that counteract apoptotic signals.

The context-dependent functions of NDRG1 in cancer make it a particularly intriguing player. While traditionally viewed as a metastasis suppressor, recent evidence demonstrates that NDRG1 can promote survival and stress tolerance in mesenchymal-like tumor cells (49), (50). Our observation that NDRG1 is elevated in resistant HCT116 cells and further induced by EMT-promoting PMA treatment in HCT15 cells suggests it functions as an adaptive stress response protein in this context. The ability of NDRG1 to modulate cellular iron homeostasis may be particularly relevant given the ferroptosis component of PA-induced cell death, as proper iron regulation is critical for preventing Fenton reaction-driven lipid peroxidation.

Notably, C-MYC expression exhibited variable regulation, reflecting its well-documented context-dependent duality: while promoting proliferation under physiological conditions, C-MYC paradoxically sensitizes cells to apoptosis during stress scenarios characterized by ERK hyperactivation or YAP suppression (51). The simultaneous activation of these stress-responsive pathways suggests that PA triggers a coordinated cellular response that ultimately favors cell death over survival.

The selective disruption of E-cadherin, β-catenin, and ZO-1 expression in PA-treated HCT15 cells reveals that saturated fatty acid exposure can trigger EMT-like changes that compromise epithelial architecture. This observation extends previous findings that PA disrupts intestinal barrier integrity (15) by

demonstrating that the effect is cell phenotype dependent. The rescue of junctional protein expression by OA co-treatment is particularly noteworthy, suggesting that unsaturated fatty acids may actively stabilize epithelial architecture through mechanisms beyond simple absence of saturated fatty acid toxicity.

The relationship between junctional disruption and lipotoxic sensitivity remains incompletely understood. Loss of E-cadherin-mediated adhesion could potentially sensitize cells to membrane stress by eliminating cooperative survival signaling between adjacent cells. Alternatively, E-cadherin downregulation may be a consequence rather than cause of cellular stress, reflecting activation of EMT-inducing transcription factors downstream of lipotoxic signals. The fact that forced EMT induction protects HCT15 cells from PA toxicity argues that phenotypic transition itself, with its attendant metabolic reprogramming, confers the protective effect, rather than simply the presence or absence of specific junctional proteins.

The protective effect of PMA-induced EMT in HCT15 cells provides compelling causal evidence that mesenchymal transition enhances lipotoxic resistance. PMA treatment not only attenuated PA-induced cytotoxicity but also enhanced LDs accumulation, suggesting that EMT co-ordinately reprograms multiple aspects of lipid metabolism. This observation aligns with emerging evidence that EMT involves comprehensive metabolic rewiring, including enhanced fatty acid oxidation, altered lipid synthesis pathways, and modified mitochondrial function (52).

The molecular changes induced by PMA, E-cadherin downregulation, PKC$\alpha$ and p53 suppression, NDRG1 upregulation, partially recapitulate the baseline phenotype of HCT116 cells, supporting the interpretation that these markers define a stress-resistant cellular state. Interestingly, the ability of PMA to reduce

p53 expression may contribute to its protective effect, as p53 stabilization was identified as a key mediator of PA-induced death in untreated HCT15 cells. This suggests that mesenchymal cells may evade lipotoxicity partly through attenuated p53 responses, allowing them to tolerate metabolic stress that would trigger apoptosis in epithelial cells.

Our findings have several potential clinical implications for understanding how dietary fat composition influences colorectal cancer progression and treatment responses. The observation that mesenchymal-like cancer cells resist saturated fatty acid-induced stress suggests that dietary interventions targeting lipid composition might differentially affect tumors based on their EMT status. Epithelial-like tumors might be particularly vulnerable to saturated fat-mediated cytotoxicity, while mesenchymal tumors could potentially thrive under high saturated fat conditions.

The identification of ferroptosis as a component of lipotoxic cell death opens potential therapeutic avenues. Ferroptosis-inducing agents are being explored as cancer therapeutics (53), and our data suggest that combining such agents with dietary or pharmacological strategies that promote saturated fatty acid exposure might synergistically eliminate epithelial cancer cells while sparing normal tissues. Conversely, inhibiting EMT in mesenchymal tumors might sensitize them to lipotoxic stress.

The protective effect of OA co-treatment observed throughout our study suggests that dietary fat quality, not just quantity, critically influences cancer cell fate. This aligns with epidemiological evidence associating Mediterranean diets, rich in monounsaturated fats from olive oil, with reduced colorectal cancer risk (54). Our mechanistic data provide cellular and molecular support for these epidemiological observations.

While our study provides comprehensive characterization of differential lipotoxic responses in EMT-distinct colorectal cancer cell lines, several questions remain. The *in vivo* relevance of our findings requires validation in animal models and human tumor samples. In addition, the relative contributions of genetic differences (particularly TP53 mutational status) in determining lipotoxic sensitivity require further dissection using isogenic cell line pairs.

## 5. Conclusions

From a broader perspective, these findings position EMT not only as a driver of invasiveness and metastasis but also as a fundamental determinant of metabolic fate under nutrient or lipid stress. The proteomic evidence supports the view that EMT confers a "metabolic armor," reorganizing mitochondrial and lipid-handling systems to sustain cell viability even in the presence of potentially cytotoxic fatty acids. Such metabolic plasticity may explain why mesenchymal-like tumors exhibit greater survival and therapeutic resistance in lipid-rich microenvironments, a scenario increasingly relevant in obesity-associated cancers.

Altogether, the comparative proteomic analysis of HCT15 and HCT116 cells reveals that EMT rewires the proteome in a manner that integrates structural, metabolic, and stress-response functions. This reprogramming transforms how cells perceive and manage lipid challenges, turning palmitic acid from a lethal insult in epithelial contexts into a manageable metabolic substrate in mesenchymal ones. Understanding this proteomic shift opens new avenues for targeting EMT-associated metabolic adaptations, potentially exploiting lipotoxic stress as a therapeutic vulnerability in epithelial-like colorectal cancers.

## 6. References


1. *Khonsary S (2017) Guyton and Hall: Textbook of Medical Physiology. Surg Neurol Int 8:275. https://doi.org/10.4103/sni.sni_327_17*
2. *Honey K (2006) DC family welcomes a new arrival. Nat Rev Immunol 6:172–172. https://doi.org/10.1038/nri1817*
3. *Nelson WJ, Nusse R (2004) Convergence of Wnt, β-Catenin, and Cadherin Pathways. Science 303:1483–1487. https://doi.org/10.1126/science.1094291*
4. *Lindley D (2001) Falling to Earth in a quantum way. Nature 410:145–146. https://doi.org/10.1038/35065500*
5. *Sánchez-Tilló E, de Barrios O, Siles L, et al (2011) β-catenin/TCF4 complex induces the epithelial-to-mesenchymal transition (EMT)-activator ZEB1 to regulate tumor invasiveness. Proc Natl Acad Sci USA 108:19204–19209. https://doi.org/10.1073/pnas.1108977108*
6. *Xu Y, Liu L, Xin W, et al (2015) The renoprotective role of autophagy activation in proximal tubular epithelial cells in diabetic nephropathy. J Diabetes Complications 29:976–983. https://doi.org/10.1016/j.jdiacomp.2015.07.021*
7. *Perler BK, Friedman ES, Wu GD (2023) The Role of the Gut Microbiota in the Relationship Between Diet and Human Health. Annu Rev Physiol 85:449–468. https://doi.org/10.1146/annurev-physiol-031522-092054*
8. *Rizzo WB, Craft DA, Somer T, et al (2008) Abnormal fatty alcohol metabolism in cultured keratinocytes from patients with Sjögren–Larsson syndrome. J Lipid Res 49:410–419. https://doi.org/10.1194/jlr.M700469-JLR200*
9. *Schröder M, Kaufman RJ (2005) The mammalian unfolded protein response. Annu Rev Biochem 74:739–789. https://doi.org/10.1146/annurev.biochem.73.011303.074134*
10. *Moliterni C, Vari F, Schifano E, et al (2024) Lipotoxicity of palmitic acid is associated with DGAT1 downregulation and abolished by PPARα activation in liver cells. J Lipid Res 65:100692. https://doi.org/10.1016/j.jlr.2024.100692*
11. *Pinçon A, Coulombe J-D, Chouinard-Watkins R, Plourde M (2016) Human apolipoprotein E allele and docosahexaenoic acid intake modulate peripheral cholesterol homeostasis in mice. J Nutr Biochem 34:83–88. https://doi.org/10.1016/j.jnutbio.2016.05.001*

12. *Kim C, Hong Y, Lee H, et al (2018) MicroRNA-195 desensitizes HCT116 human colon cancer cells to 5-fluorouracil. Cancer Lett 412:264–271. https://doi.org/10.1016/j.canlet.2017.10.022*
13. *Romani A, Ieri F, Urciuoli S, et al (2019) Health Effects of Phenolic Compounds Found in Extra-Virgin Olive Oil, By-Products, and Leaf of Olea europaea L. Nutrients 11:1776. https://doi.org/10.3390/nu11081776*
14. *Achamrah N, Coëffier M, Déchelotte P (2016) Physical activity in patients with anorexia nervosa. Nutr Rev 74:301–311. https://doi.org/10.1093/nutrit/nuw001*
15. *Stolfi C, Maresca C, Monteleone G, Laudisi F (2022) Implication of Intestinal Barrier Dysfunction in Gut Dysbiosis and Diseases. Biomedicines 10:289. https://doi.org/10.3390/biomedicines10020289*
16. *Stockwell BR, Jiang X, Gu W (2020) Emerging Mechanisms and Disease Relevance of Ferroptosis. Trends Cell Biol 30:478–490. https://doi.org/10.1016/j.tcb.2020.02.009*
17. *Sun D, Wang L, Wu Y, et al (2025) Lipid metabolism in ferroptosis: mechanistic insights and therapeutic potential. Front Immunol 16:1545339. https://doi.org/10.3389/fimmu.2025.1545339*
18. *Knutsen T, Padilla-Nash HM, Wangsa D, et al (2010) Definitive molecular cytogenetic characterization of 15 colorectal cancer cell lines. Genes Chromosomes Cancer 49:204–223. https://doi.org/10.1002/gcc.20730*
19. *Sánchez-Martínez R, Cruz-Gil S, de Cedrón MG, et al (2015) A link between lipid metabolism and epithelial–mesenchymal transition provides a target for colon cancer therapy. Oncotarget 6:38719–38736. https://doi.org/10.18632/oncotarget.5340*
20. *Monti P, Ravera S, Speciale A, et al (2022) Mutant p53K120R expression enables a partial capacity to modulate metabolism. Front Genet 13:974662. https://doi.org/10.3389/fgene.2022.974662*
21. *Carta G, Murru E, Banni S, Manca C (2017) Palmitic Acid: Physiological Role, Metabolism and Nutritional Implications. Front Physiol 8:902. https://doi.org/10.3389/fphys.2017.00902*

22. *Palomino O, Giordani V, Chowen J, et al (2022) Physiological Doses of Oleic and Palmitic Acids Protect Human Endothelial Cells from Oxidative Stress. Molecules 27:5217. https://doi.org/10.3390/molecules27165217*
23. *Domínguez-López I, Arancibia-Riveros C, Casas R, et al (2022) Changes in plasma total saturated fatty acids and palmitic acid are related to pro-inflammatory molecule IL-6 concentrations after nutritional intervention for one year. Biomedicine & Pharmacotherapy 150:113028. https://doi.org/10.1016/j.biopha.2022.113028*
24. *Heberle H, Meirelles GV, da Silva FR, et al (2015) InteractiVenn: a web-based tool for the analysis of sets through Venn diagrams. BMC Bioinformatics 16:169. https://doi.org/10.1186/s12859-015-0611-3*
25. *Zirem Y, Ledoux L, Fournier I, Salzet M (2025) Profiler: an open web platform for multi-omics analysis. Bioinformatics btaf644. https://doi.org/10.1093/bioinformatics/btaf644*
26. *Szklarczyk D, Kirsch R, Koutrouli M, et al (2023) The STRING database in 2023: protein–protein association networks and functional enrichment analyses for any sequenced genome of interest. Nucleic Acids Res 51:D638–D646. https://doi.org/10.1093/nar/gkac1000*
27. *Matyash V, Liebisch G, Kurzchalia TV, et al (2008) Lipid extraction by methyl-tert-butyl ether for high-throughput lipidomics. J Lipid Res 49:1137–1146. https://doi.org/10.1194/jlr.D700041-JLR200*
28. *Giudetti AM, Guerra F, Longo S, et al (2020) An altered lipid metabolism characterizes Charcot-Marie-Tooth type 2B peripheral neuropathy. BBA - Mol Cell Biol Lipids 1865:158805. https://doi.org/10.1016/j.bbalip.2020.158805*
29. *Uhlén M, Fagerberg L, Hallström BM, et al (2015) Tissue-based map of the human proteome. Science 347. https://doi.org/10.1126/science.1260419*
30. *Fernández LP, Gómez de Cedrón M, Ramírez de Molina A (2020) Alterations of Lipid Metabolism in Cancer: Implications in Prognosis and Treatment. Front Oncol 10:577420. https://doi.org/10.3389/fonc.2020.577420*
31. *Zhang W, Liu Y, Liao Y, et al (2024) GPX4, ferroptosis, and diseases. Biomedicine & Pharmacotherapy 174:116512. https://doi.org/10.1016/j.biopha.2024.116512*
32. *Kalluri R, Weinberg RA (2009) The basics of epithelial–mesenchymal transition. J Clin Invest 119:1420–1428. https://doi.org/10.1172/JCI39104*

33. *Lamouille S, Xu J, Derynck R (2014) Molecular mechanisms of epithelial–mesenchymal transition. Nat Rev Mol Cell Biol 15:178–196. https://doi.org/10.1038/nrm3758*
34. *Jang M, Park R, Kim H, et al (2018) AMPK contributes to autophagosome maturation and lysosomal fusion. Sci Rep 8:12637. https://doi.org/10.1038/s41598-018-30977-7*
35. *He H, Davidson AJ, Wu D, et al (2010) Phorbol ester phorbol-12-myristate-13-acetate induces epithelial to mesenchymal transition in human prostate cancer ARCaP E cells. Prostate 70:1119–1126. https://doi.org/10.1002/pros.21146*
36. *Listenberger LL, Han X, Lewis SE, et al (2003) Triglyceride accumulation protects against fatty acid-induced lipotoxicity. Proc Natl Acad Sci USA 100:3077–3082. https://doi.org/10.1073/pnas.0630588100*
37. *Walther TC, Farese RV (2012) Lipid Droplets and Cellular Lipid Metabolism. Annu Rev Biochem 81:687–714. https://doi.org/10.1146/annurev-biochem-061009-102430*
38. *Thiery JP, Acloque H, Huang RYJ, Nieto MA (2009) Epithelial–Mesenchymal Transitions in Development and Disease. Cell 139:871–890. https://doi.org/10.1016/j.cell.2009.11.007*
39. *Khan F, Elsori D, Verma M, et al (2024) Unraveling the intricate relationship between lipid metabolism and oncogenic signaling pathways. Front Cell Dev Biol 12:1399065. https://doi.org/10.3389/fcell.2024.1399065*
40. *Listenberger LL, Han X, Lewis SE, et al (2003) Triglyceride accumulation protects against fatty acid-induced lipotoxicity. Proc Natl Acad Sci USA 100:3077–3082. https://doi.org/10.1073/pnas.0630588100*
41. *Walther TC, Farese RV (2012) Lipid Droplets and Cellular Lipid Metabolism. Annu Rev Biochem 81:687–714. https://doi.org/10.1146/annurev-biochem-061009-102430*
42. *Wu Y, Chen K, Li L, et al (2022) Plin2-mediated lipid droplet mobilization accelerates exit from pluripotency by lipidomic remodeling and histone acetylation. Cell Death Differ 29:2316–2331. https://doi.org/10.1038/s41418-022-01018-8*
43. *Huang S, Cao B, Zhang J, et al (2021) Induction of ferroptosis in human nasopharyngeal cancer cells by cucurbitacin B: molecular mechanism and therapeutic potential. Cell Death Dis 12:237. https://doi.org/10.1038/s41419-021-03516-y*
44. *Feng S, Tang D, Wang Y, et al (2023) The mechanism of ferroptosis and its related diseases. Molecular Biomedicine 4:33. https://doi.org/10.1186/s43556-023-00142-2*

45. *Jia D, Park J, Jung K, et al (2018) Elucidating the Metabolic Plasticity of Cancer: Mitochondrial Reprogramming and Hybrid Metabolic States. Cells 7:21. https://doi.org/10.3390/cells7030021*
46. *Liang Y, Liu J, Feng Z (2013) The regulation of cellular metabolism by tumor suppressor p53. Cell Biosci 3:9. https://doi.org/10.1186/2045-3701-3-9*
47. *Le TL, Joseph SR, Yap AS, Stow JL (2002) Protein kinase C regulates endocytosis and recycling of E-cadherin. Am J Physiol Cell Physiol 283:C489–C499. https://doi.org/10.1152/ajpcell.00566.2001*
48. *Andreeva AY, Piontek J, Blasig IE, Utepbergenov DI (2006) Assembly of tight junction is regulated by the antagonism of conventional and novel protein kinase C isoforms. Int J Biochem Cell Biol 38:222–233. https://doi.org/10.1016/j.biocel.2005.09.001*
49. *Li A, Zhu X, Wang C, et al (2019) Upregulation of NDRG1 predicts poor outcome and facilitates disease progression by influencing the EMT process in bladder cancer. Sci Rep 9:5166. https://doi.org/10.1038/s41598-019-41660-w*
50. *Saponaro C, Damato M, Stanca E, et al (2024) Unraveling the protein kinase C/NDRG1 signaling network in breast cancer. Cell Biosci 14:156. https://doi.org/10.1186/s13578-024-01336-z*
51. *Juin P, Hueber A-O, Littlewood T, Evan G (1999) c-Myc-induced sensitization to apoptosis is mediated through cytochrome c release. Genes Dev 13:1367–1381. https://doi.org/10.1101/gad.13.11.1367*
52. *Sciacovelli M, Frezza C (2017) Metabolic reprogramming and epithelial-to-mesenchymal transition in cancer. FEBS J 284:3132–3144. https://doi.org/10.1111/febs.14090*
53. *Zhao Z, Wang J, Kong W, et al (2024) Palmitic Acid Exerts Anti-Tumorigenic Activities by Modulating Cellular Stress and Lipid Droplet Formation in Endometrial Cancer. Biomolecules 14(5):601. https://doi.org/10.3390/biom14050601*
54. *He Y, Lin Y, Song J, et al (2025) From mechanisms to medicine: Ferroptosis as a Therapeutic target in liver disorders. Cell Communication and Signaling 23:125. https://doi.org/10.1186/s12964-025-02121-2*

55. *Ungvari Z, Fekete M, Fekete JT, et al (2024) Adherence to the Mediterranean diet and its protective effects against colorectal cancer: a meta-analysis of 26 studies with 2,217,404 participants. Geroscience 47:1105–1121. https://doi.org/10.1007/s11357-024-01296-9*
56. *Perez-Riverol Y, Bandla C, Kundu DJ, et al. (2025) The PRIDE database at 20 years: 2025 update. Nucleic Acids Res 53(D1):D543–D553. https://doi.org/10.1093/nar/gkae1011*
57. *Jensen-Cody SO, Potthoff MJ. Hepatokines and metabolism: Deciphering communication from the liver. Mol Metab. 2021 Feb;44:101138. doi:10.1016/j.molmet.2020.101138.*

# 5. A multi-omics map of OEA driven lipid remodeling in intestinal cell models

## Abstract

**Background:** Intestinal epithelial cell models exhibit strong metabolic plasticity, with lipid metabolism critically shaping proliferation, stress adaptation, and cellular homeostasis. Oleoylethanolamide (OEA), an endogenous oleic acid-derived lipid mediator and established PPAR$\alpha$ agonist, is therefore a compelling regulator of intestinal metabolic programs, yet its systems-level effects on lipid remodeling remain poorly defined. To date, OEA has been investigated predominantly in hepatic and systemic metabolic settings, while intestinal studies have focused mainly on barrier function and inflammation, with limited multi-omic characterization of lipid metabolism. Importantly, OEA signaling extends beyond PPAR$\alpha$, as it can also engage GPR119 and TRPV1 and has recently been identified as an endogenous ligand of HIF-3$\alpha$. These observations suggest a broader, context-dependent signaling network. Here, we investigated whether OEA reprograms lipid metabolism in intestinal-derived colon cell models and how this response varies across distinct cellular backgrounds.

**Methods:** An integrated multi-layer workflow was applied in three colon cell lines (HCT15, HCT116, HT29), using HuH7 cells as a hepatic comparator. OEA effects were assessed by: (1) MTS assays (10, 50, 100 μM; 24-48 h) for metabolic viability ; (2) BODIPY 493/503 confocal imaging for neutral lipid droplets (LDs) accumulation; (3) RT-qPCR for lipid-handling genes (including CD36, DGAT1, DGAT2); (4) SpiderMass for untargeted lipidomic and metabolomic profiling and for time-resolved uptake kinetics using OEA-d4 (30 min, 2 h, 24 h) and (5) label-free LC-MS proteomics with pathway/network analysis.

OEA-responsive proteomes were benchmarked against the synthetic PPAR$\alpha$ agonist GW7647 to estimate the PPAR$\alpha$-dependent component of the response.

**Results:** OEA was well tolerated at 10 and 50 μM, whereas 100 μM caused a time-dependent decrease in metabolic viability. Although overt morphological changes were limited, OEA triggered a clear dose-dependent accumulation of neutral lipid droplets - most prominently in HT29 and HuH7 cells-together with CD36 upregulation and cell line-specific DGAT1/2 expression patterns, consistent with differential lipid uptake and storage capacity. Lipidomics further supported an OEA-driven remodeling of glycerophospholipids, while metabolomics highlighted an enrichment of N-acylethanolamine/N-acyl-related features alongside reduced arachidonic acid. Notably, proteomics revealed extensive but cell line-specific network rewiring, with 50 μM OEA yielding the highest number of differentially expressed proteins and aligning with the most pronounced phenotypic shifts in lipid remodulation. Comparative analysis with GW7647 showed only partial overlap, supporting the coexistence of PPAR$\alpha$-dependent and PPAR$\alpha$-independent components in the OEA response. Finally, SpiderMass kinetics demonstrated rapid cellular uptake of OEA-d4 (30 min-2 h) and a variable persistence at 24 h across cell lines. Overall, OEA rapidly enters cells and reshapes lipid metabolism and signaling in a strongly context-dependent manner.

## 1. Introduction

Colorectal cancer cells (CRC) display marked metabolic plasticity, and lipid metabolism is increasingly recognized as a central axis supporting proliferation, redox control, stress adaptation, and interactions with the tumor microenvironment. Rewiring of fatty-acid uptake and synthesis, lipid storage, and lipid-derived signaling contributes to CRC progression and inter-/intra-tumoral heterogeneity, motivating integrated strategies able to capture coordinated changes across molecular layers (1). Within this landscape, endogenous bioactive lipids function as nutrient-responsive signals that couple metabolic status to transcriptional and signaling programs. OEA, an oleic acid-derived fatty-acid ethanolamide, was initially identified as a feeding-regulated satiety factor (2) and later shown to regulate energy balance through activation of PPAR$\alpha$ (3). Beyond systemic metabolism, OEA has also been proposed as a modulator of intestinal physiology and gut homeostasis, including potential connections with the gut microbial ecosystem (4) However, despite this mechanistic foundation, how OEA reshapes lipid handling and broader cellular metabolism across diverse CRC models remains insufficiently resolved. At the systems level, there is an important knowledge gap, particularly considering that OEA is itself a lipid mediator. It is therefore likely to transmit the effects of early remodeling of lipid composition and small-molecule metabolism, ultimately leading to downstream reorganization of protein networks and phenotypic changes such as neutral lipid storage.

To address this, we implemented an integrated, multi-layer workflow to map OEA-driven molecular and phenotypic remodeling in CRC cell models (HCT15, HCT116, HT29), using HuH7 cells as a hepatic comparator. We combined functional readouts (MTS viability assays) with confocal imaging of neutral lipid

droplets using BODIPY 493/503 staining to link cellular outcomes to lipid remodeling. At the systems level, LC-MS-based proteomics was used to delineate OEA-responsive protein networks and regulated pathways and to benchmark these signatures against matched treatments with the PPAR$\alpha$ agonist GW7647, enabling assessment of shared versus distinct signaling components. In parallel, SpiderMass - a real-time, minimally invasive mass spectrometry platform developed for rapid molecular analysis and spatially resolved workflows (5) - was employed for rapid lipidomic and metabolomic profiling and for time-resolved uptake/persistence kinetics. Kinetic SpiderMass measurements were acquired at 30 min, 2 h, and 24 h following exposure to 50 μM OEA, with the isotopically labeled standard OEA-d4 enabling time-resolved tracking. Collectively, this design was conceived to capture how a bioactive lipid rapidly enters cells and reshapes lipid metabolism and signaling in a context-dependent manner, bridging early molecular trajectories to downstream network remodeling and lipid-storage phenotypes across distinct cellular backgrounds.

## 2. Materials and Methods

### 2.1. Cell treatments and reagents

HCT15, HCT116 and HT29 human colorectal cancer cell lines, and Huh7 cells, were maintained in Dulbecco's Modified Eagle Medium (DMEM; Sigma-Aldrich, D5546; low glucose) supplemented with 10% fetal bovine serum (FBS; Capricorn, HI-12A), 100 U/mL penicillin, 100 μg/mL streptomycin (Sigma-Aldrich, P4333), and 2 mM L-glutamine (Sigma-Aldrich, G7513). Cells were cultured at 37 °C in a humidified atmosphere with 5% $CO_2$. All cell lines were routinely tested for mycoplasma contamination using a Mycoplasma Detection Kit (Aurogene, REP-

MYSNC-100). OEA was dissolved in DMSO to obtain a 10 mM stock solution and diluted in DMEM immediately before treatment; vehicle controls received the same final DMSO concentration. We selected 10 μM OEA as a biologically active, non-cytotoxic concentration commonly used *in vitro* to engage PPAR-$\alpha$ related signaling (6), and 50 μM to probe dose-dependent, higher-amplitude cellular responses while remaining within a widely used non-cytotoxic *in vitro* range (148,149). For uptake kinetics, deuterated OEA (OEA-d4; MedChemExpress, Cat. No. HY-107542S) was used as specified.

## 2.2. Cell viability assay

Cell metabolic activity was assessed using an MTS-based colorimetric assay (CellTiter 96® AQueous One Solution Cell Proliferation Assay, Promega, Cat. G3582) according to the manufacturer's instructions. Cells were seeded at $1.0 \times 10^4$ cells/well in 96-well plates and allowed to adhere overnight before treatment. At the indicated time points, MTS reagent was added directly to each well (20 μL into 100 μL culture medium; 1:5 v/v), and plates were incubated for 1-4 h at 37 °C protected from light until adequate color development. Absorbance was measured at 490 nm using a microplate reader. Background was corrected by subtracting the mean absorbance of blank wells. Viability was expressed as fold change relative to time-matched DMSO controls. All conditions were tested in six technical replicates, and experiments were independently repeated at least three times. Data are reported as mean ± SD (or SEM as specified). Statistical comparisons were performed by one-way ANOVA; $p < 0.05$ was considered significant.

## 2.3. Label-free quantitative proteomics and bioinformatic analysis

Whole-cell lysates from HCT15, HT29, and HCT116 cells treated with OEA (10 μM or 50 μM) or vehicle (DMSO) were subjected to label-free quantitative proteomics. Proteins were extracted using lysis buffer supplemented with protease and phosphatase inhibitors, and protein concentration was determined by bicinchoninic acid (BCA) assay. For each sample, 50 μg protein were reduced, alkylated, and digested overnight at 37 °C with trypsin using a filter-aided sample preparation (FASP) workflow (Amicon Ultra-0.5 mL centrifugal filters, 30 kDa MWCO; Millipore). After digestion, samples were treated with NaCl and 5% trifluoroacetic acid (TFA), dried, and reconstituted in 60 μL 0.1% formic acid (FA). An aliquot (20 μL) was desalted using Evotip Pure (Evosep, Denmark) according to the manufacturer's protocol. Peptides were analyzed on an Evosep One LC system coupled to a timsTOF HT mass spectrometer (Bruker Daltonics, Germany) using the 60 samples per day (60 SPD) method. Separations were performed on a C18 performance column (EV1109; 8 cm × 150 μm, 1.5 μm particle size) maintained at 40 °C. The analytical column was connected to a fused-silica emitter (10 μm inner diameter; Bruker Daltonics) integrated into a CaptiveSpray ion source (Bruker). Data were acquired in DIA-PASEF mode over an m/z range of 100–1700 and an ion mobility range of $1/K_0$ = 1.51–0.6 $V \cdot cm^{-2}$. DIA-NN was used for peptide/protein identification and quantification. DIA-NN outputs were processed in Perseus for statistical analyses and heatmap visualization. Differential expressions were assessed by one-way ANOVA with false discovery rate (FDR) correction (FDR < 0.05). Protein overlaps were visualized using InteractiVenn. Functional enrichment analyses were performed using Profiler and Ingenuity Pathway Analysis (IPA).

## 2.4. BODIPY staining and lipid droplets quantification

BODIPY 493/503 staining was performed on cells grown on coverslips (60-80% confluency) in 12-well plates. After treatments, cells were washed with PBS and incubated for 15 min at 37 °C with BODIPY 493/503 (1:1000 dilution from a 1 mg/mL stock prepared in PBS). After three washes with PBS, coverslips were mounted using Dako Fluorescent Mounting Medium (Agilent, Santa Clara, CA, USA) and imaged using an inverted confocal microscope (Zeiss Axio Observer Z1 equipped with an LSM 780 scanning head; Zeiss, Germany). Images were acquired with ZEN Black software using a 63×/1.4 oil-immersion objective (scale bar: 20 μm) and identical acquisition settings across conditions. LDs number for single cell were quantified using FIJI (version 2.9.0/1.53) with the "Analyze Particles" function, applying size and circularity filters to exclude background. Three representative images per condition were analyzed.

## 2.5. RNA extraction and RT-qPCR

Total RNA was extracted from HCT15, HCT116, HT29 and HuH7 cells using TRI reagent® (Zymo Research, R2050-1). RNA concentration and purity were evaluated using a NanoDrop One Spectrophotometer (Thermo Scientific). cDNA synthesis was performed using HIScript III RT SuperMix for qPCR (+gDNA wiper) (Vazyme Biotech), following the manufacturer's instructions. Quantitative PCR was carried out using iTaq Universal SYBR Green Supermix (Bio-Rad) on a Rotor-Gene Q 6000 system (Qiagen). GAPDH and ACTB (β-actin) were evaluated as housekeeping genes; GAPDH was used as the reference gene. Predesigned primers were obtained from Bio-Rad (PrimePCR). Primer sequences for the genes analyzed (including CD36, GAPDH, DGAT1, and DGAT2) are reported in the table below.

| Gene | Accession Number | Sequences 5'-3' |
|---|---|---|
| *Dgat1* | NM_012079.5 | F: GACGGATCCTTGAGATGCTG<br>R: TGAGCCAGATGAGGTGATTG |
| *Dgat2* | NM_032564.4 | F: CAAGAAAGGTGGCAGGAGGT<br>R: GCTGAAGTTGCAGAAGGCAC |
| *Gapdh* | AJ005371.1 | F: ATGGCCTTCCGTGTCCCAC<br>R: ACGCGTGCTTCACCACCTTC |
| *CD36* | NM_001001548.3 | F: AGATGCAGCCTCATTTCCAC<br>R: GCCTTGGATGGAAGAACAAA |

## 2.6. Statistical analysis

Data are presented as mean ± SD unless otherwise specified. Statistical analyses for non-omics experiments were performed using GraphPad Prism (version 8.3.0 for Windows). Comparisons among groups were carried out using one-way ANOVA followed by Tukey's post hoc test, with $p < 0.05$ considered statistically significant. For proteomics, LFQ intensities were $\log_2$-transformed and normalized prior to analysis in Perseus; proteins quantified in at least two biological replicates were retained. Missing values were imputed as constants (missing = 0). Differential expression testing was performed as described in Section 2.3 with FDR correction (FDR < 0.05).

## 2.7. OEAd4 uptake kinetics by SpiderMass

For kinetic experiments, HCT15, HCT116, HT29, and HuH7 cells were seeded in 24-well plates at $4.0 \times 10^4$ cells/well. Cells were treated with deuterated oleoylethanolamide (OEA-d4; MedChemExpress, Cat. No. HY-107542S) at a final concentration of 50 μM for 30 min, 2 h, or 24 h. At each time point, conditioned media were collected for quantification of extracellular OEA-d4 levels.

In parallel, adherent monolayers were processed for intracellular uptake measurements: following media removal, cells were washed three times with PBS to minimize residual extracellular OEA-d4, and the washed monolayers were analyzed to detect the OEA-d4 isotope signal. OEA-d4 detection in both conditioned media and washed monolayers was performed by SpiderMass under identical instrumental conditions across all samples and operated in negative ion mode. A continuous infusion of isopropanol containing leucine enkephalin potassium salt (IPA/LeuK) was applied during all acquisitions to ensure signal stability and mass accuracy, and identical settings were used throughout. Quantitative measurements were normalized to the total ion current (TIC) for each run to account for differences in instrument response and sample loading.

## 2.8. SpiderMass metabolomic and lipidomic profiling

Cells were seeded at $4.0 \times 10^4$ cells/well and treated for 24 h with OEA (50 μM). After treatment, cells were washed three times with PBS and thoroughly removed to minimize residual carryover, then profiled by SpiderMass operated exclusively in negative-ion mode. A continuous isopropanol/leucine enkephalin potassium salt (IPA/LeuK) infusion was applied throughout acquisitions to ensure signal stability and mass accuracy, and all samples were acquired under identical instrumental settings. To reduce non-biological contributions, spectra acquired from DMEM alone and from the IPA/LeuK infusion solution were used for background subtraction during preprocessing. Spectral data were analyzed in two mass ranges (m/z 50–600 and m/z 600–1100), corresponding predominantly to metabolomic and lipidomic features, respectively, enabling parallel but distinct interrogation of OEA-associated metabolic and lipidomic remodeling across the four cell lines. Unsupervised multivariate analyses were

first used to explore intrinsic structure and batch/cell-line effects, showing that global variance was dominated by cell-line identity rather than treatment when all four models were pooled; therefore, supervised classification approaches were implemented to robustly discriminate OEA-treated versus control samples. Lipid and metabolite features showing differential abundance between conditions, as derived from volcano plots (not shown), with a fold change (OEA vs CTRL) > 2 and p-value ≤ 0.05 were selected and reported in the corresponding tables as "specific."

## 3. Results

### 3.1 Global proteomic differences and pathway programs across HCT15, HCT116, HT29 and HuH7

Global proteomic profiling revealed strong, cell line-dependent expression landscapes across HCT15, HCT116, HT29 and HuH7. Unsupervised hierarchical clustering robustly grouped replicates by cell line (Fig. 1a), indicating high within-group consistency and pronounced between-model divergence. For this initial exploratory comparison, proteins were pre-filtered based on a significance threshold ($p < 0.01$) to focus the clustering on the most informative features. At the protein level, the heatmap displayed six distinct clusters (highlighted in Fig. 1a). To quantify conserved versus context-restricted components, the sets of quantified proteins were compared across models (Fig. 1b). This analysis identified a large shared core of 3532 proteins detected in all four cell lines, alongside smaller subsets preferentially detected in individual models (108 in HCT15, 63 in HuH7, 145 in HCT116, and 12 in HT29) and additional fractions shared by two or three lines. Together, these data support a proteomic

architecture composed of a conserved backbone coupled to cell line-specific features that likely reflect lineage state and intrinsic metabolic/signaling wiring.

Dimensionality reduction further corroborates these relationships. PCA showed clear separation of the four cell lines, with PC1 explaining 45.4% and PC2 29.8% of the variance (Fig. 1c), and tight clustering of replicates within each group. The concordance between hierarchical clustering and PCA indicates that the dominant sources of proteomic variance are stable and reproducible and that each cell line occupies a distinct molecular space. To connect protein modules with biological processes, proteins were subjected to pathway enrichment analysis (Fig. 1d-e). The enrichment heatmap revealed cluster-specific functional signatures, with enrichment confined to a restricted number of pathways rather than broadly spread across many terms (Fig. 1d). In Fig. 1d, pathway enrichment is summarized by the combined score (a composite metric integrating enrichment strength and statistical significance), whereas in Fig. 1e enrichment is displayed as gene count. Notably, MYC Targets V1 and mTORC1 signaling contributed the largest protein counts among enriched categories (Fig. 1e-f), underscoring that proliferative/growth programs represent prominent sources of baseline variability across these models. Because these pathways also displayed the most pronounced, cluster-restricted contrasts in the enrichment summary, we prioritized them for deeper inspection and report here the corresponding proteins driving the signals. In Cluster 1, the mTORC1 signaling gene set comprised (GMPS, SLC2A1, ENO1, HSPE1, UCHL5, WARS1, SLC7A5, STIP1, LDHA, PSMA3, PNP, PPA1, ETF1, ALDOA, ABCF2, PPIA). In the same cluster, MYC Targets V1 included (DUT, RRM1, VBP1, CAD, HSPE1, SRPK1, EEF1B2, PSMA6, LDHA, PSMA1, G3BP1, PRPF31, ETF1, CYC1, MRPL9, BUB3, ABCE1, PPIA, EIF4E, EIF4G2, RAN, MAD2L1). This composition is consistent with canonical MYC- and mTORC1-linked coupling of growth control to nutrient

uptake and anabolic metabolism (SLC2A1 and glycolysis-associated proteins), as described in prior work on MYC-driven glycolytic rewiring (DOI: 10.1074/jbc.C000023200) and on mTORC1 as a metabolic growth controller (150,151). In Cluster 2 (shared between HT29 and HuH7), MYC Targets V1 comprised (YWHAE, EIF4A1, SLC25A3, PCNA, PSMD14, GLO1, U2AF1, PSMD8, CDC20, SYNCRIP, TRIM28, C1QBP, PSMD3, RACK1, DHX15, RPS3, PSMD1, SNRPD3, IARS1, RPL18, CCT7, CCT5, CCT4, CCT3, NPM1, PABPC4, PTGES3, ILF2, GNL3, TUFM, PSMC6, TCP1, NDUFAB1, MCM4, MCM5, TARDBP, MCM2, EIF3B). In the same cluster, oxidative phosphorylation included (HSPA9, FH, SLC25A3, OAT, NDUFB7, COX4I1, NDUFB3, PDHB, ATP5F1C, SDHB, LRPPRC, ACAT1, ATP5F1A, NDUFAB1, ATP5PO, ACADM, SLC25A6). The co-enrichment of MYC targets with OXPHOS-related proteins aligns with evidence that MYC transcriptional programs extend into mitochondrial biogenesis and respiratory function, supporting the biological plausibility of this shared HT29/HuH7 module (7). Hallmark pathway definitions were referenced from MSigDB (8).

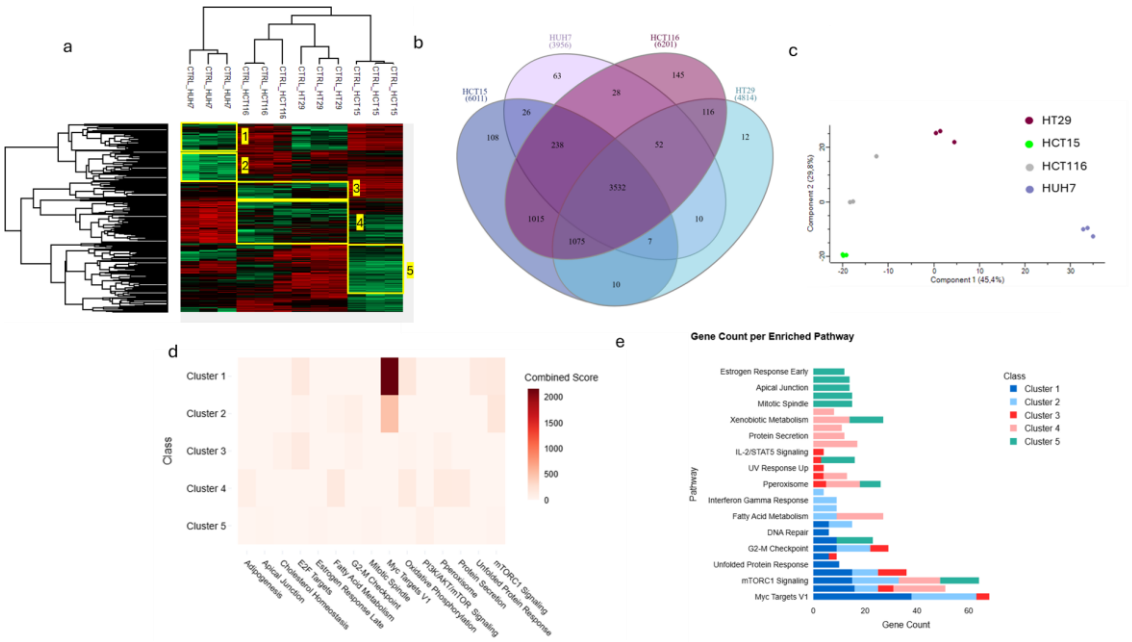


**Figure 1. Basal proteomic landscape and functional enrichment across cell models.** (a) Unsupervised hierarchical clustering of proteins selected for the initial exploratory analysis ($p < 0.01$), grouping replicates by cell line and identifying six major clusters. (b) Venn diagram showing shared and cell line-specific proteins across models. (c) PCA with separation driven predominantly by cell line identity. (d) Cluster-wise pathway enrichment heatmap reported as combined score (a composite metric integrating enrichment strength and statistical significance). (e) Enrichment displayed as gene count, the number of detected proteins mapped to each pathway. (f) Gene involvement matrix indicating the detected proteins associated with the enriched pathways.

## 3.2 Dose and time dependent effects of OEA on MTS viability.

Cell viability was assessed using the MTS tetrazolium reduction assay (a-d), which measures the conversion of MTS into a water-soluble formazan by metabolically active cells (9). HCT15, HCT116, HT29 and HuH7 were exposed to OEA (10, 50, or 100 μM) for 24 h or 48 h, and all values were normalized to the corresponding DMSO control at each time point. 10 μM OEA had no significant effects on cell viability which remained close to control at both 24 h and 48 h in

every cell line. At 50 μM viability was largely preserved at 24 h and 48 h in all the cell lines. The clearest effect emerged at 100 μM, which significantly lowered the MTS signal already apparent at 24 h in HCT15 and HuH7 , and more pronounced after 48 h across all four cell lines.

Taken together, these data suggest that OEA is generally well tolerated at 10 and 50 μM over 24-48 h, while 100 μM triggers a reproducible, time-dependent drop in metabolic viability. Under bright-field (phase-contrast) microscopy at 20× magnification (e), we observed that the overall monolayer architecture, adherence, and cell-cell contacts were largely preserved at both OEA concentrations. At 50 μM OEA, subtle stress-like features were occasionally apparent most notably in HCT15 and HCT116-including a tendency toward mild cell rounding and reduced spreading in a subset of fields, without widespread detachment or a major loss of confluence. OEA concentrations of 10 and 50 μM were selected as they proved non-cytotoxic across all four cell lines over 24-48 h. This range established a viable experimental window to investigate OEA-induced metabolic remodeling while allowing for the assessment of dose-dependent responses.

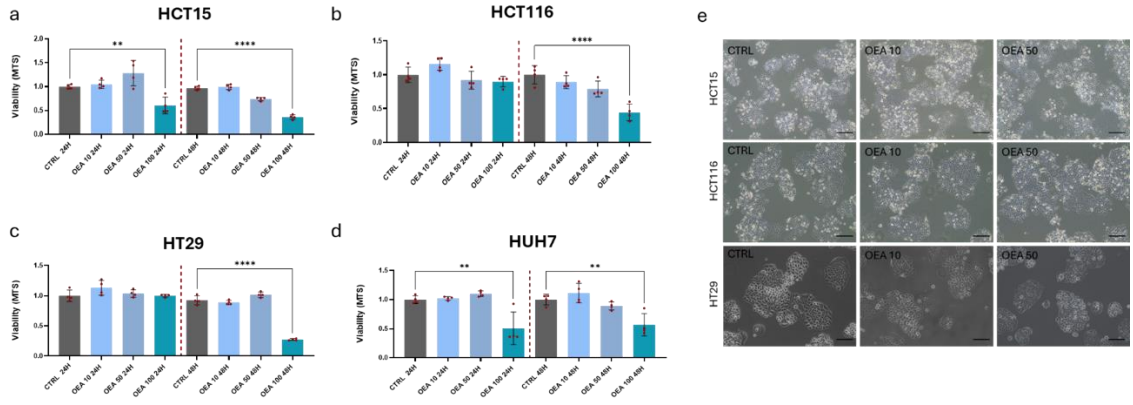


**Figure 2. OEA effects on cell metabolic viability in colorectal and hepatoma cell lines**. (a-e) MTS viability assay in HCT15 (a), HCT116 (b), HT29 (c), and HuH7 (d) cells treated with OEA (10, 50, or 100 μM) for 24 h or 48 h. Values are expressed as fold change relative to DMSO control at each time point. Bars represent mean with error bars; individual biological replicates are

overlaid as dots. (e) Representative bright-field images (20× magnification) of HCT15, HCT116 and HT29 cells treated with DMSO vehicle, OEA 10 μM, or OEA 50 μM. Data represent the mean ± SD of four independent experiments. (**p < 0.01; ***p < 0.001; ****p < 0.0001 versus DMSO).

## 3.3 OEA promotes lipid droplets accumulation and induces CD36 expression across colorectal and hepatoma cell lines

To determine whether OEA modulates neutral lipid storage, LDs were visualized by BODIPY 493/503 staining (green) with nuclear counterstaining (DAPI, blue). BODIPY 493/503 is a well-established fluorescent probe for detecting neutral lipid droplets by microscopy and for downstream quantification (10).

Fluorescence microscopy (Fig.3a) revealed that OEA increased the abundance of LDs in HCT15, HCT116, HT29 and HuH7 cell lines. LDs quantification (Fig. 3b) demonstrated a significant increase in LDs per cell following OEA exposure. In HCT15, OEA produced a moderate rise in LDs number, reaching significance at higher concentration. HCT116 exhibited a clearer dose response, with LDs per cell significantly increased at 50μM OEA compared with both control and the lower dose. The strongest induction was observed in HT29 and HuH7, where LDs number increased robustly with dose and reached high statistical significance, indicating that these lines are particularly responsive to OEA-driven neutral lipid storage. Because lipid droplets accumulation is often coupled to enhanced fatty-acid uptake, and CD36 is a well-established PPAR$\alpha$-responsive gene in the intestinal epithelium, we next quantified CD36 mRNA (Fig. 3c). OEA increased CD36 expression in a generally dose-dependent manner. Notably, HCT116, HT29, and HuH7 showed progressive induction with increasing OEA concentration, whereas HCT15 displayed a more non-linear pattern (minimal change at the lower dose and a significant increase at the higher dose). This

transcriptional response is consistent with previous reports showing that OEA activates PPAR$\alpha$, thereby inducing FAT/CD36 expression and enhancing fatty-acid uptake in metabolic tissues (11). Finally, to contextualize inter-line differences in LDs responsiveness, we compared basal expression of the terminal triglyceride-synthesis enzymes DGAT1 and DGAT2 (Fig. 3d). Baseline DGAT expression differed markedly across lines, with HuH7 showing the highest levels, while colorectal lines displayed lower expression overall and HT29 tended to occupy an intermediate range. Given that DGAT1 and DGAT2 catalyze the committed final step of triacylglycerol synthesis and are tightly linked to LDs biogenesis/expansion (12 ; 13) these baseline differences likely contribute to the cell line-specific capacity to channel incoming fatty acids into neutral lipid storage and visible LDs accumulation upon OEA treatment.

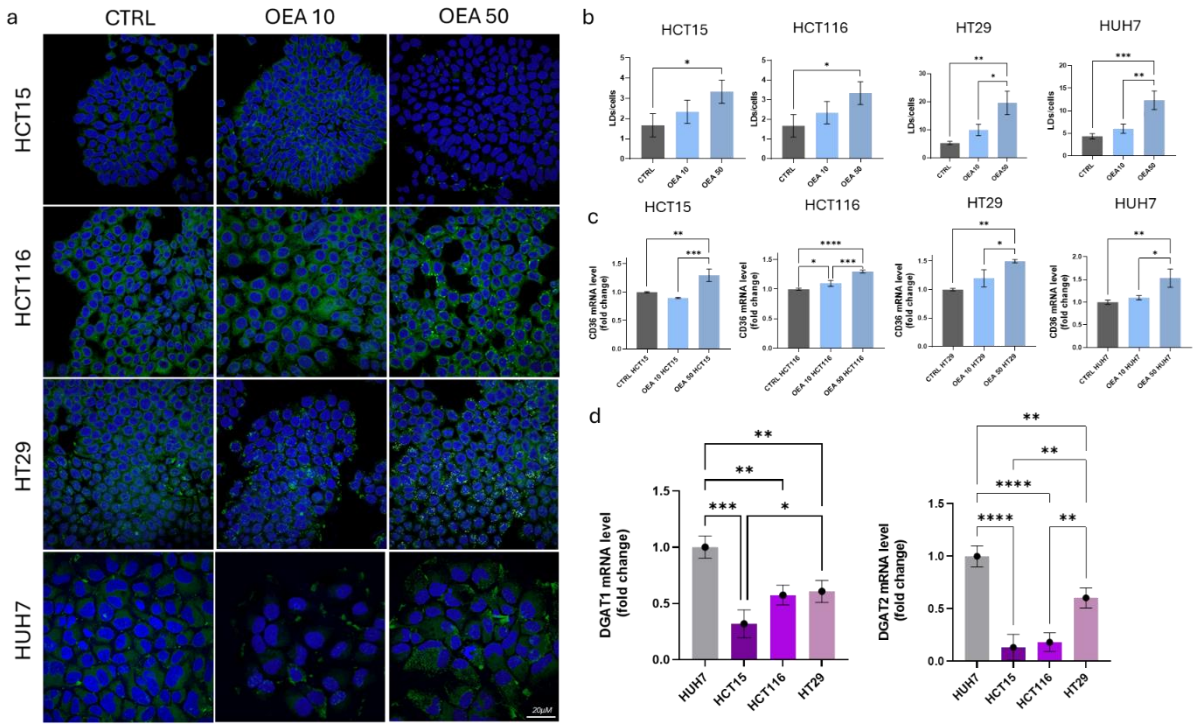


**Figure 3. OEA induces lipid droplets accumulation and modulates lipid-handling gene expression in colorectal and hepatoma cell lines.** (a) Representative fluorescence micrographs (scale bar 20 μm) of HCT15, HCT116, HT29, and HuH7 cells treated with vehicle (CTRL) or OEA (10 or 50 μM) and stained with BODIPY 493/503 to label neutral lipid droplets (green) and DAPI to label nuclei (blue). (b) Quantification of lipid droplets per cell (LDs/cell) in each cell line under CTRL, OEA 10, and OEA 50 conditions. (c) CD36 mRNA levels measured by RT-qPCR after OEA treatment and reported as fold change relative to the control for each cell line. (d) Basal DGAT1 and DGAT2 mRNA levels across the indicated cell lines (RT-qPCR; relative expression shown as fold change). Data represent the mean ± SD of three independent experiments. (**p < 0.01; ***p < 0.001; ****p < 0.0001 versus DMSO).

## 3.4 Uptake and cell line dependent persistence of OEA-d4 measured by SpiderMass

To better understand how OEA acts across different cell lines, particularly in terms of uptake, intracellular persistence, and intracellular degradation, we tracked its handling using an OEA-d4 time-course. As an amphipathic fatty-acid ethanolamide, OEA can rapidly traverse cellular membranes and/or engage protein-assisted uptake routes, consistent with the fast internalization reported for anandamide (14) In line with this, OEA displays rapid and tightly regulated intestinal kinetics *in vivo* (15), making cell line-specific differences in intracellular retention especially informative for interpreting downstream molecular remodeling. Figure 4 summarizes the time course of 50 μM OEA-d4 detected by SpiderMass (real-time ambient MS) in both the extracellular medium (green) and the cellular fraction (purple) at 0.5 h, 2 h, and 24 h. Across all four models, OEA-d4 showed rapid early redistribution, with most changes occurring within the first 0.5-2 h, consistent with fast partitioning/uptake of this amphipathic lipid. However, the subsequent trajectories were strongly cell line dependent. In HCT15 (a), OEA-d4 dropped sharply in the medium while the intracellular signal increased markedly and remained high at 24 h, indicating efficient uptake followed by slow clearance/persistence of the intact labeled species. In HCT116 (b), uptake was also rapid, but by 24 h the medium and cellular signals converged, consistent with redistribution toward an apparent near equilibrium rather than sustained intracellular accumulation. In contrast, HT29 (c) and HuH7 (d) displayed rapid depletion in the medium accompanied by minimal intracellular accumulation, consistent with faster downstream processing/turnover and limited persistence of intact OEA-d4. Importantly, the updated figure provides an orthogonal readout of N-acylethanolamine hydrolytic capacity: FAAH1 intensity levels (e) were higher in HT29 than in

HCT15 and HCT116, supporting a model in which greater FAAH-mediated hydrolysis contributes to faster removal of intact OEA-d4 and lower intracellular persistence in HT29. Conversely, the lower FAAH signal in HCT15/HCT116 is consistent with reduced hydrolytic clearance and the more persistent OEA-d4 profiles observed in these lines, in agreement with low FAAH expression reported in public resources such as the Human Protein Atlas (16). Surprisingly, in HuH7 cells the FAAH protein was not detected by proteomic analysis. In this case, its hydrolytic activity may be compensated by other endocannabinoid- and endocannabinoid-like lipid - degrading hydrolases, such as NAAA and monoacylglycerol lipase (MGAL). Figure 5 shows the bar plots of OEA-d4 ion counts measured by SpiderMass in both the extracellular medium and the intracellular (cell-associated) fraction across time (0.5 h, 2 h, and 24 h), allowing a direct comparison of OEA-d4 depletion from the medium versus retention within cells. The statistical annotations report significant pairwise differences between time points, indicating that OEA-d4 levels change dynamically over the time course rather than remaining stable.

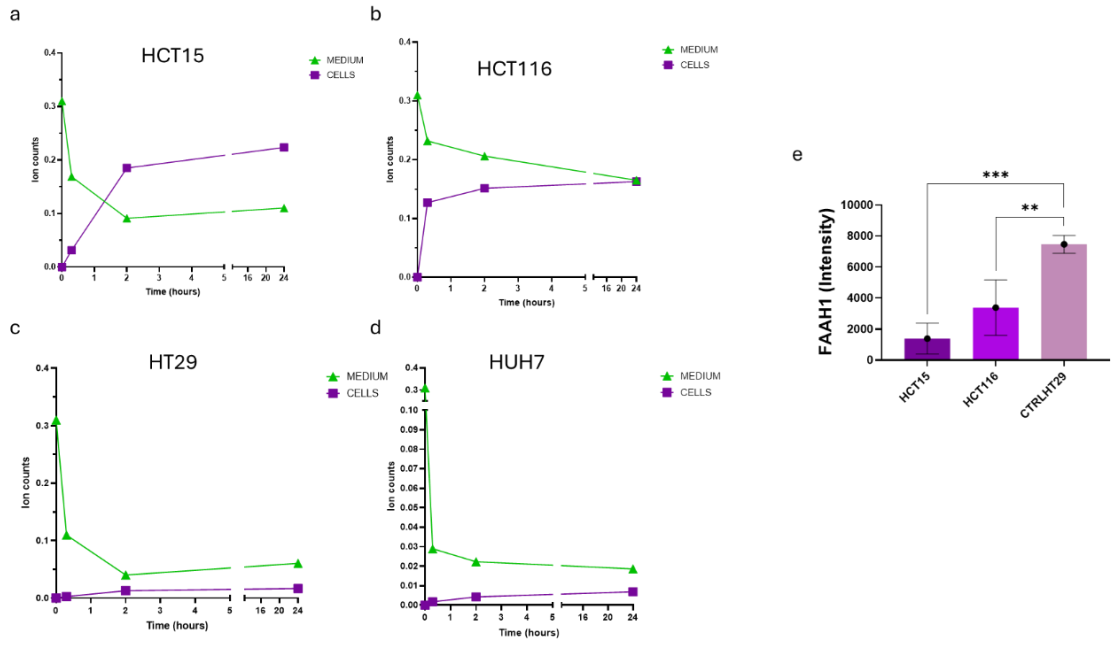


**Figure 4. SpiderMass kinetic curve of OEA-d4 (50 μM) in medium and cells across four cell lines.** OEA-d4 levels were monitored by SpiderMass ambient mass spectrometry at 30 min (0.5 h), 2 h, and 24 h after exposure to 50 μM OEA-d4. Each panel corresponds to a different cell line: (a) HCT15, (b) HCT116, (c)HT29, (d) HuH7. For each cell line, the OEA-d4 signal is reported as relative ion intensity (counts) measured in the cell culture medium (green trace) and in the cellular fraction (purple trace) at each time point. In (e) intensity level of FAAH1 measured by LC-MS at basal level in HCT15, HCT116 and HT29. Marker symbols indicate the measured values at each time point, and lines connect points to visualize the temporal trend for each compartment. Data represents the mean ± SD of six independent experiments. (**p < 0.01; ***p < 0.001; ****p < 0.0001 versus DMSO)

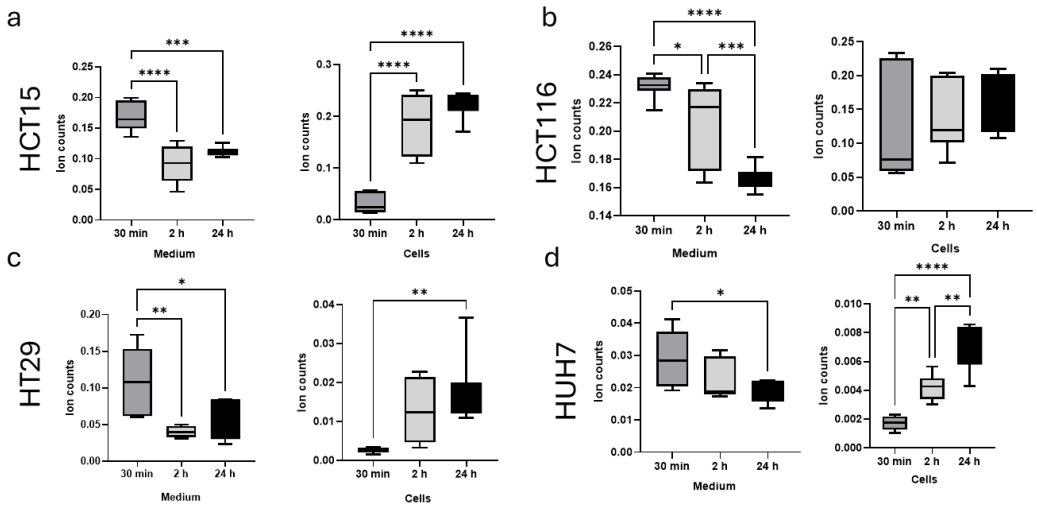

**Figure 5. Time-course of OEA-d4 handling measured by SpiderMass**. Boxplots show OEA-d4 signal (ion counts) detected by SpiderMass (real-time ambient MS) in the extracellular medium and in the cellular fraction for HCT15 (a), HCT116 (b), HT29 (c), and HuH7 (d) after exposure to 50 μM OEA-d4. Samples were collected at 30 min, 2 h, and 24 h (24 h shown in black). Boxes indicate the interquartile range with the median line; whiskers represent the distribution of values. Statistical significance is reported as $p < 0.05$ (), $p < 0.01$ (), $p < 0.001$ (), and $p < 0.0001$ (****)

## 3.5 Comparative proteomics reveal heterogeneous OEA responses across colorectal cancer models

Heatmaps with hierarchical clustering generated from FDR-corrected proteins (FDR ≤ 0.05) show a clear separation between CTRL and OEA-treated samples in all three colon cancer cell lines - HCT15 (Fig. 6a), HCT116 (Fig. 6b), and HT29 (Fig. 6c) - supporting a consistent OEA-dependent shift in protein abundance across doses. In each heatmap, two main protein clusters (highlighted as 1-2) display opposite abundance patterns, indicating coordinated protein modules that are predominantly increased versus decreased upon OEA exposure. To place these regulated protein sets into functional context, IPA network analysis of the same FDR-significant proteins highlights distinct, cell line-specific regulatory hubs and biological outputs (Fig. 6d-f), with orange indicating upregulated processes and blue indicating downregulated ones. In HCT15 cells (Fig. 6d), IPA network analysis shows a polarized response in which upregulated nodes (orange) converge on a central TP53 hub linked to microtubule dynamics and cytoskeleton/cytoplasm organization, together with stress-related outputs (including the predicted endoplasmic reticulum stress response) and cancer-associated functional annotations. Notably, HCT15 carries a TP53 p.S241F missense mutation, reported as a mutant p53 gain-of-function (GOF) allele, which can support oncogenic stress-adaptive programs rather than canonical

tumor-suppressive responses (17) . This is mechanistically relevant because p53 is also a recognized regulator of lipid and lipoprotein metabolism and broader lipid-homeostasis programs (18 ,19). In contrast, the downregulated arm (blue) is organized around a MYC-centered module, consistent with attenuation of MYC-linked growth/metabolic wiring, in line with the role of MYC as a master regulator of nutrient acquisition and metabolic reprogramming in cancer (20). In HCT116 (e), the IPA network is best interpreted as a RICTOR/mTORC2-skewed response occurring alongside repression of a MYC-driven growth module. Specifically, RICTOR is upregulated (orange) and sits as a key upstream node connected to growth-control/survival wiring, consistent with the central role of RICTOR as an essential component of mTORC2 and a determinant of Akt Ser473 phosphorylation (21 , 22) . In parallel, MYC is downregulated (blue) together with MYC-associated functional outputs (cell proliferation/colony formation/S-phase-related annotations, shown in blue), indicating attenuation of MYC-dependent proliferative/metabolic programs (23). In HT29 cells, the IPA network is dominated by a downregulated motility/invasion program, with proto-oncogene tyrosine-protein kinase Src (SRC) emerging as the central suppressed hub that connects multiple functional annotations related to cell movement, migration, and invasion across tumor line contexts. This pattern is consistent with the established role of Src-family signaling in driving colorectal cancer adhesion turnover and metastatic behavior (24). Coherently, the network shows downregulation of SDCBP (syntenin) scaffold known to promote tumor cell motility and metastasis through c-Src - linked pathways (25) together with suppression of PRL/PRL-3 (PTP4A3), a metastasis-associated phosphatase originally identified in colorectal cancer metastases (26). Additional repressed nodes include vascular endothelial growth factor A (VEGFA), which can support pro-migratory/invasive phenotypes via PI3K/AKT-linked mechanisms (27), and a decreased signal for ROBO receptor signaling, a pathway implicated in cancer

cell migration and metastasis regulation (28). Overall, this interactome supports OEA shifts HT29 toward reduced migratory/invasive wiring, centered on coordinated inhibition of SRC-associated signaling. Lipid-metabolism related proteins represented only a minority of the OEA-regulated proteome, but they formed a coherent lipid-handling signature that was most evident in HCT15 and, to a lesser extent, HT29. In HCT15, OEA increased sterol/cholesterol pathway nodes (LSS, DHCR7, DHCR24, HSD17B7, ACAT2) together with enzymes involved in fatty-acid metabolism (ACSL4, DECR1). Proteins supporting neutral-lipid storage and ER-lipid droplet coupling (GPAT4, AUP1) were also increased. Moreover, OEA upregulated membrane glycerophospholipid synthesis/remodeling nodes (PCYT2, LPCAT1, MBOAT7), providing a mechanistic bridge to the Spider Mass lipidomics. Additional lipid traffic/signaling nodes (FABP5, OSBPL2, OSBPL10, OSBPL11, DAGLB, LSR) further support broader rewiring of intracellular lipid distribution. In HT29, fewer canonical lipid enzymes were induced, but upregulation of sterol/membrane and ER/LD-associated factors (DHCR24, FAF2/UBXD8, RTN3, PIGK) is consistent with membrane/sterol adaptation and ER-lipid droplet coupling. By contrast, the limited HCT116 upregulated set primarily featured trafficking-related proteins (RAB8B, RABGGTB, CHMP7), pointing to membrane remodeling processes rather than overt induction of lipid-metabolic enzymes in this background.

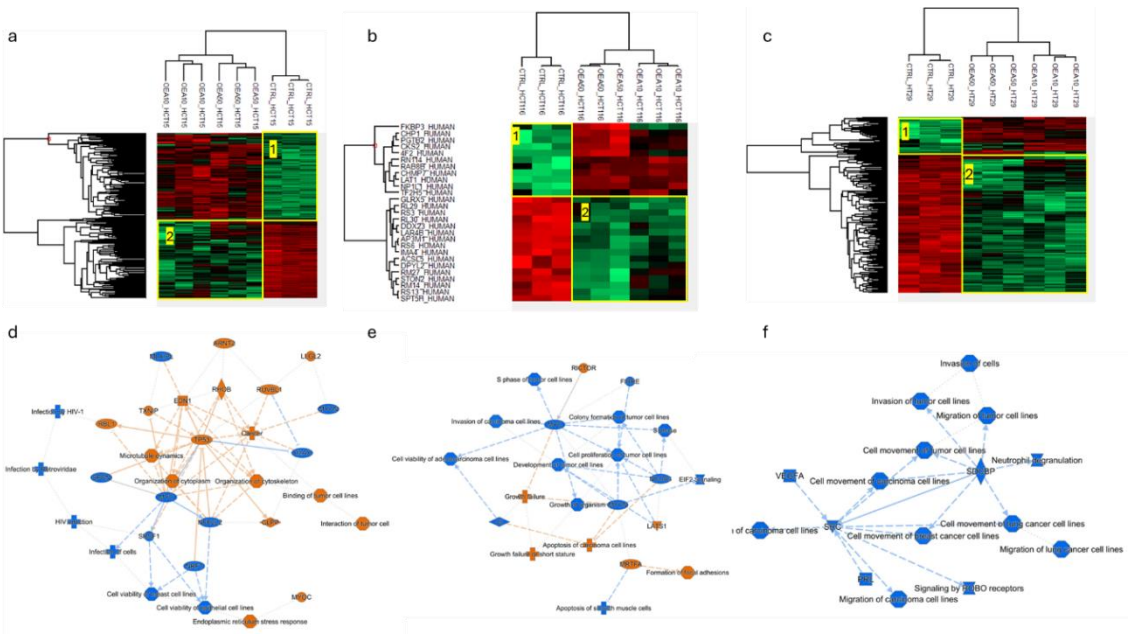


**Figure 6. OEA modulates protein-expression programs in colorectal cancer cell lines.** Unsupervised hierarchical clustering heatmaps of differentially expressed proteins in HCT15 (a), HCT116 (b), and HT29 (c) cells treated with OEA (10 or 50μM) compared with CTRL. Rows represent genes and columns represent samples/replicates; red indicates higher expression and green indicates lower expression relative to the row mean. Yellow boxes highlight two major gene clusters (1-2) showing opposite regulation patterns between conditions. (d-f) Functional interaction/enrichment networks built from the regulated proteins, highlighting biological themes associated with the OEA response, including cytoskeleton/microtubule organization, cell proliferation and apoptosis, cell migration/invasion and focal adhesion related processes (representative hub nodes include TP53, MYC, SRC, VEGFA, and SDCBP).

## 3.6 Venn diagrams confirm divergent OEA proteomic signatures across HCT15, HCT116, and HT29

Venn diagrams summarize the overlap of significantly regulated proteins (filtered by FDR<0,05) across HCT15, HCT116, and HT29 following OEA treatment. Upregulated proteins (Fig.7a) were highly cell line-specific: HCT15 displayed the largest set (716), followed by HT29 (42) and HCT116 (11). Importantly, no upregulated proteins were shared across all three cell lines (0). Overlap was limited to HCT15-HCT116 (2 proteins) and HCT15–HT29 (17 proteins), while HCT116–HT29 shared none (0), highlighting strong context dependence of the OEA-induced upregulation program. For downregulated proteins (Fig.7b), HCT15 again showed the strongest response (679), with HT29 showing an intermediate set (159) and HCT116 a small set (17).

In contrast to the upregulated direction, a small common core of downregulated proteins was shared across all three cell lines (2 proteins). The largest pairwise overlap occurred between HCT15 and HT29 (59 proteins), while overlap between HCT15 and HCT116 was modest (5 proteins) and HCT116 and HT29 shared none (0). Overall, repression signatures appear slightly more convergent than induction signatures,yet remain largely cell line restricted. Volcano plots (c-e) compare CTRL vs OEA 50 μM in each cell line, with significant proteins defined as those meeting a $-\log(\text{p-value}) \geq 2$ threshold ($p \leq 0.01$). Consistent with the Venn summaries, HCT15 shows the broadest and most densely populated significant landscape, indicating the largest magnitude and number of OEA-regulated proteins. HT29 displays an intermediate response with a notable enrichment of significant proteins on the downregulated side, whereas HCT116 shows the fewest significant changes, consistent with a comparatively weak proteomic remodeling under OEA at this dose. OEA 50 μM was selected as the highest non-

cytotoxic concentration producing the most robust and reproducible lipid phenotype (lipid droplet accumulation and increased CD36). It also yielded more significantly regulated proteins in the three cell lines versus control than the lower dose (Fig. 7c-e). Therefore, 50 μM was used for subsequent SpiderMass lipidomic/metabolomic profiling to maximize sensitivity for detecting OEA-driven molecular remodeling.

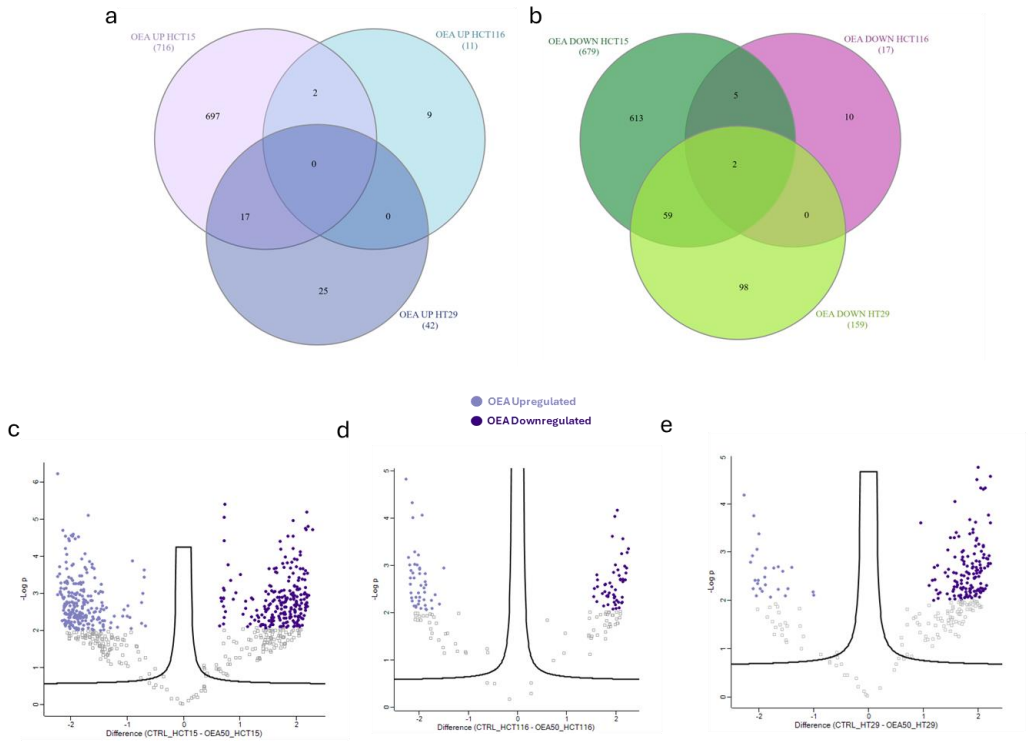


**Figure 7. Overlap and magnitude of OEA-regulated gene expression in colorectal cancer cell lines.** (a) Venn diagram of genes upregulated by OEA in HCT15, HCT116, and HT29 cells; numbers indicate genes unique to each line or shared between lines. (b) Venn diagram of proteins downregulated by OEA in HCT15, HCT116, and HT29 cells. (c-e) volcano plots comparing CTRL vs OEA 50 μM in HCT15 (c), HCT116 (d), and HT29 (e). The x-axis represents the $\log_2$ fold change (CTRL vs OEA 50 μM), while the y-axis shows the statistical significance expressed as $-\log_{10}$(p-value). Light purple dots represent OEA-upregulated proteins (negative differences), dark purple dots represent OEA-downregulated proteins (positive differences), and grey dots indicate non-significant proteins.

## 3.7 Overlap between OEA and GW7647 regulated proteomes reveals a variable PPAR$\alpha$-dependent component of the OEA response

Across the three cell lines, Venn diagrams (Fig. 8a-c) compare proteins significantly upregulated (top) or downregulated (bottom) in the comparison CTRL vs OEA and CTRL vs GW7647 after treatment for both at both at 10 and 50 μM, a high-affinity synthetic PPAR$\alpha$ agonist (29) Because OEA is an endogenous PPAR$\alpha$ ligand (30) the degree of overlap between OEA- and GW7647-regulated proteomes provides an operational estimate of the PPAR$\alpha$-aligned component of the OEA response, whereas non-overlapping protein sets point to PPAR$\alpha$-independent effects and/or differences in ligand potency, kinetics, or receptor engagement.

In HCT15 (Fig. 8a,d), OEA regulated a large number of proteins (717 increased, 680 decreased), broadly comparable in scale to GW7647 (852 increased, 1322 decreased). However, concordance between the two treatments was limited: 156 proteins were commonly increased and 202 were commonly decreased. Thus, only 22% of OEA-upregulated and 30% of OEA-downregulated proteins were also regulated by GW7647, indicating that while a clear subset of the OEA signature is consistent with PPAR$\alpha$ activation, most of the HCT15 response is not reproduced by the canonical agonist, supporting a substantial ligand-specific and/or PPAR$\alpha$-divergent component. In HCT116 (Fig. 8b,e), OEA elicited a markedly smaller signature (11 increased, 16 decreased), whereas GW7647 induced extensive remodeling (668 increased, 815 decreased). Despite the limited size of the OEA response, overlap with GW7647 was proportionally high (5 shared increases; 9 shared decreases), corresponding to 45% of OEA-upregulated

and 56% of OEA-downregulated proteins. This pattern suggests that, in HCT116, the modest proteomic changes triggered by OEA largely track with a PPAR$\alpha$-like program, but the overall amplitude of remodeling is much weaker than that achieved by GW7647. In HT29 (Fig. 8c,f), OEA increased relatively few proteins (43) but decreased a larger set (159), while GW7647 again produced a broad response (683 increased, 1373 decreased). Overlap was moderate among upregulated proteins (18 shared; 42% of OEA increases) and stronger among downregulated proteins (81 shared; 51% of OEA decreases), indicating that roughly half of the HT29 OEA signature - particularly the repressed component- maps onto a GW7647-responsive, PPAR$\alpha$-consistent program. Taken together, these comparisons indicate that OEA engages a shared core of GW7647-responsive proteins across models, supporting a PPAR$\alpha$-dependent component of the OEA response, but with pronounced cell line-specific differences in both signature size and PPAR$\alpha$ alignment. HCT15 displays broad remodeling with limited concordance to GW7647 (suggesting prominent PPAR$\alpha$-independent and/or ligand-specific effects), HCT116 shows a small but largely PPAR$\alpha$-consistent response, and HT29 exhibits an intermediate profile with a particularly strong PPAR$\alpha$-consistent component among downregulated proteins.

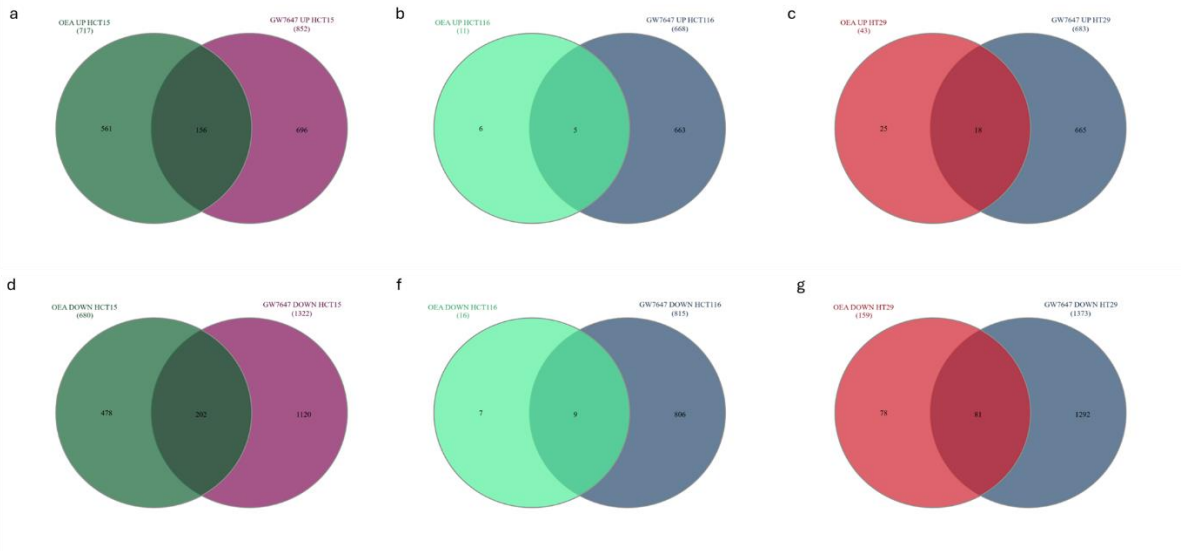


**Figure 8. Overlap between OEA and GW7647 regulated proteome in colorectal cancer cell lines.** Venn diagrams show proteins regulated by OEA versus the selective PPAR$\alpha$ agonist GW7647. Upregulated sets are shown for HCT15 (a), HCT116 (b), and HT29 (c); downregulated sets for HCT15 (d), HCT116 (e), and HT29 (f). Overlap indicates a shared PPAR$\alpha$-aligned response, whereas non-overlap highlights compound- and cell line–specific programs.

## 3.8 SpiderMass lipidomics indicates OEA-associated remodeling of membrane glycerophospholipids and lipid signaling

Untargeted lipidomic profiling by SpiderMass revealed a robust and reproducible remodeling of membrane glycerophospholipids in OEA 50 μM treated samples versus controls. This pattern reflects the shared/common response across all four cell lines (HCT15, HCT116, HT29, and HuH7), highlighting a conserved OEA-associated membrane-lipid signature despite broader cell line- specific differences elsewhere. A supervised classification model showed high performance (Fig. 9a), with 105/107 samples correctly classified (CTRL: 51 correct, 1 misclassified; OEA: 54 correct, 1 misclassified), indicating that OEA induces a distinct lipidomic fingerprint. Consistent with this,

(Fig. 9d) UMAP dimensionality reduction separated CTRL and OEA groups into clearly distinct clusters. At the feature level, (Fig. 9 b-e) several ions were significantly decreased under OEA, dominated by phosphatidylethanolamines (PEs) and a lysophospholipid signal, including m/z 716.55 (PE 34:1), 764.55 (PE 38:5), 766.55 (PE 38:4), 768.55 (PE 38:3), and 794.55 (PE 40:4), together with m/z 737.55 annotated as lysophosphatidylinositol, LPI 28:1.

Conversely, (Fig.9 c-f) OEA increased a focused set of glycerophospholipids and signaling-related species, including PE signals m/z 726.55 (PE 35:3), 770.55 (PE 38:2), 772.55 (PE 38:1), 820.55 (PE 42:5), and 822.55 (PE 42:4), as well as lysophosphatidic acid m/z 655.55 (LPA 34:3), phosphatidylserines m/z 878.55 (PS 43:5) and 880.55 (PS 43:4), and multiple phosphatidic acids m/z 893.75 (PA 50:3), 919.75 (PA 52:4), and 921.75 (PA 52:3) (additional discriminant ions such as m/z 945.55 and 938.45 also increased). Mechanistically, the simultaneous depletion of several PE species and accumulation of other PE species with distinct chain composition is consistent with activation of phospholipid remodeling via deacylation-reacylation (31). The coordinated increase in PA and LPA further suggests coupling between membrane turnover and lipid-mediated signaling: PA is a central intermediate and signaling node linked to mTOR regulation (32) and mTORC1 recruitment under stress (176), while LPA is a potent bioactive lipid acting via lysophosphatidic acid receptors (LPARs) with well-established roles in cancer-related programs (33). Finally, increased PS signals may reflect broader membrane reorganization and/or stress-associated trafficking, processes that intersect with apoptosis-related membrane dynamics (34). All reported discriminant features were supported by SMMS (SpiderMass MS/MS) fragmentation, strengthening the proposed annotations.

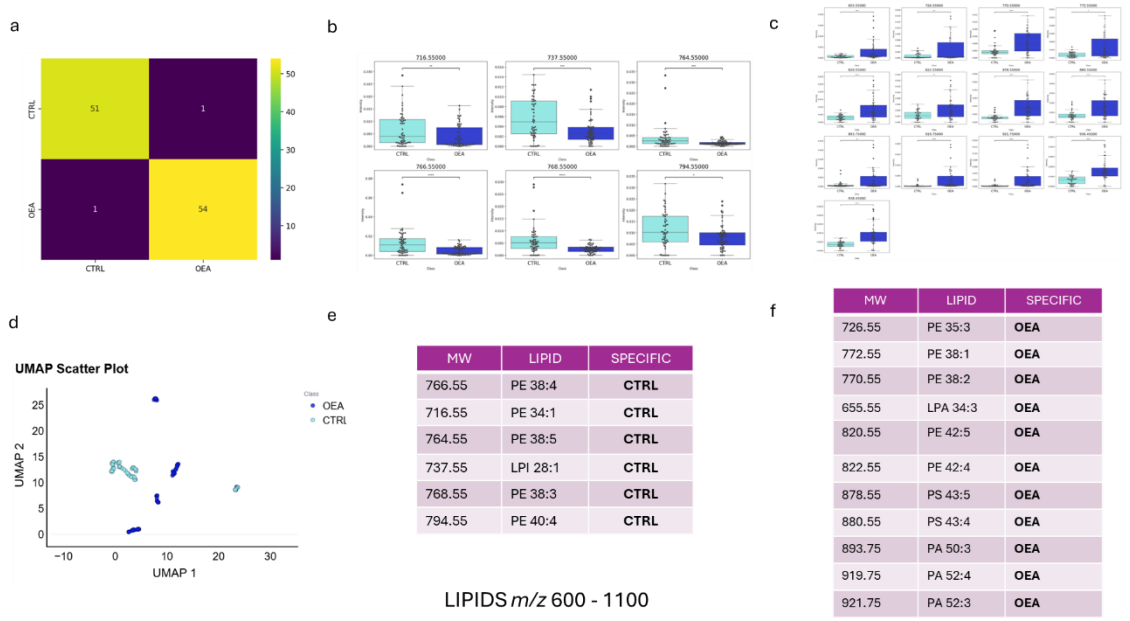


| MW | LIPID | SPECIFIC |
|---|---|---|
| 766.55 | PE 38:4 | CTRL |
| 716.55 | PE 34:1 | CTRL |
| 764.55 | PE 38:5 | CTRL |
| 737.55 | LPI 28:1 | CTRL |
| 768.55 | PE 38:3 | CTRL |
| 794.55 | PE 40:4 | CTRL |

| MW | LIPID | SPECIFIC |
|---|---|---|
| 726.55 | PE 35:3 | OEA |
| 772.55 | PE 38:1 | OEA |
| 770.55 | PE 38:2 | OEA |
| 655.55 | LPA 34:3 | OEA |
| 820.55 | PE 42:5 | OEA |
| 822.55 | PE 42:4 | OEA |
| 878.55 | PS 43:5 | OEA |
| 880.55 | PS 43:4 | OEA |
| 893.75 | PA 50:3 | OEA |
| 919.75 | PA 52:4 | OEA |
| 921.75 | PA 52:3 | OEA |

**Figure 9. SpiderMass lipidomics discriminates CTRL and OEA 50 µM and identifies OEA-driven glycerophospholipid remodeling.** (a) Confusion matrix of the supervised classification model separating CTRL and OEA samples, showing high classification performance with minimal cross-misclassification; (b) Boxplots of lipid features decreased in OEA versus CTRL; (c) Boxplots of lipid features increased in OEA versus CTRL; (d) UMAP projection showing separation of CTRL and OEA samples based on the lipidomic fingerprint; Tables representing the lipid (e) and metabolites (f) more abundant (Fold change >2, Pv <0,05) in control and OEA.

## 3.9 SpiderMass metabolomics reveals OEA-associated changes consistent with a metabolic shift in lipid mediator pools

Untargeted metabolomic profiling by SpiderMass revealed a compact set of lipid-related features that robustly discriminated CTRL from OEA 50 µM - treated samples. A supervised classification model showed high performance (Fig.10 a), with 103/107 samples correctly classified (96.3% accuracy) (50 CTRL and 53 OEA correctly assigned, with only 2 cross-misclassifications per class). At the feature level, (Fig. 10 b-e) boxplot comparisons showed significant increases in OEA for

m/z 230.1500 (NAE, N-acylethanolamine 10:0;O), m/z 360.2500 (NAE 20:5;O) and m/z 362.2500 (N-acyl species, including a NAT, N-acyl taurine 16:0 compatible assignment), together with very-long-chain polyunsaturated fatty acids (FAs) m/z 409.3500 (FA 28:7) and m/z 411.3500 (FA 28:6). In contrast, m/z 303.2500 (FA 20:4; commonly corresponding to the arachidonic acid pool) was decreased under OEA treatment (Fig10 b-e). Overall, these coordinated changes are consistent with an OEA-associated metabolic shift, characterized by enrichment of fatty-acid amide-type mediators (NAEs/N-acyl taurines) and a relative depletion of the 20:4 (arachidonic acid) substrate pool. This interpretation is biologically plausible because OEA is an endogenous lipid signal that activates PPAR-$\alpha$ (35) and can reprogram lipid utilization pathways. In addition, PPAR-$\alpha$ driven remodeling of lipid handling (potentially including increased CD36-mediated fatty-acid uptake and trafficking) could favor incorporation/turnover of non-arachidonate acyl chains (18:1), thereby reducing the relative abundance of 20:4-containing lipid pools. (Fig.10 c) Consistently, the t-SNE projection displayed a clear separation between CTRL and OEA groups, indicating that OEA induces a marked shift in the global metabolomic fingerprint. (Fig.10 f) In line with this, the pathway schematic summarizes that arachidonic acid released from membrane phospholipids feeds into the cyclooxygenase (COX), lipoxygenase (LOX), and cytochrome P450 (CYP) branches to generate eicosanoids/oxylipins, providing a mechanistic framework for how a reduction in FA 20:4 could reflect altered flux through the arachidonic acid cascade (36)

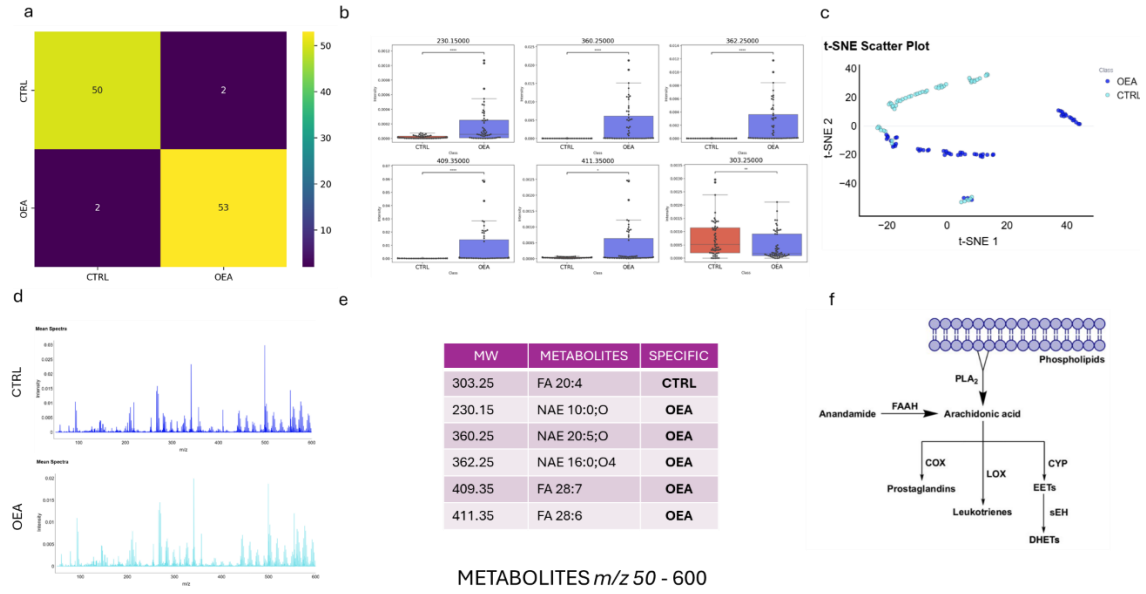


| MW | METABOLITES | SPECIFIC |
|---|---|---|
| 303.25 | FA 20:4 | CTRL |
| 230.15 | NAE 10:0;O | OEA |
| 360.25 | NAE 20:5;O | OEA |
| 362.25 | NAE 16:0;O4 | OEA |
| 409.35 | FA 28:7 | OEA |
| 411.35 | FA 28:6 | OEA |

**Figure 10. SpiderMass metabolomics discriminates CTRL and OEA and highlights an OEA-associated shift in fatty-acid amide and PUFA-related features.** (a) Confusion matrix of the supervised classification model separating CTRL and OEA samples, showing high classification performance with limited cross-misclassification. (b) Boxplots of the main discriminatory metabolomic features, showing increased abundance in OEA for m/z 230.1500 (NAE, N-acylethanolamine 10:0;O), 360.2500 (NAE 20:5;O), 362.2500 (N-acyl species, including a NAT, N-acyl taurine 16:0 compatible assignment), and very-long-chain polyunsaturated fatty acids m/z 409.3500 (FA 28:7) and 411.3500 (FA 28:6), while m/z 303.2500 (FA 20:4; commonly corresponding to the arachidonic acid pool) is decreased in OEA versus CTRL. (c) t-SNE projection showing a clear separation between CTRL and OEA groups based on the global metabolomic fingerprint. (d) Mass spectra in the m/z range 50–600 comparing control and OEA-treated samples (50 μM). (e) Table reporting the most abundant differential features (Fold change > 2) between CTRL and OEA condition. (f) Schematic overview of the arachidonic acid cascade: arachidonic acid can be released from membrane phospholipids (via $PLA_2$) or derived from endocannabinoid turnover (anandamide via FAAH), then metabolized through COX, LOX, and CYP branches to generate prostaglandins, leukotrienes, and EET/DHET derivatives, respectively.

## 4. Discussion

Colorectal cancer (CRC) cells display strong metabolic plasticity, and lipid metabolism is a key axis supporting proliferation, redox control, stress adaptation, and tumor heterogeneity (37). In this context, oleoylethanolamide (OEA) is particularly informative because it is both a bioactive lipid mediator and a molecule whose carbon backbone can be redistributed into endogenous lipid pools after uptake and enzymatic processing. OEA was first described as a feeding-regulated satiety factor (38) and later established as an endogenous PPAR$\alpha$ agonist shaping energy balance (39), yet intestinal studies have often emphasized barrier function and inflammation rather than systems-level lipid handling, despite links to gut homeostasis (40) Here, an integrated workflow (phenotyping - SpiderMass lipidomics/metabolomics/kinetics - LC-MS proteomics) captures how a lipid signal rapidly enters cells and drives coordinated remodeling across distinct CRC backgrounds. MTS assays defined a workable, non-cytotoxic window: 10-50 μM OEA is broadly tolerated at 24-48 h, whereas 100 μM causes a time-dependent drop in metabolic viability (41). Within this window, OEA increases neutral lipid droplets (LDs), most strongly in HT29 and HuH7 . Although this may seem counterintuitive for a "PPAR$\alpha$ ligand" often linked to lipid mobilization/oxidation (42), the LDs phenotype is consistent with an adaptive buffering response driven by the balance between lipid influx, processing, and storage capacity: OEA upregulates CD36, a fatty-acid transporter that can be PPAR$\alpha$-responsive (43). In parallel, cell lines differ in their baseline expression of DGAT1/2 - enzymes catalyzing the committed final step of triglyceride synthesis and tightly linked to lipid droplet biogenesis (44,45) Together, these factors likely shape how effectively each model converts increased lipid influx into neutral lipid storage and visible LD accumulation. SpiderMass lipidomics reveals a conserved OEA-associated membrane signature

across models: multiple phosphatidylethanolamine (PE) species decrease while other PE species increase, consistent with phospholipid remodeling via deacylationreacylation (46). In parallel, OEA increases phosphatidic acid (PA) and lysophosphatidic acid (LPA), linking membrane turnover to signaling: PA is a key intermediate and signaling node connected to mTOR regulation and stress-related mTORC1 recruitment (47); while LPA is a potent bioactive lipid acting through LPA receptors with established roles in cancer programs (48). Increased phosphatidylserine (PS) signals further support membrane/trafficking reorganization that can intersect stress and apoptosis-related membrane dynamics (49). The metabolomics layer complements this by highlighting enrichment of N-acylethanolamine/N-acyl-related features alongside a reduction in the m/z feature compatible with arachidonic acid (20:4), consistent with a shift in lipid-mediator substrate pools and potentially altered flux through the arachidonic-acid cascade (50). Time-resolved OEA-d4 kinetics add a mechanistic constraint: uptake is rapid (30 min-2 h) but persistence varies markedly by cell line, implying that downstream processing/clearance contributes to heterogeneous remodeling. Proteomics places these lipid shifts into broader network responses: OEA triggers extensive but cell line-specific rewiring, and comparison with the synthetic PPAR$\alpha$ agonist GW7647 shows only partial overlap, supporting a mixed PPAR$\alpha$-dependent and PPAR$\alpha$-independent response. Together, these data argue that in intestinal settings OEA should be viewed not only as a canonical PPAR$\alpha$ activator, but also as a lipid that reshapes membrane composition and lipid signaling, with LDs formation emerging as a context-dependent protective/storage endpoint. Importantly, these results are preliminary, and dedicated functional experiments are needed to validate causality- perturbing PPAR$\alpha$/CD36/DGAT1-2, testing lipid-remodeling enzymes, and directly measuring flux into β-oxidation versus triglyceride storage and mediator pathways.

# 6. General discussion and conclusions

Lipid overload is a hallmark of contemporary metabolic disease and a major perturbation for nutrient-interface epithelia such as intestine and liver. Lipotoxicity should be conceptualized not as lipid excess per se, but as a systems-level failure of fatty-acid (FA) partitioning across β-oxidation, membrane lipid remodeling, neutral-lipid sequestration into lipid droplets (LDs), and the generation of bioactive lipid intermediates that propagate stress signaling (51). Because FA flux is spatially segregated across the endoplasmic reticulum (ER), mitochondria, peroxisomes, and LDs, defects in organelle-specific lipid handling precipitate ER stress, oxidative stress, proteostasis collapse, and activation of regulated cell-death programs (53). Within this framework, saturated fatty acids (SFAs) such as palmitic acid PA constitute a prototypical lipotoxic insult, whereas monounsaturated fatty acids (MUFAs) such as oleate (OA) often exert a buffering effect by promoting triacylglycerol (TAG) synthesis and LD biogenesis, thereby limiting the accumulation of cytotoxic intermediates and membrane saturation (53,52). This dissertation examined whether targeted pharmacological modulation of lipid metabolism , centered on the OEA , PPAR$\alpha$ signaling axis and enzymatic control points governing TAG synthesis can reprogram stress adaptation under FA overload in colon and liver cellular models. A central mechanistic premise is that TAG accumulation is not intrinsically pathogenic; rather, TAG synthesis can be cytoprotective by diverting FA from lipotoxic pools and preserving membrane compositional homeostasis (54). This detoxification route is controlled by DGAT1 and DGAT2, two non-redundant acyltransferases with distinct substrate channeling properties: DGAT1 preferentially incorporates exogenous FA (notably relevant to intestinal lipid handling), whereas DGAT2 preferentially channels endogenously synthesized FA in lipogenic contexts (55) In intestinal biology, the work is positioned within the concept of the gut as a

nutrient-sensing organ in which epithelial lipid handling modulates barrier integrity and inflammatory outputs during high-fat stress (56). In this setting, oleoylethanolamide (OEA) functions as a feeding-regulated lipid mediator produced in the proximal small intestine and a potent endogenous PPAR$\alpha$ agonist coupling dietary lipid exposure to FA utilization and anti-inflammatory tone (57). Importantly, OEA can also engage PPAR$\alpha$-independent signaling nodes (e.g., TRPV1 and GPR119) and additional transcriptional programs, consistent with context-dependent pleiotropy (58).

In a hepatic PA-lipotoxicity model (Chapter 3), PA mechanistically coupled ER stress and autophagy impairment to a failure of neutral-lipid buffering, characterized by reduced LD formation and transcriptional/proteomic suppression of DGAT1, whereas OA conferred protection. DGAT1 inhibition (pharmacological or siRNA) was sufficient to trigger cell death even in the presence of OA, identifying DGAT1 as a stress-sensitive checkpoint that dictates whether incoming FA are esterified into TAG/LDs or redirected into maladaptive stress-amplifying pathways, consistent with a coordinated ER-autophagy-LDs axis (59) Bioenergetic profiling further supported a maladaptive energetic state under PA, with elevated respiration reduced coupling efficiency and increased oxidative burden, consistent with incomplete oxidation and mitochondrial stress (60). Notably, PPAR$\alpha$ activation reversed key elements of the PA phenotype, attenuating ER stress/autophagy blockade while restoring DGAT1 expression and LD buffering capacity, indicating coordinated re-alignment of catabolic and cytoprotective storage programs (61).

In CRC models (Chapter 4), epithelial–mesenchymal transition (EMT) emerged as a determinant of lipotoxic vulnerability. Epithelial-like HCT15 cells exhibited a glycolytic, LD-low phenotype and marked PA sensitivity, whereas mesenchymal-like HCT116 cells displayed a more oxidative, lipid-storage

competent program and relative resistance. OA restored viability by enhancing LD buffering, and EMT induction in HCT15 increased LD abundance and attenuated PA-induced death, supporting EMT as a metabolic plasticity state that expands lipid sequestration capacity (62). Finally, a multi-omics framework (Chapter 5) delineated OEA-driven remodeling across colon-derived models with hepatic comparison. At moderate, non-cytotoxic concentrations (10–50 μM), OEA induced LD accumulation with CD36 upregulation, remodeled glycerophospholipid composition and signaling lipid pools, and shifted metabolomic features toward fatty-acid amide - related signatures with relative depletion of arachidonic acid. Proteomic responses were highly context-dependent and only partially concordant with the selective PPAR$\alpha$ agonist GW7647, consistent with a variable PPAR$\alpha$-dependent core coupled to PPAR$\alpha$-independent components; OEA-d4 kinetics further indicated that uptake and intracellular persistence impose constraints on downstream network remodeling (63). Collectively, the dissertation supports a unifying model in which mitigating lipid-driven pathology requires reprogramming FA fate decisions: preserving TAG/LD buffering (DGAT1), coordinating catabolic flux with stress-control modules (PPAR$\alpha$, engaged by OEA), and accounting for plasticity states (EMT) that define baseline metabolic wiring and stress tolerance. These findings motivate validation in higher-fidelity systems (organoids and gut liver axis models) to establish which OEA-responsive modules are necessary and sufficient to confer stress resilience (64,65).

## 6.1 Limitations of the study and future perspectives

Despite the mechanistic insights provided by this dissertation, some limitations should be acknowledged. First, most experimental evidence was obtained using immortalized or cancer-derived cellular models. Although these systems are valuable for reproducible mechanistic studies, they may not fully recapitulate the metabolic behavior of healthy hepatic and intestinal tissues. Indeed, immortalization and tumor-associated rewiring can influence basal lipid metabolism, mitochondrial activity, lipid droplet dynamics, stress responses, and nuclear receptor signaling, potentially affecting the interpretation of lipid-partitioning phenotypes. Future studies should therefore validate the main findings in non-transformed models, including primary hepatocytes, healthy intestinal epithelial cells and organoids. Second, although *Caenorhabditis elegans* provided a useful *in vivo* platform to investigate selected lipid-metabolism-related responses at the whole-organism level, the absence of mammalian *in vivo* models represents an important limitation. Mouse models of diet-induced obesity, hepatic steatosis, or metabolic dysfunction would be necessary to determine whether DGAT1-dependent lipid buffering, PPAR$\alpha$ activation, and OEA-driven metabolic remodeling exert comparable protective effects in a more complex physiological context, where liver-intestine crosstalk, immune regulation, endocrine signals, and tissue-specific lipid fluxes can be evaluated. Finally, while proteomic and multi-omics analyses identified relevant pathways and candidate regulatory nodes, additional functional validation is required to establish causality. Future work should include targeted genetic or pharmacological manipulation of key proteins, lipid flux analyses, and focused lipidomic profiling of bioactive intermediates such as ceramides, acyl-CoAs, and phospholipid species. These approaches would strengthen the translational relevance of the present findings and clarify whether the adaptive lipid-handling

programs identified here can be exploited therapeutically to counteract lipid-induced cellular dysfunction.

## References


1. *Chen D, Zhou X, Yan P, Yang C, Li Y, Han L, et al. Lipid metabolism reprogramming in colorectal cancer. J Cell Biochem. 2023 Jan 5;124(1):3–16. doi:10.1002/jcb.30347*

2. *Rodríguez de Fonseca F, Navarro M, Gómez R, Escuredo L, Nava F, Fu J, et al. An anorexic lipid mediator regulated by feeding. Nature. 2001 Nov 8;414(6860):209–12. doi:10.1038/35102582*

3. *De Filippo C, Costa A, Becagli MV, Monroy MM, Provensi G, Passani MB. Gut microbiota and oleoylethanolamide in the regulation of intestinal homeostasis. Front Endocrinol (Lausanne). 2023 Apr 5;14. doi:10.3389/fendo.2023.1135157*

4. *Ogrinc N, Kruszewski A, Chaillou P, Saudemont P, Lagadec C, Salzet M, et al. Robot-Assisted SpiderMass for In Vivo Real-Time Topography Mass Spectrometry Imaging. Anal Chem. 2021 Nov 2;93(43):14383–91. doi:10.1021/acs.analchem.1c01692*

5. *Zhou J, Ren T, Li Y, Cheng A, Xie W, Xu L, et al. Oleoylethanolamide inhibits α-melanocyte stimulating hormone-stimulated melanogenesis via ERK, Akt and CREB signaling pathways in B16 melanoma cells. Oncotarget. 2017 Aug 22;8(34):56868–79. doi:10.18632/oncotarget.18097*

6. *Li Y, Zhang Y, Wang Q, Wu C, Du G, Yang L. Oleoylethanolamide Protects against Acute Ischemic Stroke by Promoting PPARα-Mediated Microglia/Macrophage M2 Polarization. Pharmaceuticals. 2023 Apr 20;16(4):621. doi:10.3390/ph16040621*

7. *Laplante M, Sabatini DM. An Emerging Role of mTOR in Lipid Biosynthesis. Current Biology. 2009 Dec;19(22):R1046–52. doi:10.1016/j.cub.2009.09.058*

8. *Ben-Sahra I, Manning BD. mTORC1 signaling and the metabolic control of cell growth. Curr Opin Cell Biol. 2017 Apr;45:72–82. doi:10.1016/j.ceb.2017.02.012*

9. *Kim J, Lee J hoon, Iyer VR. Global Identification of Myc Target Genes Reveals Its Direct Role in Mitochondrial Biogenesis and Its E-Box Usage In Vivo. PLoS One. 2008 Mar 12;3(3):e1798. doi:10.1371/journal.pone.0001798*

10. *Liberzon A, Birger C, Thorvaldsdóttir H, Ghandi M, Mesirov JP, Tamayo P. The Molecular Signatures Database Hallmark Gene Set Collection. Cell Syst. 2015 Dec;1(6):417–*

*25. doi:10.1016/j.cels.2015.12.004*

*11. Buttke TM, McCubrey JA, Owen TC. Use of an aqueous soluble tetrazolium/formazan assay to measure viability and proliferation of lymphokine-dependent cell lines. J Immunol Methods. 1993 Jan;157(1–2):233–40. doi:10.1016/0022-1759(93)90092-L*

*12. Qiu B, Simon M. BODIPY 493/503 Staining of Neutral Lipid Droplets for Microscopy and Quantification by Flow Cytometry. Bio Protoc. 2016;6(17). doi:10.21769/BioProtoc.1912*

*13. Yang Y, Chen M, Georgeson KE, Harmon CM. Mechanism of oleoylethanolamide on fatty acid uptake in small intestine after food intake and body weight reduction. American Journal of Physiology-Regulatory, Integrative and Comparative Physiology. 2007 Jan;292(1):R235–41. doi:10.1152/ajpregu.00270.2006*

*14. Yen CLE, Stone SJ, Koliwad S, Harris C, Farese R V. Thematic Review Series: Glycerolipids. DGAT enzymes and triacylglycerol biosynthesis. J Lipid Res. 2008 Nov;49(11):2283–301. doi:10.1194/jlr.R800018-JLR200*

*15. Harris CA, Haas JT, Streeper RS, Stone SJ, Kumari M, Yang K, et al. DGAT enzymes are required for triacylglycerol synthesis and lipid droplets in adipocytes. J Lipid Res. 2011 Apr;52(4):657–67. doi:10.1194/jlr.M013003*

*16. Kaczocha M, Glaser ST, Deutsch DG. Identification of intracellular carriers for the endocannabinoid anandamide. Proceedings of the National Academy of Sciences. 2009 Apr 14;106(15):6375–80. doi:10.1073/pnas.0901515106*

*17. Fu J, Astarita G, Gaetani S, Kim J, Cravatt BF, Mackie K, et al. Food Intake Regulates Oleoylethanolamide Formation and Degradation in the Proximal Small Intestine. Journal of Biological Chemistry. 2007 Jan;282(2):1518–28. doi:10.1074/jbc.M607809200*

*18. Uhlén M, Fagerberg L, Hallström BM, Lindskog C, Oksvold P, Mardinoglu A, et al. Tissue-based map of the human proteome. Science (1979). 2015 Jan 23;347(6220). doi:10.1126/science.1260419*

*19. Shechter S, Ya'ar Bar S, Khattib H, Gage MJ, Avni D. Riok1, A Novel Potential Target in MSI-High p53 Mutant Colorectal Cancer Cells. Molecules. 2023 May 31;28(11):4452. doi:10.3390/molecules28114452*

*20. Goldstein I, Ezra O, Rivlin N, Molchadsky A, Madar S, Goldfinger N, et al. p53, a novel regulator of lipid metabolism pathways. J Hepatol. 2012 Mar;56(3):656–62. doi:10.1016/j.jhep.2011.08.022*

*21. Stine ZE, Walton ZE, Altman BJ, Hsieh AL, Dang C V. MYC, Metabolism, and Cancer. Cancer Discov. 2015 Oct 1;5(10):1024–39. doi:10.1158/2159-8290.CD-15-0507*

*22. Ragupathi A, Kim C, Jacinto E. The mTORC2 signaling network: targets and cross-talks. Biochemical Journal. 2024 Jan 25;481(2):45–91. doi:10.1042/BCJ20220325*

*23. Glidden EJ, Gray LG, Vemuru S, Li D, Harris TE, Mayo MW. Multiple Site Acetylation of Rictor Stimulates Mammalian Target of Rapamycin Complex 2 (mTORC2)-dependent Phosphorylation of Akt Protein. Journal of Biological Chemistry. 2012 Jan;287(1):581–8. doi:10.1074/jbc.M111.304337*

*24. Stine ZE, Walton ZE, Altman BJ, Hsieh AL, Dang C V. MYC, Metabolism, and Cancer. Cancer Discov. 2015 Oct 1;5(10):1024–39. doi:10.1158/2159-8290.CD-15-0507*

*25. Jin W. Regulation of Src Family Kinases during Colorectal Cancer Development and Its Clinical Implications. Cancers (Basel). 2020 May 23;12(5):1339. doi:10.3390/cancers12051339*

*26. Boukerche H, Su Z zhong, Prévot C, Sarkar D, Fisher PB. mda -9/Syntenin promotes metastasis in human melanoma cells by activating c-Src. Proceedings of the National Academy of Sciences. 2008 Oct 14;105(41):15914–9. doi:10.1073/pnas.0808171105*

*27. Saha S, Bardelli A, Buckhaults P, Velculescu VE, Rago C, Croix B St., et al. A Phosphatase Associated with Metastasis of Colorectal Cancer. Science (1979). 2001 Nov 9;294(5545):1343–6. doi:10.1126/science.1065817*

*28. Chen CH, Lai JM, Chou TY, Chen CY, Su LJ, Lee YC, et al. VEGFA Upregulates FLJ10540 and Modulates Migration and Invasion of Lung Cancer via PI3K/AKT Pathway. PLoS One. 2009 Apr 1;4(4):e5052. doi:10.1371/journal.pone.0005052*

*29. Koohini Z, Koohini Z, Teimourian S. Slit/Robo Signaling Pathway in Cancer; a New Stand Point for Cancer Treatment. Pathology & Oncology Research. 2019 Oct 4;25(4):1285–93. doi:10.1007/s12253-018-00568-y*

*30. Koohini Z, Koohini Z, Teimourian S. Slit/Robo Signaling Pathway in Cancer; a New*

*Stand Point for Cancer Treatment. Pathology & Oncology Research. 2019 Oct 4;25(4):1285–93. doi:10.1007/s12253-018-00568-y*

*31. Fu J, Gaetani S, Oveisi F, Lo Verme J, Serrano A, Rodríguez de Fonseca F, et al. Oleylethanolamide regulates feeding and body weight through activation of the nuclear receptor PPAR-α. Nature. 2003 Sep;425(6953):90–3. doi:10.1038/nature01921*

*32. Wang B, Tontonoz P. Phospholipid Remodeling in Physiology and Disease. Annu Rev Physiol. 2019 Feb 10;81(1):165–88. doi:10.1146/annurev-physiol-020518-114444*

*33. Lee SH, Meng XW, Flatten KS, Loegering DA, Kaufmann SH. Phosphatidylserine exposure during apoptosis reflects bidirectional trafficking between plasma membrane and cytoplasm. Cell Death Differ. 2013 Jan 3;20(1):64–76. doi:10.1038/cdd.2012.93*

*34. Fu J, Gaetani S, Oveisi F, Lo Verme J, Serrano A, Rodríguez de Fonseca F, et al. Oleylethanolamide regulates feeding and body weight through activation of the nuclear receptor PPAR-α. Nature. 2003 Sep;425(6953):90–3. doi:10.1038/nature01921*

*35. Wang B, Wu L, Chen J, Dong L, Chen C, Wen Z, et al. Metabolism pathways of arachidonic acids: mechanisms and potential therapeutic targets. Signal Transduct Target Ther. 2021 Feb 26;6(1):94. doi:10.1038/s41392-020-00443-w*

*36. Rodríguez de Fonseca F, Navarro M, Gómez R, Escuredo L, Nava F, Fu J, et al. An anorexic lipid mediator regulated by feeding. Nature. 2001 Nov 8;414(6860):209–12. doi:10.1038/35102582*

*37. Fu J, Gaetani S, Oveisi F, Lo Verme J, Serrano A, Rodríguez de Fonseca F, et al. Oleylethanolamide regulates feeding and body weight through activation of the nuclear receptor PPAR-α. Nature. 2003 Sep;425(6953):90–3. doi:10.1038/nature01921*

*38. De Filippo C, Costa A, Becagli MV, Monroy MM, Provensi G, Passani MB. Gut microbiota and oleoylethanolamide in the regulation of intestinal homeostasis. Front Endocrinol (Lausanne). 2023 Apr 5;14. doi:10.3389/fendo.2023.1135157*

*39. Buttke TM, McCubrey JA, Owen TC. Use of an aqueous soluble tetrazolium/formazan assay to measure viability and proliferation of lymphokine-dependent cell lines. J Immunol Methods. 1993 Jan;157(1–2):233–40. doi:10.1016/0022-1759(93)90092-L*

*40. Yang Y, Chen M, Georgeson KE, Harmon CM. Mechanism of oleoylethanolamide on fatty acid uptake in small intestine after food intake and body weight reduction. American Journal of Physiology-Regulatory, Integrative and Comparative Physiology. 2007 Jan;292(1):R235–41. doi:10.1152/ajpregu.00270.2006*

*41. Harris CA, Haas JT, Streeper RS, Stone SJ, Kumari M, Yang K, et al. DGAT enzymes are required for triacylglycerol synthesis and lipid droplets in adipocytes. J Lipid Res. 2011 Apr;52(4):657–67. doi:10.1194/jlr.M013003*

*42. Yen CLE, Stone SJ, Koliwad S, Harris C, Farese R V. Thematic Review Series: Glycerolipids. DGAT enzymes and triacylglycerol biosynthesis. J Lipid Res. 2008 Nov;49(11):2283–301. doi:10.1194/jlr.R800018-JLR200*

*43. Wang B, Tontonoz P. Phospholipid Remodeling in Physiology and Disease. Annu Rev Physiol. 2019 Feb 10;81(1):165–88. doi:10.1146/annurev-physiol-020518-114444*

*44. Foster DA. Regulation of mTOR by Phosphatidic Acid? Cancer Res. 2007 Jan 1;67(1):1–4. doi:10.1158/0008-5472.CAN-06-3016*

*45. Frias MA, Mukhopadhyay S, Lehman E, Walasek A, Utter M, Menon D, et al. Phosphatidic acid drives mTORC1 lysosomal translocation in the absence of amino acids. Journal of Biological Chemistry. 2020 Jan;295(1):263–74. doi:10.1074/jbc.RA119.010892*

*46. Lin ME, Herr DR, Chun J. Lysophosphatidic acid (LPA) receptors: Signaling properties and disease relevance. Prostaglandins Other Lipid Mediat. 2010 Apr;91(3–4):130–8. doi:10.1016/j.prostaglandins.2009.02.002*

*47. Lee SH, Meng XW, Flatten KS, Loegering DA, Kaufmann SH. Phosphatidylserine exposure during apoptosis reflects bidirectional trafficking between plasma membrane and cytoplasm. Cell Death Differ. 2013 Jan 3;20(1):64–76. doi:10.1038/cdd.2012.93*

*48. Wang B, Wu L, Chen J, Dong L, Chen C, Wen Z, et al. Metabolism pathways of arachidonic acids: mechanisms and potential therapeutic targets. Signal Transduct Target Ther. 2021 Feb 26;6(1):94. doi:10.1038/s41392-020-00443-w*

*49. Yoon H, Shaw JL, Haigis MC, Greka A. Lipid metabolism in sickness and in health: Emerging regulators of lipotoxicity. Mol Cell. 2021 Sep;81(18):3708–30.*

*doi:10.1016/j.molcel.2021.08.027*

*50. Montgomery MK, De Nardo W, Watt MJ. Impact of Lipotoxicity on Tissue "Cross Talk" and Metabolic Regulation. Physiology. 2019 Mar 1;34(2):134–49. doi:10.1152/physiol.00037.2018*

*51. Listenberger LL, Han X, Lewis SE, Cases S, Farese R V., Ory DS, et al. Triglyceride accumulation protects against fatty acid-induced lipotoxicity. Proceedings of the National Academy of Sciences. 2003 Mar 18;100(6):3077–82. doi:10.1073/pnas.0630588100*

*52. Obaseki E, Adebayo D, Bandyopadhyay S, Hariri H. Lipid droplets and fatty acid-induced lipotoxicity: in a nutshell. FEBS Lett. 2024 May 28;598(10):1207–14. doi:10.1002/1873-3468.14808*

*53. Obaseki E, Adebayo D, Bandyopadhyay S, Hariri H. Lipid droplets and fatty acid-induced lipotoxicity: in a nutshell. FEBS Lett. 2024 May 28;598(10):1207–14. doi:10.1002/1873-3468.14808*

*54. Buhman KK, Smith SJ, Stone SJ, Repa JJ, Wong JS, Knapp FF, et al. DGAT1 Is Not Essential for Intestinal Triacylglycerol Absorption or Chylomicron Synthesis. Journal of Biological Chemistry. 2002 Jul;277(28):25474–9. doi:10.1074/jbc.M202013200*

*55. Ichinose K, Maeshima Y, Yamamoto Y, Kinomura M, Hirokoshi K, Kitayama H, et al. 2-(8-Hydroxy-6-Methoxy-1-Oxo-1H-2-Benzopyran-3-yl) Propionic Acid, an Inhibitor of Angiogenesis, Ameliorates Renal Alterations in Obese Type 2 Diabetic Mice. Diabetes. 2006 May 1;55(5):1232–42. doi:10.2337/db05-1367*

*56. Nguyen TB, Louie SM, Daniele JR, Tran Q, Dillin A, Zoncu R, et al. DGAT1-Dependent Lipid Droplet Biogenesis Protects Mitochondrial Function during Starvation-Induced Autophagy. Dev Cell. 2017 Jul;42(1):9-21.e5. doi:10.1016/j.devcel.2017.06.003*

*57. Moliterni C, Vari F, Schifano E, Tacconi S, Stanca E, Friuli M, et al. Lipotoxicity of palmitic acid is associated with DGAT1 downregulation and abolished by PPARα activation in liver cells. J Lipid Res. 2024 Dec;65(12):100692. doi:10.1016/j.jlr.2024.100692*

*58. Koves TR, Ussher JR, Noland RC, Slentz D, Mosedale M, Ilkayeva O, et al. Mitochondrial Overload and Incomplete Fatty Acid Oxidation Contribute to Skeletal Muscle*

*Insulin Resistance. Cell Metab. 2008 Jan;7(1):45–56. doi:10.1016/j.cmet.2007.10.013*

*59. Bougarne N, Weyers B, Desmet SJ, Deckers J, Ray DW, Staels B, et al. Molecular Actions of PPARα in Lipid Metabolism and Inflammation. Endocr Rev. 2018 Oct 1;39(5):760–802. doi:10.1210/er.2018-00064*

*60. Pawlak M, Lefebvre P, Staels B. Molecular mechanism of PPARα action and its impact on lipid metabolism, inflammation and fibrosis in non-alcoholic fatty liver disease. J Hepatol. 2015 Mar;62(3):720–33. doi:10.1016/j.jhep.2014.10.039*

*61. Listenberger LL, Han X, Lewis SE, Cases S, Farese R V., Ory DS, et al. Triglyceride accumulation protects against fatty acid-induced lipotoxicity. Proceedings of the National Academy of Sciences. 2003 Mar 18;100(6):3077–82. doi:10.1073/pnas.0630588100*

*62. Ogrinc N, Saudemont P, Balog J, Robin YM, Gimeno JP, Pascal Q, et al. Water-assisted laser desorption/ionization mass spectrometry for minimally invasive in vivo and real-time surface analysis using SpiderMass. Nat Protoc. 2019 Nov 9;14(11):3162–82. doi:10.1038/s41596-019-0217-8*

*63. Cravatt BF, Giang DK, Mayfield SP, Boger DL, Lerner RA, Gilula NB. Molecular characterization of an enzyme that degrades neuromodulatory fatty-acid amides. Nature. 1996 Nov;384(6604):83–7. doi:10.1038/384083a0*

*64. Tilg H, Adolph TE, Trauner M. Gut-liver axis: Pathophysiological concepts and clinical implications. Cell Metab. 2022 Nov;34(11):1700–18. doi:10.1016/j.cmet.2022.09.017*

*65. Jensen-Cody SO, Potthoff MJ. Hepatokines and metabolism: Deciphering communication from the liver. Mol Metab. 2021 Feb;44:101138. doi:10.1016/j.molmet.2020.101138.*

## Publications derived from this thesis

- Vari F. et al. Epithelial-Mesenchymal Transition Shapes the Lipotoxic Response of Colon Cancer Cells to Palmitic Acid. *Molecular & Cellular Proteomics*, 2026. doi: 10.1016/j.mcpro.2026.101554
- Vari F. et al. Pharmacological potential of endocannabinoid and endocannabinoid-like compounds in protecting intestinal structure and metabolism under high-fat conditions. *Frontiers in Pharmacology*, 2025. doi: 10.3389/fphar.2025.1567543
- Moliterni C., Vari F. et al. Lipotoxicity of palmitic acid is associated with DGAT1 downregulation and abolished by PPAR$\alpha$ activation in liver cells. *Journal of Lipid Research*, 2024. doi: 10.1016/j.jlr.2024.100692

## Additional publications not included in this thesis

- Serra I., Bisconti E., Vari F. et al. Fatty acid amide hydrolase (FAAH) and the endocannabinoid system in obesity: Mechanistic insights and pharmacological opportunities beyond incretin-based therapies. *British Journal of Pharmacology*, 2026. doi: 10.1111/bph.70511
- Saponaro C., Gammaldi N., Cavallo V., et al. Insight into the Regulation of NDRG1 Expression. International *Journal of Molecular Sciences*, 2025. doi: 10.3390/ijms26083582
- Schifano E., Vari F., Buccini L. et al. A novel scalable method for the production of rennet-treated milk-derived extracellular vesicles for improved curcumin oral delivery. *Journal of Nanobiotechnology*, 2025. doi: 10.1186/s12951-025-03724-0
- Vari F. et al. Exploring the Role of Oleic Acid in Muscle Cell Differentiation: Mechanisms and Implications for Myogenesis and Metabolic Regulation in C2C12 Myoblasts. *Biomedicines*, 2025. doi: 10.3390/biomedicines13071568
- Tacconi S., Vari F., Sbarigia C. et al. M1-derived extracellular vesicles polarize recipient macrophages into M2-like macrophages and alter skeletal muscle homeostasis in a hyper-glucose environment. *Cell Communication and Signaling*, 2024. doi: 10.1186/s12964-024-01560-7
- Sbarigia C., Dinarelli S., Mura F., Buccini L., Vari F. et al. Wild-Type and SOD1-G93A SH-SY5Y under Oxidative Stress: EVs Characterization and Topographical Distribution of Budding Vesicles. *Applied Nano*, 2023. doi: 10.3390/applnano4010004